Novel pathogenic mechanisms of myasthenic disorders and potential therapeutic approaches

DPhil thesis

Katarzyna Marta Zoltowska

Neurosciences Group

Supervisor: Prof. David Beeson

Nuffield Department of Clinical Neurosciences

Green Templeton College, University of Oxford

Funded by the Muscular Dystrophy Campaign

Novel pathogenic mechanisms of myasthenic disorders and potential therapeutic approaches

Katarzyna Marta Zoltowska, Green Templeton College, Oxford

A thesis submitted for the degree of Doctor of Philosophy, Michaelmas Term 2013

Abstract

Congenital myasthenic syndrome (CMS) and myasthenia gravis (MG) are, respectively, inherited or autoimmunological disorders caused by aberrant neuromuscular transmission, which manifests as fatiguable muscle weakness.

A novel subtype of CMS, resulting from mutations in *GFPT1* and characterised by a limb-girdle pattern of muscle weakness, has been described. The gene encodes L-glutamine:D-fructose-6-phosphate amidotransferase 1 (GFAT1) – a key rate-limiting enzyme in the hexosamine biosynthetic pathway, providing building blocks for glycosylation of proteins and lipids. The research focused on the molecular bases of the CMS resulting from mutations in the ubiquitously expressed gene, but with symptoms largely restricted to the neuromuscular junction (NMJ). The work has established a link between the NMJ and *GFPT1* CMS by demonstrating that the AChR cell surface is decreased in *GFPT1* patient muscle cells and in *GFPT1*-silenced cell lines. The decrease is likely to be caused by reduced steady-state levels of individual AChR α, δ and ε, but not β, subunits.

To optimise treatment for myasthenic disorders, a comparative *in vivo* trial of therapy with pyridostigmine bromide and salbutamol sulphate, and pyridostigmine bromide alone, was conducted. Supplementation of the AChE inhibitor-based therapy with the β_2-adrenergic receptor agonist had a beneficial effect. This offers promise for more effective treatments for CMS and MG affected individuals.

Molecular causes of MG were also investigated. The search for novel antibody targets was conducted with the use of a designed cell-based assay for the detection of anti-COLQ autoimmunoglobulins in MG patient sera. The antibodies were detected in 24 out of 418 analysed samples, but their pathogenicity has not been determined.

Acknowledgements

I would like to acknowledge my supervisor Prof. David Beeson for his invaluable dedication, constant availability and broad specialist knowledge.

I would also like to thank all members of the Neurosciences Group, especially Susan Maxwell and Dr Richard Webster.

Since my research relied heavily on the consent of the patients to participate in the research project, I would like to thank all who volunteered to take part in the study.

Finally, the investigations would not be possible without a generous funding provided by the Muscular Dystrophy Campaign.

Table of contents

List of figures

List of tables

Abbreviations

3,4-DAP – 3,4-diaminopyridine
3'UTR – 3' untranslated region
α-BuTx – α-bungarotoxin
AAV – adeno-associated virus
ACh – acetylcholine
AChE – acetylcholinesterase
AChR – acetylcholine receptor
ADAB – 4-(dimethyl amino)benzaldehyde
ADRB2 – β_2-adrenergic receptor
AGRN – agrin
ALG – asparagine-linked glycosylation
AP – action potential
APAD – 3-acetylpyridine adenine dinucleotide
ATCC – American Type Culture Collection
ATP – adenosine triphosphate
AZ – active zone
BCA – bicinchoninic acid
BSA – bovine serum albumin
cAMP – cyclic adenosine monophosphate
CaMKII – Ca^{2+}/calmodulin-dependent protein kinase II
CAS – castanospermine
CASPR2TM – contactin-associated protein-like 2
CAZ – cytoskeletal matrix at the active zone
CBA – cell-based assay
CDG – congenital disorder of glycosylation
Cer – ceramide
ChAT – choline acetyltransferase
CHRNA1 – gene encoding AChR α1 subunit
CHRNB1 – gene encoding AChR β1 subunit
CHRND – gene encoding AChR δ subunit
CHRNE – gene encoding AChR ε subunit
CHRNG – gene encoding AChR γ subunit
CHX – cycloheximide
CMAP – compound muscle action potential
CMD – congenital muscular dystrophy
CMS – congenital myasthenic syndrome
CMV – cytomegalovirus

CNS – central nervous system

COLQ – collagen Q (collagenic tail of the synaptic acetylcholinesterase)

cpm – counts per minute

CRE – cAMP-response element

CT – cytotoxic T antigen

CTD – C-terminal trimerisation domain

DMEM – Dulbecco's Modified Eagle Medium

DOK7 – downstream of tyrosine kinase 7

DON – 6-diazo-5-oxo-L-norleucine

DPAGT1 – UDP-N-acetylglucosamine-dolichyl-phosphate N-acetylglucosaminephosphotransferase

ECACC – European Collection of Cell Cultures

ECM – extracellular matrix

EDL – extensor digitorum longus muscle

EGFP – enhanced green fluorescent protein

EGFP-ER – endoplasmic reticulum-localised enhanced green fluorescent protein

EGFP-Glc-ER – endoplasmic reticulum-localised enhanced green fluorescent protein with introduced N-glycosylation site

ELISA – enzyme-linked immunosorbent assay

EPP – endplate potential

ER – endoplasmic reticulum

FCMD – Fukuyama congenital muscular dystrophy

FCS – foetal calf serum

FIPA – fluorescence immunoprecipitation assay

FPLC – fast performance liquid chromatography

Fru-6-P – fructose-6-phosphate

GAG – glycosaminoglycan

GalNAc – N-acetylgalactosamine

GAPDH – glyceraldehyde-3-phosphate dehydrogenase

GATase_2 – glutaminase domain type 2

GDH – glutamate dehydrogenase

GFAT1 – L-glutamine:D-fructose-6-phosphate amidotransferase 1

GFAT1-L – long (muscle-specific) isoform of L-glutamine:D-fructose-6-phosphate amidotransferase 1

GFPT1 – gene or mRNA encoding L-glutamine:D-fructose-6-phosphate amidotransferase 1

GFPT1-L – mRNA encoding long (muscle-specific) isoform of L-glutamine:D-fructose-6-phosphate amidotransferase 1

$GlcNH_2$ – glucosamine

$GlcNH_2$-6-P – glucosamine-6-phosphate

Glc-6-P – glucose-6-phosphate

GlmS – glucosamine-6-phosphate synthase, bacterial homologue of GFAT1

Gln – glutamine

Glu – glutamate

GPCR – G-protein-coupled receptor

GPI – glycosylphosphatidylinositol

GSL – glycosphingolipid

HEK293TSA – human embryonic kidney 293TSA cells

HEPES – 4-(2-hydroxyethyl)-1-piperazineethanesulfonic acid

HRP – horseradish peroxidase

HS – horse serum

HSBD – heparan sulphate binding domain

ICAM1 – intercellular adhesion molecule 1

iPSC – induced pluripotent stem cell

IPTG – isopropyl β-D-1-thiogalactopyranoside

IRES – internal ribosomal entry site

K_i – inhibition constant

K_M – Michaelis constant

LB – lysogeny broth

LRP4 – low-density lipoprotein receptor-related protein 4

luc2 – luciferase from *Photinus pyralis* reporter gene

MALDI – matrix-assisted laser desorption/ionisation

Man – mannose

MCS – multiple cloning site

MEB – muscle-eye-brain disease

MG – myasthenia gravis

MGFACC – Myasthenia Gravis Foundation of America Clinical Classification

M-MLV RT – moloney murine leukemia virus reverse transcriptase

miRNA – micro RNA

MS – mass spectrometry

MuSK – muscle-specific tyrosine kinase

NCAM – neural cell adhesion molecule

ND – not diagnosed

neo – neomycin resistance gene

NGS – next generation sequencing

N/K – not known

NMJ – neuromuscular junction

NP-HPLC – normal-phase high performance liquid chromatography

NRS – normal rabbit serum

O-GalNAc – O-linked N-acetylgalactosamine

O-GlcNAc – O-linked N-acetylglucosamine

OGT – O-linked N-acetylglucosamine transferase

P1, P2, P3 – patient 1, 2, 3

PBS – phosphate buffered saline

PBST – phosphate buffered saline (PBS)-0.1% Tween 20

PCR – polymerase chain reaction

PE – R-phycoerithrin

PHA-L – phytohemagglutinin-L

PNGase F – protein N-glycosidase F

PRAD – proline-rich attachment domain

PTB – phosphotyrosine binding domain

PVDF – polyvinylidene difluoride

RAPSN – 43 kDa receptor-associated protein of the synapse

RIA – radioimmunoprecipitation assay

RNAi – ribonucleic acid interference

RT – reverse transcription

RQ – relative quantification

SDS-PAGE – sodium dodecyl sulphate polyacrylamide gel electrophoresis

siRNA – small interfering RNA

SIS – sugar isomerase domain

shRNA – short hairpin RNA

SNMG – seronegative myasthenia gravis

SNP – single nucleotide polymorphism

TA – tibialis anterior muscle

TE671 – rhabdomyosarcoma cell line

TE671 DB40 – rhabdomyosarcoma cell line stably transfected with AChR β, δ and ε subunits

TM – transmembrane domain

TOF – time-of-flight

TRITC – tetramethylrhodamine isothiocyanate

qPCR – quantitative PCR

VDCC – voltage-dependent calcium channel

VGKC – voltage-gated potassium channel

V_{max} – maximum initial velocity

VVA-B_4 – *Vicia villosa* agglutinin B_4

WES – whole exome sequencing

WGA – wheat germ agglutinin

WGS – whole genome sequencing

WWS – Walker-Warburg syndrome

wt – wild type

X-Gal – 5-bromo-4-chloro-3-indolyl-β-D-galactopyranoside

Chapter 1

Introduction

1.1. The neuromuscular junction

The neuromuscular junction (NMJ) is a specialised synapse between a motor nerve terminal and a skeletal muscle fibre. It exhibits a high degree of specialisation and is designed in a way that allows an efficient transmission of an impulse between the nerve and the muscle. Recent investigations, particularly through modern molecular genetic techniques, have allowed us to gain a greater insight into the development, structure and function of this specialised synapse.

The molecular mechanism via which the innervated muscle fibre can be excited is relatively complex. First, the acetylcholine (ACh) quanta, released by the nerve terminal, activate acetylcholine receptors (AChR) clustered at the postsynaptic membrane. This results in an entry of Na^+ and Ca^{2+} ions into the muscle through the AChR channels and the generation of a transient depolarisation, known as an endplate potential (EPP). If the depolarisation reaches a threshold for the self-sustaining opening of type $Na_v1.4$ voltage-dependent sodium channels, action potentials (AP) can be generated on the muscle membrane (Ruff, 2011) and the muscle contracts.

This process would not be possible without the finely designed structure of the NMJ (Figure 1.1.), which traditionally is split into three main components: a presynaptic part, a synaptic cleft and a postsynaptic region.

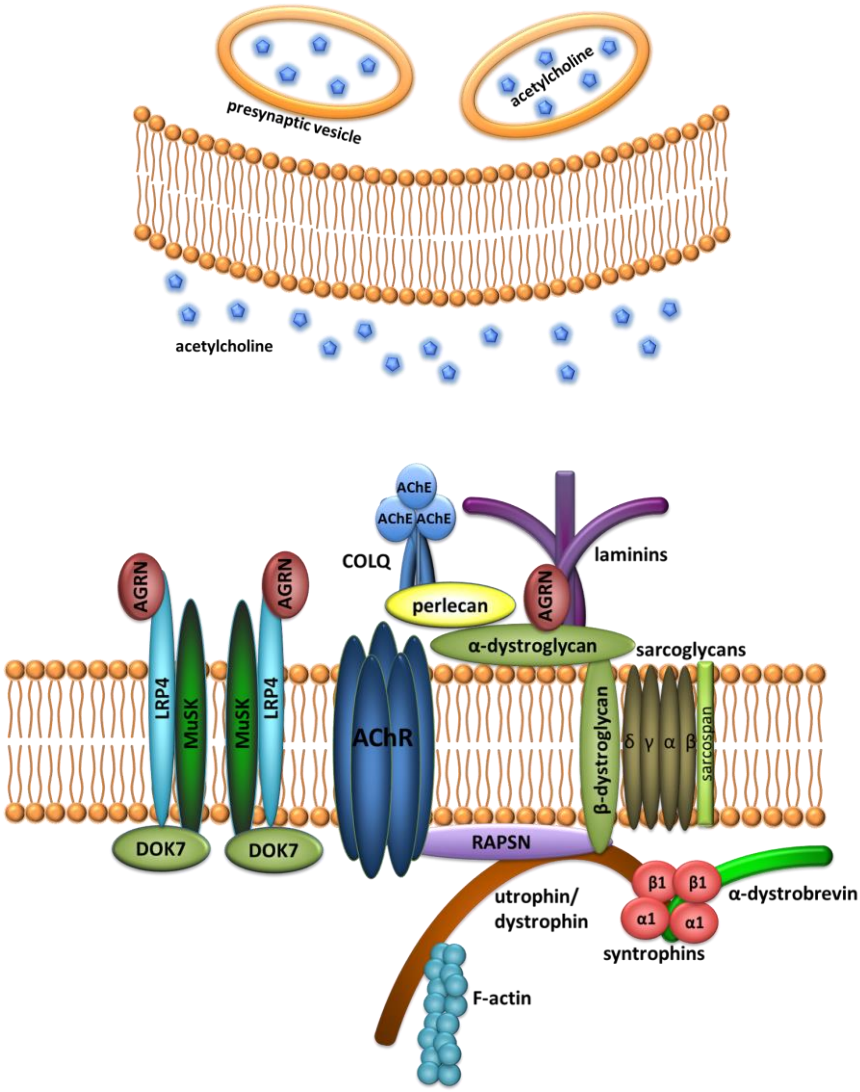

Fig.1.1. Schematic representation of the neuromuscular junction
AChE – acetylcholinesterase; AChR – acetylcholine receptor; AGRN – agrin; COLQ – collagen Q; DOK7 – downstream of tyrosine kinase 7; LRP4 – low-density lipoprotein receptor-related protein 4; MuSK – muscle-specific tyrosine kinase; RAPSN – 43 kDa receptor-associated protein of the synapse

1.1.1. The presynaptic part of the NMJ

The presynaptic side of the NMJ comprises a motor nerve terminal, which contains synaptic vesicle release sites, known as active zones (AZs). The AZs are made of a number of scaffolding proteins called the cytoskeletal matrix at the active zone (CAZ). This group of molecules includes Bassoon, CAST/ELKs/Erc family proteins, Munc13, Piccolo and regulating synaptic membrane exocytosis proteins 1/2 (RIM1/2) (Nishimune, 2012), and is essential for the development and maintenance of the

structure of the NMJ. Another major group of proteins localised at or in close proximity to the AZs are voltage-dependent calcium channels (VDCC) of N- or P/Q-type. Influx of Ca^{2+} through these channels activates a machinery (syntaxin, synaptosomal-associated protein 25 (SNAP-25) and synaptotagmin) required for synaptic vesicle release, and the transmitter, ACh, is released from the nerve terminal in multimolecular quanta (Hartzell et al., 1976). The neurotransmitter is synthesised by choline acetyltransferase (ChAT, E.C. 2.3.1.6), which catalyses the transfer of an acetyl group from acetyl-coenzyme A to choline (Govindasamy et al., 2004) and is subsequently packed into vesicles by vesicular acetylcholine transporter (VAChT) (Usdin et al., 1995).

Another molecule released from the nerve terminal at the NMJ is a heparan sulphate proteoglycan – agrin (AGRN), which is essential for both the development and maintenance of the synapse (Bezakova and Ruegg, 2003). Following release into the synaptic cleft, it binds to its receptor on the postsynaptic membrane – low-density lipoprotein receptor-related protein 4 (LRP4) (Zhang et al., 2008, Kim et al., 2008) – and induces clustering of the main ion channel at the NMJ – the AChR. The indispensable role of AGRN in the formation of the synapse has been demonstrated *in vivo* by studies of AGRN-deficient mutant mice, which lack NMJs (Gautam et al., 1996), and *in vitro* in muscle cell cultures, where AGRN induces postsynaptic differentiation, with the C-terminal part of the protein being essential for the AChR clustering process (Gesemann et al., 1995, Bezakova et al., 2001).

1.1.2. The synaptic cleft at the NMJ

The synaptic cleft is the extracellular space between a motor nerve terminal and a muscle fibre. The space is densely packed with extracellular matrix (ECM) proteins,

which compose a basal lamina. The basal lamina comprises four main types of molecules: heparan sulphate proteoglycans, such as neural AGRN, laminins (laminin 221 (α2β2γ1), 421 (α4β2γ1) and 521 (α5β2γ1)), collagens (collagen IV chains (α1-α6), XIII and collagen Q (COLQ)) and nidogens (nidogen-2), all of which play a role in the maintenance of the correct structure of the synapse (Singhal and Martin, 2011, Shi et al., 2012). The function and structure of COLQ will be described in detail in the following section since part of the project focused on this molecule.

1.1.2.1. Collagen Q and acetylcholinesterase

COLQ is crucial for anchoring the asymmetric form of acetylcholinesterase (AChE, EC 3.1.1.7) at the synapse, where AChE is responsible for the hydrolysis of ACh, thus the termination of neuromuscular transmission (Dvir et al., 2010).

AChE belongs to the family of serine hydrolases that act preferentially on choline esters. In vertebrates the enzyme is encoded by the *ACHE* gene and exists in a number of different tissue-specific isoforms ($AChE_R$, $AChE_H$ and $AChE_T$), which result from an alternative splicing of the 3' region of the transcript, hence possess the same catalytic domain but different C-terminal peptides (Chen et al., 2011, Massoulie, 2002, Taylor et al., 1993, Massoulie et al., 2005).

The unspliced "readthrough" variant ($AChE_R$) is a soluble monomeric form of the enzyme, which has been found to be up-regulated in the brain under stress stimulation (Kaufer et al., 1998). The "hydrophobic" variant ($AChE_H$) is expressed predominantly in red blood cells, where it forms glycosylphosphatidylinositol (GPI)-anchored dimers (Li et al., 1991). Finally, the "tailed" form of the enzyme ($AChE_T$) is highly expressed in the brain and at the NMJ, where it is anchored by specific interactions with proline-rich membrane anchor (PRIMA) or COLQ, respectively (Bon et al., 2004, Xie

et al., 2010, Perrier et al., 2002, Krejci et al., 1997). It possesses a highly conserved 40-amino acid long t peptide, also known as a tryptophan (W) amphiphilic tetramerisation domain (WAT), essential for homo-oligomerisation of AChE and its association with the anchoring proteins (Massoulie et al., 2005).

The molecular anchor of the AChE at the NMJ is COLQ. It exists in two variants (COLQ-1 and COLQ-1a), expressed differentially in slow-twitch and fast-twitch muscle (Krejci et al., 1999), with COLQ-1 being more abundant in the slow-twitch and COLQ-1a in the fast-twitch variant (Lee et al., 2004). The two isoforms are expressed from two distinct promoters, pCOLQ-1 and pCOLQ-1a, respectively, and differ in the N-terminal prepeptide signal sequence (exon 1 or 1a, respectively), which is cleaved in the release of the molecule. The mature COLQ-1 and COLQ-1a variants possess nearly identical sequences. The regulation of the expression of the two alternative transcripts remains poorly understood. Recent *in vitro* studies have suggested that the expression of the COLQ-1a can be induced by a nerve-derived factor – calcitonin gene-related peptide (CGRP), which may act via its downstream cyclic adenosine monophosphate (cAMP)-dependent signalling pathway. An intracellular increase in cAMP levels may activate the transcription from the pCOLQ-1a promoter, via a cAMP-response element (CRE) present in its sequence (Choi et al., 2007). The expression of COLQ also appears to be regulated by muscular activity. Application of ACh onto *in vitro* cultured C2C12 myotubes has been shown to increase an intracellular Ca^{2+} concentration, leading to an activation of Ca^{2+}/calmodulin-dependent kinase II (CaMKII), which can up-regulate the expression of myocyte enhancer factor 2 isoform C (MEF2C) – a downstream mediator of CaMKII in skeletal muscle. Finally, the activation of MEF2C leads to an up-regulation of the expression of both *COLQ* transcripts. The described pathway has been reported

to be more active in the slow-twitch muscle than in the fast-twitch muscle. This might account for a generally higher expression of both COLQ isoforms in the slow-twitch muscle fibres (Lau et al., 2008).

Irrespective of the isoform, the mature COLQ protein possesses several motifs within its sequence, which determine the localisation and the quaternary structure of the AChE-COLQ complexes (Figure 1.2.). It contains a Q_N region composed of an N-terminal signal peptide and a proline-rich attachment domain (PRAD), central collagen-like domains with characteristic repeats of glycines every three residues and a C-terminal trimerisation domain (Q_c or CTD) composed of proline-rich and cysteine-rich regions (Bon et al., 2003, Krejci et al., 1997).

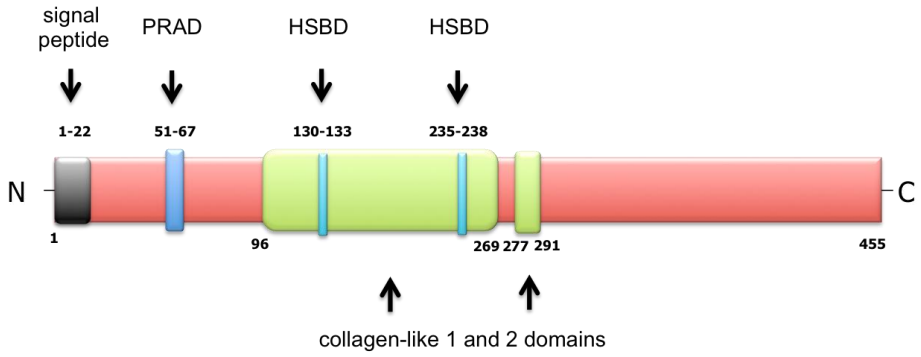

Fig.1.2. Schematic representation of human COLQ
The image was based on the data stored in the UniProt database [Q9Y215].
PRAD – proline-rich attachment domain; HSBD – heparan sulphate binding domain

Due to the presence of the CTD (307-388 segment in *Torpedo* Colq, which corresponds to 299-372 fragment in human COLQ), the protein forms homotrimeric triple helices. The assembly of these triple helical structures occurs in the endoplasmic reticulum (ER) in a zipper-like fashion, following the nucleation of the growth from the CTD and its progress through the central collagenous domain (Bon et al., 2003).

The CTD is not only essential for the formation of the COLQ trimers, but also for their association with the cell membrane. Since the protein lacks the transmembrane

domain, its presence at the postsynaptic membrane has to be mediated by a different molecular mechanism. The studies reported by Kimbell et al. have demonstrated that this mechanism involves interactions of the heparan sulphate binding domain (HSBD) and the C-terminal domain of COLQ with a heparan sulphate proteoglycan, perlecan (Kimbell et al., 2004), which itself associates with α-dystroglycan, an extracellular component of a transmembrane dystroglycan complex (Peng et al., 1999, Peng et al., 1998, Jacobson et al., 2001). Recent investigations have suggested that the mechanism might be even more complex and might involve not only the interactions between COLQ and perlecan, but also the binding of COLQ with muscle-specific tyrosine kinase (MuSK), which might occur via HSBD and CTD of COLQ (Cartaud et al., 2004).

Finally, in order to be able to play its molecular role, anchoring AChE at the NMJ, COLQ needs to form a complex with the enzyme (Figure 1.3.).

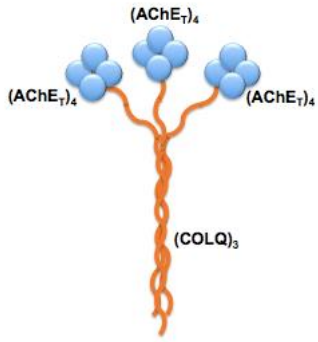

Fig.1.3. Schematic representation of the COLQ triple helix complexed with three AChE tetramers
$AChE_T$ – "tailed" form of acetylcholinesterase; COLQ – collagen Q

The formation of the COLQ-AChE complex occurs via interactions between the PRAD domain of COLQ and t peptides present in $AChE_T$ tetramer (Bon et al., 1997, Dvir et al., 2004). The minimal binding domain present in COLQ is composed of a

16-amino acid fragment: Glu-Ser-Thr-Gly_3-Pro_{10}. The quaternary structure of this complex may be stabilised by the formation of disulphide bonds between cysteines present upstream of PRAD in COLQ and in the t peptides of two AChE subunits. However, the cysteines are not required for the interaction (Krejci et al., 1991).

The assembly of the complexes occurs subsequently in two cellular compartments. First, the AChE tetramers are formed in the rough ER. They are then transported to the Golgi apparatus, where they assemble with COLQ, giving rise to various collagen-tailed AChE species (Rotundo, 1984). Each strand of the COLQ triple helix may bind one AChE tetramer, therefore the molecular interactions may give rise to the following collagen-tailed AChE species: A_4, A_8 and A_{12}, each composed of the COLQ homotrimer and one, two or three AChE tetramers, respectively (Bon et al., 1979). The abundance of particular AChE forms differs between slow- and fast-twitch muscle, with A_{12} being the main form in the fast-twitch, and A_4 and A_8 in the slow-twitch one. These variations may result from the differences in the expression of *COLQ* transcripts in the two types of muscle (Krejci et al., 1999).

1.1.3. The postsynaptic region of the NMJ

The third component of the neuromuscular synapse is its postsynaptic region. This part comprises ion channels present at the postsynaptic membrane, such as type $Na_v1.4$ voltage-dependent sodium channels and the main receptors at the NMJ – nicotinic AChR, as well as a molecular machinery essential for clustering of the AChR channels at the endplate. The structure of the postsynaptic part of the NMJ is designed to allow the most efficient transmission of the signal from a motor nerve terminal to a skeletal muscle. Characteristic features of this organisation are the extensive folding of the postsynaptic membrane (Sohn et al., 1999) and the specific localisation of various

classes of receptors at the cell surface, with the sodium channels abundant in the depths of the folds, immediately opposite the active zones in the motor nerve terminal, and the AChR clustered at the crests of the folds (Flucher and Daniels, 1989). It is thought that such a geometry of the synapse enables efficient amplification of the action of the neuromuscular transmitter, ACh (Martin, 1994).

1.1.3.1. AChR structure and function

Despite the presence of a number of densely packed synapse-specific molecules at the NMJ, muscle nicotinic AChR has always been considered to be an important functional component of the synapse. As the first purified and structurally characterised ligand-gated ion channel, it serves as a prototype for all receptors belonging to this family (Kemp et al., 1980, Nys et al., 2013).

The muscle subtype of the AChR is a pentamer composed of four homologous subunits: α1, β1, δ and ε in the adult receptor, and α1, β1, δ and γ in its foetal form. The proteins are encoded by five different genes, namely: *CHRNA1*, *CHRNB1*, *CHRND*, *CHRNE* and *CHRNG*, respectively. Additionally, the α1 subunit has been shown to be expressed in muscle fibres as two alternatively spliced isoforms, P3A+ (possessing an additional 75-base pair region between exon P3 and P4) and P3A-, but only the P3A- isoform has been found to be incorporated into functional receptors (Beeson et al., 1990, Newland et al., 1995). The functional receptors are thus formed of $2\alpha_1$(P3A-):$1\beta_1$:1δ:1ε/γ AChR subunits, which assemble around the central axis of the channel, with two α subunits separated by a γ or ε subunit and a βδ dimer (Unwin, 2005) (Figure 1.4.).

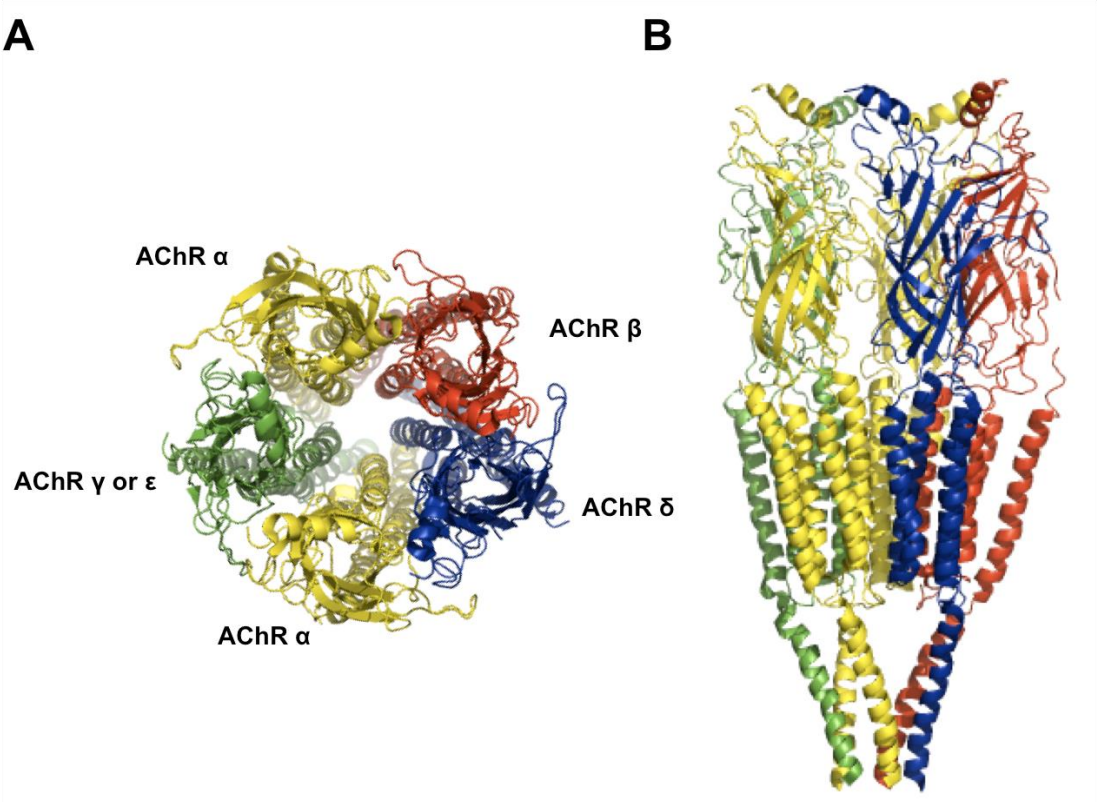

Fig.1.4. Three dimensional structure of the AChR complex (A) seen from the top or (B) from the side
AChR α subunits are coloured in yellow, AChR β is coloured in red, AChR δ in blue and AChR γ or ε in green. The image has been obtained from PDB database (PDB ID: 2BG9) and modified (Unwin, 2005).

Three main regions can be distinguished in the structure of each AChR subunit: an N-terminal extracellular (ligand binding) domain, a central membrane-spanning domain and a M3-M4 intracellular loop. The extracellular part of the protein is composed of a hydrophobic β-sandwich core, which is formed of 10 β-strands (β1-β10), and of one α-helix (α1). This fragment of the AChR subunits also possesses several loops, known as A, B, C, Cys and β1-β2 loops (Unwin, 2005). The presence of the Cys-loop, composed of 13 residues flanked by linked cysteines, designates the AChR as a prototype of a Cys-loop ligand-gated ion channel superfamily (Zouridakis et al., 2009). The other loops: A, B and C are essential for binding of the neurotransmitter, ACh (Unwin, 2005). In the muscle-type AChR the ACh can bind to two sites on the receptor, with one located on the interface between the α and δ

subunits, and the other between the α and ε or γ in the adult or the foetal receptor, respectively (Blount and Merlie, 1989). The next fragment of the receptor – the membrane-spanning domain – comprises 4 α-helices (M1-M4) and two loops: M1-M2 and M2-M3. Finally, the M3-M4 intracellular domain, involved in interactions with a number of intracellular molecules, is composed of a fragment between the M3 and M4 helices, and a MA α-helix. The described structural composition is nearly identical for all AChR subunits (Unwin, 2005).

1.1.3.2. AChR clustering mechanism

In order to mediate the neuromuscular transmission, the AChR need not only to be expressed at the postsynaptic membrane, but also tightly packed into AChR clusters. The clustering process depends on a number of NMJ proteins, among which the most important appear to be neural AGRN, LRP4, MuSK, downstream of tyrosine kinase 7 (DOK7) and 43 kDa receptor-associated protein of the synapse (RAPSN).

The AChR clustering pathway is activated by a heparan sulphate proteoglycan – AGRN, which is released from a nerve terminal and binds to its co-receptor LRP4 (Kim et al., 2008). The binding activates autophosphorylation of Tyr553 in the Asn-Pro-X-Tyr motif in the MuSK juxtamembrane region (Watty et al., 2000). Then the phosphorylation of three other tyrosines within the MuSK sequence (Tyr750, 754 and 755) occurs, which results in switching MuSK to a stably active state (Ghazanfari et al., 2011). The phosphorylated MuSK is a binding partner for DOK7, which can interact with the phosphorylated MuSK via its phosphotyrosine binding domain (PTB) (Bergamin et al., 2010).

Subsequent downstream signalling events are still poorly understood. It has been shown that the AGRN-mediated signalling activates members of the Rho family of

small guanosine triphosphatases (GTPases), such as Rac and Cdc42, which may trigger cytoskeletal rearrangements (Weston et al., 2000), and that AGRN can induce phosphorylation of the β subunit of the AChR (Borges and Ferns, 2001). Both events may contribute to the formation of the AChR clusters. The clusters are stabilised by RAPSN, which not only self-associates (Ramarao et al., 2001), but also binds to AChR subunits (Maimone and Merlie, 1993) and potentially to MuSK (Antolik et al., 2006), β-dystroglycan (Cartaud et al., 1998) and α-actinin (Dobbins et al., 2008). In addition, it can facilitate AChR phosphorylation by activating or localising protein kinases to the synaptic region. This function has been demonstrated to be mediated by a RING domain, present in the C-terminal fragment of RAPSN (Lee et al., 2008), and a cAMP-dependent protein kinase (PKA) type I has been implicated as a molecule recruited by RAPSN to the endplate region (Choi et al., 2012), where the cAMP/PKA type I pathway appears to be crucial for maintaining the synapse structure (Roder et al., 2010).

1.2. Glycosylation

Proteins, their interactions and a number of phosphorylation events are essential for the structure and function of the synapse, but the system would not be fully functional without other posttranslational modifications. One of these is modification with carbohydrate chains, known as glycosylation. A great variety of existing monosaccharides and the fact that each of them can theoretically generate an α- or a β-linkage to several positions on another molecule, results in a diversity of potential carbohydrate structures, which can be attached to proteins and lipids (Varki and Sharon, 2009) (Figure 1.5.).

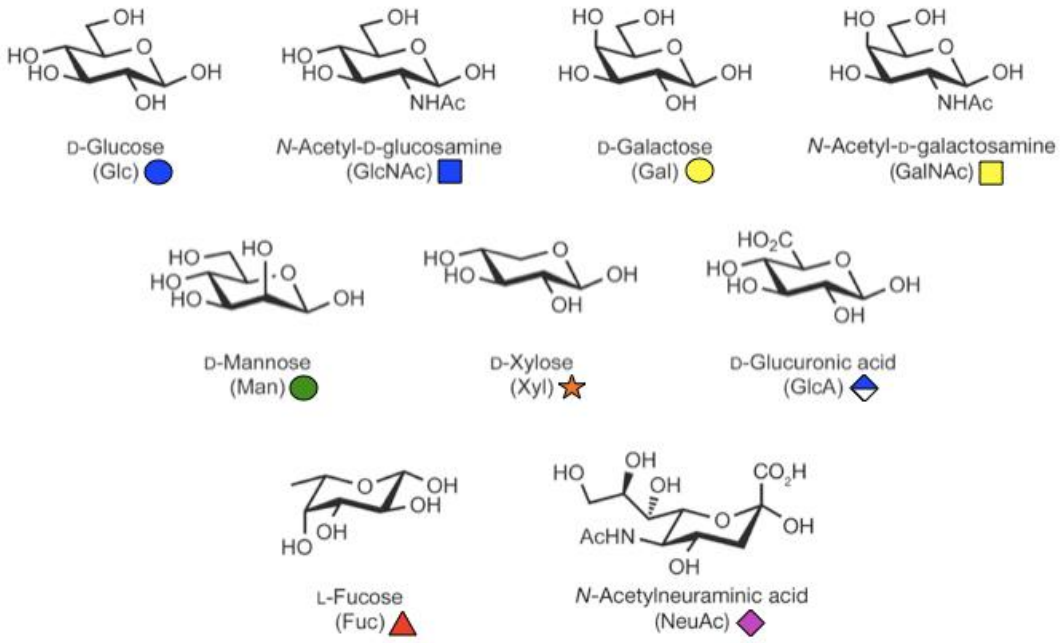

Fig.1.5. Structure and symbolic representation of monosaccharides commonly found in vertebrates (Bertozzi and Rabuka, 2009)

Current classification of glycans is based on the nature of a linkage generated between a sugar moiety and an aglycon. A covalent attachment of an oligosaccharide to a polypeptide chain results in the formation of a glycoprotein. If the sugar is attached via N-linkage, commonly to Asn present in the consensus sequence: Asn-X-Ser/Thr,

it is termed an N-oligosaccharide. On the other hand, when the carbohydrate is linked to the hydroxyl group of Ser or Thr, it is referred to as an O-glycan. Finally, if the target protein possesses one or more glycosaminoglycan (GAG) chains attached via xylose to the hydroxyl group of Ser, it is known as a proteoglycan (Moremen et al., 2012).

Not only proteins, but also lipids, can be modified with carbohydrate structures. These types of post-translationally modified molecules, officially designated as glycosphingolipids (GSLs), but often referred to as glycolipids, are composed of sugars attached to the terminal primary hydroxyl group of a ceramide (Cer), which itself consists of an alcohol sphingosine and a fatty acid.

Last but not least, glycans can comprise components of molecular anchors essential for the attachment of proteins to lipid bilayers. Such anchors, known as glycosylphosphatidylinositol (GPI) anchors, are complex structures composed of a phosphoethanolamine linker linked to the C-terminus of a target protein, a glycan core and a phospholipid (Paulick and Bertozzi, 2008, Ferguson et al., 2009).

1.2.1. Glycoproteins

The complexity of glycosylation makes it difficult to determine the structure and function of the modification. However, the discovery of a number of pathogenic mutations in the enzymes from the N- and O-glycosylation pathways, together with the development of novel molecular biology techniques, have resulted in recent progress in understanding the molecular bases of glycosylation.

1.2.1.1. N-glycosylation

The most widely studied type of glycosylation is N-glycosylation. N-glycans attached to Asn within Asn-X-Ser/Thr sequons are commonly present on a great number of membrane and secreted proteins. Each of these proteins may possess several N-glycosylation consensus sequences that can be modified with a variety of possible oligosaccharide moieties. This produces enormous diversity of possible glycoforms of a target protein.

All N-glycans that may be attached share a common Manα1-6(Manα1-3)Manβ1-4GlcNAcβ1-4GlcNAcβ1-Asn-X-Ser/Thr core, which can be further extended by the addition of various monosaccharides. The types of sugars linked to the core determine the class of the respective N-glycan. If only mannose residues are attached to the core, the glycan is termed a high-mannose one. When the core is extended by the addition of "antennae" (branching sugar chains attached to the core), the glycan is known as complex. Finally, a hybrid glycan results from the attachment of mannose residues to the Manα1-6 arm of the core and one or two "antennae" to the Manα1-3 arm (Stanley et al., 2009) (Figure 1.6.).

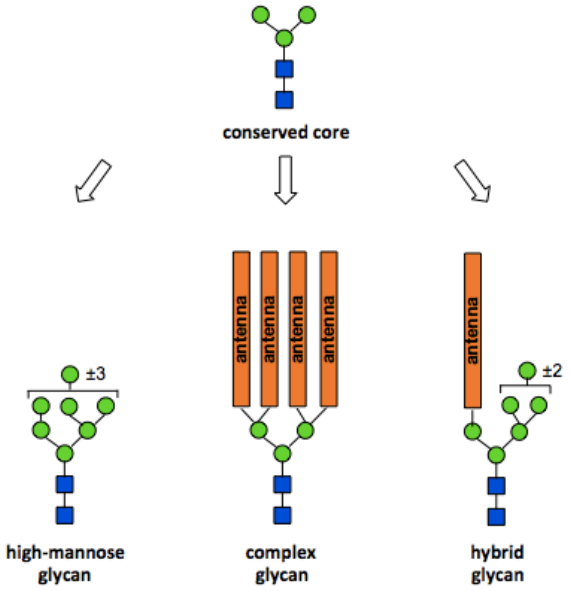

Fig.1.6. Schematic representation of a conserved glycan core and its possible extensions to high-mannose, complex and hybrid glycans

Synthesis of the N-glycans occurs at the luminal and cytoplasmic part of ER. The process is relatively complex and involves several sequential reactions catalysed by UDP-N-acetylglucosamine- dolichyl-phosphate N-acetylglucosaminephospho-transferase (DPAGT1) and a number of asparagine-linked glycosylation (ALG) enzymes. It starts from the addition of an active sugar precursor – uridine diphosphate N-acetylglucosamine (UDP-GlcNAc), derived from a hexosamine biosynthetic pathway, to the dolichol-phosphate present in the ER membrane. After several steps, the glycan is transferred onto the target protein and further processed by a variety of enzymes, including α-glucosidases, α-mannosidases and glycosyltransferases (Stanley et al., 2009). The sugars may potentially be implicated in modulating the half-life and intrinsic functions of the proteins, as well as regulating intermolecular interactions, cell-cell and cell-matrix adhesion (Varki, 1993).

1.2.1.2. O-glycosylation

O-glycosylation is another type of covalent modification of proteins with sugar moieties. O-glycans can be attached to Ser/Thr residues of the target protein via different linkages, among which the most abundant are an α-linkage of a carbohydrate chain via an N-acetylgalactosamine (GalNAc) moiety (mucin-type O-glycosylation) and a β-linkage of a single N-acetylglucosamine (GlcNAc) sugar (Brockhausen et al., 2009, Hart and Akimoto, 2009). Glycoproteins heavily decorated with O-GalNAc glycans are abundant at the cell surface and in mucous secretions (Brockhausen et al., 2009), while O-GlcNAc-modified proteins are mainly found in the cytoplasm and in the nucleus (Hahne et al., 2012).

The latter post-translational modification differs significantly from all other common types of glycosylation in a number of ways. First of all, it is extremely dynamic and O-GlcNAc can rapidly cycle on and off the target protein due to the combined action of two enzymes: O-GlcNAc transferase (OGT) and O-GlcNAcase (Figure 1.7.). Therefore, O-GlcNAcetylation appears to have more features in common with phosphorylation, and like phosphorylation, it is found on many transcription factors. DNA binding, transcriptional activity, localisation and stability of the transcription factors can be dynamically regulated by cross-talk between O-GlcNAcetylation and phosphorylation (Hart et al., 2011, Ozcan et al., 2010), and potentially other post-translational modifications, such as for instance ubiquitination (Yang et al., 2006).

One transcription factor, the transcriptional activity of which appears to be inhibited by the attachment of O-GlcNAc moieties and to correlate with the cellular UDP-GlcNAc levels, is Sp1 (Jackson and Tjian, 1988, Yang et al., 2001). The molecule may be of particular importance for the development and maintenance of the

NMJ since it has been shown to be implicated in activating the expression of a *DOK7* gene (Hamuro et al., 2011).

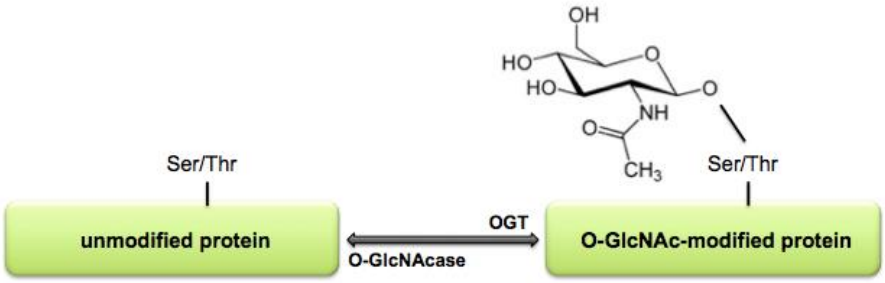

Fig.1.7. Dynamic modification of proteins with O-GlcNAc moiety
OGT – O-GlcNAc transferase

1.2.2. Glycosphingolipids

GSLs comprise a complex group of molecules which are officially divided into the following subgroups, based on the structure of the glycan core: ganglio- (Galβ1-3GalNAcβ1-4Galβ1-4GlcβCer), neolacto- (Galβ1-4GlcNAcβ1-3Galβ1-4GlcβCer), lacto- (Galβ1-3GlcNAcβ1-3Galβ1-4GlcβCer), globo- (Galα1-4Galβ1-4GlcβCer) and isoglobo- (Galα1-3Galβ1-4GlcβCer) series. In order to simplify the classification and terminology of GSLs, all sialylated GSLs, which represent the most abundant and broadly distributed group of GSLs, are traditionally referred to as gangliosides and termed with 3-character symbol. In this nomenclature the first letter G refers to gangliosides, the second (M, D, T or Q) to the number of sialic acid residues, and the last symbol (1, 2, 3, etc.) to the order of migration of the molecules on thin-layer chromatography (Schnaar et al., 2009, Svennerholm, 1964, Chester, 1998).

The molecular function of GSLs is not fully understood. They appear to be involved in cell-cell interactions or in the modulation of the activity of proteins present in cell

membranes, and are indispensable for intercellular coordination in multicellular organisms (Pontier and Schweisguth, 2012).

GSLs have been identified as a major group of glycans in the brain (Brunngraber et al., 1971). They are an abundant component of myelin sheaths (Ogawa-Goto et al., 1992), and mice lacking enzymes involved in the biosynthesis of GalCer and sulphatides exhibit a phenotype of failed myelination, slow nerve conductance and ataxia (Coetzee et al., 1996). The importance of the GSLs in myelination has been further confirmed by Sheikh et al., who reported decreased myelination and axonal degeneration in GM2/GD2 synthase knock-out mice (Sheikh et al., 1999). Surprisingly, the knock-out mice exhibited relatively subtle phenotypic changes, probably due to compensation of GM2 and GD2 expression by other gangliosides, such as GM3 or GD3 (Takamiya et al., 1996). This assumption has been corroborated by creating double knock-out mice of GM2/GD2 and GD3 synthases. These animals presented with numerous neuronal dysfunctions, including motor dysfunctions, decreased sensory functions and changes in emotional behaviour (Tajima et al., 2009).

1.3. L-glutamine:D-fructose-6-phosphate amidotransferase 1 (GFAT1)

Glycosylation would not be possible without a hexosamine biosynthetic pathway, which provides building blocks for the process. The first enzyme of the pathway is L-glutamine:D-fructose-6-phosphate amidotransferase 1 (GFAT1) (EC 2.6.1.16), encoded by the *GFPT1* gene. These two abbreviations – GFAT1 for the protein and *GFPT1* for the gene and the mRNA transcript – are commonly used in the literature and will also be used in this thesis in order to make a clear distinction between the protein and the corresponding gene or transcript.

The enzyme catalyses the conversion of glutamine (Gln) and fructose-6-phosphate (Fru-6-P) to glutamate (Glu) and glucosamine-6-phosphate ($GlcNH_2$-6-P) (Mouilleron et al., 2011). This product is then utilised in subsequent steps of the hexosamine biosynthetic pathway, to yield the major products of the pathway: UDP-GlcNAc, UDP-N-acetylgalactosamine (UDP-GalNAc) and cytidine monophosphate (CMP)-sialic acid. The most abundant product, UDP-GlcNAc is an indispensable active sugar precursor in the glycosylation pathway (Milewski, 2002) (Figure 1.8.).

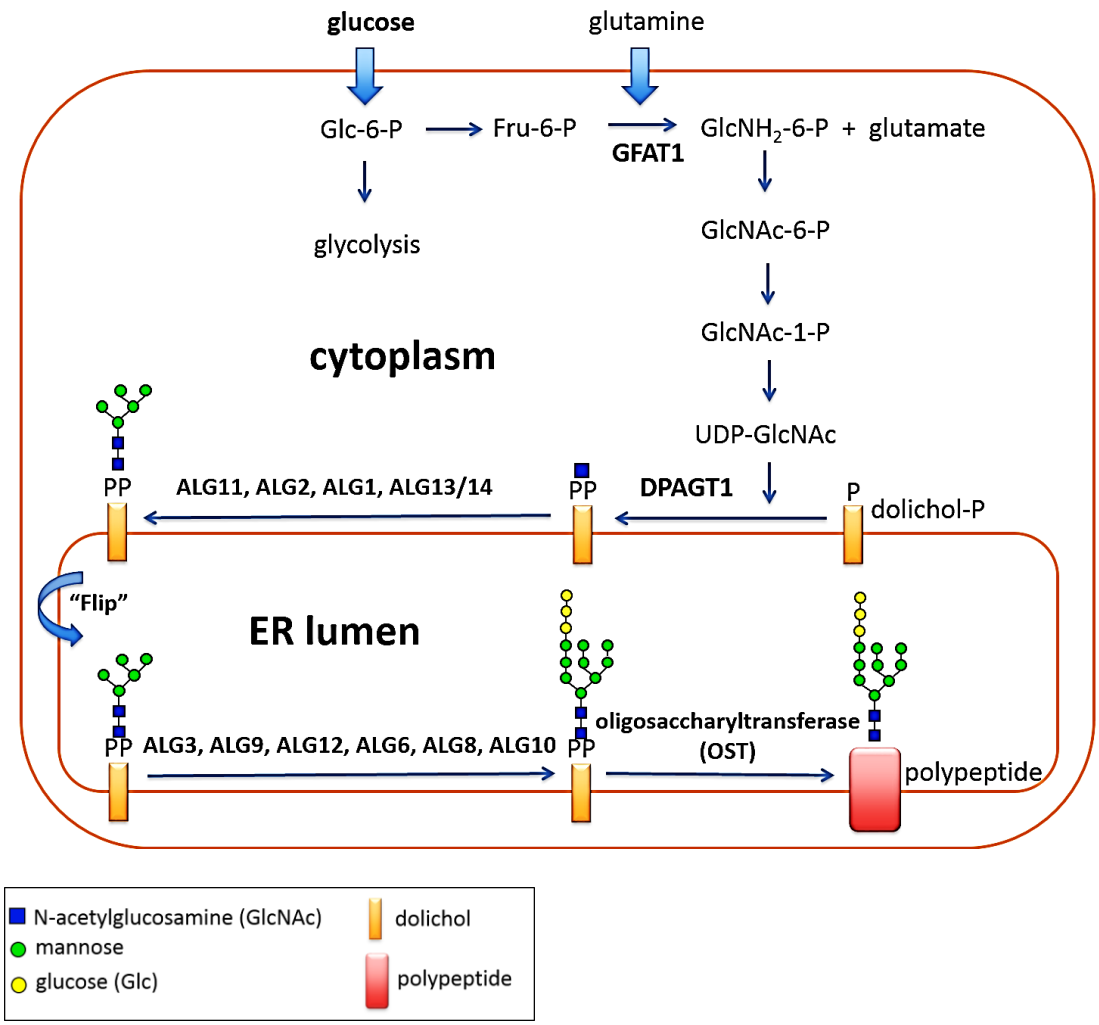

Fig.1.8. Schematic representation of the reaction catalysed by GFAT1, the subsequent steps of the hexosamine biosynthetic pathway and the N-glycosylation pathway (Zoltowska et al., 2013)
ALG – asparagine-linked glycosylation; DPAGT1 – UDP-N-acetylglucosamine-dolichyl-phosphate N-acetylglucosaminephosphotransferase; GFAT1 – L-glutamine:D-fructose-6-phosphate amidotransferase 1;
Glc-6-P – glucose-6-phosphate; GlcNAc – N-acetylglucosamine; $GlcNH_2$-6-P – glucosamine-6-phopshate; Gln – glutamine; Glu – glutamate; Fru-6-P – fructose-6-phosphate; UDP-GlcNAc – uridine diphosphate N-acetylglucosamine

1.3.1. Molecular diversity of GFAT1 isoforms

Human GFAT1 has long been considered as a simple 681-amino acid enzyme converting Fru-6-P and Gln to $GlcNH_2$-6-P and Glu; the *GFPT1* gene encoding the enzyme has been mapped to chromosome 2p13 (Whitmore et al., 1995, Zhou et al., 1995). Although northern blot experiments conducted by Zhou et al. pointed towards the presence of distinct *GFPT1* mRNA species in different tissues, the group did not investigate the molecular bases of this variability (Zhou et al., 1995).

Complexity to the GFAT catalysed reaction was added with the discovery of a GFAT1 homologue in mammals, mapped in the region corresponding to human chromosome 5q23-35. The newly reported enzyme has been designated GFAT2 and shares 75% homology at the amino acid level with GFAT1. Both enzymes appear to possess the same catalytic function. However, their mRNA expression profiles differ significantly in different tissues. The most apparent differences are found in the ratio of the expression of the two homologues in the central nervous system (CNS), where high levels of *GFPT2* mRNA and almost no *GFPT1* mRNA have been detected (Oki et al., 1999).

An additional level of complexity exists in that GFAT1 exists in two different isoforms, resulting from an alternative splicing of the *GFPT1* mRNA transcript. The second *GFPT1* isoform possesses an additional 54-base pair exon, which corresponds to an 18-amino acid insertion at position 229 in the human GFAT1 protein sequence (Niimi et al., 2001, DeHaven et al., 2001). The novel *GFPT1* splice variant, designated *GFPT1-L* (Niimi et al., 2001) or *GFPT1Alt* (DeHaven et al., 2001), has been shown to be expressed selectively in skeletal muscle and heart (DeHaven et al., 2001, Niimi et al., 2001).

1.3.2. Tertiary and quaternary structure of GFAT1

GFAT1 possesses two types of domains: an N-terminal glutaminase domain, which catalyses the hydrolysis of Gln to ammonia and Glu, and a C-terminal sugar isomerase domain, converting Fru-6-P into $GlcNH_2$-6-P (Denisot et al., 1991) (Figure 1.9.).

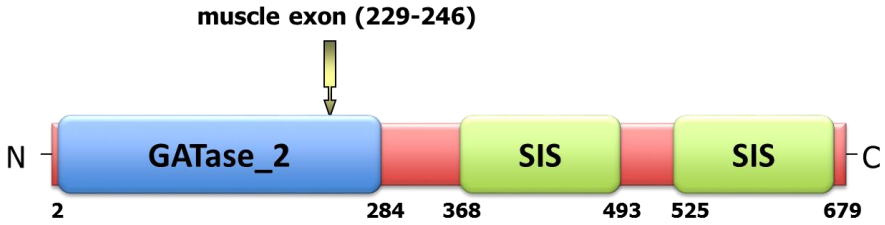

Fig.1.9. Schematic representation of GFAT1 (Zoltowska et al., 2013)
GATase_2 – glutaminase domain type 2
SIS – sugar isomerase domain

The detailed tertiary and quaternary structure of the full-length GFAT1 has only been resolved for its bacterial homologue – GlmS (Isupov et al., 1996, Teplyakov et al., 2001). For human GFAT1only the three-dimensional (3D) structure of the isomerase domain has been described (Nakaishi et al., 2009) due to the difficulties caused by the instability of the enzyme during its purification However, there is a high level of sequence homology between the prokaryotic and the eukaryotic enzyme at the amino acid level and also the 3D structures of the isomerase domain of human GFAT1 and bacterial GlmS are highly similar, hence it is likely that the structure of the glutaminase domain is conserved as well (Figure 1.10.).

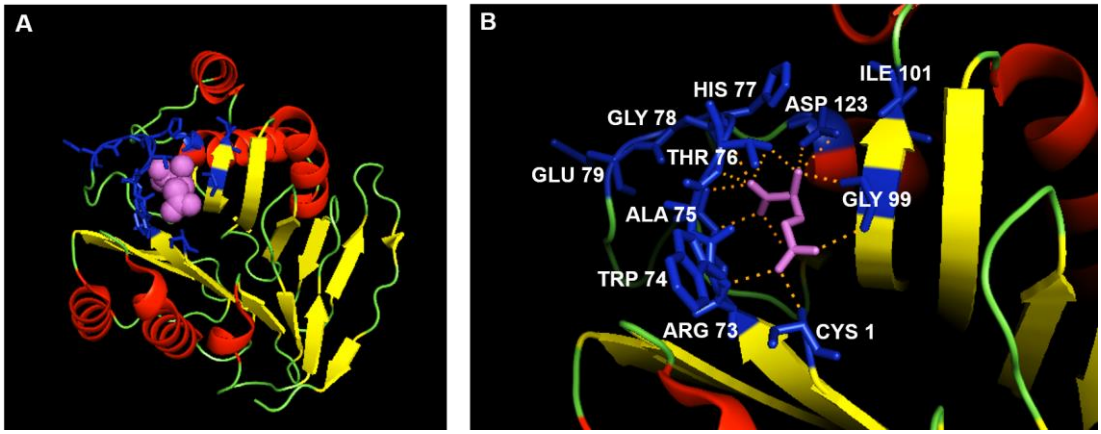

Fig.1.10. 3D structure of the glutaminase domain of *Escherichia coli* GlmS (residues 1-240)
(A) α-helices are coloured in red, β-sheets in yellow and loops in green. The residues involved in the binding of the substrate – Gln (marked with magenta spheres) – are coloured in blue.
(B) Enlarged image of the 3D structure of the Gln binding site. α-helices are coloured in red, β-sheets in yellow and loops in green. The residues interacting with the substrate (labelled with magenta sticks) via the interactions marked with orange dashed lines are coloured in blue.
The image was modified based on a 3D structure stored in PDB database (PDB ID: 1XFF) (Isupov et al., 1996).

The glutaminase domain of GlmS is formed by two antiparallel β sheets, which are sandwiched between α-helices connected with the β strands by relatively short loops. The binding site for Gln is mainly formed by the loops connecting β-strands 4 and 5, and β-strand 6 and helix 3. The substrate is recognised by Arg73 and Asp123, with the orientation maintained by interactions with the main chain residues 77-79 and the amino group of Ala101. The pocket for Gln binding is covered by residues 73-79, and the amino acids responsible for the hydrolysis of Gln are Cys1, Trp74 and Gly99 (Isupov et al., 1996).

The second domain present in GFAT1 is the isomerase domain (Figure 1.11.).

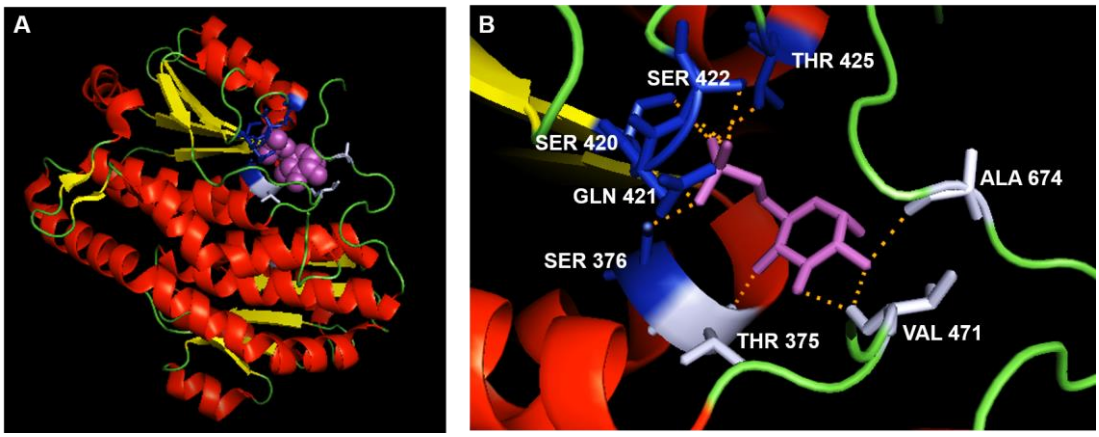

Fig.1.11. 3D structure of the isomerase domain of human GFAT1-L (residues 332-699)
(A) α-helices are coloured in red, β-sheets in yellow and loops in green. The residues involved in the binding of the substrate – Fru-6-P (marked with magenta spheres) – are coloured in light blue (binding the sugar ring) or dark blue (binding the 6-phosphate group).
(B) Enlarged image of the 3D structure of the Fru-6-P binding site. α-helices are coloured in red, β-sheets in yellow and loops in green. The residues interacting with the substrate (labelled with magenta sticks) via the interactions marked with orange dashed lines are coloured in light blue (binding the sugar ring) and dark blue (binding the 6-phosphate group).
The image was modified based on a 3D structure stored in PDB database (PDB ID: 2ZJ4) (Nakaishi et al., 2009).

The structure of the isomerase domain has been resolved both for bacterial GlmS and for human GFAT1. In the human, this domain is composed of two similar subdomains, each of which is formed by a five-stranded parallel β sheet flanked by α-helices. The binding site for Fru-6-P is formed by a C-tail of one subunit and a His-loop from the other. Several residues are involved in the interactions with the substrate. These

include Ser376, Ser420, Gln421, Ser422 and Thr425 (binding the 6-phosphate group), Thr375, Val471, His576 and Ala674 from the neighbouring subunit (binding the sugar ring), and Thr375, Val471, Ser473, Lys557 and Gln560 (binding the $GlcNH_2$ from $GlcNH_2$-6-P – the product of the reaction) (Nakaishi et al., 2009).

To perform its catalytic function, GFAT1 needs not only to acquire the correct tertiary structure, but also form a homo-oligomeric complex. Although it is well-established that homo-oligomerisation is essential for GFAT1 activity, it is not clear whether the active form of the enzyme is a homodimer or a homotetramer. Ultracentrifugation and size-exclusion chromatography experiments have indicated that human GFAT1, similar to *Candida albicans* Gfa, forms homotetramers (Richez et al., 2007, Raczynska et al., 2007). However, the data published by Nakaishi et al., obtained from the analysis of GFAT1 crystal structure, have shown that the interactions responsible for the homotetramerisation are significantly weaker when compared with those involved in the dimer formation, thus this group has suggested that the biologically relevant form of human GFAT1, similarly to *E.coli* GlmS, is a homodimer (Nakaishi et al., 2009, Teplyakov et al., 2001).

1.3.3. The reaction catalysed by GFAT1

GFAT1 catalyses the conversion of Fru-6-P and Gln to $GlcNH_2$-P and Glu. It possesses an absolute specificity for both substrates, and the binding of the substrates occurs in an ordered fashion, with Fru-6-P binding preceding that of Gln (Mouilleron et al., 2011). Unlike other amidotransferases, ammonia cannot replace Gln as a donor of the amine group (Milewski, 2002).

The detailed mechanism of the GFAT1-catalysed reaction has been well-described for the bacterial homologue of GFAT1, GlmS, which shares 41% identity and 75%

similarity at the amino acid level with human GFAT1, with all residues important for catalytic activity being conserved (Figure 1.12.). Therefore, the reaction mechanism will be described for the bacterial enzyme, with the corresponding residues in human GFAT1 specified in Table 1.1.

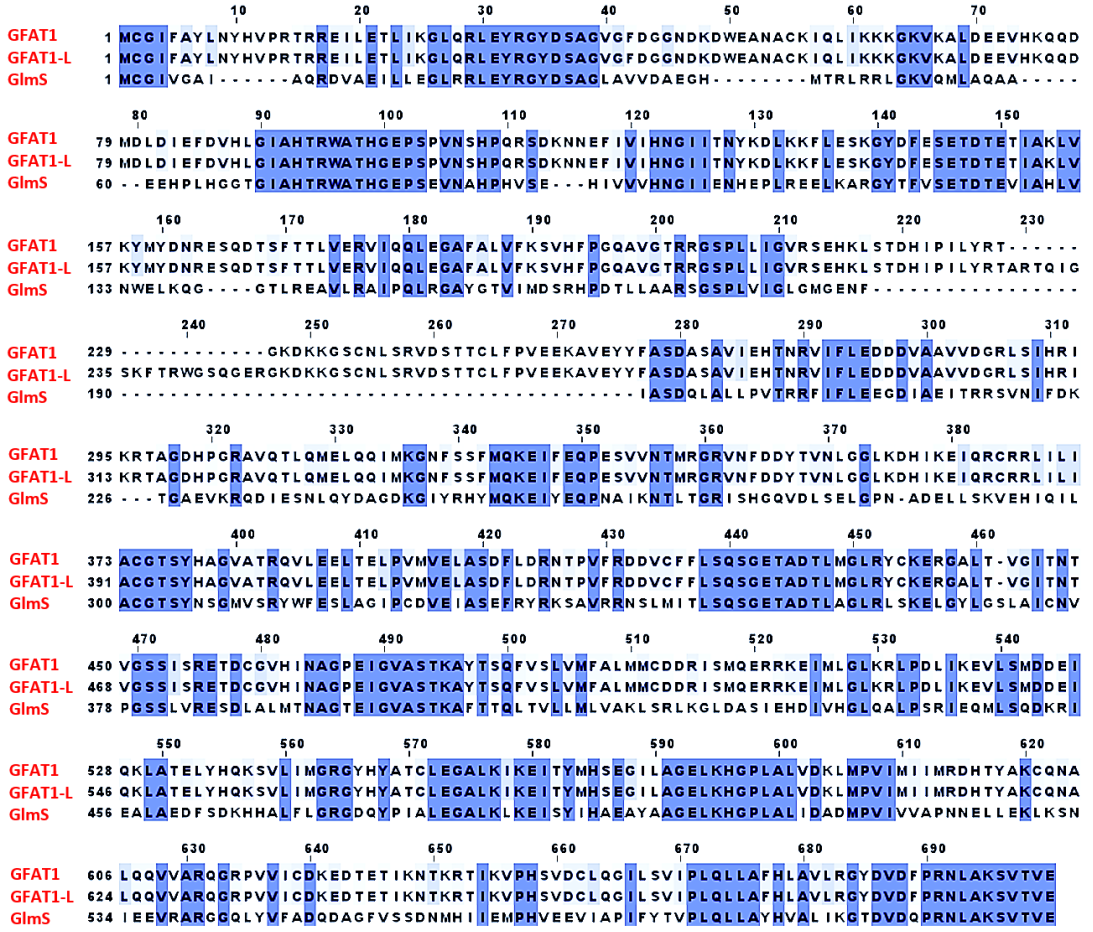

Fig.1.12. Alignment of amino acid sequences of human GFAT1 and GFAT1-L, and *Escherichia coli* GlmS, coloured according to the level of the conservation of the residues
The unconserved residues remain unshaded, the low conserved ones are shaded in light blue and the highly conserved ones are shaded in dark blue.
The alignment was based on the reference sequences of *Homo sapiens* GFAT1 [Q06210-2] and GFAT1-L [Q06210-1], and *Escherichia coli* GlmS [P17169] stored in UniProt database, and prepared using ClustalW2 (Larkin et al., 2007, Goujon et al., 2010) and Jalview applications.

Table 1.1. Amino acids crucial for the activity of *Escherichia coli* GlmS and its human homologues GFAT1 and GFAT1-L
The initiator methionine has been removed from the bacterial sequence.

Amino acid residue in *E.coli* GlmS	Corresponding amino acid residue in human GFAT1/GFAT1-L	Molecular function in catalytic activity of the enzyme
Cys1	Cys2/Cys2	glutaminase activity
Arg26	Arg33/Arg33	glutaminase activity, formation of ammonia channel
Tyr28	Tyr35/Tyr35	formation of ammonia channel
Trp74	Trp96/Trp96	closure/opening of ammonia channel closure of Fru-6-P binding site
Arg73-Ser81	Arg95-Ser103/ Arg95-Ser103	loop Q - closure of glutamine binding site
Asn98	Asn123/Asn123	glutaminase activity
Gly99	Gly124/Gly124	glutaminase activity
Lys503-Gly505	Lys576-Gly578/ Lys594-Gly596	sugar isomerase activity
His504	His577/His595	sugar isomerase activity
Glu535	Glu608/Glu626	closure of sugar isomerase site
Ala602	Ala675/Ala693	closure/opening of ammonia channel
Val605	Val678/Val696	closure/opening of ammonia channel
Thr606	Thr679/Thr697	glutaminase activity
Arg600-Glu608	Arg673-Glu681/ Arg691-Glu699	loop C – formation of ammonia channel, closure of Fru-6-P binding site

The reaction catalysed by GFAT1 starts with Fru-6-P binding. After the binding, an initially disordered C-terminal C-loop (600-608) is ordered and anchored to aromatic residues (Tyr28 and Trp74) present in the glutaminase domain. In this conformation of the enzyme, the bound Fru-6-P is prevented from contacts with solvent and the glutaminase domain gets fixed relative to the sugar isomerase domain, in a way that

two sugar isomerase domains form an interface of a dimer, and two glutaminase domains are located on the sites. The structural rearrangements result in several important changes. First, Trp74 and His-loop (499-512) get located close to each other. Second, as a result of a conformational change of Lys503-Gly505, the catalytic His504 moves towards the sugar isomerase domain, facilitating the opening of the sugar ring. Finally, the His-loop is linked with the C-loop of the other monomer via a salt bridge formed between Glu535 and Glu608. This contributes to the closure of the sugar isomerase site (Mouilleron et al., 2011, Mouilleron et al., 2008). Another important change, which occurs upon Fru-6-P binding, is the formation of the ammonia channel, which is composed mainly of hydrophobic residues present in the C-loop, the His-loop from one of the monomers, and Arg26 and Trp74 from the glutaminase domain of the other. However, in the absence of Gln, the channel remains obstructed by Trp74, Ala602 and Val605 (Floquet et al., 2007).

Following the binding of Fru-6-P and the subsequent structural rearrangements, the enzyme is ready to bind the second substrate, Gln. This binding triggers a rotation of Trp74, leading to opening of the ammonia channel and closure of the glutaminase site by the Q-loop (73-81). The Gln is then converted to Glu and ammonia. The essential catalytic elements for the reaction are Cys1, Asn98 and Gly99 present in the glutaminase domain. The glutaminase activity is also dependent on Arg26 and Thr606, which enhance the nucleophilic character of the α-amino group of Cys1 and ensure a proper conformation of this residue (Mouilleron et al., 2006).

1.3.4. Regulation of GFAT1 enzymatic activity

GFAT1, as the first enzyme of the hexosamine biosynthetic pathway, regulates glucose flux through the pathway and an abundance of active sugar precursors essential for glycosylation. Its activity needs to be tightly controlled in order to maintain intracellular homeostasis, which is done at several levels.

First, the expression of *GFPT1* is regulated on a transcriptional level. This results in the differences in the abundance of the enzyme in various tissues. The transcribed mRNA is also alternatively spliced, giving rise to two tissue-specific splice variants: *GFPT1* and *GFPT1-L* (DeHaven et al., 2001, Niimi et al., 2001).

Second, GFAT1 catalytic activity appears to be regulated by post-translational modifications. Three serine residues (Ser205, Ser235 and Ser243) have been identified within the human GFAT1, all of which can be modified with phosphate groups, by PKA in the case of Ser205 and Ser235 (Chang et al., 2000), or by AMP-activated protein kinase and CaMKII in the case of Ser243 (Li et al., 2007, Eguchi et al., 2009). The modification of Ser205 has been reported to inhibit GFAT1 enzymatic activity (Chang et al., 2000, Eguchi et al., 2009), while the phosphorylation of Ser235 appears to play no detectable role (Chang et al., 2000). The residues modified by phosphate groups are located in close proximity to the alternatively spliced muscle exon, thus it is possible that this exon modulates the regulation of GFAT1 and GFAT1-L in a tissue-specific manner. Tissue-dependent regulation of the hexosamine biosynthetic pathway might also be a consequence of distinct regulation of the GFAT2 homologue, expressed predominantly in the CNS. Although both Ser205 and Ser243 are conserved between GFAT1 and GFAT2, as Ser202 and Ser244, respectively, so far only Ser202 has been found to be modified with phosphate groups in GFAT2 (Figure 1.13.). The phosphorylation of this residue, similarly to GFAT1, appears to be catalysed by PKA.

However, by contrast with the phosphorylation of GFAT1, the addition of a phosphate group to GFAT2 has been reported to increase its enzymatic activity (Hu et al., 2004).

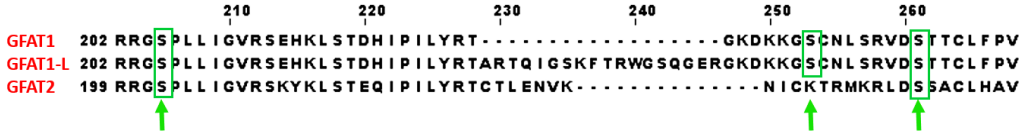

Fig.1.13. Alignment of amino acid sequences, adjacent to phosphorylated residues, of human GFAT1, GFAT1-L and GFAT2
The arrows show serine residues which can be phosphorylated.
The alignment was based on the reference sequences of *Homo sapiens* GFAT1 [Q06210-2], GFAT1-L [Q06210-1] and GFAT2 [O94808] stored in UniProt database and prepared using ClustalW (Goujon et al., 2010, Larkin et al., 2007) and Jalview software.

Another proposed mechanism for regulating GFAT1 is a potent feedback inhibition of the catalytic activity of the enzyme by $GlcNH_2$-6-P (product of GFAT1 catalysed reaction) and UDP-GlcNAc (product of the hexosamine biosynthetic pathway). Both prokaryotic GlmS and eukaryotic GFAT1 are susceptible to the inhibition by $GlcNH_2$-6-P, which possesses a high affinity for the Fru-6-P binding site, while the regulation by UDP-GlcNAc is a characteristic feature of mammalian GFAT1 only (Broschat et al., 2002, Winterburn and Phelps, 1971, Kornfeld, 1967).

It has also been reported that the two GFAT1 isoforms (GFAT1 and GFAT1-L) differ in their sensitivity to the inhibition by UDP-GlcNAc, with GFAT1-L having a lower inhibition constant (K_i) for UDP-GlcNAc, thus being more susceptible to the feedback inhibition, compared to GFAT1 (DeHaven et al., 2001). Another difference in the kinetic properties of the two alternatively spliced isoforms is a lower affinity of GFAT1-L for Fru-6-P relative to GFAT1 (DeHaven et al., 2001, Niimi et al., 2001).

1.4. Glycosylation of the NMJ

GFAT1 is an ubiquitously expressed enzyme that is crucial for providing building blocks for glycosylation of proteins and lipids. Since the NMJ contains a number of molecules modified with carbohydrate structures and the repertoire of sugar moieties in this region appears to be unique with respect to the extrasynaptic parts of the muscle, it is likely that this post-translational modification plays an essential role at the endplate (Martin et al., 1999, Martin, 2003). However, due to the complexity of the modification, the diversity of the potential configurations of sugars within the carbohydrate chains, and the fact that many molecules expressed at the cell surface are modified with carbohydrates, the molecular function of glycosylation at the NMJ is poorly understood.

Studies with lectins and antibodies directed to gangliosides, globosides and cytotoxic T antigens have provided some clues about the structures of the sugar moieties present uniquely at the synaptic sites, and not expressed in extrasynaptic regions (Martin et al., 1999).

One of the most abundant carbohydrates present exclusively at the synapse is a terminal β-linked GalNAc, recognised by *Vicia villosa* agglutinin B_4 (VVA-B_4) and *Dolichos biflorus* agglutinin (DBA) lectins (Scott et al., 1988). It has been reported that VVA-B_4 not only binds selectively to the NMJ, but can also itself induce and potentiate AChR clustering, independently of MuSK and AChR β subunit phosphorylation (McDearmon et al., 2001, Martin and Sanes, 1995, Grow et al., 1999). There are several molecules at the NMJ which might be recognised by the VVA-B_4 lectin, hence potentially mediating the VVA-B_4 clustering activity. These include α-dystroglycan (Grow et al., 1999, McDearmon et al., 2001) and AChE (Scott et al., 1988). They both appear to exist in a number of glycoforms, recognised not only by

VVA-B_4, but also by other lectins. For instance, AChE is also recognised by *Concanavalin A* (ConA) – lectin binding to terminal α-D-glucosyl and α-D-mannosyl residues, characteristic for high-mannose glycans (Scott et al., 1988, McDearmon et al., 2001).

The high-mannose glycans are abundant on AChR from *Torpedo californica*, with ConA binding to each of the subunits of the receptor, but ConA is not the only lectin binding to the AChR subunits. The γ subunit is also recognised by phytohemagglutinin-L (PHA-L), possessing high affinity to triantennary and tetraantennary glycans, while AChR δ can be bound by ConA, PHA-L and wheat germ agglutinin (WGA) specific for sialic acids and GlcNAc. These data indicate that AChR expressed in *Torpedo californica* are modified with high-mannose as well as complex glycans (Nomoto et al., 1986). The findings have been confirmed later by mass spectrometry analysis (Poulter et al., 1989).

Although AChR subunits possess homologous sequences, a number of glycosylation sites and the role of the attached sugars differ significantly between them. The α and β subunits have one glycosylation site in a homologous position, γ and ε have a second glycosylation site, and δ has third (Witzemann et al., 1990). Site-directed mutagenesis of glycosylation sites present in the individual subunits results in a significant decrease in the protein levels of AChR α (Blount and Merlie, 1990, Gehle et al., 1997, Gehle and Sumikawa, 1991) and γ subunits (Gehle et al., 1997), but has no effect on the steady state levels of β (Gehle et al., 1997, Gehle and Sumikawa, 1991) and δ subunits (Gehle et al., 1997, Ramanathan and Hall, 1999). However, mutations of AChR δ that prevent glycosylation reduces its ability to assemble with AChR α subunit (Ramanathan and Hall, 1999).

In addition to the studies of the glycosylation of the AChR using lectins, mass spectrometry and mutagenesis, the function of the glycan structures has also been investigated using inhibitors of N-glycosylation, such as tunicamycin, and of glucose trimming, such as castanospermine (CAS). Incubation of AChR-expressing cells with these decreases the assembly and cell surface expression of the channels (Wanamaker and Green, 2005, Prives and Bar-Sagi, 1983), but the receptors which reach the cell surface, despite underglycosylation, appear to be functional, although they present reduced binding affinity to the ligand, carbamylcholine (Prives and Bar-Sagi, 1983).

Another key NMJ protein is MuSK. It has been shown that the protein extracted from *Torpedo californica* electric organs is recognised by *Maackia amurensis* and *Datura stramonium* agglutinins. The pattern of lectin binding indicates the presence of terminal sialic acids attached to galactose in an α2,3-linkage and terminal galactose attached to GlcNAc in β1,4-linkage. Further analysis has revealed that the sugars are attached to two well-conserved N-glycosylation sites: Asn222 and Asn338 in human MuSK. The modification appears to reduce AGRN-independent MuSK phosphorylation and AChR clustering, but does not play a part in AGRN-dependent signalling (Watty and Burden, 2002).

The carbohydrate structures at the NMJ have also been studied using specific antibodies that target cytotoxic T antigens: CT1 and CT2 (Hoyte et al., 2002). The results of the immunofluorescence studies indicate concentration of the CT antigens at the NMJ with an abundant expression of CT GalNAc transferase (an enzyme responsible for creating a β1,4GalNAc-linkage on CT antigens) in the endplate region (Xia et al., 2002).

Another major group of oligosaccharides which can be detected in skeletal muscle with specific antibodies are GAGs, components of proteoglycans (Dennissen et al.,

2002). The most commonly studied proteoglycans present at the NMJ are AGRN and perlecan. AGRN, which is important for the induction of AChR clustering, possesses two sites modified by heparan sulphate and chondroitin sulphate, respectively (Winzen et al., 2003). However, the role of the GAGs attached to AGRN is not clear since both GAG-modified sites are localised in the N-terminal part of the protein, while only the C-terminal fragment of AGRN is indispensable for the induction of the AChR cluster formation (Gesemann et al., 1995). It has been suggested that the post-translational modification may be involved in the interactions with other proteins present in the synaptomatrix, such as fibroblast growth factor 2 (FGF2), thrombospondin, merosin, laminin (Cotman et al., 1999) and neural cell adhesion molecule (NCAM) (Storms et al., 1996). Another proteoglycan, which is essential for the correct structure and function of the NMJ, is perlecan. It consists of four heparan sulphate chains attached to the 400 kDa protein core. Three GAG attachment sites are located in the N-terminal and one in the C-terminal region of the protein (Noonan et al., 1991, Friedrich et al., 1999). This modification may be involved in the binding to a number of proteins present in the ECM, including COLQ (Peng et al., 1999, Kimbell et al., 2004).

The last group of carbohydrate-modified molecules found at the NMJ are glycolipids, the most abundant of which are globosides and gangliosides. The first group appears to be present predominantly at the postsynaptic site and is important for synaptic transmission (Martin et al., 1999). Gangliosides are concentrated at both post- and pre-synaptic sites, with GM2 being present at the nerve terminal (Hoyte et al., 2002) and GD2 at the postsynaptic membrane (Martin et al., 1999). Despite the abundance at the NMJ, gangliosides appear not to be required for neuromuscular transmission (Bullens et al., 2002).

1.5. Disorders of the NMJ

The structure and function of the neuromuscular synapse can be disrupted by mutations in proteins expressed at the endplate or involved in the formation and maintenance of the synapse (in congenital myasthenic syndrome (CMS)) or by autoantibodies targeting neuromuscular molecules (in myasthenia gravis (MG)).

1.5.1. Congenital myasthenic syndrome

CMS comprises a group of genetically and phenotypically heterogenous disorders, which manifest themselves with aberrant neuromuscular transmission caused by mutations in molecules essential for the structure and function of the synapse. The most common feature observed in the affected individuals is fatiguable muscle weakness, usually presenting from birth and affecting different groups of muscles: limb, trunk, bulbar, respiratory, facial or extraocular. The group of muscles affected, together with the treatment response, provide important clues for targeting the genetic screen for mutations (Abicht et al., 2012).

The most common classification of CMS is based on the site of the identified defect. According to this classification, various types of CMS can be classified as: presynaptic, synaptic or postsynaptic (Engel, 2011). However, this classification is not always appropriate since some mutations, especially those identified in a glycosylation pathway (Guergueltcheva et al., 2011, Senderek et al., 2011, Belaya et al., 2012, Cossins et al., 2013b), may simultaneously affect presynaptic, synaptic and postsynaptic sites.

1.5.1.1. CMS due to mutations in the NMJ proteins

Most CMS cases result from mutations in genes encoding NMJ proteins. Thus far, mutations in 14 pre-, post- and synaptic molecules have been implicated in the causation of CMS (Table 1.2.) (Engel, 2011).

Table 1.2. Genetic defects, phenotype and treatment in CMS caused by mutations in NMJ proteins
The CMS subtypes were classified according the location and the acting site of the respective molecules at the NMJ, as postsynaptic, presynaptic and synaptic. Additional subdivision, based on the molecular consequences of the underlying genetic defect, was used for the CMS resulting from the mutations in AChR subunits.

Gene	Protein	CMS type	Phenotype	Treatment
AGRN (Huze et al., 2009)	AGRN	synaptic/ postsynaptic	ptosis, mild weakness of facial and limb muscles	salbutamol, no response to AChE inhibitors and 3,4-diaminopyridine (3,4-DAP)
CHAT (Schara et al., 2010)	choline acetyltransferase	presynaptic	sudden episodes of apnoea, bulbar weakness	AChE inhibitors
CHRNA1 (Chaouch et al., 2012, Webster et al., 2004)	AChR α1	postsynaptic, fast-channel syndrome (Palace et al., 2012) (recessive mutations causing abnormally brief AChR openings)	respiratory crises in infancy, ptosis, abnormal eye movements, ophthalmoplegia, weakness of neck and jaw muscles, more proximal limb weakness	AChE inhibitors, 3,4-DAP
CHRNB1 (Chaouch et al., 2012, Quiram et al., 1999)	AChR β1			
CHRND (Palace et al., 2012, Chaouch et al., 2012)	AChR δ	postsynaptic, slow-channel syndrome (Chaouch et al., 2012) (dominant "gain of function" mutations causing rapid AChR channel opening, slow channel closure or increased affinity for ACh)	generalised muscle weakness more predominant in cervical and forearm muscles	open channel AChR blockers – quinidine and fluoxetine, no response to AChE inhibitors

CHRNE (Palace et al., 2012, Croxen et al., 2002, Chaouch et al., 2012)	AChR ε	postsynaptic, AChR deficiency syndrome (Ohno et al., 1997) (recessive mutations, usually in AChR ε, resulting in reduced AChR expression)	ptosis, bulbar symptoms, generalised fatiguable weakness	AChE inhibitors
CHRNG	AChR γ	postsynaptic	Escobar variant of multiple pterygium syndrome (EVMPS), lethal form of multiple pterygium syndrome (LMPS), arthrogryposis, scoliosis	not available
COLQ (Wargon et al., 2012)	collagen Q	synaptic	ptosis, proximal muscle weakness, neck weakness, cramps, myalgia	3,4-DAP, ephedrine, salbutamol
DOK7 (Beeson et al., 2006, Lashley et al., 2010, Palace et al., 2007)	downstream of tyrosine kinase 7	postsynaptic	limb-girdle muscle weakness, mild ptosis and facial weakness	ephedrine, salbutamol
LAMB2 (Maselli et al., 2009)	laminin β2	synaptic	Pierson syndrome with ocular, respiratory and proximal limb muscle weakness, severe ptosis	ephedrine
MUSK (Chevessier et al., 2004)	muscle-specific tyrosine kinase	postsynaptic	ptosis, respiratory distress	salbutamol, no response to AChE inhibitors
RAPSN (Milone et al., 2009, Ohno et al., 2002)	43 kDa receptor-associated protein of the synapse	postsynaptic	arthrogryposis at birth, respiratory crises, arched palate	AChE inhibitors, 3,4-DAP
PLEC1 (Maselli et al., 2011)	plectin	synaptic	epidermolysis bullosa simplex, myopathy, myasthenic syndrome with ptosis	AChE inhibitors, ephedrine
SCN4A (Tsujino et al., 2003)	$Na_v1.4$ type voltage-dependent sodium channel	postsynaptic	apnoeic attacks, facial, trunk and limb muscle weakness	AChE inhibitors, acetazolamide

1.5.1.2. CMS due to mutations in the glycosylation pathway

Recent studies have suggested that CMS can result from mutations not only in the NMJ proteins, but also in the molecules involved in glycosylation, and a number of CMS causative mutations have been identified in *GFPT1* (Guergueltcheva et al., 2011, Senderek et al., 2011, Huh et al., 2012), *DPAGT1* (Belaya et al., 2012), *ALG2* and *ALG14* genes (Cossins et al., 2013b). The mutations in GFAT1, which is the main focus of the presented thesis, are shown in Figure 1.14.

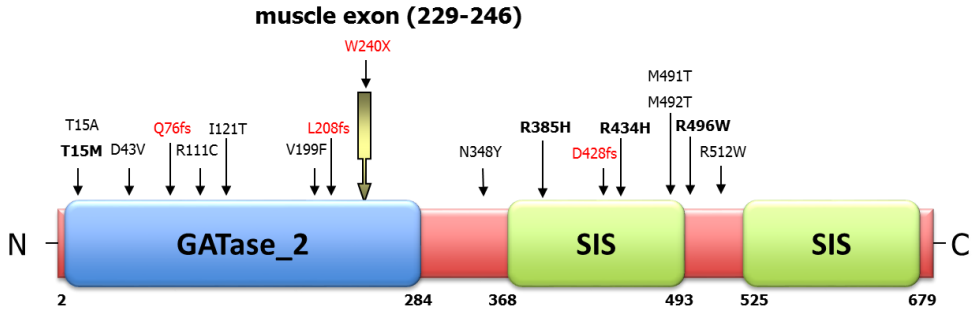

Fig.1.14. Schematic representation of GFAT1 and the mutations identified in the protein in *GFPT1* CMS cases (Zoltowska et al., 2013)
The missense mutations are labelled in black and the frameshift and nonsense changes are labelled in red. The mutations analysed in the present thesis are marked in bold.
GATase_2 – glutaminase domain type 2
SIS – sugar isomerase domain

The mutations in *GFPT1* underlie a CMS typically presenting with marked shoulder and pelvic girdle weakness, and minimal involvement of facial and ocular muscles. First symptoms are usually noted in the first decade of life. Analyses of muscle biopsies taken from the CMS patients carrying mutations in *GFPT1*, *DPAGT1* and *ALG2* genes have revealed the presence of tubular aggregates, simplification of the postsynaptic membrane and a reduction in the density of AChR at the endplates (Senderek et al., 2011, Guergueltcheva et al., 2011, Belaya et al., 2012, Cossins et al., 2013b). The patients are usually treated with AChE inhibitors, such as pyridostigmine, which leads to a significant improvement in muscle strength in most cases. However, the beneficial effects of the drug are often not fully sustained. Therefore, pyridostigmine is frequently combined with 3,4-diaminopyridine (3,4-DAP), a potassium channel blocker, which has been reported to improve or stabilise the condition in a number of patients (Guergueltcheva et al., 2011, Belaya et al., 2012, Senderek et al., 2011, Huh et al., 2012).

Mutations in *ALG2* and *DPAGT1* have also been identified in individuals with severe multisystemic disorders. The multisystemic disease resulting from ALG2 deficiency, termed congenital disorder of glycosylation type Ii (CDG-Ii), manifests itself with

mental retardation, defective myelination, seizures, coloboma of the iris, hepatomegaly and coagulation abnormalities (Thiel et al., 2003). Similarly, severe clinical symptoms have been noted in individuals diagnosed with CDG-Ij, resulting from mutations in *DPAGT1*. These symptoms include a number of neurological and ophthalmological abnormalities, developmental delay, seizures and muscular hypotonia. Some cases with the severe phenotype end in premature death (Wu et al., 2003, Wurde et al., 2012, Carrera et al., 2012), but cases with milder symptoms have also been described (Iqbal et al., 2012). By contrast, no multisystemic disorders have been reported to date that result from mutations in *GFPT1* and *ALG14*.

1.5.2. Myasthenia gravis

Distinct myasthenic disease is MG, which is an autoimmune neuromuscular disorder caused by autoantibodies targeting NMJ proteins. The disease manifests itself with fatiguable muscle weakness, with the first symptoms generally noted in adulthood and involving ptosis and weakness of extraocular muscles. They may progress to affect bulbar and limb-girdle muscles, and to a generalised weakness (Conti-Fine et al., 2006).

The following guidelines can be used to classify subtypes of MG (Conti-Fine et al., 2006, Gilhus et al., 2011):

1. early-onset MG: onset at <50 years, thymic hyperplasia
2. late-onset MG: onset at >50 years, thymic atrophy
3. thymoma-associated MG
4. MG with anti-MuSK antibodies
5. ocular MG
6. seronegative MG (without detectable anti-AChR or anti-MuSK IgG)

1.5.2.1. Autoantibodies in MG patients

Pathogenic autoantibodies in MG patients target molecules expressed highly at the NMJ. Most frequently, the target of the immunoglobulins is the AChR. The second molecule commonly recognised by the autoantibodies is MuSK (Hoch et al., 2001). Recent advances in autoimmunology have resulted in the detection of other targets, which include voltage-dependent calcium channel (VDCC) (Lennon et al., 1995) and active zone protein ERC1 (Huijbers et al., 2013) in Lambert Eaton myasthenic syndrome (LEMS), K_V1.4 voltage-gated potassium channel (VGKC K_V1.4) (Romi et al., 2012), titin, ryanodine receptor (RyR) and AChE (Wang et al., 2010).

However, there are still affected individuals with unknown antibody targets. Such patients are referred to as seronegative (SNMG) (Pal et al., 2011). Development of novel methods, such as cell-based assay (CBA), may help to identify antibody targets in these individuals. The CBA involves over-expression of the potential target at the cell surface, incubation of the cells with serum samples and subsequent detection of bound autoimmunoglobulins with fluorescent anti-human IgG secondary antibody (Yang et al., 2011). In the case of AChR the sensitivity of the assay has been additionally improved by co-transfection of the cells with RAPSN, which clusters the receptors expressed at the cell surface (Jacob et al., 2012, Vincent et al., 2012). These new methodologies have enabled the detection of low-affinity anti-AChR antibodies and immunoglobulins targeting novel antigens, such as LRP4 (Pevzner et al., 2012). The autoantibodies may act via several molecular mechanisms that include: activation of complement at the NMJ (Romi et al., 2000, Engel et al., 1981), antigenic modulation, such as accelerated endocytosis (Clementi and Sher, 1985) or prevention of the binding of the target protein to its ligands (Jahn et al., 2000) or interacting partners (Ohno, 2012).

1.6. Treatment of neuromuscular junction disorders

NMJ disorders can be devastating and sometimes life-threatening, especially in patients with respiratory involvement. However, when diagnosed early, they can usually be treated successfully. The choice of pharmacological treatment is dictated by the underlying molecular defect in a given CMS. Therefore, a specific diagnosis is crucial for rational therapy. Of note, medications beneficial in one CMS subtype can be detrimental in another one.

1.6.1. Drug treatment

Currently most CMS cases are treated with drugs, the most common of which are AChE inhibitors (pyridostigmine, edrophonium), open channel AChR blockers (quinidine sulphate and fluoxetine), potassium channel blockers (3,4-DAP) and β_2-adrenergic receptor (ADRB2) agonists (salbutamol and ephedrine). Similar therapeutic approaches, but with the addition of immunosuppressive drugs, may also be used in the treatment of autoimmune myasthenia (Finlayson et al., 2013).

AChE inhibitors prolong the lifetime of the neurotransmitter, ACh, by inhibiting its hydrolysis. They have been successfully used as therapy for several types of CMS, including *ALG2, ALG14* (Cossins et al., 2013b), *CHAT* (Barisic et al., 2005), *DPAGT1* (Belaya et al., 2012, Muller et al., 2006), *GFPT1* (Guergueltcheva et al., 2011, Senderek et al., 2011), *RAPSN* (Ohno et al., 2002), fast-channel (Palace et al., 2012) and the most common AChR deficiency CMS (Webster et al., 2004). However, if the disorder results from mutations in COLQ (Wargon et al., 2012, Mihaylova et al., 2008), DOK7 (Palace et al., 2007) or a "gain of function" mutation in AChR (Chaouch et al., 2012), the drugs may worsen the clinical course. The slow channel syndrome caused by the "gain of function" AChR mutations can be successfully treated with

open channel blockers of the AChR, such as quinidine sulphate and fluoxetine (Colomer et al., 2006, Harper and Engel, 1998).

Another commonly used medication is 3,4-DAP, which leads to increased calcium entry in the terminal bouton by blocking the outward potassium channels at the nerve terminal, and thus promotes increased release of the neurotransmitter (Metcalf and Boegman, 1989). The drug has been reported to be effective in a number of CMS resulting from mutations in AChR (Palace et al., 2012) and RAPSN (Milone et al., 2009).

Finally, myasthenic syndromes can be treated with ADRB2 agonists, such as salbutamol or ephedrine. These chemicals may act via stimulation of ADRB2 and activation of the PKA type I pathway (Stiles et al., 1984). This may consequently lead to the stabilisation of AChR clusters (Choi et al., 2012). These medicines have shown positive effects in *COLQ* (Liewluck et al., 2011), *DOK7* (Burke et al., 2012) and slow-channel CMS (Finlayson et al., 2012).

1.6.2. Gene therapy

Although CMS and MG can be successfully treated by administration of appropriate chemical agents, there are certain disadvantages to such therapies. First, treatment may be symptomatic and often non-specific, and can cause a number of side effects. Moreover, it requires repeated drug administration. At least some of these disadvantages could potentially be overcome with gene therapy focused on down-regulating (by RNA interference (RNAi)) or up-regulating the expression of target genes.

The first attempt to explore RNAi approach for myasthenic disorders was described by Abdelgany et al., who demonstrated an efficient allele-specific silencing of a

pathogenic AChR α1 subunit (CHRNA1.p.S226F) *in vitro* using allele-specific small interfering RNA (siRNA) and short hairpin RNA (shRNA) (Abdelgany et al., 2003). This was followed by similar studies to down-regulate another slow-channel AChR α1 mutated variant (p.C418W) (Shen et al., 2006). Finally, gene therapy has also been proposed for the treatment of AChE deficiency resulting from COLQ mutations. A single intravenous injection of adeno-associated virus serotype 8 (AAV8)-COLQ to *Colq*$^{-/-}$ mice has been demonstrated to restore the ultrastructure of the NMJ and synaptic transmission (Ohno et al., 2012). However, it is not yet practical to try these approaches in patients.

Objectives

This thesis focuses on inherited and autoimmunological causes of myasthenic weakness and on the development of novel therapies, which might be used to treat muscle disorders. The project was divided into three major parts. The first focused on the pathogenesis of L-glutamine:D-fructose-6-phosphate amidotransferase 1 (*GFPT1*) congenital myasthenic syndrome (CMS), the second aimed to develop new potential therapeutic approaches for myasthenic disorders, while the third concentrated on collagen Q (COLQ) as a potential target in autoimmune myasthenic weakness.

Molecular pathogenesis of *GFPT1* CMS

GFPT1 mutations have recently been implicated in the pathogenesis of CMS (Guergueltcheva et al., 2011, Senderek et al., 2011), but how these mutations lead to the aberrant neuromuscular transmission has not yet been defined. The first part of the project aimed to provide insight into the following aspects:

1. Molecular consequences of individual missense mutations (p.T15M, p.R385H, p.R434H, p.T479N and p.R496W) identified in two unrelated *GFPT1* CMS cases and siblings diagnosed with a severe multisystemic disease
2. The pattern and importance of carbohydrates at the neuromuscular junction (NMJ) *in vitro* and *in vivo*
3. The link between *GFPT1* mutations and AChR expression

Therapy of myasthenic disorders

Most subtypes of CMS can be treated, but the response is often partial and may not be fully sustained over time. The second part of the project aimed to study the use of β_2-adrenergic receptor (ADRB2) agonists as a therapy in AChR deficiency syndrome.

Targeting COLQ as a cause of an autoimmune myasthenic weakness

In myasthenia gravis (MG) muscle weakness is caused by autoantibodies targeting molecules expressed at the cell surface at the NMJ, but the antibody targets remain unknown in many cases. A possible target for the antibodies is COLQ, which is highly and specifically expressed at the NMJ, and is mutated in a number of CMS cases. Specific aims were to:

1. Search for the autoantibodies targeting COLQ in a cohort of MG patients
2. Determine whether anti-COLQ autoimmunoglobulins may cause myasthenic weakness

Chapter 2

Patients, materials and methods[1]

2.1. Biopsies

Muscle biopsies were taken from two unrelated individuals of white European ethnic origin (P1 and P2), who both harboured compound heterozygous mutations in the L-glutamine:D-fructose-6-phosphate amidotransferase 1 (*GFPT1*) gene, p.R385H/R434H and p.T15M/R496W, respectively, and had a clinical diagnosis of *GFPT1* congenital myasthenic syndrome (CMS). Control human skeletal muscle cells were obtained from a commercial source (Cell Applications, 150-05a) or from the MRC Centre for Neuromuscular Diseases BioBank, London.

A skin biopsy was taken from one British patient (P3), who was diagnosed with a severe multisystem disorder, and harboured a homozygous missense variant in *GFPT1*, p.T479N. Fibroblasts from muscle biopsies from CMS patients, from thymuses of myasthenia gravis (MG) patients and from a skin biopsy from a healthy individual were used for control purposes.

Patient consents were obtained with ethical approval OXREC B: 04.OXB.017 and Oxfordshire REC C 09/H0606/74.

[1] The methods described in this chapter are specific for the presented thesis. Standard molecular biology techniques can be found in the Appendix.

2.2. DNA methods

2.2.1. Polymerase Chain Reaction (PCR)

2.2.1.1. Standard PCR

Standard PCR was performed using MegaMix-Blue (Microzone$^{\mu}$, 2MMB) containing recombinant *Taq* polymerase in 1.1x reaction buffer (2.75 mM $MgCl_2$) with 220 µM deoxyribonucleotide triphosphates (dNTPs), blue agarose loading dye and stabiliser. Usually, 18 µl MegaMix-Blue were mixed with 1 µl 10 nM primers and 1 µl DNA template, and the PCR reactions were run under standard conditions:

1x94^{o}C for 5 minutes

20-30x(94^{o}C for 30 seconds, primer T_M-5^{o}C for 30 seconds, 72^{o}C for 1 minute/1 kb of target DNA)

1x72^{o}C for 10 minutes

The primers used in the reactions are specified in Table 2.1.

Table 2.1. Sequences of the oligonucleotides used in standard PCR
The sequences are shown from 5' to 3'.

Target	Primer name	Primer sequence
EGFP	*EGFP* F	GGATACCGGTATGGTGAGCAAGGGCGAGGAGCTG
EGFP	*EGFP R*	GGATACCGGTTTACTTGTACAGCTCGTCCATGCC
Gapdh	*Gapdh F*	AGAACATCATCCCTGCATCC
Gapdh	*Gapdh R*	CCCTGTTGCTGTAGCCGTAT
***GFPT1* promoter**	*GFPT1* promoter F1	GGTTATGGAGGCAACGGATGCGGAGG
***GFPT1* promoter**	*GFPT1* promoter R1	GACGGCCAAGGCAACGACAGCCTTCT
***GFPT1* promoter**	*GFPT1* promoter F2	GTCTCCAAGTCTGTCTAGGGGGGATA
***GFPT1* promoter**	*GFPT1* promoter R2	GCCCCAAAGGTCAGCCTCTCTGGTAA
***GFPT1* exon 1**	*GFPT1* exon 1 F	ATTCCCTGCCAGGTGCTGAGTTTCTC
***GFPT1* exon 1**	*GFPT1* exon 1 R	GCCTTCCTCTCAGGTGCCTTTCTCCC
***GFPT1* exon 2**	*GFPT1* exon 2 F	TTCACATACTTGACATAATTATGCTA
***GFPT1* exon 2**	*GFPT1* exon 2 R	AAACAGACTTTAATAGTCTAGTCTCC
***GFPT1* exon 3**	*GFPT1* exon 3 F	GCCTCACATTAATAATTTTATCAGTA
***GFPT1* exon 3**	*GFPT1* exon 3 R	TTCAATGTTACAGACCATTATCATTA
***GFPT1* exon 4**	*GFPT1* exon 4 F	ATTCCAAGAGAGCAGCATTGTAATAA

***GFPT1* exon 4**	*GFPT1* exon 4 R	ATGAGCCAGCACTCTCAGCTCCATAT
***GFPT1* exon 5**	*GFPT1* exon 5 F	TGCTGATCTACCTGATGATAATCTGG
***GFPT1* exon 5**	*GFPT1* exon 5 R	TGTTTGTTGCACATCCCAACAACCGA
***GFPT1* exon 6**	*GFPT1* exon 6 F	GGGATATGGTGTTCAAAGAATATTAG
***GFPT1* exon 6**	*GFPT1* exon 6 R	AAATAGCACAGTTCCTGCTTATCAAA
***GFPT1* exon 7**	*GFPT1* exon 7 F	GTCTTGGATACACCAAAGCTTAGGAG
***GFPT1* exon 7**	*GFPT1* exon 7 R	TATGCTCACATGAATATATCTAATAA
***GFPT1* exon 8-9**	*GFPT1* exon 8-9 F	CTGAAGTTGAGCTTGGGGAGGATGAT
***GFPT1* exon 8-9**	*GFPT1* exon 8-9 R	AAAAGAGGATAAGATCCTCCCCATCC
***GFPT1* exon 10**	*GFPT1* exon 10 F	ATGCATATTTCTACATTGGACATGAT
***GFPT1* exon 10**	*GFPT1* exon 10 R	AAAAGTTATCTCACAGAGCACAACTA
***GFPT1* exon 11**	*GFPT1* exon 11 F	ACTGCAGAGTGATAGAGTTTATATTG
***GFPT1* exon 11**	*GFPT1* exon 11 R	GGAAGATTCCACTCATCATTCATTAC
***GFPT1* exon 12**	*GFPT1* exon 12 F	GGCAGTCATGTCTATTGCATGAACTT
***GFPT1* exon 12**	*GFPT1* exon 12 R	TGTTAATGGCACCTCCTACTGTCAGA
***GFPT1* exon 13**	*GFPT1* exon 13 F	ACAGCAGTATTCTTCCTCATATTGGC
***GFPT1* exon 13**	*GFPT1* exon 13 R	AAGCAGCTGGTAAATTTCTCCCCTTA
***GFPT1* exon 14**	*GFPT1* exon 14 F	CTATACATTGAATCCAAAGAAGTCCG
***GFPT1* exon 14**	*GFPT1* exon 14 R	TCGTCAAGTCATCTGCAATGCCAGTT
***GFPT1* exon 15**	*GFPT1* exon 15 F	ACAGCATATGTTAAAACTGTTCTGTG
***GFPT1* exon 15**	*GFPT1* exon 15 R	GTGTGAGTTCTATAACTGCTAACAAA
***GFPT1* exon 16**	*GFPT1* exon 16 F	AAATTCTTCAGATGCAGCTGCAACTA
***GFPT1* exon 16**	*GFPT1* exon 16 R	AGAGAATTTTACCTATTACCCACTCC
***GFPT1* exon 17**	*GFPT1* exon 17 F	AATACCCATACTGATTGATAGCACAG
***GFPT1* exon 17**	*GFPT1* exon 17 R	TCTGCAGGTCAATGGACTGATACTAA
***GFPT1* exon 18**	*GFPT1* exon 18 F	CAGTGGCTTGACATATCAGATGCTTT
***GFPT1* exon 18**	*GFPT1* exon 18 R	TAAGCTAGCGTAACTCCCCTCTTTGA
***GFPT1* exon 19**	*GFPT1* exon 19 F	GGCTTCATATGGATTATGCAGTGCAA
***GFPT1* exon 19**	*GFPT1* exon 19 R	GATGTAACCTACAAATTGGGCCATGA
***GFPT1* exon 20**	*GFPT1* exon 20 F	CAGTCTATATAATCTCTCAAATCTTG
***GFPT1* exon 20**	*GFPT1* exon 20 R	CTTCCCTAACTGTCCAAGTATGAGCA
GFPT1-L	*GFPT1-L*-m.exon F	ATTCACAATGGAATCATCACCAACTACAAA
GFPT1-L	*GFPT1-L*-m.exon R	GTGTTCACGACAGACTCTGGCTGCTCAAAT
GFPT1* and *GFPT1-L	*GFPT1* F	TGTTGATTGGTGTACGGAGTG
GFPT1* and *GFPT1-L	*GFPT1* R	AACCACCCAAATTCACAGTATAGTC
GFPT1* and *GFPT1-L	*GFPT1*.p.T15M F splice site	GTGGTATATTTGCTTACTTAAACTACC
GFPT1* and *GFPT1-L	*GFPT1*.p.T15M R splice site	CGATAAATTCATTATTTTTATCAGAGC
GFPT1* and *GFPT1-L	*GFPT1*.p.R385H F splice site	GCTTCTGATGCAAGTGCTGT

GFPT1* and *GFPT1-L	*GFPT1*.p.R385H R splice site	TCTGCTGTCTCACCTGATTGA
GFPT1* and *GFPT1-L	*GFPT1*.p.R434H/ T479N/R496W F splice site	GCTGGTGTAGCAACACGTCA
GFPT1* and *GFPT1-L	*GFPT1*.p.R434H/ T479N/R496W R splice site	TCAATTCACCAGCAAGGATG

2.2.1.2. Hot start PCR

Hot start PCR reactions were conducted using *PfuUltra* II Fusion HS DNA polymerase (Agilent Technologies, 600670), which is a thermostable DNA polymerase possessing a 3'→5' proof-reading activity and enhanced processivity. Reaction mixtures contained 40.6 µl distilled water, 5 µl *PfuUltra* II reaction buffer, 0.4 µl dNTPs (25 nM each), 1 µl DNA template (100 ng/µl), 1 µl each primer (1 µg/µl) and 1 µl (2.5 U) *PfuUltra* II Fusion HS DNA polymerase.

The following PCR cycling parameters were used:

1x95^{o}C for 2 minutes

30x(95^{o}C for 30 seconds, primer T_M-5^{o}C for 30 seconds, 72^{o}C for 1 minute/1 kb of target DNA)

1x72^{o}C for 10 minutes

The primers used in the PCR are specified in Table 2.2.

Table 2.2. Sequences of the oligonucleotides used in hot start PCR
The sequences are shown from 5' to 3'.

Target	Primer name	Primer sequence
EGFP-Glc-ER* and *EGFP-ER	*EGFP-ER* cloning F	TTAGATGCTAGCATGCTGCTATCAGTACCACTT
EGFP-Glc-ER* and *EGFP-ER	*EGFP-ER* cloning R	CTAGTCGGATCCTTACAGCTCATCCTTCTTGTA
GFPT1* and *GFPT1-EGFP	*GFPT1*.cloning F	GGTAGCGGCCGCCGTGTCTCCGGCATCATGTGTGGTATAT
GFPT1	*GFPT1*.cloning R	GGTAGGATCCTTGTATAGATATTCCTCACTCTACAGTCAC
GFPT1-EGFP	*GFPT1-EGFP*.cloning R	GGAAGGATCCTTTGTATAGATATACCGGTTTACTTGTACA

2.2.1.3. Reverse transcription PCR

Total RNA was transcribed into cDNA by reverse transcription PCR (RT-PCR) using a RETROscript® Kit (Ambion, AM1710). 1-2 µg RNA and 2 µl random decamers (50 µM) were mixed with nuclease-free water to obtain a total volume of 11 µl. The reaction mixes were heated for 3 minutes at 85^{o}C and placed on ice. 2 µl 10xRT Buffer, 4 µl dNTP mix (25 µM each), 1 µl RNase inhibitor and 2 µl moloney murine leukemia virus reverse transcriptase (M-MLV RT) were added to the samples. The reactions were incubated for 1 hour at 44^{o}C and then for 10 minutes at 92^{o}C. The cDNA was stored at -20^{o}C.

2.2.1.4. RT-qPCR

RNA was extracted from *in vitro* cultured cells or tissue using RNeasy Mini Kit (Qiagen, 74104) according to the manufacturer's recommendations (Appendix, section I.2.1.). Contaminating DNA was digested using a TURBO DNA-*free*™ kit (Invitrogen, AM1907) following the supplier's protocol (Appendix, section I.2.2.). 2 µg total purified RNA was reverse transcribed using RETROscript™ kit with random decamers (Invitrogen, AM1710) (Chapter 2, section 2.2.1.3). A sample not containing any RNA was reverse transcribed as a negative control.

Quantitative PCR (qPCR) was conducted using the Applied Biosystems 7500 Real-Time PCR System and TaqMan® Gene Expression Master Mix (Applied Biosystems, 4369016) following the manufacturer's protocol. Each qPCR reaction was performed in triplicate in a MicroAmp Fast Optical 96-well plate (Applied Biosystems, 4346907) and the data were recorded using 7500 Software (Applied Biosystems). mRNA expression levels of the target gene, encoding AChR α1 subunit (*CHRNA1*), were

normalised to the levels of glyceraldehyde-3-phosphate dehydrogenase (*GAPDH*) housekeeping gene expression.

Predesigned assays for the amplification of the target and the reference cDNA were purchased from Integrated DNA Technologies. The assay for the amplification of *CHRNA1* contained 5'-CAGTAAGACAGAGATGCTCAGAG-3' and 5'-TCTACTTCATCGTCAACGTCATC-3' as primers, and 5'-/56-FAM/ACCAGGCCA/ZEN/GTTAAGAAGGAGAAGAG/3IABkFQ/-3' as a probe. The assay used for the *GAPDH* amplification contained the following primers: 5'-TGTAGTTGAGGTCAATGAAGGG-3' and 5'-ACATCGCTCAGACACCATG-3', and 5'-/56-FAM/AAGGTCGGA/ZEN/GTCAACGGATTTGGTC/3IABkFQ/-3' as a probe. The relative quantification (RQ) values were calculated using 7500 Software (Applied Biosystems).

2.2.2. Mutagenesis

The GeneArt®Site-Directed Mutagenesis System (Invitrogen, A13282) was used to generate single base substitutions or small insertions (up to 20 nucleotides) in DNA constructs. For each mutation two complementary mutagenic primers with centrally located mutation sites were designed. The primer sequences are shown in Table 2.3.

Table 2.3. Sequences of the oligonucleotides used for mutagenesis
The sequences are shown from 5' to 3'.

Construct name	Primer name	Primer sequence
GFAT1-L.pT15M	GFAT1-L. p.T15MmutF	AACTACCATGTTCCTCGAATGAGACGAGA AATCCTGG
GFAT1-L.pT15M	GFAT1-L. p.T15MmutR	CCAGGATTTCTCGTCTCATTCGAGGAACA TGGTAGTT
GFAT1-L.pR385H	GFAT1-L.p.R385HmutF	ACCATGCTGGTGTAGCAACACATCAAGTT CTTGAGGAGC
GFAT1-L.pR385H	GFAT1-L. p.R385HmutR	GCTCCTCAAGAACTTGATGTGTTGCTACA CCAGCATGGT
GFAT1-L.pR434H	GFAT1-L. p.R434HmutF	ATACTTTGATGGGTCTTCATTACTGTAAGG AGAGAGGAGC

GFAT1-L.pR434H	GFAT1-L. p.R434HmutR	GCTCCTCTCTCCTTACAGTAATGAAGACCC ATCAAAGTAT
GFAT1.pT479N	GFAT1.p.T479NmutF	CAGTACAAAGGCTTATAACAGCCAGTTTG TATCC
GFAT1.pT479N	GFAT1.p.T479NmutR	GGATACAAACTGGCTGTTATAAGCCTTTG TACTG
GFAT1-L.pR496W	GFAT1-L. p.R496WmutF	TTATGATGTGTGATGATTGGATCTCCATGC AAGAAAGACG
GFAT1-L.pR496W	GFAT1-L. p.R496WmutR	CGTCTTTCTTGCATGGAGATCCAATCATCA CACATCATAA
GFAT1.AgeI	GFAT1.AgeIF	TCTGTGACTGTAGAGACCGGTATATCTAT ACAAAATGTACG
GFAT1.AgeI	GFAT1.AgeIR	CGTACATTTTGTATAGATATACCGGTCTCT ACAGTCACAGA
COLQ.BslI	COLQ.BslIF	CAATCTCAGCAGCCCTTCCACCGGTAAGC CTGGATCAGAAGAAGC
COLQ.BslI	COLQ.BslIR	GCTTCTTCTGATCCAGGCTTACCGGTGGA AGGGCTGCTGAGATTG
Myc-COLQ	Myc-COLQF	CAATCTCAGCAGCCCTTCCACCGGTAAGC CTGGATCAGAAGAAGC
Myc-COLQ	Myc-COLQR	GCTTCTTCTGATCCAGGCTTACCGGTGGA AGGGCTGCTGAGATTG

The designed oligonucleotides were used to amplify previously methylated target plasmids. To enhance the colony output, PCR reactions were followed by *in vitro* recombination. The final products were introduced into DH5α™-T1R competent *Escherichia coli* strain. The host cells should circularise the linear mutated DNA and also, due to the presence of *Mcr*BC endonuclease, they should digest the methylated template DNA, leaving only the unmethylated, mutated products. The transformed cells were plated on lysogeny broth (LB)-agar plates containing the appropriate selection antibiotic. Three antibiotic-resistant colonies were screened for the presence of the plasmids with the desired mutations. This was done by extracting the DNA from the cells using QIAprep Spin Miniprep Kit (QIAGEN, 27106) (Appendix, section I.1.1.) and sequencing the target genes (Appendix, section I.1.13.).

2.3. RNA methods

2.3.1. siRNA design

Small interfering RNA (siRNA) molecules were designed in a way that target sequences were 24 nucleotides in length, did not contain runs of more than three of the

same nucleotides, had 35-55% GC content and contained minimal homology to other genes. Two siRNA sequences were designed, one targeting ubiquitously expressed *GFPT1* and the other targeting *GFPT1-L* only. The targeted DNA sequences were 5'-CAGAGGATATGATTCTGCTGGTGT-3' and 5'-GAACAGCTAGGACTCAGATTGGAT-3', respectively. As a negative control, scrambled sequences were used: 5'-GTGCAGGATAGATTCGCTGGTATT-3' and 5'-GTGTCACGAGTCGAATCCAAGATA-3', respectively. The oligonucleotides were ordered from Sigma.

2.4. Protein, glycoprotein and glycolipid methods

2.4.1. Western blotting

Before immunoblotting, polyvinylidene difluoride (PVDF) membranes containing separated proteins transferred from polyacrylamide gels (Appendix, section I.3.2. and I.3.3.) were incubated in a blocking solution of 5% dry skimmed milk in phosphate buffered saline (PBS)-0.1% Tween 20 (PBST) for at least 2 hours at 4^{o}C. Primary antibodies diluted in 2% dry skimmed milk in PBST were applied to the membranes and incubated with them for 1-12 hours. The membranes were washed 3 times for 10 minutes in PBST and incubated for 2 hours at room temperature with horseradish peroxidase (HRP)-conjugated secondary antibodies diluted in 2% dry skimmed milk in PBST. The immunoblotted membranes were washed 3 times for 30 minutes in PBST. The primary and the secondary antibodies used in the western blotting are summarised in Table 2.4.

Table 2.4. Primary and secondary antibodies used in western blotting

Antibody	Dilution	Species raised in
α-tubulin (Sigma, T5168)	1:1000	mouse monoclonal IgG
AChR α (mAb155, gift from S.Tzartos)	1:500-1:1000	rat monoclonal IgG
AChR β (mAb124, gift from S.Tzartos)	1:1000	rat monoclonal IgG
AChR δ (Santa Cruz, sc-1451)	1:1000	goat polyclonal IgG
AChR ε (Santa Cruz, sc-1454)	1:1000	goat polyclonal IgG
EGFP (Abcam, ab6556)	1:1000	rabbit polyclonal IgG
GFAT1 (Cell Signaling, 3818)	1:500	rabbit polyclonal IgG
GFAT1 (Epitomics, 3651-1)	1:1000	rabbit monoclonal IgG
mCherry (Biovision, 5993-100)	1:1000	rabbit polyclonal IgG
MuSK (R&D Systems, AF562)	1:500	goat polyclonal IgG
Myc-Tag (Cell Signaling, 2276)	1:1000	mouse monoclonal IgG
O-GlcNAc CTD110.6 (Santa Cruz, sc-59623)	1:200	mouse polyclonal IgM
phosphotyrosine (Millipore, 05-321)	1:500	mouse monoclonal IgG
RAPSN (Abcam, ab11423)	1:200	mouse monoclonal IgG
anti-goat immunoglobulins/HRP (DakoCytomation, P0449)	1:1000	rabbit polyclonal IgG
anti-human IgG/HRP (DakoCytomation, P0214)	1:500	rabbit polyclonal IgG
anti-mouse IgM (μ) HRP (Invitrogen, M31507)	1:500	goat polyclonal IgG
anti-mouse immunoglobulins/HRP (DakoCytomation, P0447)	1:1000	goat polyclonal IgG
anti-rabbit immunoglobulins/HRP (DakoCytomation, P0448)	1:1000	goat polyclonal IgG
anti-rat immunoglobulins/HRP (DakoCytomation, P0450)	1:1000	rabbit polyclonal IgG

The HRP-conjugated secondary antibodies were developed using Amersham ECL or ECL Prime Western Blotting Detection Reagents (GE Healthcare, RPN2105 and RPN2132, respectively) following the manufacturer's recommendations, and the membranes were exposed in the dark to X-ray films. The choice of the detection reagent was influenced by the abundance of the target proteins and the binding strength of the primary antibodies used in the procedure.

The densities of the bands were measured by densitometry using GelDoc-It2 310 Imager (UVP) and VisionWorks®LS Image Acquisition and Analysis Software (UVP 97-0186-03).

2.4.2. Immunoprecipitation

Target proteins were isolated from the cell surface by immunoprecipitation. Cells were incubated for 1 hour with appropriate antibodies (Table 2.5.) diluted in a buffer containing Dulbecco's Modified Eagle Medium (DMEM) (Sigma, D6429) supplemented with 1% bovine serum albumin (BSA) and 200 mM 4-(2-hydroxyethyl)-1-piperazineethanesulphonic acid (HEPES). The cells were washed 3 times for 5 minutes with the buffer and lysed in 220 µl protein extraction buffer (10 mM Tris, 100 mM NaCl, 1 mM ethylenediaminetetraacetic acid (EDTA), 1% Triton X-100, pH8.0) per well of 24-well plate. The lysates were collected and centrifuged for 15 minutes at 14000rpm at 4^{o}C to remove cell debris. 200 µl of the lysates were added to 1.5 mg magnetic beads coupled with a recombinant protein G (Dynabeads®Protein G, Invitrogen, 100-03D) and the samples were incubated for 30 minutes at 4^{o}C with gentle rotation. The beads were washed 5 times with 200 µl PBS, resuspended in 100 µl PBS and transferred into new eppendorf tubes. The PBS was removed and the beads were resuspended in a mixture containing 14.28 µl 4xNuPAGE® LDS Sample Buffer (Invitrogen, NP0008) and 5.71 µl 10xNuPAGE® Reducing Agent (Invitrogen, NP0004). Immunocomplexes captured on the beads were eluted by a 10-minute incubation at 70^{o}C.

Table 2.5. Antibodies used in immunoprecipitation

Antibody	Dilution	Species raised in
MuSK (R&D Systems, AF562)	1:50	goat polyclonal IgG
Myc-Tag (Cell Signaling, 2276)	1:500	mouse monoclonal IgG

2.4.3. Pull-down of acetylcholine receptors

Acetylcholine receptors (AChR) were isolated from the cell surface using XX-biotin α-bungarotoxin (α-BuTx) (Invitrogen, B-1196) and Dynabeads® M-270 Streptavidin (Invitrogen, 65305). Cells were incubated for 45 minutes with the α-BuTx diluted 1:500 in tissue culture medium (DMEM (Sigma, D6429) supplemented with 2% horse serum (HS) (Sigma, H1138) and antibiotics (Invitrogen, 15240-062)). Then, the cells were washed 3 times for 5 minutes with the medium and lysed in 450 µl protein extraction buffer (10 mM Tris, 100 mM NaCl, 1 mM ethylenediaminetetraacetic acid (EDTA), 1% Triton X-100, pH8.0) per well of a 6-well plate. The lysates were collected and centrifuged for 15 minutes at 14000rpm at 4^{o}C to remove cell debris. 400 µl of the lysates were added to 50 µl Dynabeads® M-270 Streptavidin, and the samples were incubated for 30 minutes at 4^{o}C with gentle rotation. The beads were washed 5 times with 200 µl PBS, resuspended in 100 µl PBS and transferred into new eppendorf tubes. The PBS was removed and the beads were resuspended in a mixture containing 14.28 µl 4xNuPAGE® LDS Sample Buffer (Invitrogen, NP0008) and 5.71 µl 10xNuPAGE® Reducing Agent (Invitrogen, NP0004). The protein bound to the beads was eluted by a 10-minute incubation at 70^{o}C.

2.4.4. Cycloheximide pulse chase assay

In order to determine the effects of the mutations on the stability of GFAT1-L, human embryonic kidney cells (HEK293TSA) were transfected with wild type and mutated GFAT1-L-encoding constructs, respectively. 12 hours after the transfection, cycloheximide (CHX) (Sigma, C4859) was added to the growth medium to a final concentration of 20 µg/ml and the cells were incubated for 0, 4, 6, 8 or 24 hours. They were collected and lysed. The cell lysates were resolved by sodium dodecyl sulphate

polyacrylamide gel electrophoresis (SDS-PAGE) (Appendix, section I.3.2.) and immunoblotted with rabbit polyclonal anti-GFAT1 antibodies (Cell Signaling, 3818) and HRP-conjugated anti-rabbit secondary antibodies (Chapter 2, section 2.4.1.).

The densities of the bands were measured by densitometry using GelDoc-It2 310 Imager (UVP) and VisionWorks®LS Image Acquisition and Analysis Software (UVP 97-0186-03).

2.4.5. Inhibition of GFAT1 enzymatic activity

Enzymatic activity of GFAT1 was inhibited by a 48-hour incubation of target cells with a glutamine analogue 6-diazo-5-oxo-L-norleucine (DON) (Sigma, D2141) diluted in an appropriate growth medium to a final concentration of 100 μM-1 mM.

2.4.6. Immunocytofluorescence

Cells plated on poly-L-leucine-coated coverslips were fixed by a 20-minute incubation with 3% paraformaldehyde in PBS and permeabilised in 0.1% Triton X-100 in PBS for 5 minutes. The latter step was omitted when the target protein was expressed at the cell surface. The fixed cells were incubated for 30 minutes in a blocking solution (3% BSA in PBS). Primary antibodies diluted in the blocking solution were applied and the cells were incubated with the antibodies for 1 hour with gentle rocking. The coverslips were washed 3 times for 5 minutes with PBS and incubated for one hour with fluorescent secondary antibodies diluted in the blocking solution. Finally, the coverslips were washed 3 times for 10 minutes with PBS and mounted using Dako Faramount mounting medium (Dako, S3025). The primary and secondary antibodies used are specified in Table 2.6. The labelled cells were analysed by widefield or confocal fluorescence microscopy using an Olympus X71 Fluorescence Microscope

and a SimplePCI Software, or a Zeiss 780 Inverted Microscope and a ZEN 2012 Lite software, respectively.

Table 2.6. Antibodies used in immunocytofluorescence

Antibody	Dilution	Species raised in
GFAT1 (Epitomics, 3651-1)	1:50	rabbit monoclonal IgG
LRP4 (Santa Cruz, sc-98775)	1:50	rabbit polyclonal IgG
MuSK (R&D Systems, AF562)	1:50	goat polyclonal IgG
Myc-Tag (Cell Signaling, 2276)	1:1000	mouse monoclonal IgG
Alexa Fluor 568 anti-goat IgG (Invitrogen, A-11057)	1:500	donkey polyclonal IgG
Alexa Fluor 568 anti-human IgG (Invitrogen, A-21090)	1:1000	goat polyclonal IgG
Alexa Fluor 594 anti-mouse IgG (Invitrogen, A-11032)	1:500	goat polyclonal IgG
Alexa Fluor 488 anti-rabbit IgG (Invitrogen, A-21206)	1:500	donkey polyclonal IgG

2.4.7. Induction and detection of AChR clusters in *in vitro* cultured muscle cells

AChR cluster formation in *in vitro* cultured myotubes was induced by a 12-hour incubation with a full-length human agrin (AGRN). The formed clusters were labelled by a 1-hour incubation of the cells at 37ºC, 5% CO_2 with 1 µg/ml Alexa Fluor 594 α-bungarotoxin (α-BuTx) (Invitrogen, B13423) diluted in DMEM (Sigma, D6429) supplemented with 2% foetal calf serum (FCS) (Sigma, F2442) and antibiotics (Invitrogen, 15240-062). Excess of the toxin was removed by washing 3 times for 5 minutes with the medium. The cells were then fixed by a 20-minute incubation with 3% paraformaldehyde diluted in the medium and washed 3 times for 5 minutes with PBS. The labelled AChR clusters were visualised by fluorescence microscopy using an Olympus X71 Fluorescence Microscope and a SimplePCI Software.

2.4.8. Cell surface ^{125}I-α-bungarotoxin binding assay

A cell surface ^{125}I-α-bungarotoxin (^{125}I-α-BuTx) binding assay was conducted on mammalian cells cultured in 6-well Corning® Costar® Cell Culture plates (Corning, CLS3516-50EA). The cells were washed 3 times with PBS and incubated for 1 hour with ^{125}I-α-BuTx (10^6 cpm/ml) (PerkinElmer, NEX126050UC) diluted in PBS. If necessary, to estimate the background signal, a step with a 15-minute preincubation with excess (5 µg/ml) unlabelled α-BuTx (Invitrogen, B1601), prior to the addition of the radiolabelled one, was introduced. The α-BuTx-containing mixtures were then aspirated and the cells were washed 3 times for 5 minutes with PBS. The radiolabelled cells were dissolved in 1 ml extraction buffer (10 mM Tris, 100 mM NaCl, 1 mM EDTA, 1% Triton X-100, pH8.0) and the amount of the ^{125}I-α-BuTx bound to the cells was counted in a γ-counter. To ensure the reproducibility of the results, the assay was performed in triplicate.

2.4.9. N-acetylgalactosamine detection in cultured cells

N-acetylgalactosamine (GalNAc) carbohydrate moieties present at the cell surface were stained using tetramethylrhodamine isothiocyanate (TRITC)-conjugated *Vicia villosa* agglutinin B_4 (VVA-B_4) (EY Laboratories Inc., R-4601-2). C2C12 myotubes were incubated for 1 hour at 37ºC, 5% CO_2, with 50 µg/ml TRITC-VVA-B_4 diluted in an appropriate growth medium. Excess of the lectin was removed by washing 3 times for 5 minutes with the medium. The cells were then fixed by a 20-minute incubation in 3% paraformaldehyde diluted in the medium, washed 3 times for 5 minutes with PBS and imaged using an Olympus X71 Fluorescence Microscope and a SimplePCI Software.

2.4.10. Flow cytometry

Cell surface expression of intercellular adhesion molecule 1 (ICAM1, CD54) or a fluorescence intensity of enhanced green fluorescent proteins (EGFP-Glc-ER and EGFP-ER) and DsRed were measured by flow cytometry. 10^6 cells were collected, resuspended in growth medium supplemented with 10 mM EDTA and transferred to eppendorf tubes. The cells were centrifuged for 8 minutes at 1200rpm at 4^{o}C to form a pellet. If immunolabelling was required, the cells were resuspended in 100 µl of a staining buffer (DMEM (Sigma, D6429) supplemented with 1% BSA and 200mM HEPES) containing 5 µl of a respective R-phycoerithrin (PE)-conjugated antibody (Table 2.7.). After a 30-minute incubation with the antibody, 500 µl of the buffer was added to the cell suspension and the cells were centrifuged for 8 minutes at 1200rpm at 4^{o}C. The cell pellets were resuspended in 40 µl 1% paraformaldehyde diluted in the staining buffer and incubated for 5 minutes at 4^{o}C. They were then washed in 500 µl of the staining buffer and centrifuged for 5 minutes at 1200rpm at 4^{o}C. The immunolabelled cells or the cells presenting intrinsic EGFP-Glc-ER, EGFP-ER or DsRed fluorescence were resuspended in 200 µl PBS supplemented with 10 mM EDTA (PBS-EDTA). The cells were run through sieves to round-bottom polypropylene tubes. To collect all the cells, the eppendorf tubes were washed with 200 µl PBS-EDTA and then the sieves were also washed with 200 µl PBS-EDTA. The intensity of the PE fluorescence, corresponding to the cell surface expression of ICAM1, was measured using a CyAn™ ADP analyser. The fluorescence intensity of EGFP-Glc-ER, EGFP-ER and DsRed was quantified using a BD LSRFortessa™ Cell Analyser. The data were analysed using Summit 4.3 software.

Table 2.7. Antibodies used in flow cytometry

Antibody	Dilution	Species raised in
anti-human CD54 (ICAM1) PE (eBioscience, 12-0549)	1:20	mouse monoclonal IgG
mouse IgG1 K isotype control PE (eBioscience, 12-4714)	1:20	mouse monoclonal IgG

2.4.11. Immunofluorescence staining of muscle sections

Muscles were dissected, snap-frozen in liquid nitrogen-isopentane and sectioned into 10 µm-thick sections using a cryostat (Leica, CM1900). The sections were attached to glass slides and dried for 12 hours under vacuum. Before immunostaining, the muscle sections were rehydrated by the brief incubation in PBS, fixed by a 20-minute incubation in 3% paraformaldehyde in PBS and permeabilised by a 5-minute incubation in 0.1% Triton X-100 in PBS. The permeabilised sections were incubated for 1 hour with primary antibodies diluted in PBS supplemented with 3% BSA. Excess of the antibodies was removed by washing 3 times for 5 minutes with PBS, and the slides were incubated for 1 hour with secondary antibodies diluted in PBS supplemented with 3% BSA. The antibodies used in the labelling are specified in Table 2.8. For staining with serum samples obtained from MG patients and healthy individuals, SuperBlock (PBS) Blocking Buffer (Pierce, 37580) was used during the entire procedure in place of PBS supplemented with 3% BSA. The slides were washed 3 times for 10 minutes and mounted using Dako Faramount mounting medium (Dako, S3025). They were then analysed by widefield or confocal fluorescence microscopy using an Olympus X71 Fluorescence Microscope and a SimplePCI software, or a Zeiss 780 Inverted Microscope and a ZEN 2012 Lite software, respectively.

Table 2.8. Antibodies used in immunohistofluorescence

Antibody	Dilution	Species raised in
EGFP (Abcam, ab6556)	1:100	rabbit polyclonal IgG
GFAT1 (Epitomics, 3651-1)	1:100	rabbit monoclonal IgG
Alexa Fluor 488 anti-rabbit IgG (Invitrogen, A-21206)	1:500	donkey polyclonal IgG
Alexa Fluor 568 anti-rabbit IgG (Invitrogen, A-11011)	1:500	goat polyclonal IgG

2.4.12. AChR and AChE detection on muscle sections

AChR and acetylcholinesterase (AChE) were detected on muscle sections by a 1-hour incubation with 1 µg/ml Alexa Fluor 488 or 594 α-BuTx (Invitrogen, B13422, B13423) or Alexa Fluor 488 fasciculin (Invitrogen, custom-made), respectively, diluted in PBS supplemented with 1% BSA. Excess of the neurotoxins was removed by washing 3 times for 10 minutes with PBS. The muscle sections were then fixed by a 20-minute incubation with 3% paraformaldehyde diluted in PBS, and mounted using Dako Faramount mounting medium (Dako, S3025). They were analysed by widefield or confocal fluorescence microscopy using an Olympus X71 Fluorescence Microscope and a SimplePCI software, or a Zeiss 780 Inverted Microscope and a ZEN 2012 Lite software, respectively.

2.4.13. N-acetylgalactosamine detection on muscle sections

10 µm-thick tibialis anterior muscle sections were fixed by a 20-minute incubation in 3% paraformaldehyde diluted in PBS and permeabilised by a 5-minute incubation with 0.1% Triton X-100 in PBS. The permeabilised sections were incubated for 1 hour with 50 µg/ml TRITC-VVA-B_4 (EY Laboratories Inc., R-4601-2) diluted in PBS supplemented with 1% BSA. The slides were washed 3 times for 10 minutes to remove excess of TRITC-VVA-B_4, and mounted using Dako Faramount mounting medium

(Dako, S3025). They were analysed by fluorescence microscopy using an Olympus X71 Fluorescence Microscope and a SimplePCI software.

2.4.14. Immunofluorescence labelling of teased muscle fibres

To explore the structure and innervation of neuromuscular junctions (NMJ) in mouse skeletal muscles in greater detail, extensor digitorum longus muscles were dissected and fluorescently labelled. The muscles were pinned out on Sylgard 184 and incubated for 30 minutes with fluorescent Alexa Fluor 488 or 594 α-BuTx (Invitrogen, B13422 or B13423) diluted 1:150 in PBS. Excess toxin was removed by 6 times 10-minute washing of the muscles with PBS. The muscles were fixed by a 30-minute incubation in 1% paraformaldehyde in PBS and washed overnight at 4^{o}C with PBS.

Each muscle was divided into four separate bundles and dehydrated by subsequent 10-minute incubations in prechilled 100% ethanol and 100% methanol at -20^{o}C. The dehydrated fibres were permeabilised by a 15-minute incubation in 0.1% Triton X-100 in PBS. The reagent was removed by washing with PBS for 2 hours with at least 3 changes of the buffer. Then the muscles were incubated overnight at 4^{o}C with primary antibodies diluted in PBS supplemented with 3% BSA. Excess of the antibodies was removed by 12 times 10-minute washing with PBS and the fibres were incubated for 3 hours with secondary antibodies diluted in PBS supplemented with 3% BSA. The labelled muscles were washed overnight at 4^{o}C in PBS and mounted on glass slides using Dako Faramount mounting medium (Dako, S3025). The antibodies used for the labelling are specified in Table 2.9. The labelled muscles were analysed by confocal microscopy using a Zeiss 780 Inverted Microscope and a ZEN 2012 Lite software.

Table 2.9. Antibodies used in labelling of teased skeletal muscle fibres

Antibody	Dilution	Species raised in
GFAT1 (Epitomics, 3651-1)	1:250	rabbit monoclonal IgG
Alexa Fluor 594 anti-rabbit IgG (Invitrogen, A21207)	1:500	donkey polyclonal IgG

2.4.15. Staining for type I and type II muscle fibres

The proportion of type I and type II fibres in mouse extensor digitorum longus, soleus and tibialis anterior muscles was estimated using immunohistochemistry. The dissected muscles were snap-frozen in liquid nitrogen-isopentane and sectioned into 10 µm-thick transverse sections using a cryostat (Leica, CM1900). The sections were mounted on glass slides and dried under vacuum. Before immunolabelling, the sections were rehydrated, fixed by a 20-minute incubation in 1% paraformaldehyde in PBS and blocked for 20 minutes with 5% foetal calf serum/normal rabbit serum (FCS/NRS) in PBS. Primary antibodies were diluted 1:50 in 1% FCS/NRS in PBS and incubated with the sections for 1 hour at room temperature. Excess of the immunoglobulins was removed by washing 3 times for 5 minutes with PBS. The rinsed sections were incubated for 30 minutes at room temperature with HRP-conjugated secondary antibodies diluted 1:100 in FCS/NRS in PBS. The antibodies were washed off by rinsing the slides 3 times for 10 minutes with PBS and the peroxidase activity was developed using 3-amino-9-ethylcarbazole (AEC) (Sigma, A5754). A mixture of 14 ml sodium acetate (NaAc) buffer (0.1 M, pH5.2), 1 ml AEC in dimethylformamide (DMF) (5 mg/ml) and 9 µl H_2O_2 was prepared, filtered before use, and applied to the slides. After 10 minutes, the slides were rinsed and mounted using Dako Faramount mounting medium (Dako, S3025). All antibodies applied in the procedure are specified in Table 2.10. The slides were analysed by light microscopy.

The proportion of type I and type II fibres was determined by counting labelled and unlabelled fibres in the central part of each muscle section on 20 images taken at 10x magnification.

Table 2.10. Antibodies used in staining for type I and type II muscle fibres

Antibody	Dilution	Species raised in
anti-myosin heavy chain (fast) (Novocastra, NCL-MHCf)	1:50	mouse monoclonal IgG
anti-myosin heavy chain (slow) (Novocastra, NCL-MHCs)	1:50	mouse monoclonal IgG
anti-mouse immunoglobulins/HRP (DakoCytomation, P0447)	1:100	goat polyclonal IgG

2.4.16. GFAT1 enzymatic activity assay

2.4.16.1. Glutamate dehydrogenase method

Enzymatic activity of GFAT1 over-expressed in HEK293TSA cells was determined by monitoring the formation of L-glutamate (L-Glu) in a coupled assay employing glutamate dehydrogenase (GDH) (Ye et al., 2004) (Figure 2.1.).

The experiment was started by transfecting HEK293TSA cells with plasmids encoding GFAT1-L with or without 3'UTR, or pcDNA™3.1/Hygro$^{(-)}$ as a negative control. 48 hours after transfection, the cells were harvested, washed with PBS, and homogenised in 200 µl lysis buffer (50 mM KH_2PO_4/K_2HPO_4, 10 mM EDTA, 12 mM glucose-6-phosphate (Glc-6-P), 5 mM reduced L-glutathione (GSH), 1 mM phenylmethylsulphonyl fluoride (PMSF), pH7.6). The lysates were then cleared by centrifugation, first for 5 minutes at 5000rpm at 4ºC and then for 30 minutes at 14000rpm at 4ºC. Following that, the protein concentration in the samples was determined using a Pierce™ BCA Protein Assay Kit (Thermo Scientific, 23227) and 100 µg protein samples were brought up to 100 µl volume with the lysis buffer. The samples were transferred into a 96-well plate, mixed with 80 µl reaction buffer

(100 mM KH_2PO_4/K_2HPO_4, 50 mM KCl, 10 mM D-fructose-6-phosphate (D-Fru-6-P), 6 mM L-glutamine (L-Gln), 0.3 mM 3-acetylpyridine-adenine dinucleotide (APAD), 6U GDH, pH7.6) and incubated for 90 minutes at 37°C. All the reagents, unless otherwise stated, were purchased from Sigma. The changes in the absorbance caused by the reduction of APAD were measured at the wavelength of 370 nm by a microplate spectrometer (μQuant, BIO-TEK Instruments, Inc.).

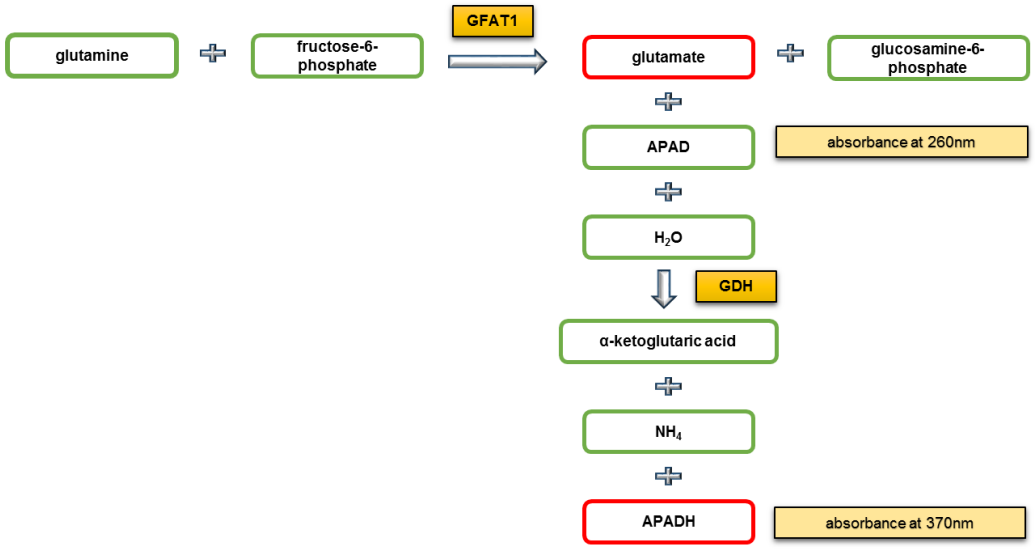

Fig.2.1. Schematic representation of the application of the GDH method for the determination of glutamate in the reaction catalysed by GFAT1
APAD – 3-acetylpyridine-adenine dinucleotide
GDH – glutamate dehydrogenase

2.4.16.2. The Morgan-Elson method

Enzymatic activity of GFAT1 over-expressed in a bacterial system was determined using the Morgan-Elson method in collaboration with Prof. Slawomir Milewski at Gdansk University of Technology.

2.4.16.2.1. Protein production and purification

Escherichia coli Rosetta (DE3) pLysS (F^- *ompT* $hsdS_B(r_B^- m_B^-)$ *gal dcm* (DE3) pLysSRARE (Cam^R)) strain was transformed with pET-22b(+) plasmids encoding

respective GFAT1 and GFAT1-L variants. The cells were grown for 10 hours at 37^{o}C in 10 ml LB medium supplemented with 100 µg/ml ampicillin. Then 4 ml of the culture was transferred to 800 ml fresh LB medium supplemented with 100 µg/ml ampicillin and the cells were grown until the culture reached optical density (OD)=0.5 (measured at a wavelength of 600 nm using a spectrophotometer). Then the protein expression was induced using 0.1 mM isopropyl β-D-1-thiogalactopyranoside (IPTG) and the cells were cultured for 8 hours at 37^{o}C in a rocking incubator.

To collect the cells, the culture was centrifuged for 15 minutes at 3500rpm. The cell pellets were resuspended in 10 ml of buffer A (25 mM KH_2PO_4/K_2HPO_4, 0.5 mM PMSF, 1 mM dithiothreitol (DTT), 1 mM EDTA, pH7.0) and sonicated (three 30-second pulses at 30% amplitude) on ice. The mixtures were centrifuged for 20 minutes at 12000rpm at 4^{o}C and the supernatants were collected.

DNA was removed from the samples by the addition of streptomycin sulphate to a final concentration of 1.1%. The samples were mixed on ice during the entire procedure and for 15-30 minutes afterwards. Then the mixtures were centrifuged for 20 minutes at 12000rpm at 4^{o}C and the supernatants were collected.

Protein was precipitated from the samples by the addition of ammonium sulphate ($(NH_4)_2SO_4$) to a final concentration of 60%. The mixtures were then centrifuged for 20 minutes at 12000rpm at 4^{o}C. The pellets were resuspended in 10 ml buffer A supplemented with 40 mM NaCl and 10 mM $MgCl_2$, and mixed on ice for 10 minutes. The samples were centrifuged for 10 minutes at 12000rpm at 4^{o}C and the supernatants were collected.

Ammonium sulphate was removed from the supernatants using Amicon® Ultra-15 Centrifugal Filter Units (Millipore, UFC901008). The samples were applied on the columns and the tubes were filled to the top with buffer A. They were then centrifuged

for 10 minutes at 3500rpm at 4°C several times, until the volumes of the samples reached approximately 3-5 ml. Then the tubes were filled once again with buffer A and the entire procedure was repeated two more times. The ammonium sulphate-free samples were collected and GFAT1 was purified by fast performance liquid chromatography (FPLC) on a ResourceQ column.

2.4.16.2.2. Ion exchange chromatography using a ResourceQ column

Before the purification of GFAT1, a ResourceQ (FPLC) column (GE Healthcare Life Sciences) was preconditioned using buffer B (20 mM KH_2PO_4/K_2HPO_4, pH7.0). Samples were loaded on the column and the protein was eluted using a linear gradient of 0-0.4 M NaCl in buffer C (20 mM KH_2PO_4/K_2HPO_4, 1 M NaCl, pH7.0). The flow rate was 20 column volumes per minute. Eluted 2 ml fractions were collected and divided into subgroups based on the obtained chromatogram. The activity of GFAT1 in each subgroup was measured to determine which one contained the purified enzyme.

2.4.16.2.3. The Morgan-Elson assay

The enzymatic activity of GFAT1 purified by ion exchange chromatography was measured using the Morgan-Elson method (Elson and Morgan, 1933) (Figure 2.2.). Standard reaction mixtures contained 40 µl 100 mM L-Gln, 40 µl 75 mM D-Fru-6-P, 30-100 µl enzyme and the appropriate amount of buffer A (25 mM KH_2PO_4/K_2HPO_4, pH7.0, 0.5 mM PMSF, 1 mM DTT, 1 mM EDTA) to a final volume of 400 µl. When it was necessary to determine the Michaelis constant (K_M) and the maximum initial velocity (V_{max}), the substrate concentrations varied from 0 mM to 11.25 mM for Fru-6-P and from 0 mM to 5 mM for Gln. A positive control contained 40 µl 100 mM

glucosamine-6-phosphate ($GlcNH_2$-6-P) and 360 µl buffer A. A negative control contained 400 µl buffer A. The reaction mixtures were incubated for 30 minutes at 37°C. Then the reactions were terminated by a 1-minute incubation at 100°C. The samples were cooled and mixed with 200 µl saturated $NaHCO_3$ solution and 100 µl 10% acetic anhydrate in acetone, and incubated for 3 minutes at room temperature. They were then kept for 3 minutes at 100°C, cooled and mixed with 200 µl $K_2B_4O_7$ (0.8 M) and incubated again for 3 minutes at 100°C. Following the incubation, the samples were cooled and mixed with 5 ml of solution prepared by mixing 1 g 4-(dimethyl amino)benzaldehyde (ADAB), 100 ml acetic acid and 1.5 ml hydrochloric acid. The mixtures were then incubated for 20 minutes at 37°C and the absorbance at a wavelength of 585 nm, corresponding to the amounts of $GlcNH_2$-6-P, was measured using a spectrophotometer. All chemicals, unless stated otherwise, were purchased from Sigma.

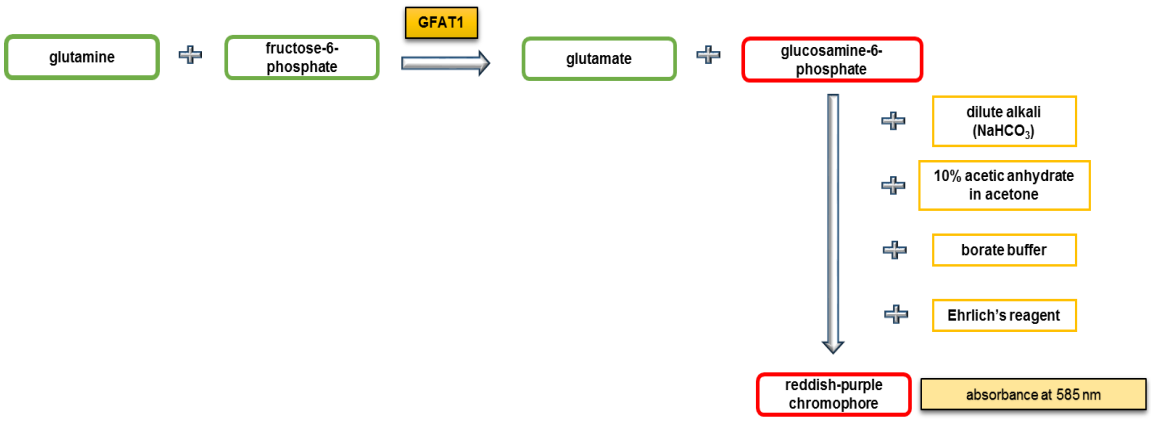

Fig.2.2. Schematic representation of the application of the Morgan-Elson method for the determination of glucosamine-6-phosphate in the reaction catalysed by GFAT1
Ehrlich's reagent – 4-(dimethylamino)benzaldehyde (ADAB) acidified with hydrochloric acid

2.5. Cell culture

2.5.1. Human skeletal muscle cell culture

2.5.1.1. Growth conditions

Wild type (control) human skeletal muscle cells and muscle cells derived from biopsies taken from *GFPT1* patients were grown in Corning® Cell Culture flasks in Skeletal Muscle Cell Growth Medium (Cell Applications, 151K-500) supplemented with antibiotics (penicillin, streptomycin, amphotericin B) (Invitrogen, 15240-062). This medium was later replaced with Skeletal Muscle Growth Medium (Promocell, C-23060) supplemented with 10% FCS (Sigma, F2442) and antibiotics since this medium was recommended by MRC Centre for Neuromuscular Disease BioBank, London, and appeared to increase a cell division rate. If necessary, cells were cultured in serum-free medium (Cell Progen, M36077-03S) supplemented with antibiotics. The non-immortalised cells were grown at 37ºC and the immortalised ones at 33ºC in a humidified 5% CO_2 incubator.

2.5.1.2. Differentiation conditions

Myoblasts were differentiated into multinucleated myotubes in order to replicate the formation of muscle fibres. They were plated into 6-well (CLS3516-50EA) or 24-well Corning® Costar® Cell Culture plates (CLS3527-100EA) tissue culture plates at the density of $4x10^5$/well or $6x10^4$/well, respectively, and fusion of the myoblasts was induced by serum starvation. Three different differentiation media were tested: DMEM (Sigma, D6429) supplemented with 2% FCS (Sigma, F2442), 2% FCS and 10 µg/ml insulin (Sigma, I6634) or 2% HS (Sigma, H1138) and 10 µg/ml insulin and antibiotics (penicillin, streptomycin, amphotericin B) (Invitrogen, 15240-062). The supplementation of the medium with insulin was tried since the peptide has been

reported to be required for an optimal performance of serum-free media (Florini and Roberts, 1979). It has been shown to have pleiotropic anabolic effects on mammalian cells, promoting glucose and amino acid uptake, lipogenesis, monovalent cation and phosphate transport, and protein and nucleic acid synthesis (Wilcox, 2005). The performance of the media was assessed by comparing times needed for the formation of the myotubes, their stability and their capacity to form AChR clusters following the treatment with AGRN.

It was observed that, regardless of the medium used, the myotubes were formed in 5 days. However, they appeared to be more stable and more capable of forming AChR clusters when the medium was supplemented with insulin. Based on the above observations, for most experiments, DMEM supplemented with 2% FCS was used. Only for the ones which required a longer culture time or the AChR cluster formation the medium was supplemented with 10 µg/ml insulin.

2.5.1.3. Selection of myoblasts

To obtain myoblast-enriched cell cultures, primary cultures were selected based on the expression of neural cell adhesion molecule (NCAM, CD56) by an immunomagnetic selection method. 50 µl sheep anti-mouse magnetic beads (Invitrogen, 1201-D) were incubated with 1 µg mouse monoclonal anti-human CD56 antibodies (AbD Serotec, MCA591XZ) for 30 minutes and washed with PBS. The antibody-coated magnetic beads were added to $2.5x10^6$ cells resuspended in growth medium supplemented with 200 mM HEPES and the cells were incubated with the beads for 1 hour at 4^oC with gentle rotation. The beads were washed 3 times with the growth medium, resuspended in 5 ml fresh growth medium and transferred to new tissue culture flasks.

2.5.1.4. Immortalisation of human primary myoblasts

Human primary myoblasts were immortalised by infection with *Simian virus* 40 (SV40) expressing simian virus T antigen. The cells were incubated with 1 ml adenovirus (10^6 cfu/ml) for 90 minutes at 37ºC in a humidified 5% CO_2 tissue culture incubator. The virus was then removed and replaced with fresh growth medium. The transduced cells were cultured at 33ºC in a humidified 5% CO_2 incubator.

2.5.2. Human primary fibroblast culture

2.5.2.1. Growth conditions

Human fibroblasts derived from skin, muscle or thymus biopsies were grown in Corning® Cell Culture flasks in DMEM (Sigma, D6429) supplemented with 12% FCS (Sigma, F2442) and antibiotics (penicillin, streptomycin, amphotericin B) (Invitrogen, 15240-062) in a humidified 5% CO_2 incubator at 37ºC. If required, the cells were cultured in FM-sf serum-free medium (ScienCell, 2311) supplemented with antibiotics.

2.5.3. Amplification of adenovirus SV40

SV40 adenovirus was amplified in HEK293TSA. The cells were seeded in 75 cm^2 Corning® Cell Culture flasks (Corning, CLS430641-100EA) and infected with the adenovirus by a 1-hour incubation with the virus diluted in DMEM (Sigma, D6429) supplemented with ultra-low IgG FCS (Invitrogen, 16250-086). The virus was removed, replaced with fresh medium and the cells were cultured for 72 hours at 37ºC, 5% CO_2. The medium was collected and centrifuged for 10 minutes at 2000rpm to remove cell debris. Supernatant containing the adenovirus (10^6 cfu/ml) was stored at -80ºC.

2.5.4. Production of recombinant AGRN

AGRN, used for the stimulation of AChR clustering *in vitro*, was produced in HEK293TSA. The cells were transfected with pcDNA-*AGRN* vector, which encoded a full-length human AGRN. 12 hours after the transfection, the growth medium was refreshed and the cells were cultured for 72 hours at 37ºC, 5% CO_2. After incubation, the medium was collected and cleared of cell debris by a10-minute centrifugation at 2000rpm. The clarified AGRN-containing medium was stored at -80ºC in aliquots.

2.6. *in vivo* methods

2.6.1. Transgenic mice and genotyping

C57BL/6 mice lacking the expression of an endogenous AChR ε subunit, but instead expressing human AChR γ under a muscle α-actin promoter were applied as a model of CMS (Cossins et al., 2004). The animals were obtained by crossing human AChR γ subunit cDNA into a mouse *Chrne*$^{-/-}$ (msε$^{-/-}$) background. In order to confirm the genotype of the generated litters, the mice were ear-clipped and the DNA was extracted from the tissue using DirectPCR® Extraction Reagent (ViagenBiotech, 401-E) (Appendix, section I.1.3.). The DNA corresponding to the *Chrne* gene and AChR γ subunit cDNA, and to a neomycin resistance gene (*neo*) was amplified by PCR. The presence of the neomycin resistance gene would indicate the targeted disruption of the *Chrne* gene. The amplification was performed using MegaMix-Blue (Microzone$^{\mu}$, 2MMB) and the primers specified in Table 2.11. Only *Chrne*$^{-/-}$, *neo*$^{+/+}$, AChR γ cDNA^{+} (msε$^{-/-}$neo$^{+/+}$hγ^{+}) animals were used in subsequent experiments as disease models.

Table 2.11. Primers used for genotyping
The sequences are shown from 5' to 3'.

Target	Primer name	Primer sequence
CHRNG	***CHRNG* F**	GAGTTAGGGCTGAGCCAGTTCTGTG
CHRNG	***CHRNG* R**	GTCTGGTGAGGGCAGGTAGGGGCGTG
Chrne	***Chrne* F**	CTCTTCGACAATTATGATCCAGA
Chrne	***Chrne* R**	GAGCCGATAGTCGTGCCAGT
neo	***neo* F**	CAACAGACAATCGGCTGCTCT
neo	***neo* R**	GAATGGGCAGGTAGCCGGAT

2.6.2. Drug administration

2.6.2.1. Treatment with chemical drugs

6-week-old CMS mouse models ($ms\varepsilon^{-/-}neo^{+/+}h\gamma^{+}$) were treated with drugs commonly used for myasthenic syndromes, pyridostigmine bromide (Sigma, 29797) and/or salbutamol sulphate (Sigma, 59803). Both medicines were administered orally in drinking water. The doses used were 7 mg/kg/day of pyridostigmine bromide and 45 mg/kg/day of salbutamol sulphate. The following treatment regimens were tested:

- 4-week treatment with pyridostigmine bromide followed by 6-week treatment with a combination of pyridostigmine bromide and salbutamol sulphate
- 10-week treatment with pyridostigmine bromide

2.6.2.2. Inverted screen test

The muscle strength of control and treated animals was assessed using an inverted screen test. The test involved hanging an animal upside-down on a 40-cm-square wire grid held 40 cm above a padded surface and measuring the length of time each animal was able to hold on. Three subsequent attempts without resting were recorded and summed.

Chapter 3

Pathogenicity of mutations in GFAT1 and GFAT1-L

3.1. Introduction

L-glutamine:D-fructose-6-phosphate amidotransferase 1 (GFAT1) is a complex enzyme, which exists in two isoforms translated from distinct, tissue-specific, alternatively spliced mRNA transcripts (*GFPT1* and *GFPT1-L*) (DeHaven et al., 2001, Niimi et al., 2001). A growing interest in the enzyme has resulted from the implication of the protein in the susceptibility to diabetes mellitus and diabetic nephropathy (Elbein et al., 2004), and very recently also in the pathogenesis of congenital myasthenic syndrome (CMS) (Senderek et al., 2011). However, it remains unclear how identified mutations and single nucleotide polymorphisms (SNPs) may affect molecular properties of the protein. The only available data on the consequences of the SNPs come from studies of the association of the identified polymorphisms with obesity, intramyocellular lipid content (Weigert et al., 2005), diabetes and diabetic nephropathy (Elbein et al., 2004, Kunika et al., 2006). The research has revealed the presence of a number of tissue-specific regulatory regions in the *GFPT1* promoter in mesangial cells and in C2C12 myotubes. The tissue-specificity has been implied by distinct functional effects of two SNPs in the promoter region (-913G/A and -1412G/C) on the expression of *GFPT1* mRNA (Burt et al., 2005). Potential regulatory elements have also been described in the 3' untranslated region (3'UTR), where 61804C/T SNP has been found to be associated with diabetes and diabetic nephropathy in the Caucasian population. This SNP potentially leads to an increased expression of *GFPT1*, thus an increased glucose flux through the

hexosamine biosynthetic pathway, in patients diagnosed with diabetic nephropathy (Elbein et al., 2004). In contrast with the diabetic patients, the *GFPT1* CMS-affected individuals have been shown to exhibit lower levels of GFAT1 and GFAT1-L in skeletal muscle (Senderek et al., 2011). However, since more than 9-fold disease-unrelated variations in *GFPT1/18S* RNA ratios have been reported among different individuals (Elbein et al., 2004), the data need to be confirmed by analysing molecular consequences of the pathogenic mutations in a model system. Missense changes may affect the expression of *GFPT1* and *GFPT1-L* mRNA transcripts by altering their processing or stability. Both processes are dependent on cis-elements in the RNA, located not only in the 5' and 3' UTR, but also in the coding sequence, as well as on trans-acting factors (Brennan and Steitz, 2001). The most comprehensively studied elements are located in the 3'UTR and are known as AU-rich elements (ARE). They consist of the stretches of adenylate and uridylate residues and target mRNA for a rapid degradation (Chen and Shyu, 1995). Such elements are also present in the *GFPT1* 3'UTR. Another important aspect of the pre-mRNA processing is an excision of introns and a subsequent ligation of exons. The splicing occurs through an action of a ribonucleoprotein complex referred to as a spliceosome. It depends on a recognition of specific sequences at the exon/intron boundaries and on silencer and enhancer elements present in introns as well as in exons (De Conti et al., 2013), hence any nucleotide changes can affect the splicing and result in the exon or intron inclusion or exclusion.

A mature mRNA transcript is further translated to the amino acid sequence, which determines the formation of the secondary, tertiary and quaternary structures of the target protein. The correct structure is essential for the function of molecules. There are a number of factors that contribute to the protein folding process. The most

important are forces between residues within the amino acid chain, such as hydrogen bonds, van der Waals, electrostatic and hydrophobic interactions. These depend on physical properties of the residues within the amino acid sequence (Dill and MacCallum, 2012). The acquisition of a correct quaternary structure is indispensable for the enzymatic activity of GFAT1 and GFAT1-L, which both exist in homodimeric (Nakaishi et al., 2009) or homotetrameric (Richez et al., 2007, Huynh et al., 2000) forms, and thus the mutations of the amino acids that occur at the interfaces of the GFAT1 oligomers might potentially influence the formation of the complexes.

Finally, in order to perform their functional role, proteins need to acquire the ability of binding with a number of small molecules. In the case of enzymes, the small molecules include, most importantly, substrates, intermediates and products of a catalysed reaction, and also allosteric regulators. Substrate binding occurs in an active site of an enzyme, which is often formed by evolutionarily conserved residues and is commonly found in the largest or deepest cleft of the molecule, creating an optimal molecular niche for a catalysed reaction. The active site is usually dynamic and undergoes a number of conformational changes after binding the substrates, especially when some amino acids involved in the formation of the site are located within flexible loops. GFAT1 possesses two such sites, one located within the glutaminase domain, responsible for the hydrolysis of glutamine (Gln) to glutamate (Glu), and the other present within the sugar isomerase domain, involved in ketose/aldose isomerisation of the aminosugar phosphate (Milewski, 2002) (Figure 3.1.). The two regions, presenting distinct catalytic functions, are connected by an intramolecular channel, indispensable for the transfer of ammonia (Teplyakov et al., 2001). The mutations identified in the enzyme may lead to alterations in the binding and processing of the substrates or compromise the channelling of ammonia between the domains. They may also alter

regulation of the enzyme by having detrimental effects on its interactions with feedback inhibitors, such as uridine diphosphate N-acetylglucosamine (UDP-GlcNAc) (Kornfeld, 1967) and glucosamine-6-phosphate ($GlcNH_2$-6-P) (Broschat et al., 2002). Since the catalytic properties of GFAT1 are not only regulated by these feedback inhibitors, but also by post-translational modifications, such as cyclic adenosine monophosphate (cAMP)-dependent serine phosphorylation (Eguchi et al., 2009, Li et al., 2007), this regulatory mechanism might also be altered in mutated GFAT1 variants.

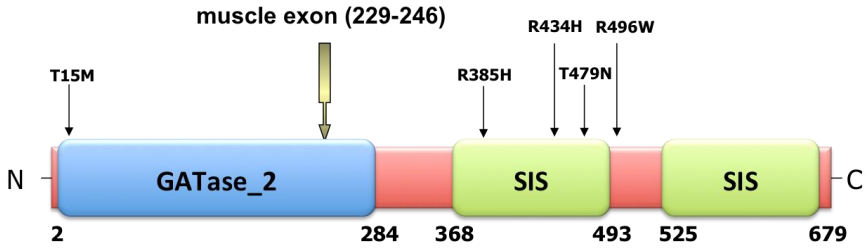

Fig.3.1. Schematic representation of GFAT1 and the location of the mutations analysed in the presented thesis (Zoltowska et al., 2013)
GATase_2 – glutaminase domain type 2
SIS – sugar isomerase domain

The pathogenicity of GFAT1 mutations can be confirmed by investigations into molecular properties of the protein and also by novel sensitive biomarkers of aberrant glycosylation since the enzyme is a key regulator of the hexosamine biosynthetic pathway providing building blocks for glycosylation. The markers include endogenous intercellular adhesion molecule 1 (ICAM1, CD54), which is a glycoprotein that needs to be N-glycosylated for its efficient cell surface expression (He et al., 2012). Patients diagnosed with inherited genetic defects in enzymes responsible for N-linked glycosylation might be expected to have reduced cell surface expression of ICAM1 compared to healthy controls. This would be expected for both types of congenital disorders of glycosylation: type I (CDG-I), resulting from unoccupied glycosylation

sites, and type II (CDG-II), caused by altered processing of attached sugar chains. To date, the marker has only been reported in CDG-I patient fibroblasts (He et al., 2012, Jones et al., 2012). Another potential marker of an aberrant N-glycosylation is a modified endoplasmic reticulum (ER)-localised enhanced green fluorescent protein (EGFP) containing an N-glycosylation consensus sequence (Asn-X-Ser/Thr), which has been introduced by changing threonine to asparagine at the position 147 of EGFP (Figure 3.2.). The occupation of the glycosylation site by an N-glycan impairs green fluorescence. By contrast with ICAM1, this biomarker can be applied only in research into CDG-I. This is consistent with defects in CDG-II affecting the processing, but not the addition, of N-glycans (Losfeld et al., 2012).

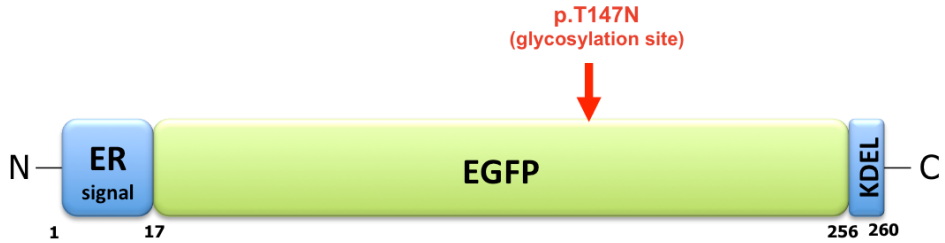

Fig.3.2. Schematic representation of EGFP-Glc-ER – a biomarker of an N-glycosylation site occupancy
EGFP.p.T147N – enhanced green fluorescent protein with an introduced N-glycosylation site
ER signal – signal peptide from calreticulin, targeting to endoplasmic reticulum
KDEL – (lysine-aspartic acid-glutamic acid-leucine) endoplasmic reticulum retention signal

3.2. Patients diagnosed with mutations in *GFPT1*

Two unrelated, white, British individuals (P1 and P2) were diagnosed with *GFPT1* CMS. They were chosen for the studies due to the availability of the cells derived from their muscle biopsies. The patients carried compound heterozygous mutations in GFAT1: p.R385H/R434H and p.T15M/R496W, respectively.

Both of them presented in clinics in their childhood, at age 8 and 6, respectively, with fatiguable muscle weakness (Figure 3.3.). At age 8, P1 lost his ability to run and tended to fall after prolonged exercise. Progression of the disorder made him wheelchair-dependent by the age of 12. Clinical examination revealed a marked weakness of shoulders, hip flexion, elbow and wrist extensors, but facial and ocular muscles were spared. Electromyography on anconeus muscle showed a decrement of compound muscle action potential on repetitive nerve stimulation, and abnormal single fibre electromyography jitter.

Similarly, P2 presented in clinic in his childhood with fatigue and tendency to fall, marked proximal weakness of shoulders and hips, and weakness at the elbow, wrists and small muscles of the hand, but ocular and respiratory muscles were spared. Electromyography examination showed a decrement of compound muscle action potentials following repetitive stimulation at 3 Hz.

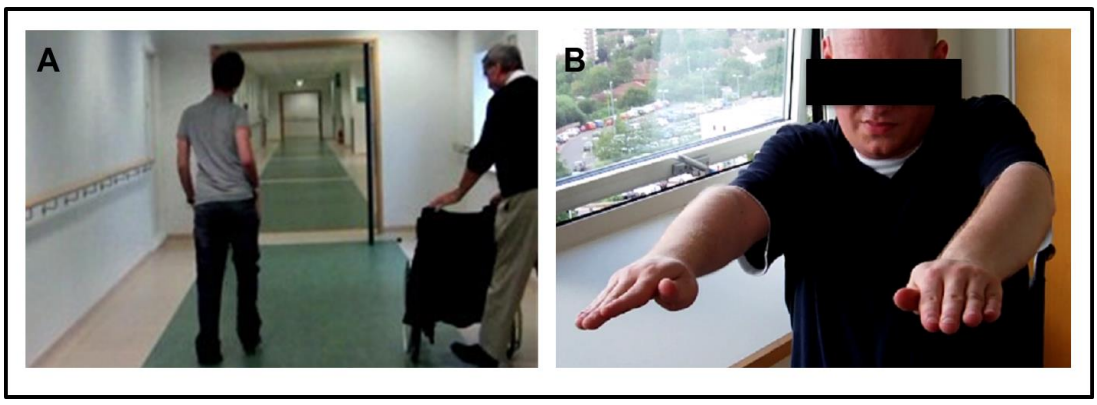

Fig.3.3. Fatiguable weakness of (A) limb-girdle and (B) upper limb muscles in *GFPT1* CMS patients

After the diagnosis of a myasthenic syndrome, acetylcholinesterase (AChE) inhibitor (pyridostigmine) treatment was started in both cases. This was later supplemented with 3,4-diaminopyridine (3,4-DAP), which appeared to stabilise the condition in both patients. Recently, treatment with ephedrine has also been tried and has been found to lead to further significant improvement.

Muscle biopsies obtained from the patients showed presence of tubular aggregates in muscle fibres and an aberrant structure of the neuromuscular junctions (NMJ). Detailed electron microscopy analyses of the intercostal biopsy taken from P2 revealed reduction in postsynaptic folding and in ^{125}I-α-bungarotoxin (^{125}I-α-BuTx) binding to around 25% of control values ($0.25\pm0.1 \times 10^7$/endplate compared to $1.0\pm0.2 \times 10^7$/endplate in control samples, n=8).

Similar symptoms were observed in a number of patients presented in clinics, for whom there was no known underlying genetic cause of the disease. The DNA from these individuals was analysed for the presence of mutations in the *GFPT1* gene. Additionally, one DNA sample, obtained from an individual diagnosed with a multisystem disorder, was analysed since whole exome sequencing pointed towards a homozygous missense change in *GFPT1*.

Despite sequencing all *GFPT1* exons, the *GFPT1* promoter and the 3'UTR, no mutations in the gene were detected in a cohort of patients with tubular aggregates observed on muscle biopsy. By contrast, the sequencing of the DNA obtained from the individual diagnosed with a multisystem disorder confirmed the previous results, indicating the presence of a homozygous change c.1436C>A in *GFPT1*, resulting in a p.T479N amino acid substitution in the GFAT1 protein sequence (Figure 3.4.). To the best of our knowledge, this was the first time that a missense change in the *GFPT1* gene was proposed as a potential cause of a multisystem disorder. This case (P3) was

also included in the investigations due to the availability of skin fibroblasts from the affected individual.

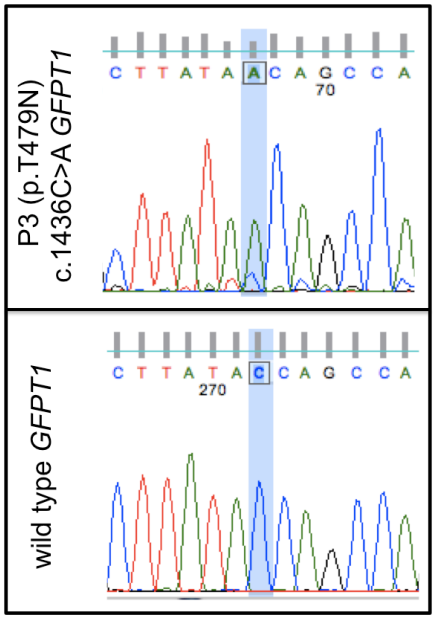

Fig.3.4. Sequencing chromatogram indicating the presence of a homozygous c.1436C>A change in *GFPT1* gene

3.3. Molecular consequences of mutations in GFAT1 and GFAT1-L

Amino acid substitutions in GFAT1 and GFAT1-L may affect various properties of the proteins, including their expression, stability and enzymatic activity, and hence these were analysed both in patient cells and in heterologous expression systems.

3.3.1. Protein levels of GFAT1 and GFAT1-L in human skeletal muscle cells and skin fibroblasts from *GFPT1* patients

GFAT1 protein levels were investigated in wild type, and patient (P1) p.R385H/R434H and (P2) p.T15M/R496W myoblasts and myotubes. The cells were harvested, lysed and the protein extracts were immunoblotted with a rabbit polyclonal anti-GFAT1 antibody. Great care was taken to ensure that any variations in the GFAT1 levels could have not been attributed to an unequal amount of the protein loaded onto the gel. Before electrophoresis, the protein concentration in each sample was estimated using the Pierce™ BCA Protein Assay Kit and, following immunoblotting with an anti-GFAT1 antibody, the membranes were reprobed with a mouse monoclonal anti-α-tubulin antibody. GFAT1 expression was normalised to the α-tubulin amounts (Figure 3.5.).

A

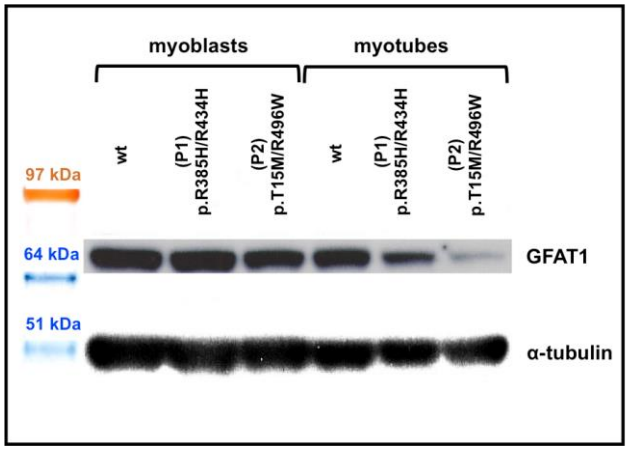

B

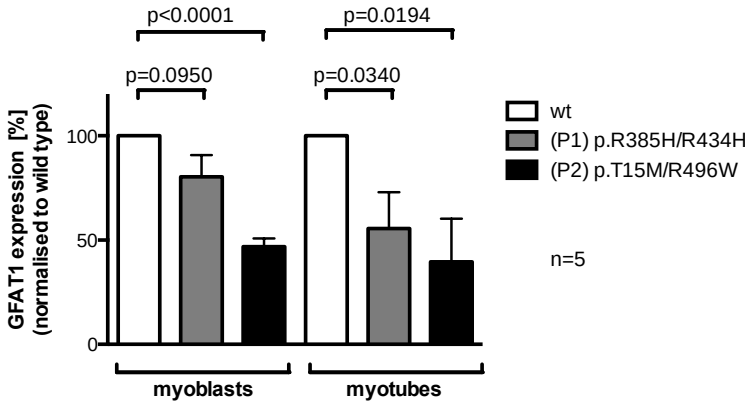

Fig.3.5. GFAT1 expression in wild type and *GFPT1*-mutated myoblasts and myotubes from (P1 and P2) *GFPT1* patients (Zoltowska et al., 2013)
(A) Protein extracts from wild type and *GFPT1*-mutated myoblasts and myotubes were immunoblotted with anti-GFAT1 and anti-α-tubulin antibodies, and the appropriate secondary HRP-conjugated antibodies.
(B) The intensities of the bands were measured by densitometry and GFAT1 expression was normalised to the α-tubulin levels. Each bar represents the mean±SEM GFAT1 protein levels, recorded in n=5 independent experiments, in human skeletal myoblasts and myotubes. All the data are expressed relative to the levels of GFAT1 expression in wild type myoblasts and myotubes, respectively. p values were obtained using a student t-test.

A significant decrease in the GFAT1 protein levels was observed in (P1) p.R385H/R434H myotubes (to 55.54±17.41%, p=0.0340, n=5) and in (P2) p.T15M/R496W myoblasts and myotubes (to 46.88±3.89%, p<0.0001, n=5 and 39.76±20.72%, p=0.0194, n=5, respectively). Thus one potential effect of the mutations is to reduce levels of the GFAT1 expression.

Skin fibroblasts only were available from the (P3) p.T479N patient, and so the effects of the mutation on the GFAT1 protein levels were estimated in the fibroblasts and compared to wild type controls. As the controls, adult dermal fibroblasts derived from a skin biopsy taken from a healthy individual, fibroblasts from the thymuses from two myasthenia gravis (MG) patients and fibroblasts from a skeletal muscle from a downstream of tyrosine kinase 7 (*DOK7*) CMS patient were used.

The estimation of the GFAT1 protein levels in the fibroblasts was performed by extracting protein from the cells, separating it by electrophoresis on a polyacrylamide gel and immunoblotting with a rabbit monoclonal anti-GFAT1 antibody. The membranes were also reprobed with a mouse monoclonal anti-α-tubulin antibody and the intensities of the bands corresponding to GFAT1 were normalised to the α-tubulin levels (Figure 3.6.).

A

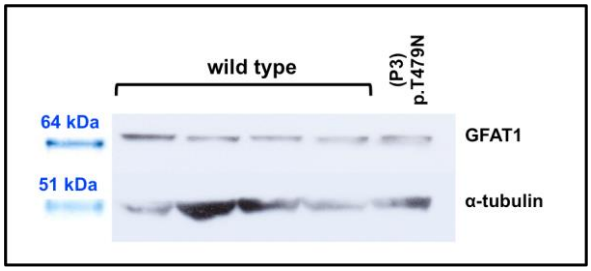

B

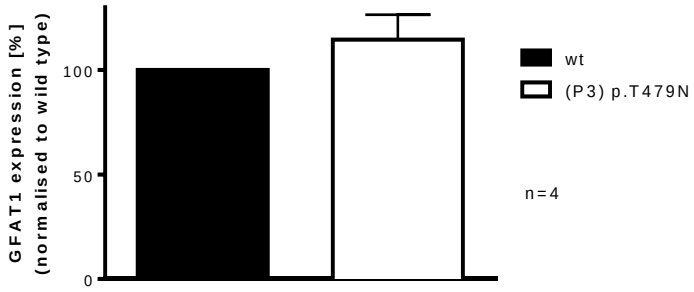

Fig.3.6. GFAT1 expression in wild type and *GFPT1*-mutated fibroblasts from (P3) *GFPT1* patient
(A) Protein extracts from wild type and *GFPT1*-mutated fibroblasts were immunoblotted with anti-GFAT1 and anti-α-tubulin antibodies, and the appropriate secondary HRP-conjugated antibodies.
(B) The intensities of the bands corresponding to GFAT1 and α-tubulin in wild type and (P3) p.T479N human dermal fibroblasts were measured by densitometry. Each bar represents the mean±SEM GFAT1 protein levels, recorded in n=4 independent experiments. All the data are expressed relative to the levels of the GFAT1 expression in the wild type fibroblasts.

The intensity of the bands corresponding to GFAT1 was similar in wild type (lanes 1-4) and (P3) p.T479N (lane 5) fibroblasts. This indicates that the p.T479N substitution does not alter the GFAT1 protein expression, and hence the experiment did not provide evidence of the pathogenicity of this amino acid change.

3.3.2. Over-expression of GFAT1 and GFAT1-L in heterologous expression systems

The analyses of GFAT1 protein levels in patient cells, due to the heterozygosity of the mutations identified in the individuals, did not reveal molecular consequences of the individual amino acid substitutions. This aspect was studied by over-expressing respective GFAT1 and GFAT1-L variants in HEK293TSA cell line and in bacterial cells.

3.3.2.1. Optimisation of GFAT1 and GFAT1-L expression in HEK293TSA cells

Expression of the studied proteins in HEK293TSA cell line was aimed to be achieved by subcloning *GFPT1* and *GFPT1-L* cDNA into pcDNA™3.1/Hygro$^{(-)}$ vector that possesses human cytomegalovirus immediate early promoter (CMV), which drives a high, constitutive expression of target genes. The mutations identified in the *GFPT1* CMS patients (p.T15M, p.R385H, p.R434H and p.R496W) were introduced by site-directed mutagenesis into the GFAT1-L coding sequence. The constructs were then co-transfected with pEGFP-N1 into HEK293TSA cells. The pEGFP-N1 plasmid encoded enhanced green fluorescent protein (EGFP) – a cytoplasmic reporter protein, which gives rise to bright fluorescence that is readily detectable after a short transfection interval (Zhang et al., 1996), and served as a marker of the transfection efficiency. To analyse the expression of GFAT1, protein extracted from the cells was resolved by electrophoresis and immunoblotted with an anti-GFAT1 antibody.

Despite subcloning the *GFPT1* and *GFPT1-L* cDNA into the vector possessing a strong constitutive CMV promoter, the target proteins exhibited a relatively low expression in the transfected HEK293TSA cells. A potential reason for the relatively low expression was the presence of a long 3'UTR in the plasmids. The 3'UTR was

removed from all GFAT1- and GFAT1-L-encoding vectors and HEK293TSA cells were transfected with the constructs without and with the 3'UTR, respectively. The protein was extracted from the cells and immunoblotted with an anti-GFAT1 antibody (Figure 3.7.).

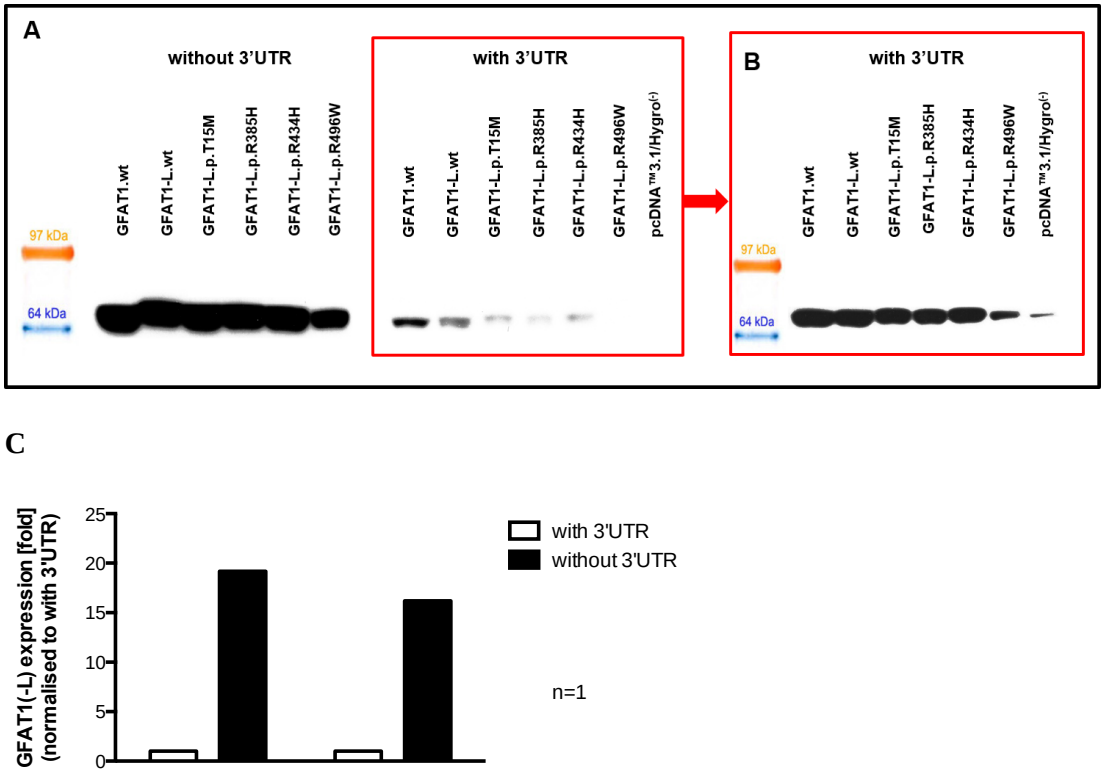

Fig.3.7. Effects of the removal of the 3'UTR on the expression of GFAT1 and GFAT1-L
HEK293TSA cells were transfected with constructs encoding wild type GFAT1 and GFAT1-L, and mutated GFAT1-L variants (A) without or (B) with the 3'UTR, respectively. pEGFP-N1 vector was added to the transfection mixes as a marker of transfection efficiency.
Protein extracted from the cells was immunoblotted with an anti-GFAT1 antibody and the appropriate HRP-conjugated secondary antibody. B shows longer exposure of the western blot.
(C) The intensities of the bands corresponding to wild type GFAT1 and GFAT1-L were measured by densitometry. Each bar represents the GFAT1 and GFAT1-L protein levels, recorded in n=1 experiment, in the transfected HEK293TSA cells. All the data are expressed relative to the levels of GFAT1 or GFAT1-L, respectively, with the 3'UTR.

The intensities of the bands corresponding to GFAT1 over-expressed from the constructs with 3'UTR were lower compared to the GFAT1 over-expressed from the constructs without 3'UTR. This demonstrated that the removal of the 3'UTR led to an increase in the expression of GFAT1 and GFAT1-L. Quantification of the expression

of the wild type GFAT1 and GFAT1-L indicated that the constructs without the 3'UTR exhibited approximately 19 and 16 fold higher expression, respectively, compared to the constructs possessing the long 3'UTR.

Similar low expression levels were found for C-terminally EGFP-tagged GFAT1 and GFAT1-L proteins, so the 3'UTR was also removed from these constructs. To confirm that the removal of the 3'UTR had analogous effects on these vectors, the plasmids were transfected into HEK293TSA cells. A pcDNA-*mCherry* plasmid was added to the transfection mixes to normalise the transfection efficiency. The transfected cells were visualised by fluorescence microscopy (Figure 3.8.).

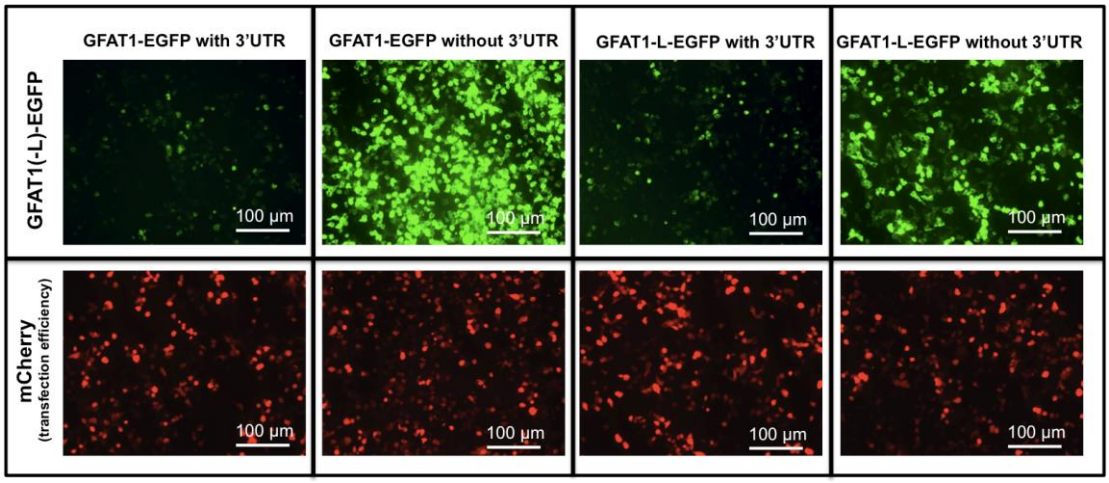

Fig.3.8. Effects of the removal of the 3'UTR on the expression of GFAT1-EGFP and GFAT1-L-EGFP analysed by immunofluorescence
HEK293TSA were co-transfected with GFAT1-EGFP- or GFAT1-L-EGFP-encoding constructs with or without the 3'UTR, respectively and pcDNA-*mCherry* as a marker of the transfection efficiency. Green and red fluorescence of the over-expressed proteins were visualised by fluorescence microscopy.

Green fluorescence of the over-expressed GFAT1-EGFP and GFAT1-L-EGFP, respectively, was much brighter in the cells transfected with the constructs without 3'UTR compared to the ones transfected with the plasmids with 3'UTR. At the same time, no differences in the levels of red fluorescence, corresponding to mCherry, were

observed. This indicated that the removal of the 3'UTR led to a substantial elevation in the expression of both GFAT1-EGFP and GFAT1-L-EGFP.

The expression of the proteins was also analysed by immunoblotting protein lysates obtained from the cells with anti-GFAT1, anti-α-tubulin and anti-mCherry antibodies (Figure 3.9.).

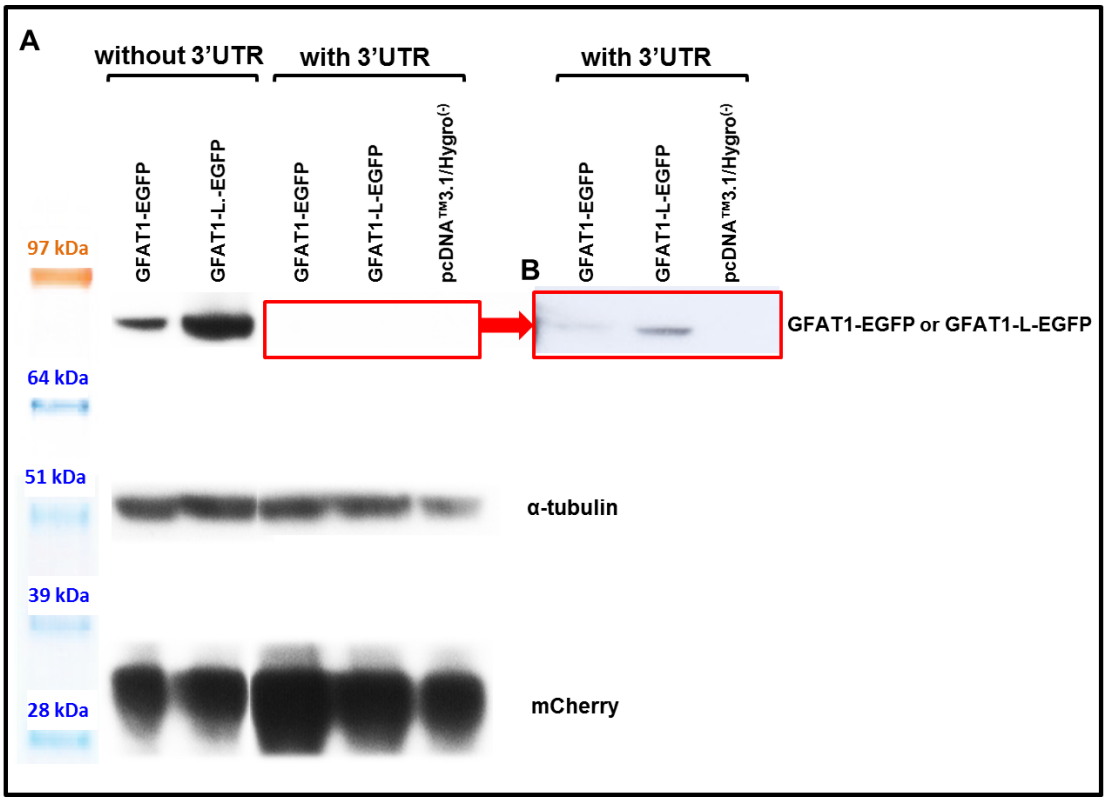

Fig.3.9. Effects of the removal of the 3'UTR on the expression of GFAT1-EGFP and GFAT1-L-EGFP analysed by western blotting
HEK293TSA cells were transfected with constructs encoding wild type GFAT1-EGFP and GFAT1-L-EGFP. mCherry-encoding vector was added to the transfection mixes as a marker of the transfection efficiency.
(A) Protein extracted from the cells was immunoblotted with anti-GFAT1, anti-α-tubulin and anti-mCherry antibodies, and the appropriate HRP-conjugated secondary antibodies.
(B) Longer exposure was needed to visualise the bands corresponding to GFAT1-EGFP and GFAT1-L-EGFP with the 3'UTR.

The intensities of the bands corresponding to GFAT1-EGFP and GFAT1-L-EGFP over-expressed from the constructs without the 3'UTR (lanes 1 and 2) were stronger relative to the bands detected in the cells transfected with the 3'UTR-possessing constructs (lanes 3 and 4). This was consistent with the previous findings, emerging

from the fluorescence microscopy imaging, demonstrating a substantial increase in GFAT1-EGFP and GFAT1-L-EGFP expression following the removal of the 3'UTR. Although GFAT1-L possesses an additional exon and therefore a greater molecular weight than GFAT1, no differences in the migration between the molecules were observed on the polyacrylamide gel. This was probably due to the relatively small size of the additional fragment compared to the entire protein.

3.3.2.2. Effects of the mutations on GFAT1 and GFAT1-L protein levels

The optimised system was used to investigate protein levels of wild type and mutated GFAT1 and GFAT1-L. The untagged GFAT1 and GFAT1-L variants were chosen since the EGFP tag may alter the properties of the proteins. The p.T15M, p.R385H, p.R434H and p.R496W amino acid substitutions were introduced into the muscle-specific isoform (GFAT1-L) since these mutations were identified in the patients who presented with a fatiguable muscle weakness. The p.T479N substitution was introduced into the non-muscle GFAT1 isoform because it had been identified in the siblings diagnosed with a multisystem disorder.

The respective constructs were transfected into HEK293TSA cells, together with a pEGFP-N1 vector as a transfection efficiency control. The cells were collected and lysed, and the protein extracts immunoblotted with an anti-GFAT1 antibody. At the same time, the EGFP fluorescence was quantified using a fluorescence plate reader and the expression of GFAT1 was normalised to the EGFP fluorescence to account for potential differences in the efficiency of the DNA delivery (Figures 3.10. and 3.11.).

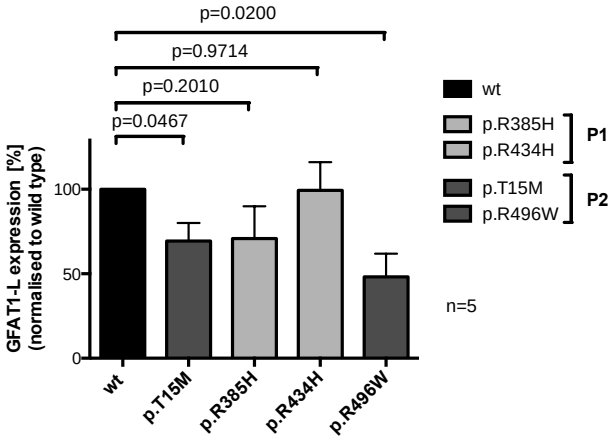

Fig.3.10. Effects of the p.T15M, p.R385H, pR434H and p.R496W mutations on GFAT1-L expression

HEK293TSA cells were transfected with constructs encoding wild type and mutated GFAT1-L variants, respectively. pEGFP-N1 vector was added to the transfection mixes as a marker of transfection efficiency. Protein extracts were immunoblotted with an anti-GFAT1 antibody and the appropriate HRP-conjugated secondary antibody. The intensities of the bands were measured by densitometry and the GFAT1-L expression was normalised to the EGFP fluorescence determined with a fluorescence plate reader. Each bar represents the mean±SEM GFAT1-L protein levels, recorded in n=5 independent experiments, in the transfected HEK293TSA cells. All the data are expressed relative to the levels of the GFAT1-L.wt expression. p values were obtained using a student t-test.

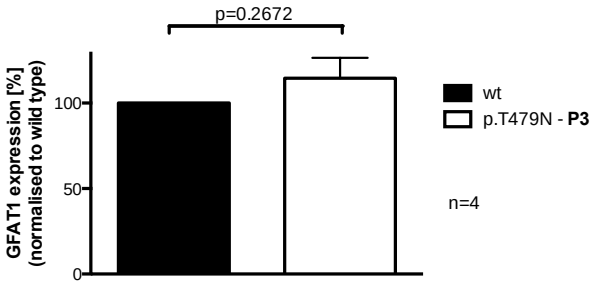

Fig.3.11. Effects of the p.T479N substitution on GFAT1 expression

HEK293TSA cells were transfected with constructs encoding wild type and mutated GFAT1, respectively. pEGFP-N1 vector was added to the transfection mixes as a marker of transfection efficiency. Protein extracts were immunoblotted with an anti-GFAT1 antibody and the appropriate HRP-conjugated secondary antibody. The intensities of the bands were measured by densitometry and the GFAT1 expression was normalised to the EGFP fluorescence determined with a fluorescence plate reader. Each bar represents the mean±SEM GFAT1 protein levels, recorded in n=4 independent experiments, in the transfected HEK293TSA cells. All the data are expressed relative to the levels of the GFAT1.wt expression. p value was obtained using a student t-test.

Quantification of the over-expression of different GFAT1-L variants in HEK293TSA cells demonstrated that GFAT1-L.p.T15M and GFAT1-L.p.R496W exhibited significantly reduced expression (by 30.60±10.76%, p=0.0467, n=5 and by 51.87±13.84%, p=0.0200, n=5, respectively) compared to wild type GFAT1-L. By contrast, no statistically significant differences were observed between wild type

GFAT1-L and the two other analysed mutants: GFAT1-L.p.R385H and GFAT1-L.p.R434H. Similarly, no noticeable alterations in the expression of GFAT1.p.T479N compared to GFAT1.wt were found. However, due to the semi-quantitative nature of western blotting experiments, caution is needed in the interpretation of the obtained data, especially for the p.T15M substitution, which only modestly decreased the expression of GFAT1-L, with the result just reaching the statistical significance ($p=0.0467$, $n=5$).

3.3.2.3. Changes in the protein stability of the mutated GFAT1-L variants

To assess whether the decreased protein levels resulted from the changes in the protein stability upon the introduction of the mutations (p.T15M, p.R385H, p.R434H, p.R496W), a cycloheximide (CHX) assay was performed. The assay was conducted by transfecting HEK293TSA cells with constructs encoding wild type and the mutated GFAT1-L variants, and subsequently inhibiting protein synthesis by the addition of CHX to the growth medium to a final concentration of 20 µg/ml. The cells were collected at 0, 4, 6, 8 and 24 hours after the addition of CHX, lysed and the protein lysates were immunoblotted with an anti-GFAT1 antibody. The intensities of the bands corresponding to GFAT1-L were measured and normalised to the initial expression (considered as 100%) of the respective GFAT1-L variant (Figure 3.12.).

A

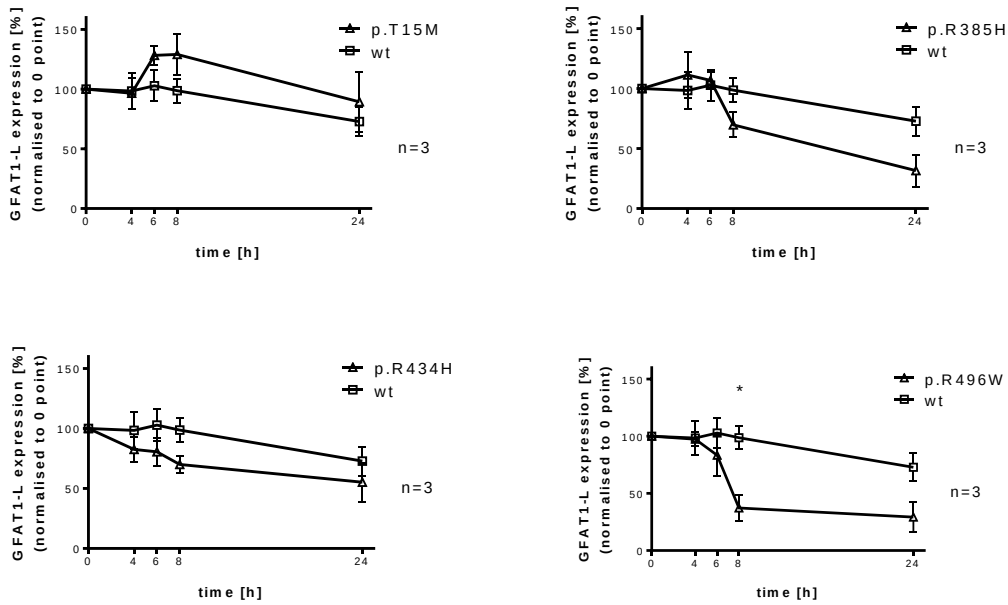

B

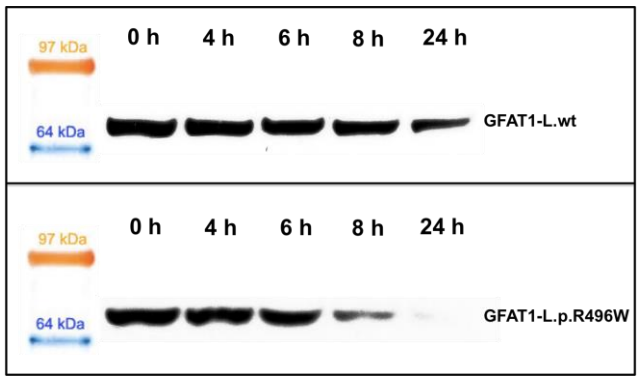

Fig.3.12. Effects of the mutations on GFAT1-L stability
HEK293TSA cells were transfected with plasmids encoding wild type and mutated GFAT1-L variants, respectively. 36 hours after the transfection, CHX (20 µg/ml) was added to the growth medium. The cells were collected at 0, 4, 6, 8 and 24 hours after the addition of CHX, lysed and the protein lysates were immunoblotted with an anti-GFAT1 antibody and the appropriate HRP-conjugated secondary antibody.
(A) The intensities of the bands in n=3 independent experiments were measured by densitometry and plotted on the graphs. The expression of the proteins at 0 time points was considered as 100%. The data were analysed using 2-way ANOVA statistics with Bonferroni multiple comparison post-test.
(B) The protein levels of relatively unstable GFAT1-L variant with p.R496W substitution decreased significantly faster compared to wild type GFAT1-L following the addition of CHX.

Figure 3.12. shows that the intensities of the bands corresponding to GFAT1-L.pR496W decreased faster over time compared to the wild type protein.

When their densities were quantified, it was found that the protein levels of GFAT1 with the p.R496W substitution were 62.26±15.32%, $p<0.05$, $n=3$ lower 8 hours after the addition of CHX, compared to the wild type. This suggested that the half-life of GFAT1-L.p.R496W was significantly reduced relative to the wild type control.

3.3.2.4. Effects of the mutations on GFAT1-L homo-oligomerisation

Analysis of the GFAT1 3D structure reveals that the enzyme is active as a homodimer (Nakaishi et al., 2009) or a homotetramer (Richez et al., 2007). *GFPT1* mutations, especially those occurring at the residues comprising the oligomer interfaces, may affect the formation of a stable and enzymatically active GFAT1 complex. The formation of the oligomer by wild type and mutated GFAT1-L was investigated by native western blotting, which uses electrophoresis to separate native proteins according to their molecular weight and 3D structure.

The experiments were conducted by transfecting HEK293TSA cells with wild type and mutated GFAT1-L-encoding plasmids. The constructs possessing 3'UTR were chosen for the investigations since the very high expression of GFAT1-L from the vectors lacking the 3'UTR might have resulted in a non-specific aggregation of the over-expressed proteins. 48 hours after the transfection, the cells were harvested, lysed and the protein extracts were resolved by non-denaturating electrophoresis, and immunoblotted with a rabbit monoclonal anti-GFAT1 antibody. Additionally, before the incubation with the immunoglobulins, the western blot membranes were stained with Ponceau S in order to visualise the NativeMark™ unstained protein standard and to ensure an equal transfer of the protein from the gel to the polyvinylidene difluoride (PVDF) membrane (Figure 3.13.).

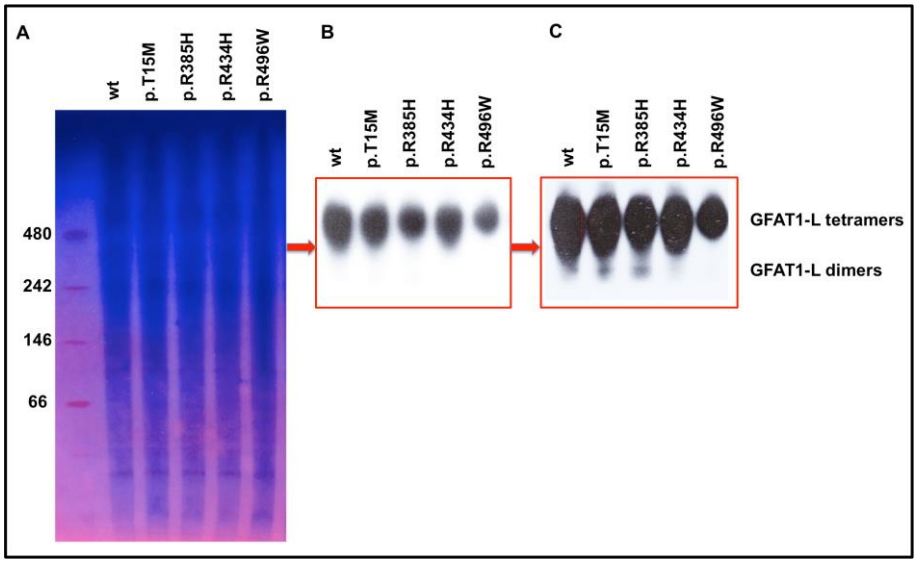

Fig.3.13. Effects of the mutations on GFAT1-L homo-oligomerisation
HEK293TSA cells were transfected with constructs encoding wild type and mutated GFAT1-L variants, respectively.
(A) Protein extracted from the cells was resolved by non-denaturating electrophoresis and transferred onto a PVDF membrane, which was stained with Ponceau S.
(B) The membranes were immunoblotted with an anti-GFAT1 antibody and the appropriate HRP-conjugated secondary antibody.
(C) A longer exposure was needed to visualise the GFAT1-L dimers.

As depicted in Figure 3.13., GFAT1-L migrated as two distinguishable bands, potentially corresponding to two distinct oligomeric structures: tetramers and dimers. The intensities of the bands corresponding to the dimers showed especially high expression relative to the levels of the tetramers for GFAT1-L.p.R385H (lane 4) compared to wild type GFAT1-L (lane 1). This suggested that the p.R385H substitution might affect the formation of the GFAT1-L complex.

3.3.2.5. Enzymatic activity of the mutated GFAT1 and GFAT1-L

GFAT1 is an enzyme catalysing the first step of the hexosamine biosynthetic pathway by transferring amide nitrogen from glutamine (Gln) to fructose-6-phosphate (Fru-6-P) and producing glucosamine-6-phosphate ($GlcNH_2$-6-P) and glutamate (Glu) (Milewski, 2002). The process is highly dependent on intra- and intermolecular interactions between amino acids within the GFAT1 sequence and the substrates and

products of the reaction, and thus the mutations in GFAT1 may affect catalytic properties of the enzyme.

The estimation of GFAT1-L enzymatic activity was first attempted by over-expressing the protein in HEK293TSA, extracting the total protein and assaying the GFAT1-L activity using a glutamate dehydrogenase (GDH) method, which determines the levels of Glu, one of the products in the GFAT1-catalysed reaction (Figure 3.14.). With Glu, GDH reduces acetylpyridine adenine dinucleotide (APAD) to APADH, which can be determined directly at a wavelength of 370 nm (Ye et al., 2004).

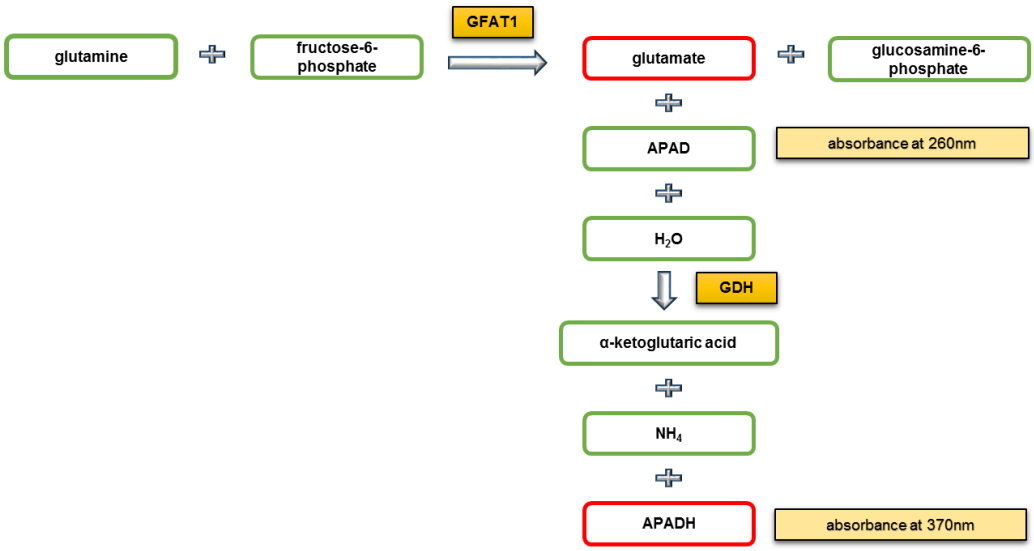

Fig.3.14. Schematic representation of the application of the GDH method for the determination of glutamate in the reaction catalysed by GFAT1
APAD – 3-acetylpyridine-adenine dinucleotide
GDH – glutamate dehydrogenase

Although the method is commonly used for assaying GFAT1 activity, it required careful optimisation, the aim of which was to determine an optimal amount of GDH and the type of the enzymatic solution. After a number of initial experiments, 6 U of GDH were found to be optimal, and the advantage of the buffered aqueous glycerol solution over the ammonium sulphate suspension was determined, thus these conditions were applied in the subsequent investigations (Figure 3.15.).

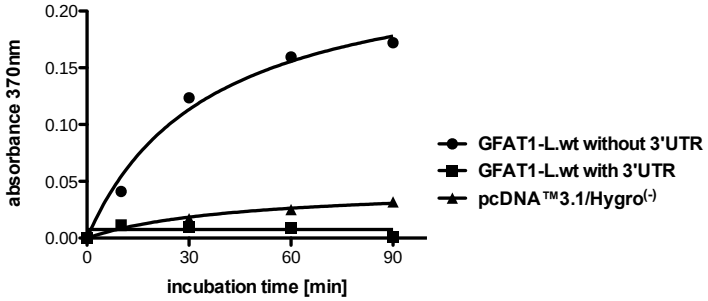

Fig.3.15. Enzymatic activity of wild type GFAT1-L over-expressed in HEK293TSA cells
HEK293TSA cells were transfected with constructs encoding wild type GFAT1-L, possessing or lacking 3'UTR, respectively. Total protein was extracted from the cells and the activity of GFAT1-L in the whole cell lysate was determined by the GDH method. As a control the cells were transfected with pcDNA™3.1/Hygro$^{(-)}$ plasmid. The graph shows increase over time in the absorbance measured at 370 nm, corresponding to the production of APADH.

An over-time increase in the absorbance at a wavelength of 370 nm was observed in the reaction containing protein extracted from the cells transfected with plasmids encoding GFAT1-L.wt without 3'UTR, although the amount of the APADH appeared to be only modestly above the mock-transfected cells. However, no APADH accumulation over time was detected when protein extracts from the cells over-expressing GFAT1-L from the constructs with the 3'UTR were used. Such observations confirms the enzymatic activity of GFAT1-L over-expressed in HEK293TSA as well as suggest that larger amounts of protein are required to measure relative enzymatic activity of the GFAT1-L variants.

A collaboration with Prof. Slawomir Milewski at Gdansk University of Technology was set up in order to over-express recombinant GFAT1 and GFAT1-L variants in a bacterial system, purify the active protein and determine its kinetic characterisations. cDNA encoding GFAT1, GFAT1-L and their mutated variants was cloned into the pET-22b(+) plasmid, which allows for efficient expression of the target proteins in *Escherichia coli* Rosetta (DE3) pLysS strain. The over-expressed proteins were purified using fast performance liquid chromatography (FPLC). Catalytic properties

of the enzymes were measured by the Morgan-Elson method, which is commonly used for the detection of glucosamine, acetylated or not, in analysed samples (Figure 3.16.).

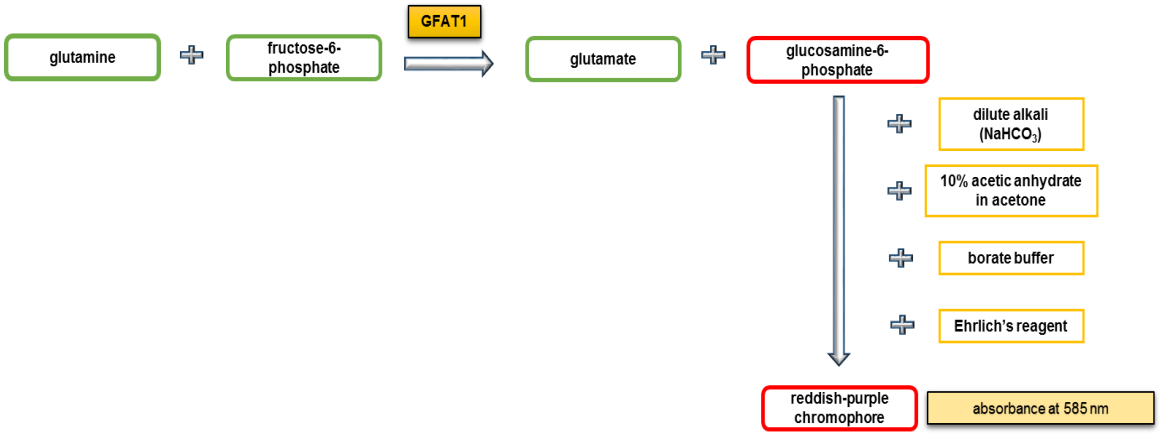

Fig.3.16. Schematic representation of the application of the Morgan-Elson method for the determination of glucosamine-6-phosphate in the reaction catalysed by GFAT1
Ehrlich's reagent – 4-(dimethylamino)benzaldehyde (ADAB) acidified with hydrochloric acid

The Morgan-Elson method is based on the fact that the N-acetylated aminosugar derivatives, pretreated with diluted alkali, and mixed with an Ehrlich's reagent (p-dimethylaminobenzaldehyde (ADAB) acidified with hydrochloric acid) produce an intense reddish-purple chromophore, the intensity of which can be quantified with a spectrophotometer at a wavelength of 585 nm (Elson and Morgan, 1933). Based on the most recent investigations, the reddish-purple colour stems from the formation of mesomeric forms of N^3-protonated 3-acetylimino- 2-(4-dimethylaminophenyl) methylidene- 5-(1,2-dihydroxyethyl) furane (Muckenschnabel et al., 1998). The procedure can be modified for the detection of non-acetylated aminosugars by an addition of a reacetylation step. This step involves treating samples with 10% acetic anhydrate in acetone (Morgan and Elson, 1934). Further modifications may include an addition of a borate buffer, which has been observed to increase the intensity of the reddish-purple colour of the chromophore, and hence enhance the sensitivity of the method (Reissig et al., 1955).

The modified approach was used to determine the amounts of $GlcNH_2$-6-P in the reaction catalysed by GFAT1. The concentrations of the substrates varied from 0 mM to 11.25 mM for Fru-6-P and from 0 mM to 5 mM for Gln. The reactions proceeded for 30 minutes before the product ($GlcNH_2$-6-P) was quantified. Maximum initial velocity (V_{max}) and Michaelis constants (K_M) for both substrates were determined using a non-linear regression (Table 3.1.).

Table 3.1. Catalytic properties of wild type and mutated GFAT1 and GFAT1-L
Kinetic parameters (V_{max} and K_M for Fru-6-P and Gln, respectively) were determined using the Morgan-Elson method. The values represent mean±SEM of V_{max}, K_M for Fru-6-P or K_M for Gln, respectively, recorded in n=3 repeats of the assay. The values were calculated using a non-linear regression. The major changes in the catalytic properties of the enzyme are marked in red.

Protein	V_{max} [mmol/min/mg]	K_M for Fru-6-P [mM]	K_M for Gln [mM]
GFAT1.wt	0.209±0.006	1.585±0.200	0.449±0.059
GFAT1.p.T479N	0.165±0.004	1.411±0.146	0.495±0.076
GFAT1-L.wt	0.193±0.010	1.535±0.321	0.436±0.069
GFAT1-L.p.T15M	**0.031±0.001**	**3.112±0.415**	0.484±0.062
GFAT1-L.p.R385H	**0.105±0.003**	**2.059±0.224**	0.374±0.072
GFAT1-L.p.R434H	0.150±0.009	**2.972±0.529**	0.353±0.066
GFAT1-L.p.R496W	**0.104±0.002**	1.211±0.142	0.387±0.042

As summarised in Table 3.1., the investigations revealed that V_{max} for GFAT1.wt and GFAT1-L.wt were 0.209±0.006 mmol/min/mg and 0.193±0.006 mmol/min/mg, respectively. This parameter was decreased for GFAT1-L.p.T15M, GFAT1-L.pR385H and GFAT1-L.p.R496W, with the values of 0.031±0.001, 0.105±0.003 and 0.104±0.002, respectively. A minor decrease in the V_{max} values was also recorded for GFAT1.p.T479N and GFAT1-L.p.R434H. Further analyses of the enzymatic activity of the target protein revealed that the K_M values for Fru-6-P were 1.585±0.200 mM and 1.535±0.321 mM for GFAT1.wt and GFAT1-L.wt, respectively. These were markedly increased, to 3.112±0.415 mM, 2.059±0.224 mM and 2.972±0.529 mM, for GFAT1-L.p.T15M, GFAT1-L.p.R385H and

GFAT1-L.p.R434H, respectively. Finally, the K_M for Gln for GFAT1.wt and GFAT1-L.wt were 0.449±0.059 mM and 0.436±0.069 mM, and did not appear to be markedly affected by any of the amino acid substitutions.

In summary, the data demonstrated that the p.T15M mutation led to the loss of the enzymatic activity of GFAT1-L and a reduction in its affinity for Fru-6-P. Similar, but less marked, changes were recorded for the GFAT1-L.p.R385H variant. The studies also suggested that the substitution of arginine for histidine at position 434 resulted in a diminished affinity for Fru-6-P and that the p.R496W mutation led to the reduction in the enzymatic activity of GFAT1-L, but the reduction recorded in the activity of GFAT1-L.p.R496W could be the result of the relative instability of this variant. The only amino acid substitution, which did not result in any marked changes in the catalytic properties of GFAT1, was p.T479N.

3.4. Bioinformatics predictions

Molecular consequences of the mutations were also analysed using bioinformatics tools, which might indicate the consequences of the mutations for stability, formation of a 3D structure and interactions with ligands (Thusberg and Vihinen, 2009).

3.4.1. Predictions based on the sequence conservation

First, the consequences of the mutations were analysed based on the evolutionary conservation of the mutated residues, using PolyPhen2.0 software (Flanagan et al., 2010) (Table 3.2.).

Table 3.2. PolyPhen2.0 prediction of molecular consequences of the amino acid substitutions in GFAT1
The mutations which were found to be damaging are labelled in red.

Amino acid change	Probability score of being damaging	Consequence
p.T15M	**0.940**	**damaging**
p.R385H	**0.995**	**damaging**
p.R434H	0.018	benign
p.T479N	0.242	benign
p.R496W	**0.980**	**damaging**

The predictions indicated that the p.T15M, p.R385H and p.R496W mutations in GFAT1 were likely to be damaging to the protein, with probability scores of 0.940, 0.995 and 0.980, respectively. By contrast, the substitutions at positions 434 and 479, although occurring at relatively conserved sites, were found to be benign, with probability scores of 0.018 and 0.242, respectively.

3.4.2. Effects of the mutations on *GFPT1* pre-mRNA splicing

The next step was to analyse molecular consequences of the missense changes on the *GFPT1* pre-mRNA splicing. This was done using Spliceman software (Lim and Fairbrother, 2012, Lim et al., 2011) (Table 3.3.).

Table 3.3. Bioinformatics predictions of the effects of the mutations on *GFPT1* pre-mRNA splicing using Spliceman software
The higher the L1 distance and the ranking (L1), the more likely that the mutation alters the pre-mRNA splicing. Two substitutions (p.R434H and p.T479N) with the highest scores are marked in red.

Amino acid change	DNA change	L1 distance	Ranking (L1)
p.T15M	5'-TCGAA(C/T)GAGAC-3'	34878	67%
p.R385H	5'-GACAC(G/A)TCAAG-3'	33544	60%
p.R434H	5'-TCTTC(G/A)TTACT-3'	37747	**81%**
p.T479N	5'-TTATA(C/A)CAGCC-3'	36302	**74%**
p.R496W	5'-ATGAT(C/T)GGATC-3'	34377	64%

As summarised in Table 3.3., the substitutions p.R434H and p.T479N were predicted to affect the splicing of the *GFPT1* pre-mRNA.

To verify these findings, RNA was extracted from the wild type and the patient-derived *GFPT1*-mutated cells, transcribed into cDNA and the fragments of *GFPT1* cDNA adjacent to the location of the respective substitutions amplified in a polymerase chain reaction (PCR). The PCR products were resolved by electrophoresis on ethidium bromide-stained agarose gels (Figures 3.17. and 3.18.).

A

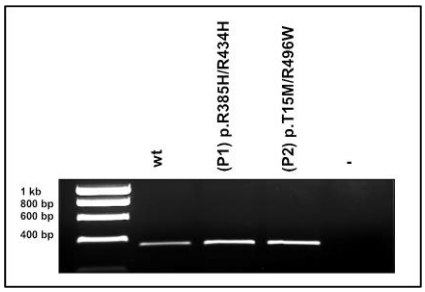

B

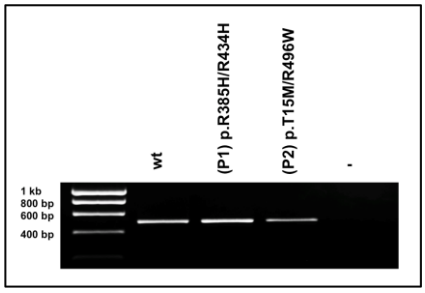

C

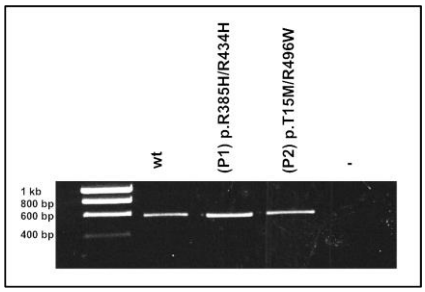

Fig.3.17. *GFPT1* pre-mRNA splicing in wild type and *GFPT1*-mutated (P1 and P2) human skeletal muscle cells

Total RNA was extracted from the wild type and the *GFPT1*-mutated myoblasts, transcribed into cDNA and the *GFPT1* fragments adjacent to the substitutions (A) p.T15M (exons 2, 3 and 4), (B) p.R385H (exons 12, 13, 14 and 15) and (C) p.R434H and p.R496W (exons 13, 14, 15 and 16) were amplified by PCR. The PCR products were resolved on agarose gels.

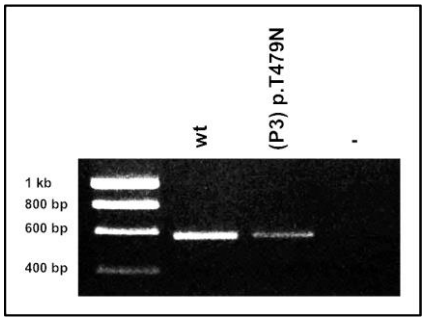

Fig.3.18. *GFPT1* pre-mRNA splicing in wild type and *GFPT1*-mutated (P3) human dermal fibroblasts

Total RNA was extracted from the wild type and the *GFPT1*-mutated fibroblasts, transcribed into cDNA and the *GFPT1* fragments adjacent to the p.T479N substitution (exons 13, 14, 15 and 16) was amplified by PCR. The PCR products were resolved on agarose gels.

No differences in the gel migrations of the PCR products amplified from the wild type and the *GFPT1*-mutated cells were detected. This might suggest that the mutations do not alter the splicing of *GFPT1* pre-mRNA. However, it may not be possible to observe relatively small insertions and deletions by gel electrophoresis, and thus to confirm the integrity of the PCR products, they were extracted from the gels and sequenced (Figure 3.19.).

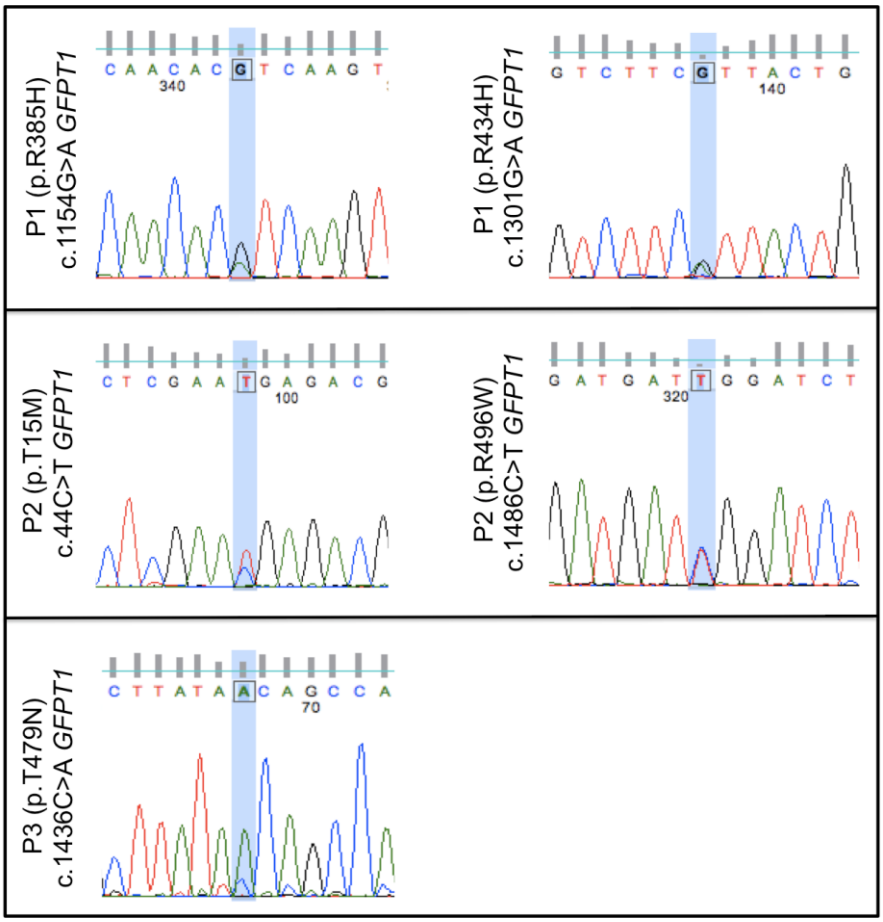

Fig.3.19. Sequencing chromatograms presenting the mutations detected in *GFPT1* patients
The peaks, which represent the missense changes, are shaded in blue.

The sequencing results corroborated the presence of the respective changes in the DNA sequence and reaffirmed that the splicing of *GFPT1* pre-mRNA was not altered in the mutated cells.

3.4.3. Predictions of the effects of the mutations on GFAT1 and GFAT1-L structure

Another potential consequence of amino acid changes is an introduction of intramolecular forces, destructive for the structure of the protein. This was analysed using PyMol mutagenesis wizard (Schrodinger, 2010) (Figure 3.20.).

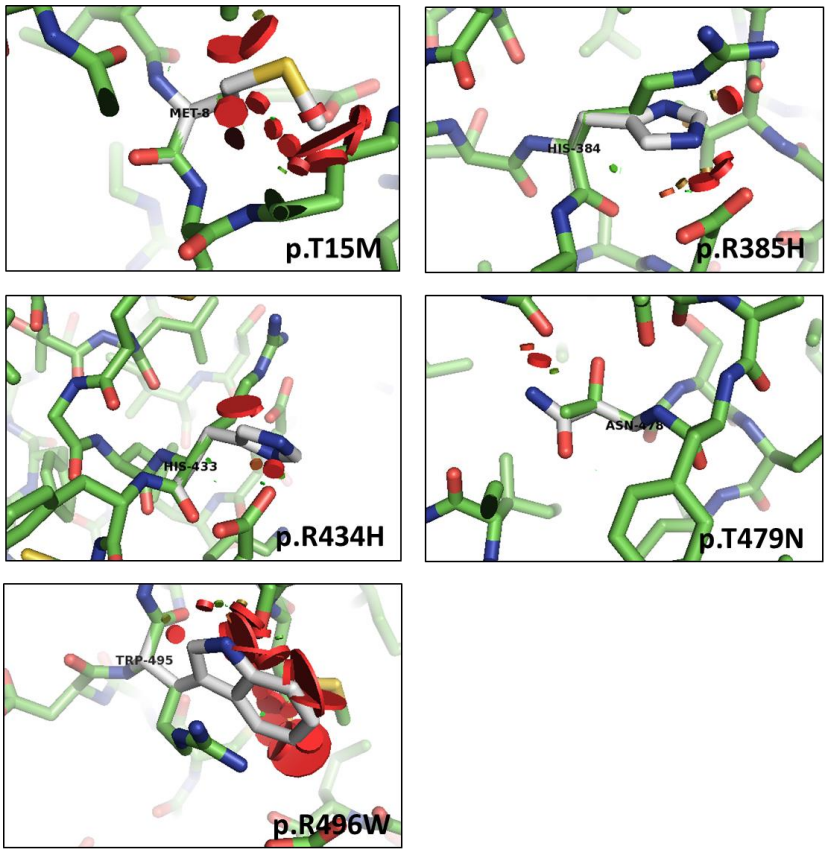

Fig.3.20. *In silico* mutagenesis of GFAT1
The mutations identified in GFAT1 (represented with grey sticks) were introduced into the 3D structure of GFAT1 using a PyMol mutagenesis wizard. A structure of the sugar isomerase domain of human GFAT1 deposited in PDB (PDB ID: 2ZJ3) (Nakaishi et al., 2009) was used as a model for p.R385H, p.R434H, p.T479N and p.R496W substitutions. The p.T15M mutation was introduced into the structure of the glutaminase domain of *E.coli* GlmS stored in PDB (PDB ID: 1XFF) (Isupov et al., 1996). The small green disks indicate a close proximity of residues or a slight van der Waals overlap and the large red ones a significant van der Waals overlap.

As shown in Figure 3.20., the introduction of the mutations resulted in a number of significant van der Waals overlaps, represented with the red disks. The clashes were especially apparent in GFAT1.p.T15M and GFAT1.p.R496W.

3.4.4. Predictions of the effects of the mutations on GFAT1 oligomerisation

Amino acid substitutions may also impair the formation of a correct quaternary structure. Since GFAT1 is an enzyme, which is active as a homodimer (Nakaishi et al., 2009) or a homotetramer (Richez et al., 2007), it was of interest to analyse whether any of the amino acid substitutions was likely to disrupt the formation of the complex. This was done using PDBePISA software (Krissinel and Henrick, 2007).

The examinations indicated that GFAT1 was likely to form a complex, with a relatively high Complex Formation Significance Score=0.574, and that the arginine at position 385 comprised the interface of the complex, forming hydrogen bonds with methionine at position 397, and hydrogen bonds and salt bridges with glutamine at position 399 of the partner monomer. At the same time, none of the mutated residues was involved in the binding of Fru-6-P.

The formation of GFAT1 complex was further analysed using a PyMol software (Figure 3.21.).

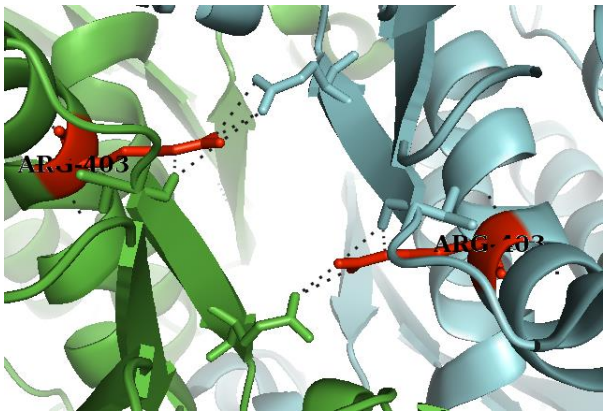

Fig.3.21. Implication of Arg403 in GFAT1-L (corresponding to Arg385 in GFAT1) in the oligomerisation of human GFAT1-L
The image presents the bonds formed between Arg403 and other amino acids in human GFAT1-L oligomer. The distinct monomers are labelled in green and blue, the Arg403 are shown as red sticks and the bonds are represented with grey dashed lines.
The image was modified based on the unpublished 3D structure of GFAT1 stored in PDB database (PDB ID: 2V4M) deposited by Moche et al. (awaiting publication).

The studies show that Arg403 in GFAT1-L (corresponding to Arg385 in GFAT1) comprises the interface of the oligomer.

3.5. Application of biomarkers of glycosylation to study the pathogenicity of *GFPT1* mutations

To analyse further the pathogenicity of the identified mutations, the alterations in the glycosylation between wild type and *GFPT1*-mutated cells were studied using molecular biomarkers of the process. These include (1) endogenous glycoprotein ICAM1 (CD54) and (2) a modified exogenously expressed EGFP with an engineered N-glycosylation site, which when occupied by a sugar moiety, affects the structure of the protein resulting in its diminished fluorescence (He et al., 2012, Losfeld et al., 2012).

3.5.1. ICAM1 cell surface expression in wild type and *GFPT1*-mutated cells

The first biomarker analysed was ICAM1 (CD54), which is a cell surface glycoprotein, possessing 8 potential N-glycosylation sites. The carbohydrate structures comprise ~30% of the molecular weight of the molecule (Tomassini et al., 1989, Bloom et al., 1996). When the glycosylation sites are not occupied with sugar chains, ICAM1 is degraded by glycoprotein quality control mechanisms and fails to reach the cell surface membrane. This results in its reduced expression in glycosylation-deficient cells, obtained from CDG-affected individuals (He et al., 2012).

Cell surface expression of ICAM1 in myoblasts derived from the biopsies taken from *GFPT1* patients and healthy individuals was analysed by flow cytometry. The percentage of the cells expressing ICAM1 at the cell surface above the background and the median fluorescence of the cell surface protein labelled with a phycoerythrin (PE)-conjugated anti-ICAM1 antibody were chosen as estimators of the ICAM1 cell surface expression (Figure 3.22.).

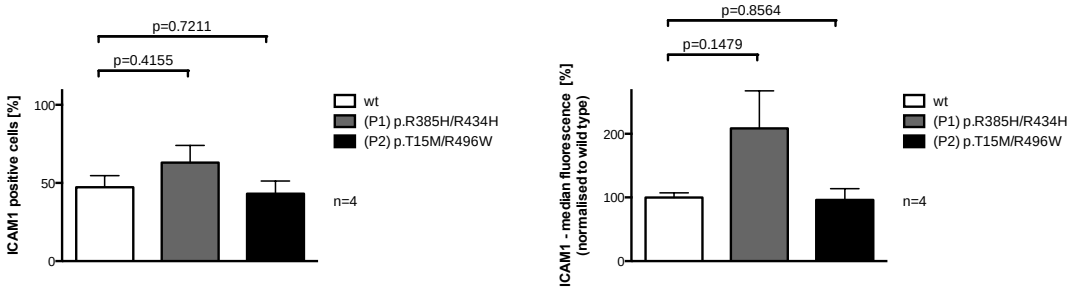

Fig.3.22. ICAM1 cell surface expression in wild type and *GFPT1*-mutated (P1 and P2) myoblasts
Wild type and *GFPT1*-mutated myoblasts were stained with PE-conjugated mouse monoclonal anti-CD54 (ICAM1) antibody and the intensity of the fluorescence was measured by flow cytometry. Each bar represents (A) average±SEM% of ICAM1 positive cells and (B) average median±SEM ICAM1 fluorescence, recorded in n=4 independent experiments, in the wild type and the *GFPT1*-mutated cells. All the data are presented relative to the expression of ICAM1 in the control cells. p values were obtained using a student t-test.

No significant changes in the ICAM1 cell surface expression in the *GFPT1*-mutated myoblasts, compared to the healthy control, were observed. This would indicate a lack of any alterations in the levels of the N-glycosylation in the cells.

The expression of ICAM1 at the cell surface was also analysed in the *GFPT1*-mutated fibroblasts with p.T479N amino acid substitution (Figure 3.23.).

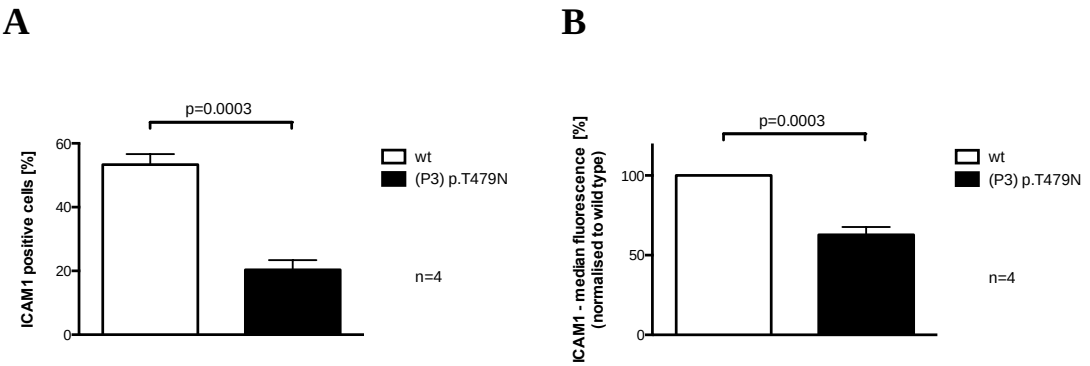

Fig.3.23. ICAM1 cell surface expression in wild type and *GFPT1*-mutated (P3) p.T479N dermal fibroblasts
Wild type and *GFPT1*-mutated fibroblasts were stained with a PE-conjugated mouse monoclonal anti-CD54 (ICAM1) antibody or a PE-conjugated mouse monoclonal isotype K IgG1 antibody as a negative control, and the intensity of the fluorescence was measured by flow cytometry. Each bar represents (A) average±SEM% of ICAM1 positive cells and (B) average median±SEM ICAM1 fluorescence, recorded in n=4 independent experiments, in the wild type and the *GFPT1*-mutated cells. All the data are presented relative to the expression of ICAM1 in control cells. p values were obtained using a student t-test.

By contrast with the *GFPT1*-mutated myoblasts, (P3) p.T479N fibroblasts exhibited reduced ICAM1 cell surface expression. Only 20.37±3.00% of the mutated fibroblasts were found to express ICAM1 at the cell surface above the background. This value was significantly lower (p=0.0003, n=4) compared to the wild type dermal fibroblasts, 53.4±3.29% of which were found to express ICAM1 above the background. The median fluorescence of ICAM1 at the cell surface was also reduced (to 62.71±4.92%, p=0.0003, n=4) in the *GFPT1*-mutated cells. The lower ICAM1 levels in the *GFPT1*-mutated fibroblasts might indicate that the activity of the N-glycosylation pathway is diminished in these cells. However, the differences could be the result of non-GFAT1-related variability between individuals, and hence needed confirmation using a different approach.

3.5.2. EGFP-Glc-ER fluorescence in wild type and *GFPT1*-mutated human skin fibroblasts

Another novel sensitive biomarker that can be used in the identification of CDG-I is an ER-located EGFP with an engineered N-glycosylation site. Glycosylation at this site impairs fluorescence of the protein and so glycosylation-deficient cells are expected to exhibit enhanced green fluorescence compared to controls. The plasmid encoding the protein, together with the construct encoding wild type ER-located EGFP, as a control, was obtained from Prof. Hudson Freeze (Losfeld et al., 2012). The DNA encoding EGFP-Glc-ER and EGFP-ER were separately subcloned into a pIRES2-DsRed2 vector. This plasmid possesses an internal ribosomal entry site (IRES), which allows for a simultaneous expression of the target protein and the DsRed2 selection marker from a single mRNA. This enables specific selection of the

transfected cells expressing both the DsRed2 reporter and the target EGFP-Glc-ER or EGFP-ER.

The constructs were introduced into wild type and (P3) p.T479N skin fibroblasts, and green fluorescence in the transfected cells, selected based on the DsRed2 expression, was estimated using LSRFortessa cell analyser and a BD Biosciences FACSDiva™ software (Figure 3.24.).

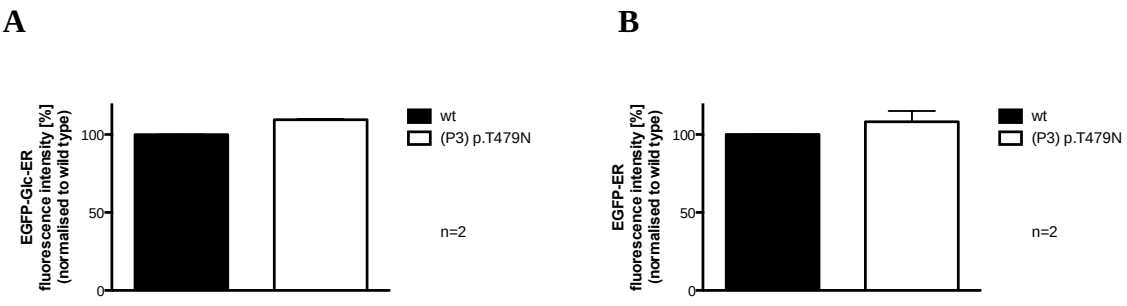

Fig.3.24. Intensity of green fluorescence recorded in wild type and *GFPT1*-mutated (P3) p.T479N dermal fibroblasts transfected with (A) EGFP-Glc-ER-IRES-DsRed2-, or (B) EGFP-ER-IRES-DsRed2-encoding plasmids, analysed using flow cytometry
Each bar represents the median±SEM fluorescence intensity of EGFP-Glc-ER or EGFP-ER, recorded in n=2 independent experiments, in the transfected wild type and mutated cells. All the data are presented relative to green fluorescence in control cells.

EGFP-Glc-ER fluorescence was marginally less affected by the attachment of sugars in the (P3) p.T479N fibroblasts compared to the wild type cells. At the same time, the mutated cells transfected with the control EGFP-ER-encoding plasmid also presented marginally brighter green fluorescence. Therefore, it is probable that the recorded changes were not due to a glycosylation defect.

3.6. Discussion

The present chapter studied mutations in the *GFPT1* gene identified in the selected *GFPT1* patients. The experiments clearly indicated that at least some of the mutations led to GFAT1 deficiency since the GFAT1 protein levels were found to be lower in the (P1) p.R385H/R434H myotubes and in both myoblasts and myotubes from the (P2) p.T15M/R496W case. Similar findings have emerged from the analyses of GFAT1 levels in muscle biopsies from *GFPT1* CMS cases (Senderek et al., 2011). The only individual in whom the molecular consequences of the amino acid substitution remained unresolved was the (P3) p.T479N patient. In the fibroblasts obtained from this patient neither the protein expression nor the *GFPT1* pre-mRNA splicing appeared to be altered, suggesting a possibility that the mutation was not an underlying cause of the multisystem disease.

The limitation of the analyses of GFAT1 expression in patient cells was that they could have not revealed molecular consequences of individual amino acid substitutions in GFAT1 since two of the individuals harboured heterozygous mutations in the protein. To investigate the effects of the amino acid substitutions (p.T15M, p.R385H, p.R434H, p.T479N, p.R496W) in GFAT1 individually, the respective proteins were over-expressed in heterologous expression systems – HEK293TSA and *Escherichia coli* cells. The studies included analyses of the enzyme's protein levels and stability as well as homo-oligomerisation and catalytic properties.

Optimisation steps performed prior to the experiments resulted in the removal of the 3'UTR from the target constructs since this fragment significantly reduced the expression of the protein. This might have been due to the presence of regulatory RNA sequences within the 3'UTR (Chen and Shyu, 1995, Brennan and Steitz, 2001). Such an assumption is corroborated by the identification of a CMS-causing mutation

c.*22C>A, leading to reduced levels of GFAT1 (Maselli et al., 2013, Senderek et al., 2011).

Although the removal of the 3'UTR led to the high expression of the target protein, it might have also resulted in an increased or a decreased stability of the *GFPT1* mRNA. This might have hindered the studies into the molecular consequences of the mutations which led to changes in the mRNA stability, without affecting the stability or the enzymatic activity of the protein. Nonetheless, the plasmids which allowed the higher expression of the target protein were chosen for most of the experiments.

The research clearly indicated that the p.R496W mutation led to the production of a relatively unstable protein, which exhibited decreased protein levels when over-expressed in HEK293TSA cells. The protein levels of the GFAT1-L.p.T15M were also slightly reduced, but its stability appeared not to be affected.

Based on further experiments, the molecular consequences of the p.T15M substitution are more likely to be a reduced maximum initial velocity (V_{max}) and an increased Michaelis constant (K_M) for Fru-6-P, compared to GFAT1-L.wt. Similar, potentially pathogenic, changes in the affinity for Fru-6-P were recorded for GFAT1-L.p.R434H. The enzymatic assay also pointed to a minor decrease in V_{max} of GFAT1-L.p.R385H and GFAT1-L.p.R496W, and to a reduced affinity for Fru-6-P of GFAT1-L.p.R385H, but the reduced activity of the GFAT1-L.p.R496W in the assay might have resulted from the relative instability of this GFAT1-L variant.

Finally, native western blotting and *in silico* predictions suggested the potential for the aberrant homo-oligomerisation of GFAT1-L.p.R385H.

The molecular consequences of the p.T479N substitution are uncertain. It does not appear to affect either the protein levels or the mRNA splicing, or the catalytic properties of the protein. The lack of any evident differences between GFAT1.wt and

GFAT1.p.T479N may suggest that this substitution is not an underlying cause of the disease in the patient. Further evidence for this is that no defect of neuromuscular transmission was detected by neurophysiology.

In summary, the results presented in this chapter demonstrate that decreased amounts of GFAT1 or its altered activity may impair neuromuscular transmission (Guergueltcheva et al., 2011, Senderek et al., 2011) (Table 3.4.).

Table 3.4. Summary of molecular consequences of the mutations in GFAT1

Amino acid substitution	Protein levels	Protein stability	Oligomerisation	Enzymatic activity
p.T15M	↓	=	=	V_{max} ↓ $K_{M(Fru\text{-}6\text{-}P)}$↓; $K_{M(Gln)}$=
p.R385H	=	=	↓	V_{max} ↓ $K_{M(Fru\text{-}6\text{-}P)}$↓; $K_{M(Gln)}$=
p.R434H	=	=	=	V_{max}= $K_{M(Fru\text{-}6\text{-}P)}$↓; $K_{M(Gln)}$=
p.T479N	=	N/A	N/A	V_{max}= $K_{M(Fru\text{-}6\text{-}P)}$=; $K_{M(Gln)}$=
p.R496W	↓	↓	=	V_{max} ↓ $K_{M(Fru\text{-}6\text{-}P)}$=; $K_{M(Gln)}$=

↓ - decreased, ↑ - increased, = - unchanged, N/A - not available
Fru-6-P - fructose-6-phosphate, Gln - glutamine, K_M - Michaelis constant, V_{max} - maximum initial velocity

Chapter 4

Potential links between GFAT1, GFAT1-L, glycosylation and the neuromuscular junction

4.1. Introduction

Mutations in the *GFPT1* gene can cause congenital myasthenic syndromes (CMS) (Guergueltcheva et al., 2011, Senderek et al., 2011). This discovery indicates that the defects in the hexosamine biosynthetic pathway may cause aberrant neuromuscular transmission, but thus far no links have been established between L-glutamine:D-fructose-6-phosphate amidotransferase 1 (GFAT1), glycosylation and the neuromuscular junction (NMJ) so the pathogenic mechanism of *GFPT1* CMS has yet to be uncovered.

GFAT1, the enzyme encoded by the *GFPT1* gene, catalyses the first and rate-limiting step of the hexosamine biosynthetic pathway, which is a minor branch (encompassing approximately 3% of glucose utilised by cells) of the glycolytic pathway. This enzyme regulates glucose flux through the pathway, determining how much glucose is converted into uridine diphosphate N-acetylglucosamine (UDP-GlcNAc), and how much is left for glycolysis and glycogen synthesis (Figure 4.1.). The latter are essential for energy homeostasis and play particularly important roles in metabolically active tissues, such as skeletal muscle, while the UDP-GlcNAc serves as an activated sugar precursor utilised in glycosylation, including O-linked and N-linked glycosylation, and the synthesis of glycolipids. The importance of GFAT1 in glucose metabolism might suggest that the pathological features of *GFPT1* CMS could result from either alterations in the energy homeostasis or from defective glycosylation. The latter is more likely to be affected since the hexosamine biosynthetic pathway, regulated by

GFAT1, is only a minor branch of the glycolytic pathway, and thus the alterations in hexosamine synthesis would have minimal consequences on the main glycolytic events. These minor consequences would be unlikely to lead to disease.

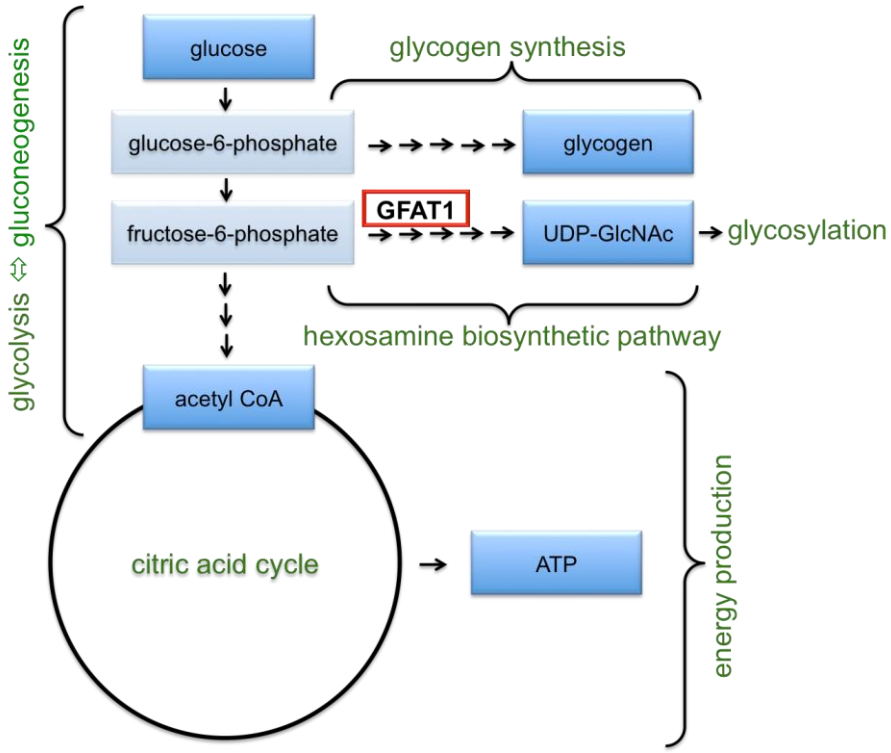

Fig.4.1. Schematic representation of metabolic pathways related to GFAT1 and processes potentially affected by mutations in *GFPT1*
acetyl CoA – acetyl coenzyme; ATP – adenosine triphosphate; GFAT1 – L-glutamine:D-fructose-6-phosphate amidotransferase 1; UDP-GlcNAc – uridine diphosphate N-acetylglucosamine

Defective glycosylation as a pathogenic mechanism in *GFPT1* CMS would be in line with the reports that attachment of O-GlcNAc moieties is compromised in *GFPT1* cases (Senderek et al., 2011) and with phenotypic similarities between *GFPT1*, UDP-N-acetylglucosamine-dolichyl-phosphate N-acetylglucosaminephosphotransferase (*DPAGT1*), asparagine-linked glycosylation 2 and 14 (*ALG2* and *ALG14*) CMS cases (Guergueltcheva et al., 2011, Senderek et al., 2011, Belaya et al., 2012, Cossins et al., 2013b). DPAGT1, ALG2 and ALG14 play important roles in the early steps of the

N-glycosylation pathway, which utilises the major product of the hexosamine biosynthetic pathway – UDP-GlcNAc.

It is well known that both classes of sugars (N-linked and O-linked) are abundantly present in muscle fibres, where they are attached to proteins and lipids, and that mutations in a number of genes, encoding enzymes from glycosylation pathways, can cause severe muscular dystrophies, often accompanied with brain abnormalities (Haliloglu and Topaloglu, 2004). These include muscle-eye-brain disease (MEB) and Walker-Warburg syndrome (WWS), caused by O-mannosylation defects arising from mutations in *POMGnT1* (Yoshida et al., 2001) in MEB, and *POMT1* (Beltran-Valero de Bernabe et al., 2002) or *POMT2* in WWS (van Reeuwijk et al., 2005), Fukuyama congenital muscular dystrophy (FCMD) and a number of other types of congenital muscular dystrophies (CMD), resulting from mutations in the genes encoding putative glycosyltransferases, such as for instance *FUKUTIN* (Kobayashi et al., 1998) and *LARGE* (Longman et al., 2003). The *LARGE* gene has been proposed as a potential candidate since mutations have been shown to lead to muscular dystrophy in the $Large^{myd}$ mouse model, which is commonly used in studies of aberrant glycosylation in muscle. The pathological features of $Large^{myd}$ mice are dystrophic muscle fibres, abnormal migration of central nervous system (CNS) neurons and defects in the structure of the NMJ (Holzfeind et al., 2002). The latter include neuronal sprouting, exuberant nerve growth and reduced expression of muscle-specific tyrosine kinase (MuSK) and acetylcholine receptors (AChR), resulting in less densely packed AChR clusters (Herbst et al., 2009). The compromised structure of the NMJ may indicate a particular importance of glycans at the synapse.

The importance of glycans at the NMJ has been further confirmed by research into the pathogenesis of Guillan-Barré (Willison, 2005) and Miller Fisher syndromes (Overell

and Willison, 2005), which are caused by antibodies targeting glycolipids. The main pathological features observed in patients and in animal models of the disease include motor neuropathy and aberrant neuromuscular transmission, which are due to the abundance of glycans in lipid rafts at the NMJ (Willison et al., 2008). However, a sensory neuropathy is also often present (Hughes and Cornblath, 2005).

In sharp contrast to the muscular dystrophies and immunological disorders, CMS caused by glycosylation defects show little or no signs of muscle dystrophy and minimal pathological features elsewhere in the body. Such a clinical picture is difficult to explain since glycosylation enzymes are expressed ubiquitously and hence, in most congenital disorders of glycosylation (CDG), NMJ dysfunctions are accompanied by muscle dystrophy, abnormalities in CNS functions and by various pathological morphologies (Theodore and Morava, 2011, Taniguchi et al., 2006).

Approaches that can be undertaken to investigate alterations in glycosylation include analyses of glycan profiles with mass spectrometry (North et al., 2009). This method should reveal any potential alterations in the global patterns of glycosylation, but would not address the question why the NMJ is particularly sensitive to the *GFPT1* mutations.

The susceptibility of the NMJ to defective glycosylation might be caused by a relative concentration of a unique repertoire of carbohydrates at the synapse, as revealed by studies involving the application of lectins and carbohydrate-specific antibodies (Martin, 2003). A specific pattern of glycans might result from a neuromuscular localisation of some enzymes from glycosylation pathways (Xia et al., 2002, Singhal et al., 2012) or their particular regulation in this region. However, no direct link between the *GFPT1* gene and the NMJ has yet been established.

A feature of GFAT1 is that it exists in two alternative splice variants, GFAT1 and GFAT1-L, with the latter possessing an 18-amino acid insertion specific to skeletal muscle and heart (DeHaven et al., 2001, Niimi et al., 2001). This alternatively spliced exon might influence the regulation and enzymatic activity of the protein or target the enzyme to a specific location within a tissue, such as the NMJ. The latter could partially explain the susceptibility of the synapse to the mutations in *GFPT1*. The existence of a homologous enzyme – GFAT2 that catalyses the same reaction and is highly expressed in the CNS (Oki et al., 1999), may reduce the likelihood of brain involvement in *GFPT1* CMS. However, the pathogenic mechanism of the disease and the restriction of the defects to the NMJ have yet to be uncovered.

4.2. Why do *GFPT1* patients present aberrant neuromuscular transmission?

The discovery of the novel mutations in the *GFPT1* gene as a cause of a pure myasthenic syndrome, presenting with aberrant neuromuscular transmission, but minimal pathological symptoms elsewhere, was surprising since GFAT1 is an ubiquitously expressed enzyme, the activity of which should be essential for the function of all cell types. Links between the protein, hexosamine biosynthetic pathway and the NMJ remain to be established.

4.2.1. Role of GFAT1 and protein glycosylation in AChR cluster formation

The similarity in the clinical picture of *GFPT1* CMS and CMS caused by mutations in DPAGT1, ALG2 and ALG14 – proteins involved in the N-glycosylation – suggests that aberrant neuromuscular transmission in these disorders may result from a similar mechanism, potentially involving glycosylation defects, but it remains unclear why the NMJ is particularly prone to these defects (Guergueltcheva et al., 2011, Senderek et al., 2011, Belaya et al., 2012, Cossins et al., 2013b).

4.2.1.1. Demonstration of the enrichment of N-acetylgalactosamine moieties at the sites of AChR clusters *in vitro* in C2C12 myotubes

First, carbohydrate moieties, which might, at least, be partially dependent on the efficient function of the hexosamine biosynthetic pathway, were investigated in C2C12 muscle cells that can be differentiated from myoblasts into multinucleated myotubes. Incubation of the myotubes with agrin (AGRN) induces a formation of AChR clusters (Denzer et al., 1997, Gesemann et al., 1995) that partially mimics the formation of the NMJ. The AChR clusters can be visualised by staining with a

fluorescent α-bungarotoxin (α-BuTx), which binds with a high affinity to nicotinic AChR (Vincent et al., 1998).

The localisation of carbohydrates at the cell surface was analysed by co-staining AGRN-treated myotubes with fluorescent Alexa Fluor 488 α-BuTx and tetramethylrhodamine isothiocyanate (TRITC)-conjugated *Vicia villosa* agglutinin B_4 (VVA-B_4) – a lectin that specifically binds N-acetylgalactosamine (GalNAc) moieties (Puri et al., 1992) (Figure 4.2.).

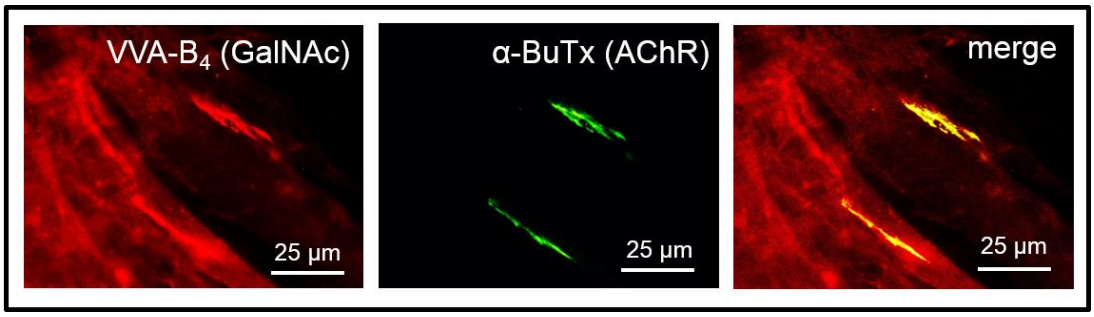

Fig.4.2. Enrichment of N-acetylgalactosamine moieties at the sites of AChR clusters in C2C12 myotubes
AGRN-treated C2C12 myotubes were co-stained with TRITC-VVA-B_4 and Alexa Fluor 488 α-BuTx.

Red fluorescence of TRITC-VVA-B_4 was enriched at the α-BuTx binding sites (green fluorescence). This indicated a relative enrichment of GalNAc moieties at the sites of AChR clusters. The concentration of the specific repertoire of carbohydrates at the neuromuscular synapse may suggest that sugars are of particular importance for the structure and function of the NMJ.

4.2.1.2. Is the expression of GFAT1 and GFAT1-L enriched at the AChR cluster sites *in vitro* in C2C12 myotubes?

The enrichment of GFAT1 at the sites of AChR clusters would suggest that the enzyme might be directly involved in the synthesis of the glycan moieties concentrated at the synapse, possibly by providing building blocks (UDP-GlcNAc) for the glycosylation.

The localisation of GFAT1 in AGRN-treated C2C12 myotubes was studied. AChR clusters were labelled with Alexa Fluor 594 α-BuTx and endogenous GFAT1 was immunostained with a rabbit monoclonal anti-GFAT1 antibody, and the appropriate Alexa Fluor 488 secondary antibody. The stained cells were visualised by fluorescence microscopy (Figure 4.3.).

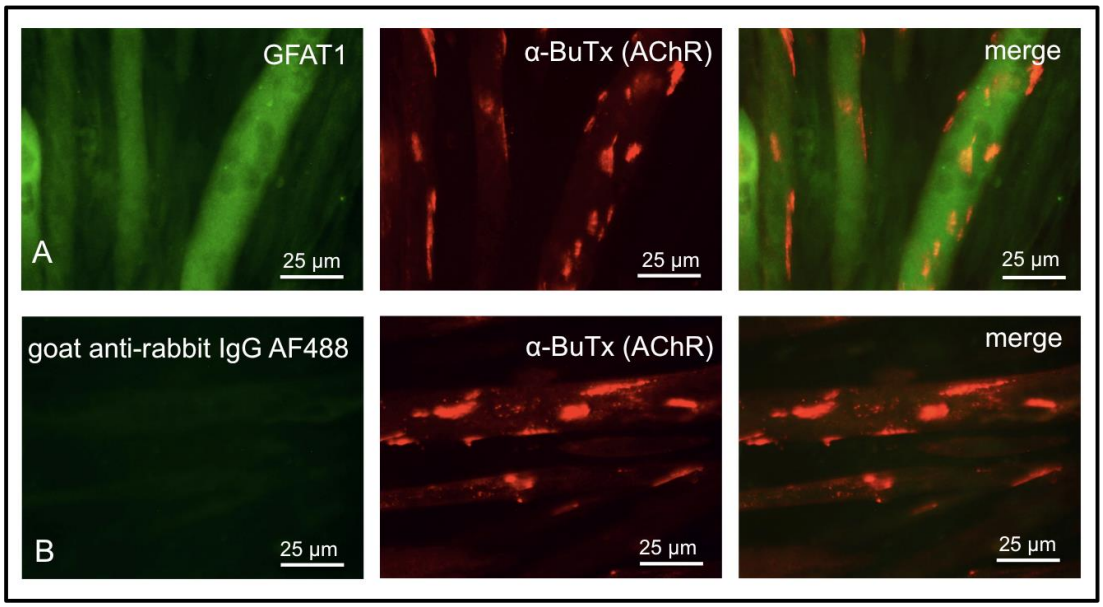

Fig.4.3. Localisation of GFAT1 in C2C12 myotubes
(A) AGRN-treated C2C12 myotubes were permeabilised and co-stained with an anti-GFAT1 antibody and the appropriate Alexa Fluor 488 secondary antibody, and Alexa Fluor 594 α-BuTx. (B) As a control, C2C12 myotubes were co-stained with the Alexa Fluor 488 secondary antibody and Alexa Fluor 594 α-BuTx.

GFAT1 was distributed throughout the cytoplasm and did not appear to be concentrated in the regions of the AChR clusters in *in vitro* cultured C2C12 myotubes.

4.2.1.3. N-acetylgalactosamine moieties at the neuromuscular junction *in vivo*

Cultured cells may not replicate the physiological conditions observed *in vivo*. Therefore, similar experiments were performed on muscle from C57BL/6 wild type mice.

Tibialis anterior muscle was stained with Alexa Fluor 488 α-BuTx and TRITC-VVA-B_4 lectin and analysed by fluorescence microscopy (Figure 4.4.).

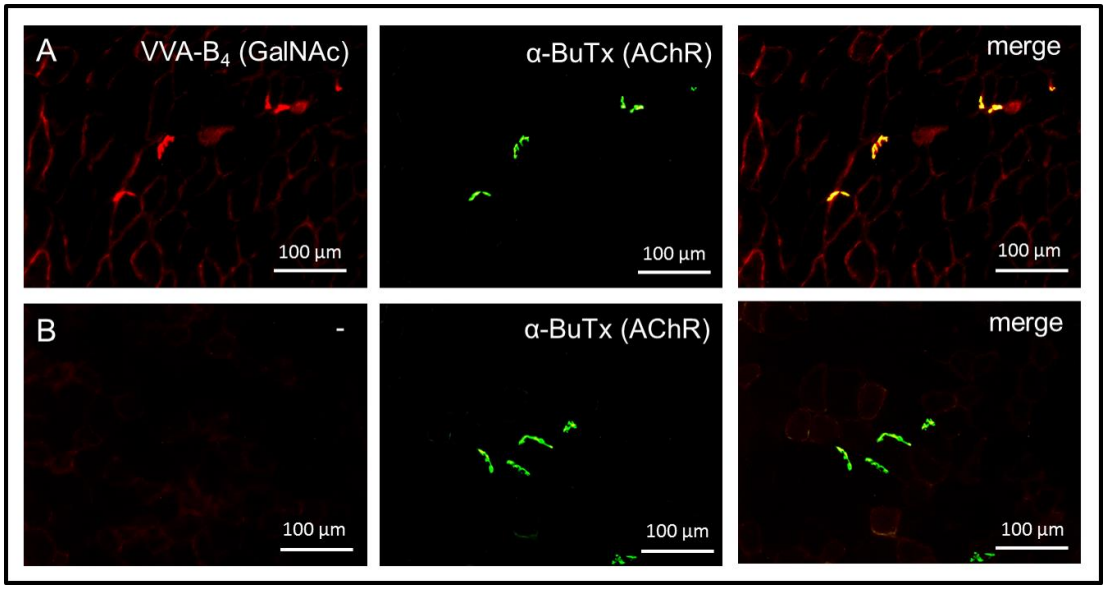

Fig.4.4. Enrichment of N-acetylgalactosamine moieties at the NMJ in mouse tibialis anterior muscle
(A) Mouse tibialis anterior muscle sections were co-stained with TRITC-VVA-B_4 and Alexa Fluor 488 α-BuTx.
(B) For control purposes the muscle was stained with Alexa Fluor 488 α-BuTx only.

Co-localisation of red and green fluorescence, corresponding to GalNAc moieties and AChR, respectively, was observed, which indicated a concentration of GalNAc in the regions of AChR clusters in the muscle tissue. This corresponds with the observations made in C2C12 myotubes and with published data (Martin and Sanes, 1995, Martin et al., 1999), and may further confirm the importance of sugars for the structure and function of the synapse.

4.2.1.4. Is the expression of GFAT1 and GFAT1-L enriched at the neuromuscular junction *in vivo*?

A synaptic localisation of GFAT1 and/or GFAT1-L *in vivo* might indicate a particular role for the enzyme in this region and partially explain why the *GFPT1* mutations

affect neuromuscular transmission. It would also correlate with the concentration of glycan moieties at the neuromuscular endplate.

The subcellular localisation of GFAT1 was analysed by co-staining sectioned mouse tibialis anterior muscle and teased fibres of mouse extensor digitorum longus muscle with Alexa Fluor 488 α-BuTx and a rabbit monoclonal anti-GFAT1 antibody, and the appropriate Alexa Fluor 568 secondary antibody (Figures 4.5. and 4.6.).

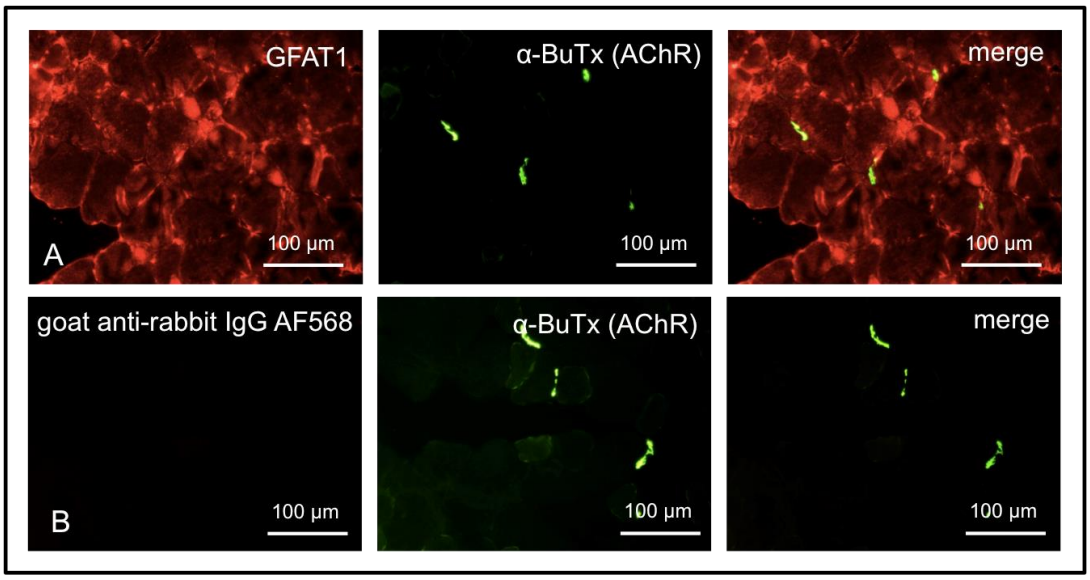

Fig.4.5. Localisation of endogenous GFAT1 in mouse tibialis anterior muscle
Frozen tibialis anterior muscle sections were fixed, permeabilised and co-stained with (A) an anti-GFAT1 antibody and the appropriate Alexa Fluor 568 secondary antibody, and Alexa Fluor 488 α-BuTx or (B) the Alexa Fluor 568 secondary antibody and Alexa Fluor 488 α-BuTx.

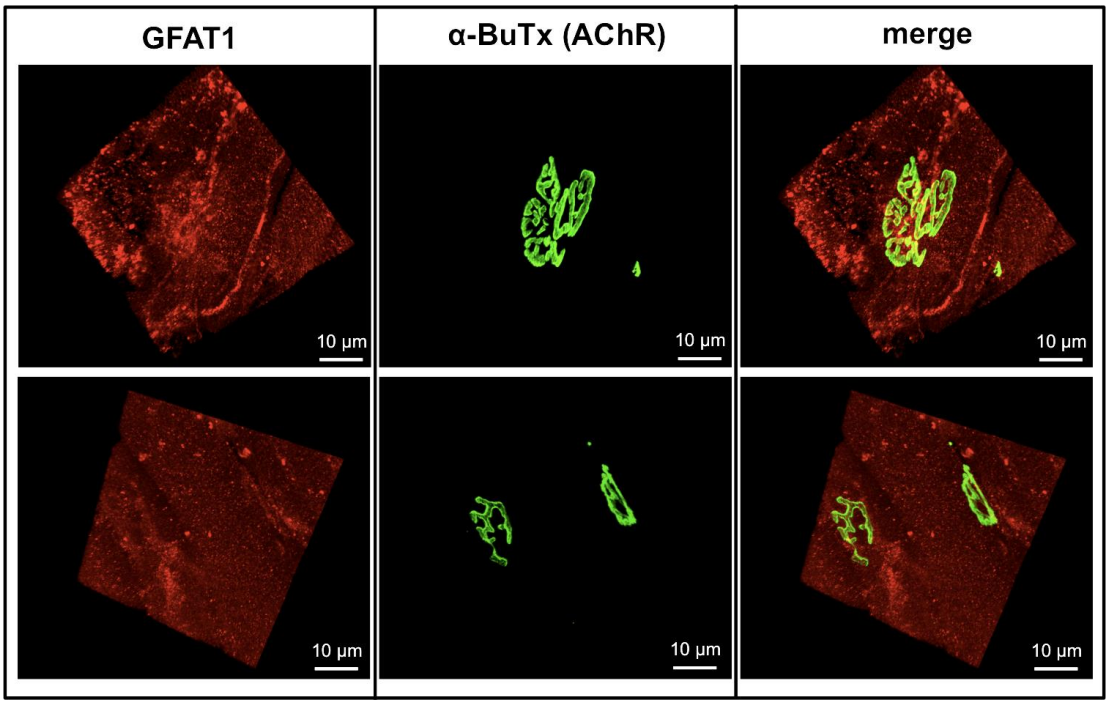

Fig.4.6. Localisation of endogenous GFAT1 in mouse extensor digitorum longus muscle
Teased extensor digitorum longus muscle fibres were co-stained with an anti-GFAT1 antibody and the appropriate Alexa Fluor 568 secondary antibody, and Alexa Fluor 488 α-BuTx. Two representative images are presented.

Staining of endogenous GFAT1 was diffuse within the cytoplasm, and no concentration of the enzyme in the endplate regions in mouse tibialis anterior and extensor digitorum longus muscles was observed. However, there is still a possibility that different GFAT1 isoforms are present at distinct subcellular localities.

4.2.1.5. Role of muscle-specific exon in the subcellular localisation of GFAT1-L

There are two protein products of the *GFPT1* gene, GFAT1 and GFAT1-L, with the latter possessing an 18-amino acid insertion at position 229, with expression restricted to skeletal muscle and heart (DeHaven et al., 2001, Niimi et al., 2001). The role of this alternatively spliced exon remains unclear. It could target the protein to a specific localisation in the tissue, such as for instance to the NMJ. Antibodies that differentiated between the two isoforms were not available, and thus *in vivo* expression of the constructs for the two isoforms was undertaken.

4.2.1.5.1. DNA delivery into mouse muscle using the electroporation technique

One method to deliver DNA *in vivo* is electrogenetransfer, which is commonly used as a non-viral method for introduction of a transgene into a target organ. This technique possesses several advantages over viral delivery systems. It reduces safety risks and costs, and avoids the problems of antibody formation against the viral vectors (Gehl, 2003). This technique has been used successfully by many groups to deliver transgenes into mouse tibialis anterior muscle (Aihara and Miyazaki, 1998). The method uses a brief, high intensity electric field to induce transient yet reversible breakdown of the membrane, allowing an influx of molecules by simple diffusion or through an electrophoretically driven process (Gehl, 2003, Lu et al., 2003).

Control experiments were performed to establish conditions for the gene transfer. Mouse tibialis anterior muscle was injected with 10 µg of a reporter plasmid encoding DsRed. Muscle in the contralateral leg was injected with an empty pcDNA^{TM}3.1/Hygro$^{(-)}$ vector. Following the injections, four pulses of 200 V/cm each were applied to the muscles at a rate of one pulse per s, each pulse lasting 20 ms. Polarity across the electrodes was reversed and the pulses were applied again. Five days later, the muscles were dissected, frozen in liquid nitrogen-isopentane, sectioned at 10 µm thickness and analysed by fluorescence microscopy (Figure 4.7.).

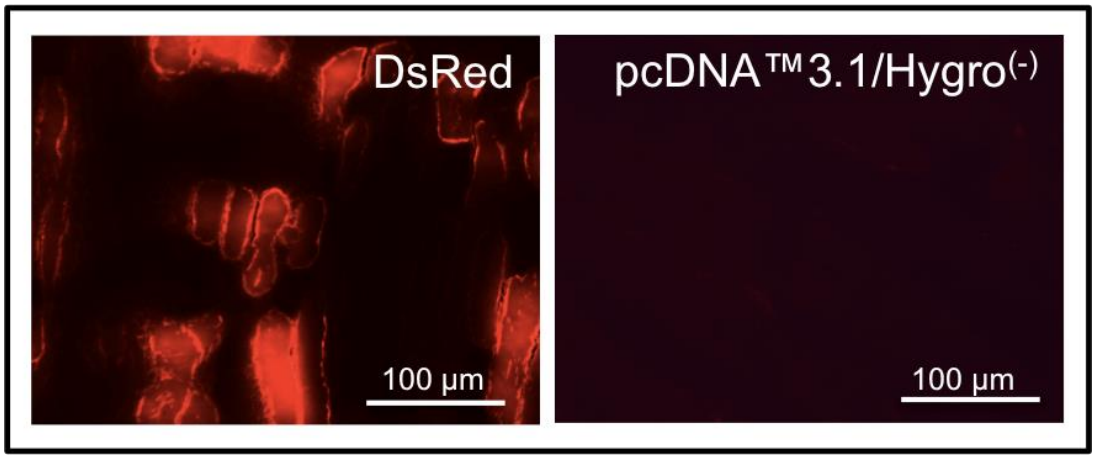

Fig.4.7. DsRed expression in mouse tibialis anterior muscle
Mouse tibialis anterior muscles were electroporated with pDsRed-Monomer-N1 or pcDNA^{TM}3.1/Hygro$^{(-)}$ vectors, respectively. After 5 days, muscles were dissected, frozen and sectioned. Red fluorescence of DsRed was visualised by fluorescence microscopy.

High levels of red fluorescence were observed only in the muscle injected with the DsRed-encoding construct. This proved a successful gene transfer.

4.2.1.5.2. Does the muscle-specific exon localise GFAT1-L to the neuromuscular junction?

To follow the expression in skeletal muscle, the GFAT1 isoforms were tagged with enhanced green fluorescent protein (EGFP). These constructs were electroporated into mouse tibialis anterior muscle and the protein localisation was visualised by fluorescence microscopy.

Initial experiments demonstrated efficient gene delivery into the muscle, but high background autofluorescence of the tissue caused difficulties distinguishing between transfected and non-transfected muscle fibres. To overcome these above difficulties, the signals from the expressed proteins were amplified by immunostaining with a rabbit polyclonal anti-EGFP antibody and a goat anti-rabbit Alexa Fluor 488 secondary antibody (Figure 4.8.).

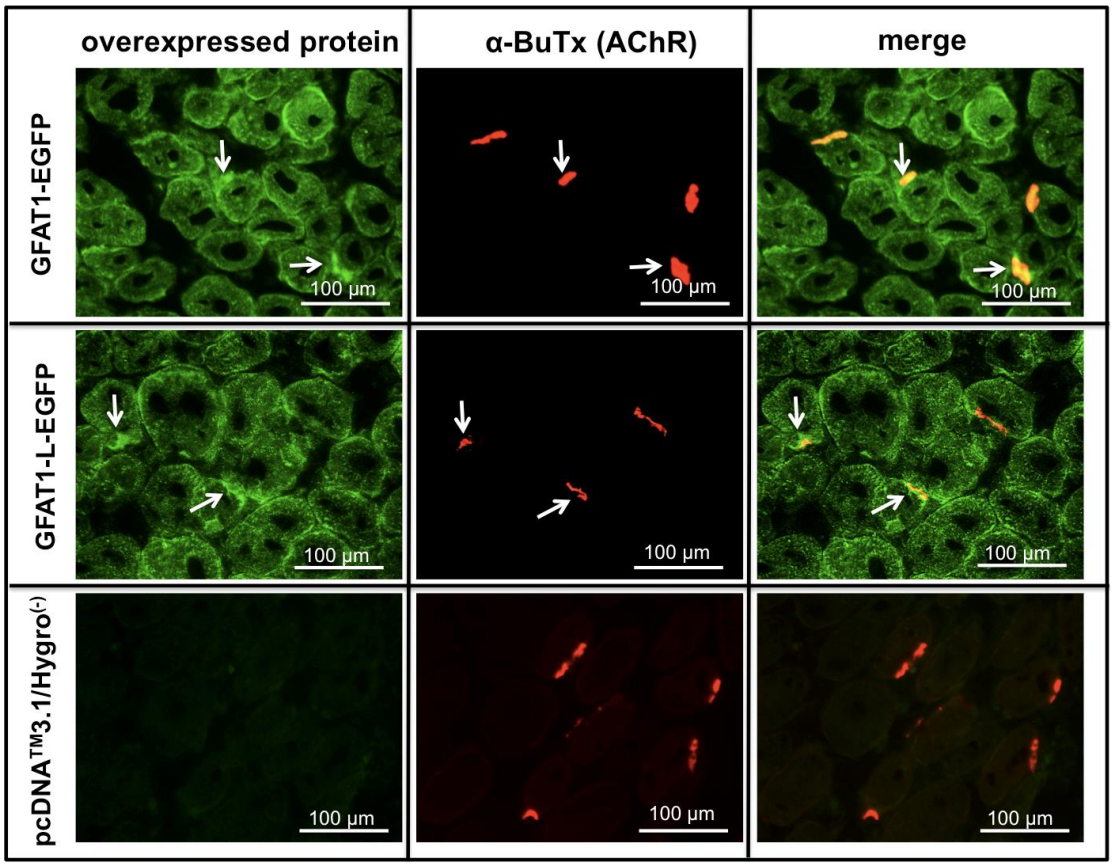

Fig.4.8. Apparent increase in GFAT1-EGFP and GFAT1-L-EGFP expression at the NMJ in mouse tibialis anterior muscle
Mouse tibialis anterior muscles were electroporated with GFAT1-EGFP- or GFAT1-L-EGFP-encoding vectors, or empty pcDNA™3.1/Hygro(-) plasmid as a control. Muscles were frozen, sectioned, fixed, permeabilised and green fluorescence of EGFP was amplified by staining with an anti-EGFP antibody and the appropriate Alexa Fluor 488 secondary antibody. NMJ were stained with Alexa Fluor 594 α-BuTx. The arrows show representative neuromuscular endplates.

As shown in Figure 4.8., the over-expressed GFAT1-EGFP and GFAT1-L-EGFP were widely distributed in the cytoplasm. However, a small increase was seen in both GFAT1-EGFP and GFAT1-L-EGFP green fluorescence at some NMJs. This was not noticeable when the mock-electroporated muscles were stained with the anti-EGFP antibody. These findings are likely to be the result of increased membrane folding, which occurs in the NMJ region, and often leads to an increase in fluorescence signal. No differences were observed in the subcellular localisation of GFAT1-EGFP and GFAT1-L-EGFP, suggesting that the muscle-specific exon is not acting to localise the enzyme at the synapse.

4.2.1.6. Does GFAT1 or GFAT1-L play a role in the formation of the neuromuscular synapse?

Clustering of AChR in response to AGRN was used as a model for the formation of the NMJ. Primary human myoblasts were differentiated into myotubes using optimised conditions (Chapter 2, section 2.5.1.2.), and AChR cluster formation was induced by incubating with AGRN (Figure 4.9.).

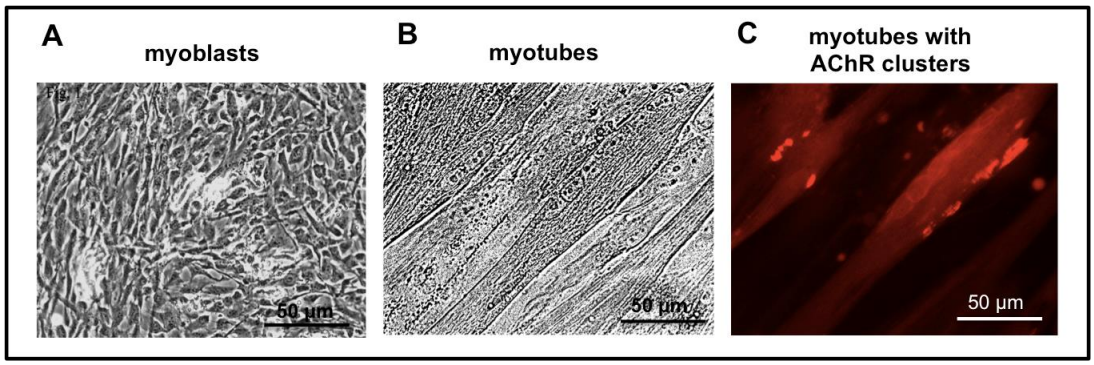

Fig.4.9. Human skeletal muscle cells in culture as a model system to study muscle disorders
The images represent subsequent stages of muscle cells in culture: (A) undifferentiated myoblasts, (B) differentiated multinucleated myotubes and (C) myotubes with AChR clusters stained with Alexa Fluor 594 α-BuTx.

To study GFAT1 expression levels, differentiated myotubes and myotubes treated overnight with AGRN were harvested and total protein was extracted from the cells. Its concentration in each sample was measured using a bicinchoninic acid (BCA) assay and equal amounts of protein were resolved on polyacrylamide gels, and transferred to polyvinylidene difluoride (PVDF) membranes. GFAT1 protein levels were estimated by western blot. The western blot membranes were also reprobed with a mouse monoclonal anti-α-tubulin antibody (Figure 4.10.).

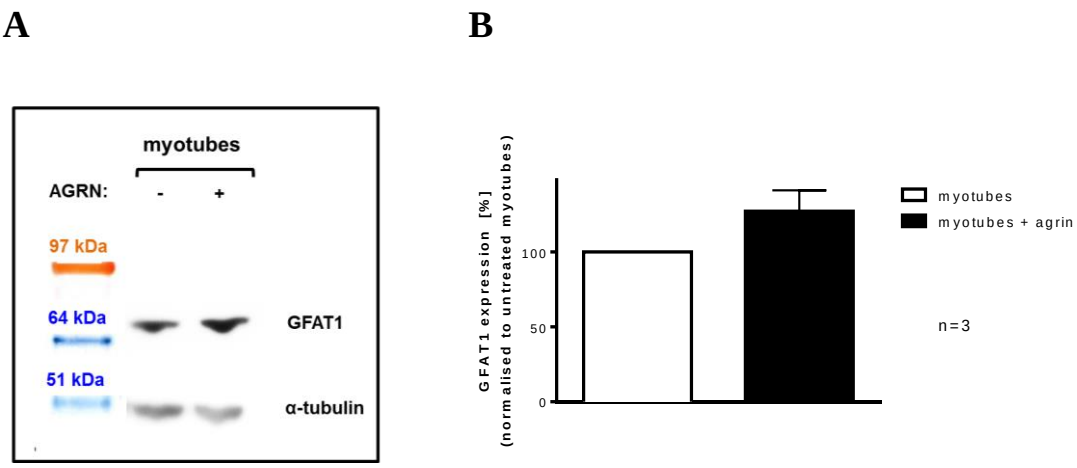

Fig.4.10. GFAT1 expression in untreated and AGRN-treated human skeletal myotubes
(A) Protein extracts from untreated and AGRN-treated myotubes were immunoblotted with anti-GFAT1 and anti-α-tubulin antibodies, and the appropriate secondary HRP-conjugated antibodies.
(B) The intensity of the bands was measured by densitometry and GFAT1 expression was normalised to the α-tubulin levels. Each bar represents the mean±SEM GFAT1 protein levels, recorded in n=3 independent experiments, in untreated and AGRN-treated wild type myotubes, respectively. All the data are expressed relative to the levels of GFAT1 in the untreated cells.

No significant changes were detected in the intensity of the bands that corresponded to GFAT1 between the untreated cells and those treated with AGRN. This indicated that the expression of GFAT1 was not grossly altered during the AGRN-induced clustering of AChR.

4.2.2. Global glycosylation patterns in wild type and *GFPT1*-mutated cells

No clear links were established between GFAT1 and the NMJ, but there was still the potential for *GFPT1* mutations to alter the synthesis of particular glycan classes, found by us and others to be enriched at the neuromuscular endplates (Martin and Sanes, 1995, Martin et al., 1999, Scott et al., 1988, Martin, 2003). The changes could be detected on global glycosylation profiles.

4.2.2.1. N-glycosylation in wild type and *GFPT1*-mutated human skeletal myoblasts and dermal fibroblasts

Preliminary data from clinical biochemical studies suggested that *GFPT1* mutations were not detected using serum transferrin isoform analysis. To investigate general effects on glycosylation patterns, the N-glycan profiles of wild type and *GFPT1*-mutated cells were studied. The research was conducted in collaboration with Prof. Anne Dell and Dr Stuart Haslam at Imperial College London in The Glycobiology Training, Research and Infrastructure Centre (GlycoTRIC).

Glycans were extracted from muscle cells and fibroblasts derived from healthy controls or *GFPT1* patients. Their composition and relative abundance were analysed by matrix-assisted laser desorption ionisation - time-of-flight mass spectrometry (MALDI-TOF MS). This method enables one to analyse the relative amounts of glycans composed of particular monosaccharides. Each peak detected on the MS spectrum can be assigned to a specific carbohydrate chain, based on its molecular weight. The height of the peak indicates the relative amount (%) of a particular sugar moiety in the analysed extract. To analyse whether the *GFPT1* mutations lead to any changes in the global N-glycosylation profiles in the cells, we looked at the relative ratios of different types of sugars present in myoblasts derived from two healthy individuals and two *GFPT1* CMS patients (P1 and P2) harbouring p.R385H/R434H and p.T15M/R496W mutations in GFAT1, respectively, and in skin fibroblasts obtained from one healthy individual and one potential *GFPT1* patient (P3) harbouring p.T479N amino acid substitution in GFAT1. The detected sugars were divided into several subclasses, namely: high mannose glycans, bi-, tri- and tetra- antennary ones, and sugars decorated with fucose or sialic acid, and the ratios of these were compared between the samples obtained from the healthy individuals and the patients. The

muscle cells and the fibroblasts were analysed separately since N-glycosylation patterns are likely to vary among different tissues (Figures 4.11., 4.12., 4.13., 4.14., 4.15. and 4.16.).

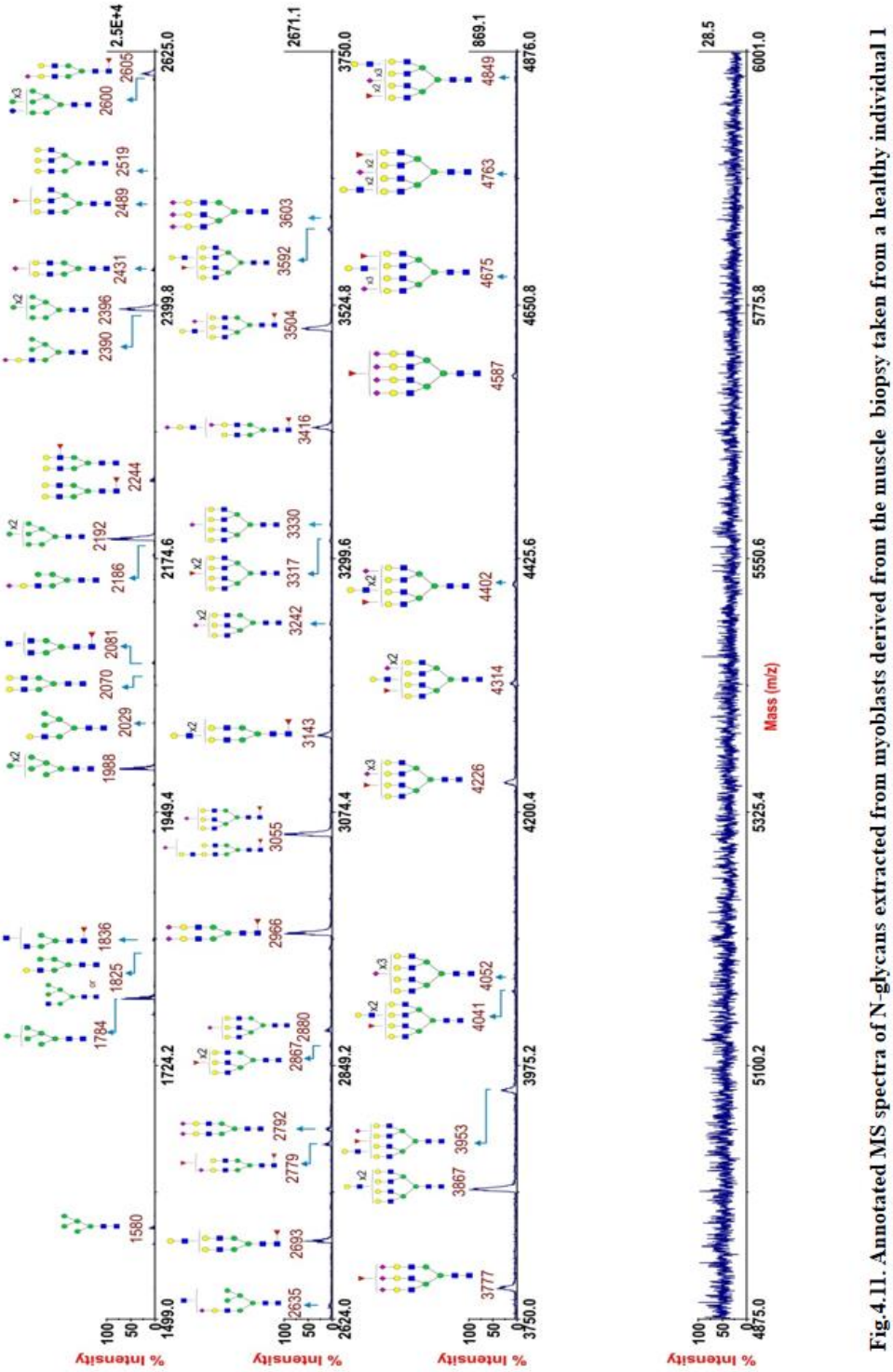

Fig.4.11. Annotated MS spectra of N-glycans extracted from myoblasts derived from the muscle biopsy taken from a healthy individual 1

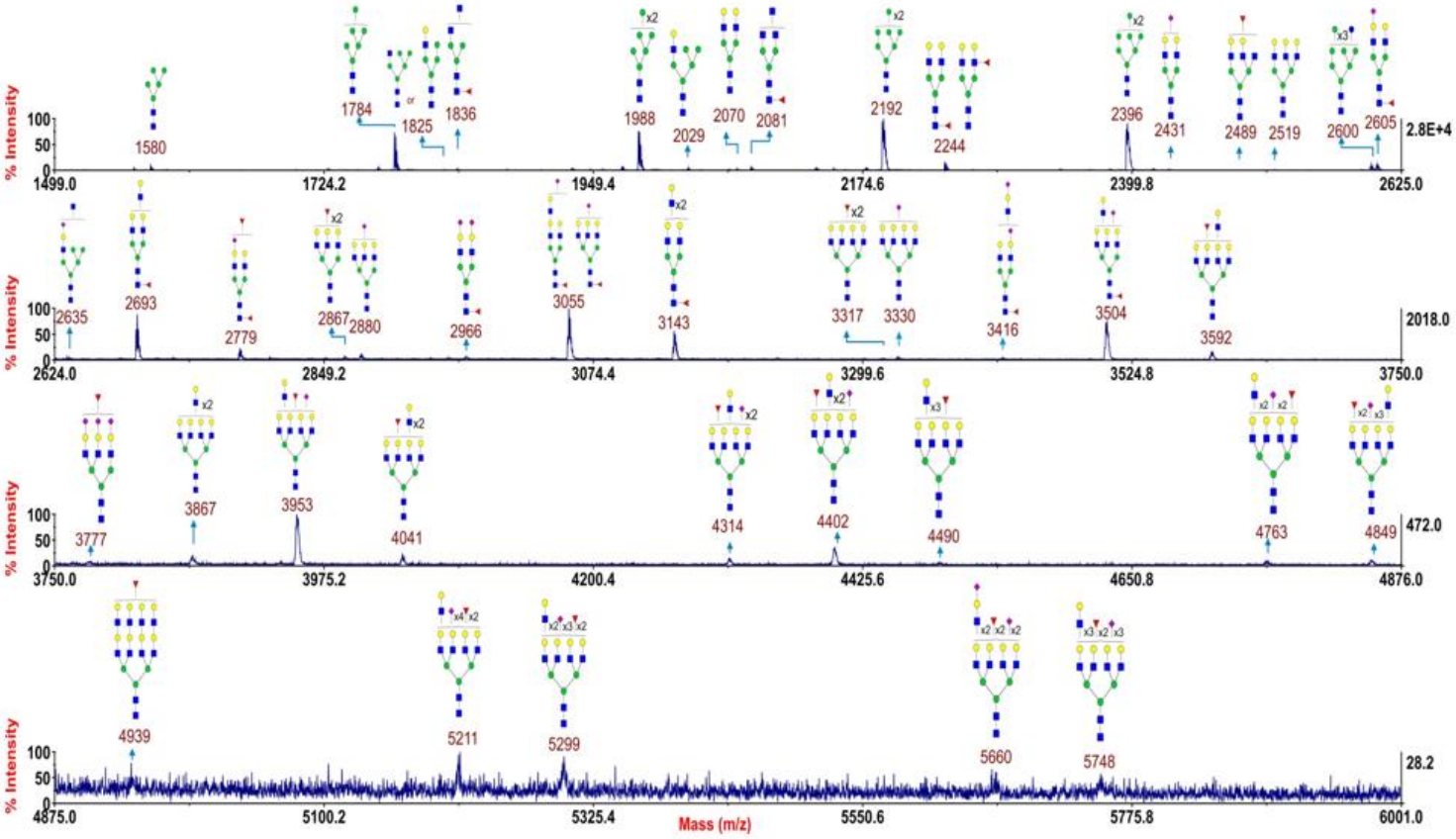

Fig.4.12. Annotated MS spectra of N-glycans extracted from myoblasts derived from the muscle biopsy taken from a healthy individual 2

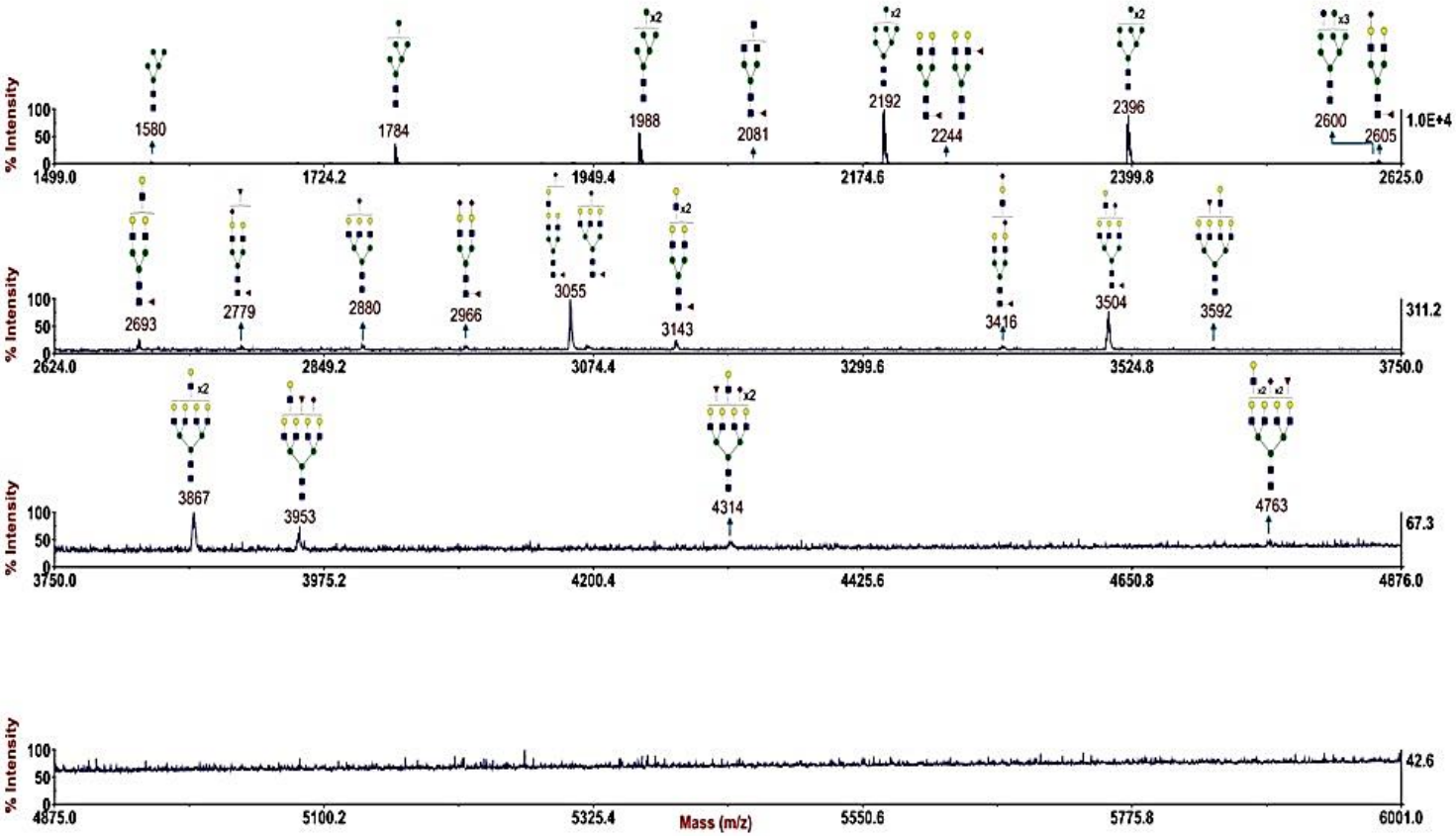

Fig.4.13. Annotated MS spectra of N-glycans extracted from myoblasts derived from the muscle biopsy taken from (P1) p.R385H/R434H patient

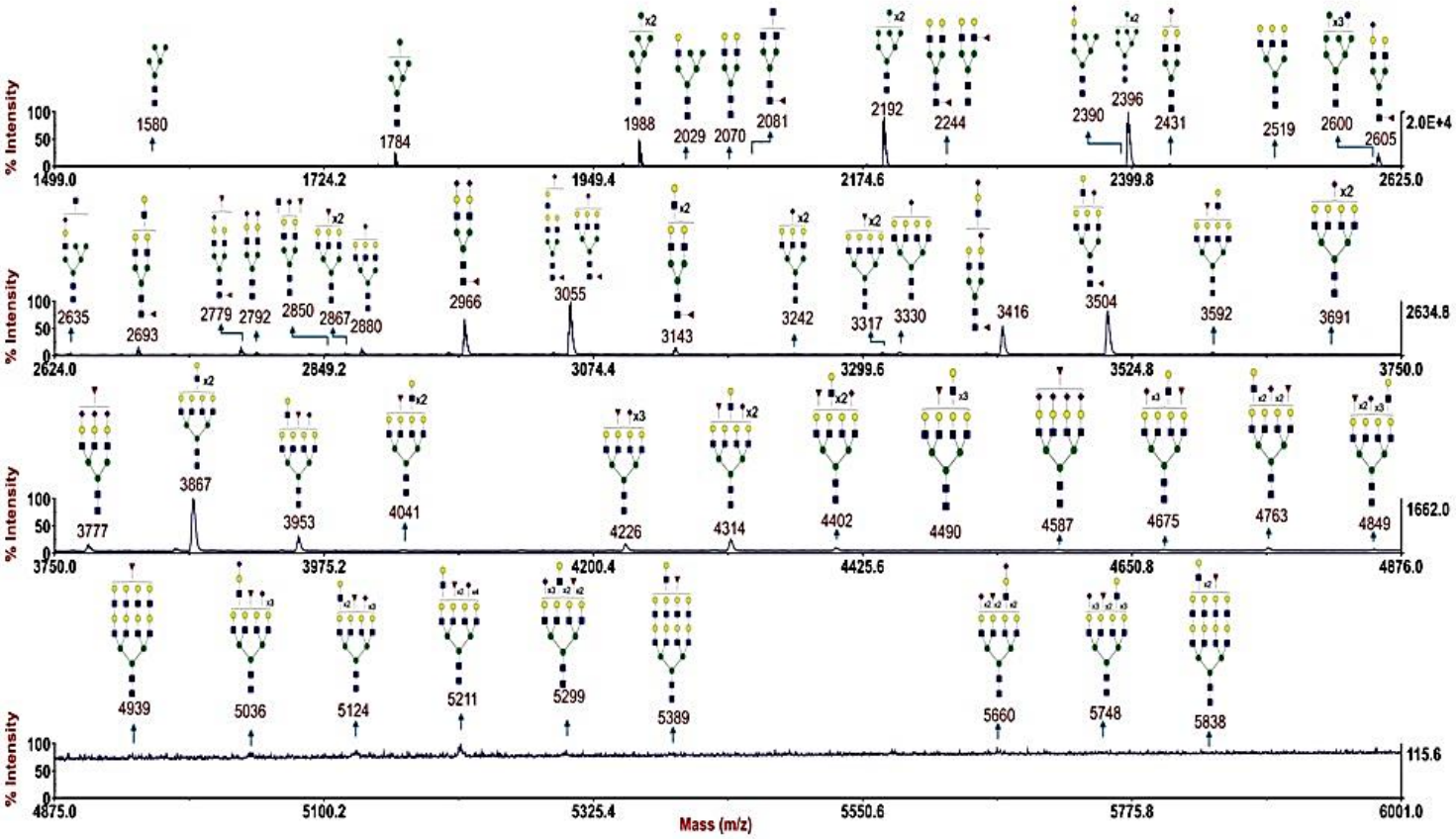

Fig.4.14. Annotated MS spectra of N-glycans extracted from myoblasts derived from the muscle biopsy taken from (P2) p.T15M/R496W patient

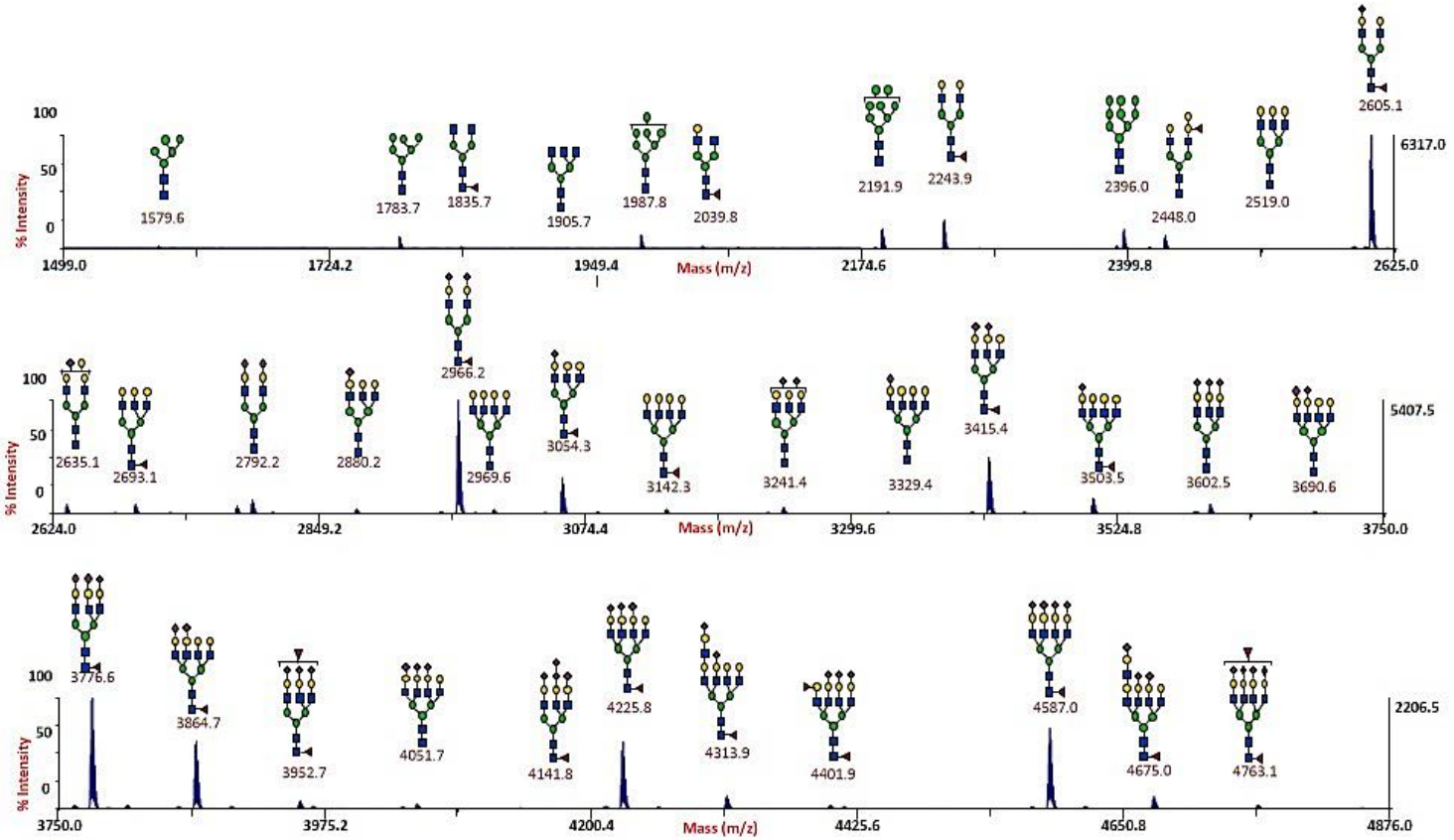

Fig.4.15. Annotated MS spectra of N-glycans extracted from human dermal fibroblasts from a healthy individual

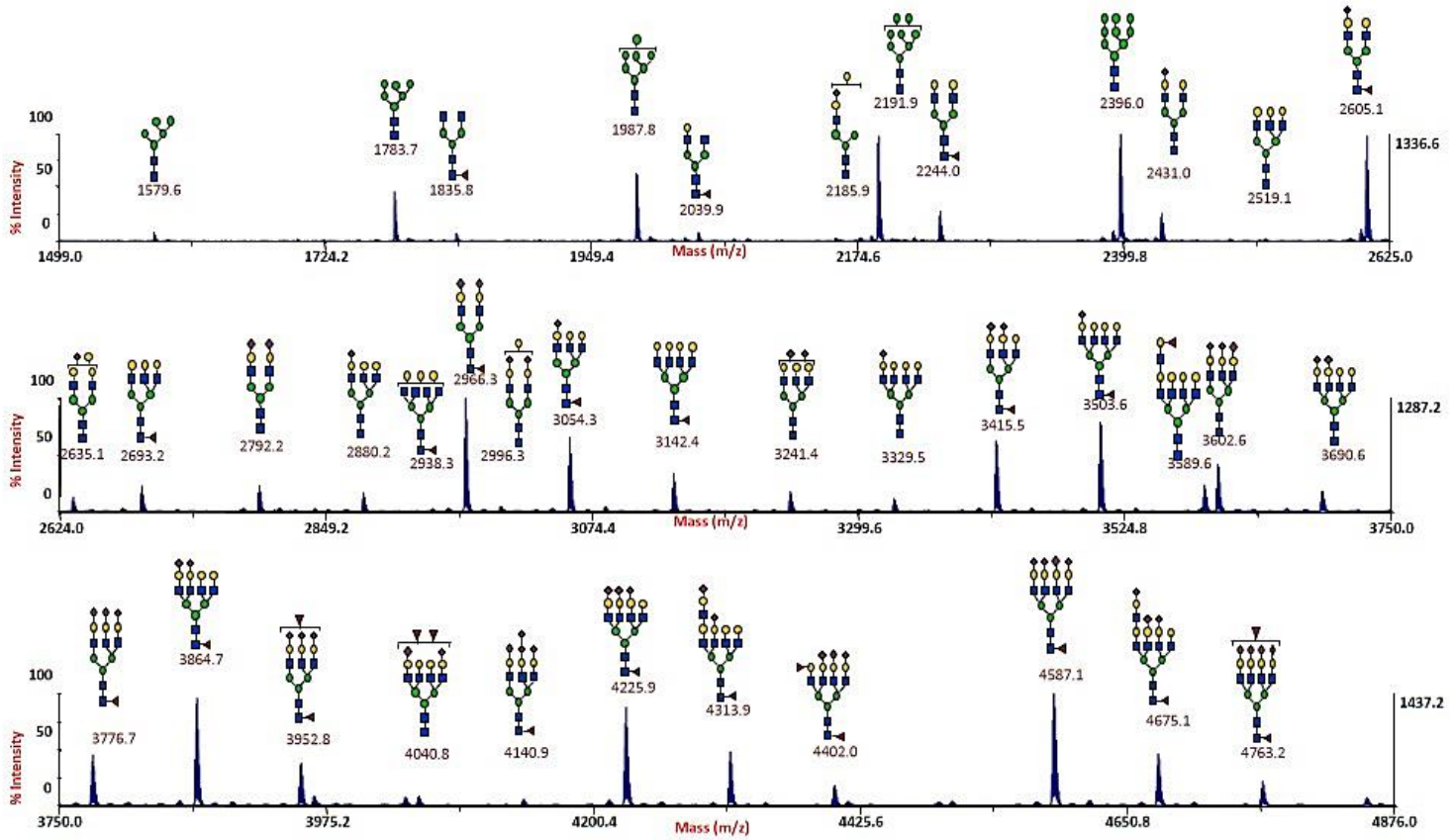

Fig.4.16. Annotated MS spectra of N-glycans extracted from human dermal fibroblasts from (P3) p.T479N patient

Various types of carbohydrates (both high mannose and complex) were detected in all samples. When these were divided into the aforementioned subclasses and their ratios was compared between extracts obtained from control and patient samples, there were no consistent alterations in the abundance of sugars classified into different groups, and hence these experiments did not indicate any clear changes in the levels of particular classes of glycans in the *GFPT1*-mutated cells compared to the wild type controls. This would suggest that the *GFPT1* disease cannot be classified as CDG-II (resulting in changes in glycosylation profiles), but might still belong to the group of CDG-I diseases (affecting total levels of glycosylation). This experimental method cannot, however, be used to study alterations in total levels of modification.

4.2.2.2. Protein O-GlcNAcetylation in *GFPT1*-mutated muscle cells

UDP-GlcNAc – the final product of the hexosamine biosynthetic pathway is also required for O-linked β-N-acetylglucosamine (O-GlcNAc) modification. The attachment of O-GlcNAc moieties is important for many cellular processes, including differentiation, metabolism, contractile function of striated muscle (Cieniewski-Bernard et al., 2004) and protection against oxidative stress (Cieniewski-Bernard et al., 2009, Zachara and Hart, 2006). Alterations in its levels have been reported to contribute to the pathogenesis of many diseases (Hart et al., 2011).

Experiments were performed to determine whether differences in O-GlcNAc patterns between wild type and *GFPT1*-mutated human skeletal myotubes could be detected. Total and nuclear protein lysates obtained from cells were immunoblotted with a mouse monoclonal anti-O-GlcNAc antibody for selective detection of the O-GlcNAc moieties (Figure 4.17.).

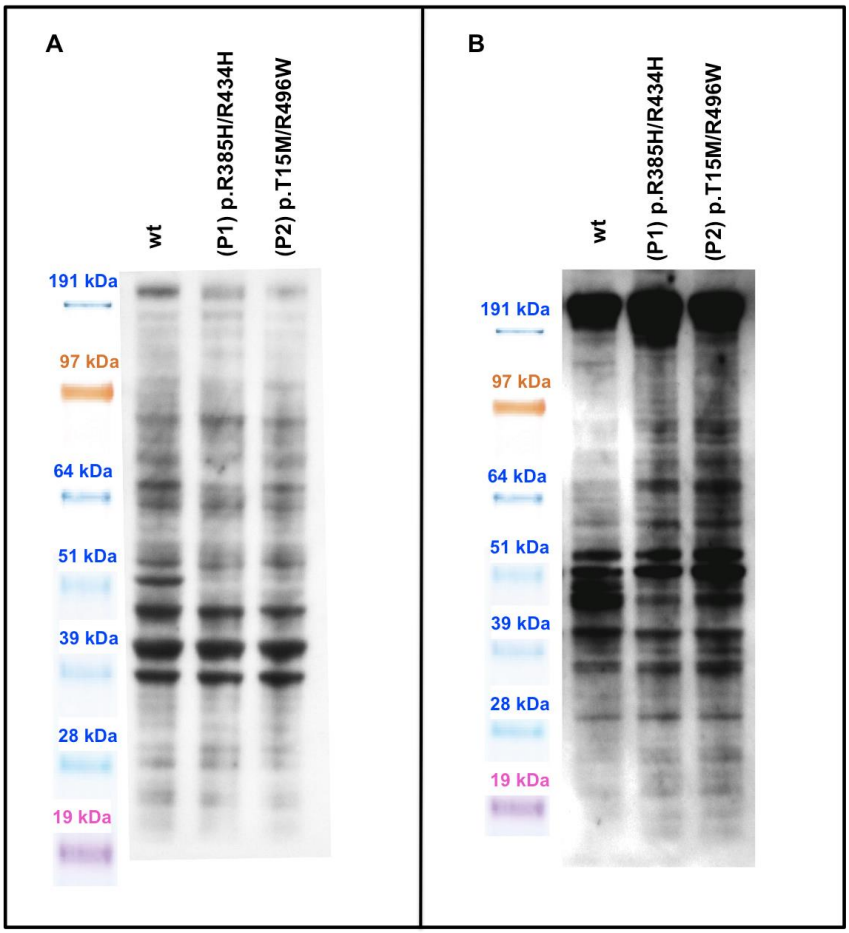

Fig.4.17. O-GlcNAcetylation in wild type and *GFPT1*-mutated myotubes
(A) Total or (B) nuclear protein was extracted from wild type and *GFPT1*-mutated human skeletal myotubes, and immunoblotted with an anti-O-GlcNAc antibody and the appropriate HRP-conjugated secondary antibody.

The antibody recognised several bands in all samples, with the intensity of many of them varying between the analysed cells. However, subsequent repeats of the experiments showed such a variability in the O-GlcNAc patterns that it was decided not to continue with this line of investigation.

4.2.2.3. Glycosphingolipids in wild type and *GFPT1*-mutated human skeletal muscle cells

Another major group of glycosylated cellular molecules are glycosphingolipids (GSLs), which are the most structurally diverse class of complex sphingolipids, modified with more than 500 different carbohydrate structures. Main sugar

components of GSLs are glucose, galactose, fucose, GlcNAc, GalNAc and sialic acid (N-acetylneuraminic acid) (Lahiri and Futerman, 2007, Merrill, 2011).

Samples were studied in collaboration with Dr David Priestman. The method involved extraction and purification of GSLs from wild type or *GFPT1*-mutated human muscle cells and release of glycan moieties by ceramide glycanase digestion. The ceramide-glycanase-released oligosaccharides were labelled with anthranilic acid (2-amino-benzoic acid; 2-AA) and separated by normal-phase high performance liquid chromatography (NP-HPLC) (Neville et al., 2004). First, the chromatograms were studied in terms of the relative expression of different GSLs between the myoblasts and the myotubes and then between the wild type and the *GFPT1*-mutated cells. Each peak detected on the chromatograms corresponds to a particular GSL, the abundance of which is indicated by the height of the peak (Figure 4.18.).

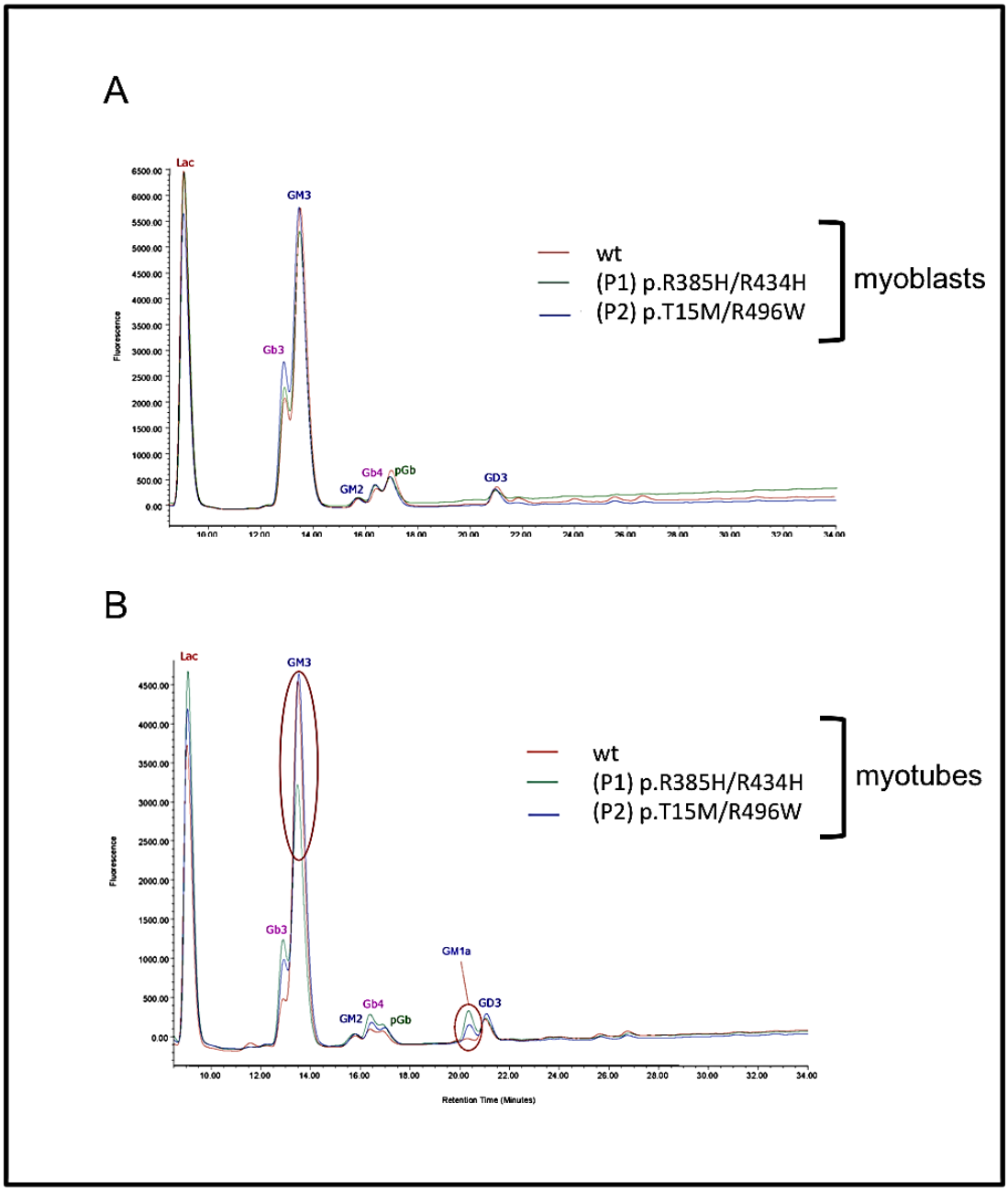

Fig.4.18. Glycosphingolipids extracted from wild type and *GFPT1*-mutated human skeletal (A) myoblasts and (B) myotubes
Glycolipids were extracted from the wild type and the *GFPT1*-mutated muscle cells. Glycan moieties were released and analysed using NP-HPLC.
Major differences observed between the wild type and the mutated cells are circulated in red.

Following differentiation of the myoblasts into myotubes, considerable changes occurred in the expression ratio of Gb4 and pGb, and an increase in the expression of GM1a. The latter glycolipid was present in the myotubes only and exhibited an elevated expression in the *GFPT1*-mutated myotubes from both patients compared to

the healthy control. Another alteration was a minor reduction in the GM3 levels in the (P1) p.R385H/R434H myotubes. The differences detected between the wild type and the *GFPT1*-mutated myotubes may indicate that glycolipid biosynthesis is altered by GFAT1 deficiency.

4.3. Discussion

The discovery of the defects in GFAT1 was quickly followed by the identification of CMS-underlying mutations in three proteins (DPAGT1, ALG2 and ALG14) (Belaya et al., 2012, Cossins et al., 2013b) from the N-glycosylation pathway, whose function at least partially depends on the efficiency of the hexosamine biosynthetic pathway. *GFPT1, DPAGT1, ALG2* and *ALG14* CMS patients present with a number of phenotypic similarities (Belaya et al., 2012, Cossins et al., 2013b, Guergueltcheva et al., 2011, Senderek et al., 2011), which suggests that the mutations in all these genes lead to aberrant neuromuscular transmission through a similar mechanism, such as compromised N-glycosylation. However, the final product of the hexosamine biosynthetic pathway (UDP-GlcNAc) is also used in O-glycosylation as well as the synthesis of glycolipids, therefore we cannot exclude the possibility that the detrimental consequences of these gene mutations occur also in these processes. Theoretically, it is possible that the defects in the *GFPT1* gene lead to CMS through multiple mechanisms.

The question of whether GFAT1 and glycosylation are especially important at the NMJ was approached by the analysis of the glycoprotein patterns *in vitro* in C2C12 myotubes and *in vivo* in mouse tibialis anterior muscle. These investigations pointed to a relatively high expression of carbohydrate moieties at the sites of AChR clusters. One of the sugars found to be highly concentrated at the synapse was GalNAc. These findings agreed with the previous studies of the carbohydrate patterns in muscle cells (Martin and Sanes, 1995, Scott et al., 1988).

The concentration of a specific repertoire of sugars at the synapse may indicate that they play a far from passive role in this region. It could also suggest that there might be a specific cellular mechanism responsible for concentrating carbohydrates at the

NMJ. A potential mechanism involves localisation of the glycosylation enzymes, such as β-1,4-N-acetyl-galactosaminyl transferase 1 (B4Galnt1) (Xia et al., 2002) and 2 (B4Galnt2) (Singhal et al., 2012) and ALG14 (Cossins et al., 2013b) in the synaptic region. The possibility that the same might also be true for GFAT1 and/or GFAT1-L, with the muscle-specific exon possibly being essential for the process, was investigated. The data obtained from immunofluorescence studies showed a diffused cytoplasmic expression of the endogenous GFAT1 or GFAT1-L, both *in vitro* in C2C12 myotubes and *in vivo* in muscle fibres. We were unable to study the specific distribution of the two GFAT1 isoforms (GFAT1 and GFAT1-L) in the cells because there are, at present, no antibodies that can distinguish the two isoforms. Therefore, over-expression of tagged GFAT1 and GFAT1-L in *in vivo* experiments was used. The tag allowed distinction between the endogenous and exogenous proteins. When the EGFP-tagged enzyme was over-expressed in mouse tibialis anterior muscle, a modest increase in green fluorescence was observed at the NMJ for both GFAT1-EGFP and GFAT1-L-EGFP. This was most probably the result of considerable membrane folding at the synapse leading to an increased fluorescence signal.

The ubiquitous expression of GFAT1 and GFAT1-L suggested looking first at global glycosylation patterns in *GFPT1*-mutated cells and so we analysed total N-glycan and glycolipid profiles. No significant alterations in the levels of particular N-glycan classes were found, which is consistent with reports that mutations in the enzymes catalysing the early steps of glycosylation do affect total levels of the modification with carbohydrates, but not the relative abundance of particular glycans (Jones et al., 2012).

By contrast, studies of glycolipid patterns indicated an increased expression of GM1a GSL in the myotubes from both *GFPT1* CMS patients and a reduction in the levels of

GM3 gangliolipid, the main GSL within skeletal muscle (Muthing and Cacic, 1997), in the (P1) p.R385H/R434H myotubes. However, these changes could result from the myotubes being in different developmental phases. The increased expression of GM1a could be explained by the fact that the wild type cells were in an earlier stage of differentiation since this glycolipid exhibited higher expression in the myoblasts compared to the myotubes, irrespective of the mutations. The reduction in GM3 levels in one of the patients possibly warrants further investigation. Studies of GM2/GD2-synthase*GD3-synthase double-knock-out mice, after enzymatic removal of the remaining GM3, have suggested that the complete ablation of the gangliosides results in aberrant neurotransmission (Zitman et al., 2010). It is not clear whether the relatively small reduction observed in one of the *GFPT1* cases would produce similar effects.

Some alterations in the patterns of the O-GlcNAc modification in the *GFPT1*-mutated myotubes were also observed, but the observations proved inconsistent in subsequent experiments, and therefore this line of investigation was discontinued. The variations might be the result of changes in the cell cycle phase and the differentiation status of the cells (Ogawa et al., 2012).

The lack of clear-cut changes of global glycosylation in the *GFPT1*-mutated cells may point to only local (specific only to particular neuromuscular proteins) consequences of the *GFPT1* mutations. This warrants further investigation.

Chapter 5

The link between GFAT1 and AChR expression

5.1. Introduction

The likely causes of L-glutamine:D-fructose-6-phosphate amidotransferase 1 (*GFPT1*) congenital myasthenic syndrome (CMS) are reduced protein levels or an impaired activity of GFAT1 (Ohno, 2013), but it remains unclear why a deficiency of this ubiquitously expressed enzyme should cause impaired neuromuscular transmission. This question can be investigated in patient muscle cells or with model systems that reduce activity of the target enzyme or diminish its protein levels.

Catalytic activity of GFAT1 can be reduced by chemical inhibitors that bind to the active site of the protein, but are not utilised in the catalysed reaction. A number of glutamine (Gln) analogues, such as 6-diazo-5-oxo-L-norleucine (DON), anticapsin, N3-(4-methoxyfumaroyl)-L-2,3-diaminopropanoic acid (FMDP) and azaserine, have been shown to inactivate the enzyme in a time- and a concentration-dependent manner (Milewski, 1993). The use of these chemicals is limited by their potential to inhibit not only the target enzyme, but also other enzymes that utilise Gln in catalysed reactions. This has the potential to cause non-specific off-target effects.

Off-target action of the inhibitors can be reduced by utilising RNA interference (RNAi) pathways. A number of specific classes of small RNA have been described: small interfering RNA (siRNA), short hairpin RNA (shRNA), microRNA (miRNA), piwi-interacting RNA (piRNA) and 21-U RNA. Despite their differences, they all have an overlapping requirements for double-stranded RNA as a precursor, and Dicer and Ago subfamily proteins for further processing (Naqvi et al., 2009b).

The most common class of RNA used as a tool in molecular biology is siRNA. These are single-stranded 20-24 nucleotide-long nucleic acids generated from double-stranded RNA molecules by an RNase III-type endonuclease – Dicer. This cleaves the double-stranded RNA, and then Argonaute proteins, members of an siRNA-induced silencing complex (siRISC), unwind the duplex siRNA. One of the strands, referred to as a guide strand, is retained with the protein complex, while the other, known as a passenger strand, is degraded by exonucleases. The guide strand can target an RNA sequence and mediate the gene silencing by degrading the target transcript or inhibiting its translation. The silencing properties of siRNA depend upon a critical region within its sequence, designated as a "seed region", and located between the second and the seventh nucleotide of the siRNA (Naqvi et al., 2009a).

These molecular biology tools can be used to model GFAT1 deficiency and its effect on the neuromuscular junction (NMJ) proteins. Clinical observations and muscle biopsy studies provide some indication that the myasthenic weakness in *GFPT1* CMS might be caused by impaired function of the acetylcholine receptor (AChR). Each subunit of the receptor has been shown to be modified with carbohydrate structures (Nomoto et al., 1986, Kostelidou et al., 2006) that are essential for correct assembly of the pentamer and for export of the complexes from the endoplasmic reticulum (ER) through the Golgi to the cell surface (Gehle et al., 1997, Ramanathan and Hall, 1999, Wanamaker and Green, 2005). However, other targets cannot be excluded.

5.2. Is there a link between AChR expression and *GFPT1* mutations?

Preliminary experiments have so far not demonstrated any gross global alterations in the expression of the glycans in *GFPT1*-mutated muscle cells. This does not exclude the possibility that GFAT1 deficiency affects the glycosylation of specific protein targets that are potentially crucial for neuromuscular transmission.

5.2.1. AChR cell surface expression in wild type and *GFPT1*-mutated human muscle cells

The first potential target to be analysed was AChR, which is a pentamer composed of homologous subunits with multiple glycosylation sites (Nomoto et al., 1986, Poulter et al., 1989). Previous studies into the kinetics of maturation and assembly of the AChR subunits have suggested that glycosylation is required for efficient formation of the receptor complex and subsequent cell surface expression (Gehle and Sumikawa, 1991, Gehle et al., 1997, Merlie et al., 1982, Prives and Olden, 1980).

AChR cell surface expression was studied in wild type and *GFPT1*-mutated human skeletal myoblasts by incubating the cells with radiolabelled ^{125}I-α-bungarotoxin (^{125}I-α-BuTx). Control experiments involved preincubating the cells with unlabelled (cold) α-BuTx before incubation with the radiolabelled agent. This provided a background signal since the cold toxin would saturate the cell surface AChR and prevent specific binding of ^{125}I-α-BuTx to the cells. As a positive control for the assay, TE671 DB40 cell line stably transfected with AChR subunits was used (Beeson et al., 1996a) (Figure 5.1.).

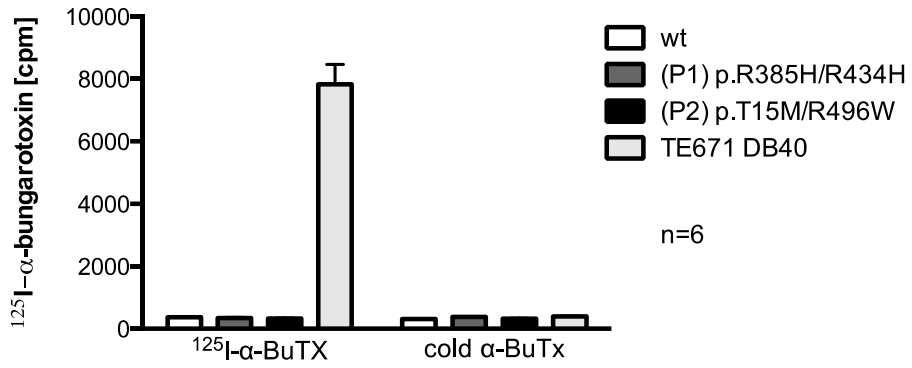

Fig.5.1. Cell surface ^{125}I- α-BuTx binding to wild type and *GFPT1*-mutated human skeletal myoblasts and to TE671 DB40 cells
Each bar represents the mean±SEM cell surface ^{125}I-α-BuTx binding to human skeletal myoblasts and TE671 DB40 cells, or these cells preincubated with cold α-BuTx, respectively, recorded in n=6 independent experiments.

There were no apparent differences observed between the myoblasts incubated with the ^{125}I-α-BuTx and those preincubated with the cold toxin. It is therefore likely that the levels of AChR at the cell surface of these cells were too low to give a clear result. AChR cell surface expression increases significantly following the differentiation of myoblasts into multinucleated myotubes (Prives et al., 1975), therefore the study was repeated for differentiated cells (Figure 5.2.).

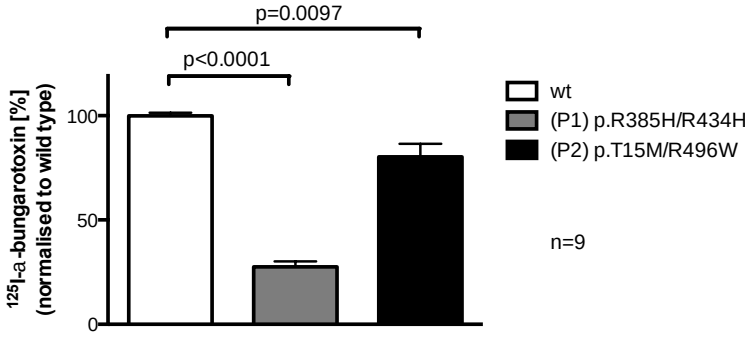

Fig.5.2. Cell surface ^{125}I-α-BuTx binding to wild type and *GFPT1*-mutated human skeletal myotubes (Zoltowska et al., 2013)
Each bar represents the mean±SEM cell surface ^{125}I-α-BuTx binding, recorded in n=9 independent experiments, to human skeletal myotubes. The data are expressed relative to the cell surface ^{125}I-α-BuTx binding to the wild type cells. p values were obtained using a student t-test.

Much higher counts were recorded in this experiment compared to that performed on the myoblasts (~5000 cpm vs. ~400 cpm for wild type cells), and thus allowed comparison of the cell surface expression of AChR between the wild type and the *GFPT1*-mutated myotubes. A significant decrease in the receptor cell surface expression was observed in the (P1) p.R385H/R434H and the (P2) p.T15M/R496W myotubes, to 27.55±2.59%, $p<0.0001$, $n=9$ and 80.25±6.13%, $p=0.0097$, $n=9$ of the control values, respectively. This suggests that GFAT1 is important for the efficient expression of the receptor at the cell surface.

5.2.2. Model systems for investigating *GFPT1* CMS

Mutations in GFAT1 identified in *GFPT1* CMS cases result in lower expression or decreased activity of the protein, and hence model systems of *GFPT1* CMS should involve a reduction in GFAT1 protein expression or an inhibition of its enzymatic activity using specific inhibitors or RNAi pathways. Establishing model systems was important to confirm that the pathogenic changes, detected in muscle cell lines derived from *GFPT1* CMS patients, were the result of mutations in GFAT1 and not intrinsic, non-GFAT1-related, differences between individuals.

5.2.2.1. Silencing of *GFPT1* using siRNA

siRNA sequences were used to silence *GFPT1* expression, one targeting both *GFPT1* isoforms (*GFPT1*) and the other complement to the *GFPT1-L* variant only (*GFPT1-L*). The sequences of the molecules are shown in Chapter 2, section 2.3.1. The siRNA, enhanced green fluorescent protein (EGFP)-tagged GFAT1- or GFAT1-L-encoding constructs and a pcDNA-*mCherry* vector, as a marker of transfection efficiency, were

transfected into human embryonic kidney cells (HEK293TSA). *EGFP*-specific siRNA was used as a control (Table 5.1. and Figures 5.3., 5.4. and 5.5.).

The choice of the EGFP-tagged constructs was determined by several factors. First, the expression levels of the proteins tagged with EGFP could be detected readily by fluorescence microscopy. Secondly, the tagged proteins could be identified on a polyacrylamide gel and separated from the endogenously expressed GFAT1 due to their higher molecular weight. Finally, the *EGFP*-specific siRNA can be used as a control.

Table 5.1. Summary of DNA and siRNA transfected into HEK293TSA cells

	GFAT1 construct	siRNA target	transfection marker
1	GFAT1-EGFP	*GFPT1* and *GFPT1-L*	pcDNA-*mCherry*
2	GFAT1-EGFP	scrambled *GFPT1* and *GFPT1-L* (negative control)	pcDNA-*mCherry*
3	GFAT1-L-EGFP	*GFPT1* and *GFPT1-L*	pcDNA-*mCherry*
4	GFAT1-L-EGFP	scrambled *GFPT1* and *GFPT1-L* (negative control)	pcDNA-*mCherry*
5	GFAT1-L-EGFP	*GFPT1-L*	pcDNA-*mCherry*
6	GFAT1-L-EGFP	scrambled *GFPT1-L* (negative control)	pcDNA-*mCherry*
7	GFAT1-EGFP	*EGFP* (positive control)	pcDNA-*mCherry*
8	GFAT1-EGFP	scrambled *EGFP* (negative control)	pcDNA-*mCherry*
9	GFAT1-L-EGFP	*EGFP* (positive control)	pcDNA-*mCherry*
10	GFAT1-L-EGFP	scrambled *EGFP* (negative control)	pcDNA-*mCherry*

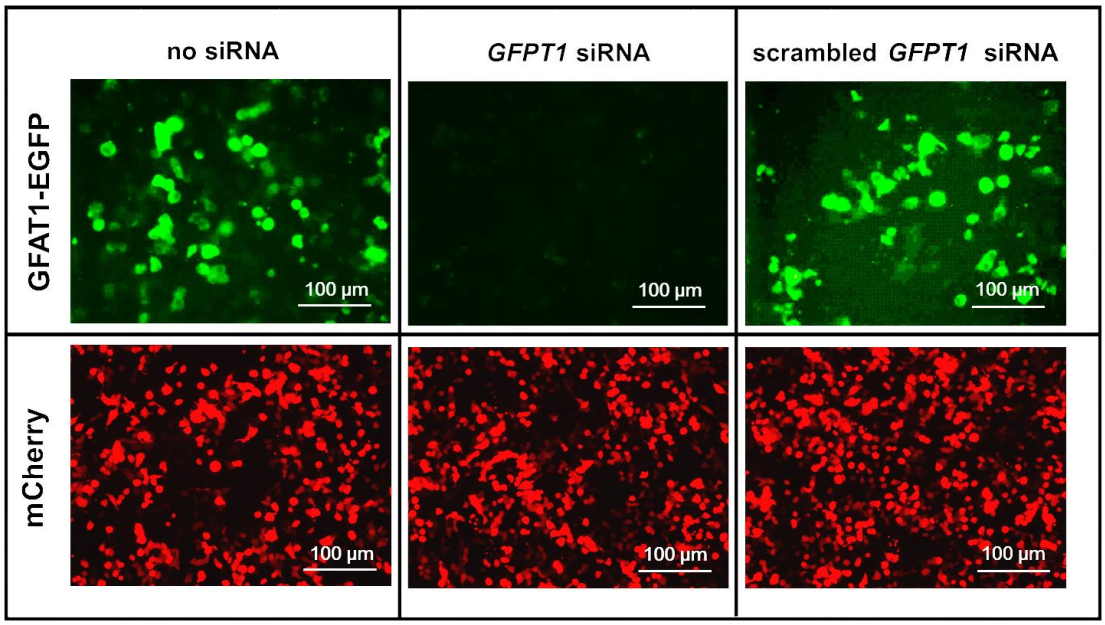

Fig.5.3. Knock-down of exogenous GFAT1-EGFP in HEK293TSA cells with *GFPT1* siRNA
HEK293TSA cells were co-transfected with GFAT1-EGFP- and mCherry-encoding plasmids, and specific or scrambled siRNA against *GFPT1* and *GFPT1-L*. Transfections without siRNA were also performed. 48 hours after the co-transfection, the cells were imaged using fluorescence microscopy. Example panels are shown.

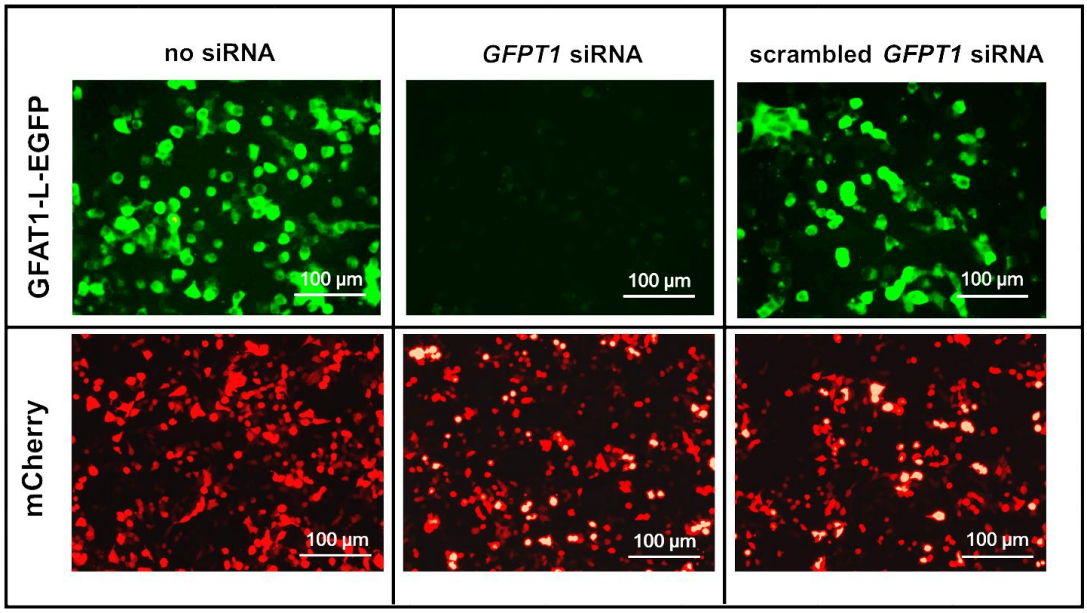

Fig.5.4. Knock-down of exogenous GFAT1-L-EGFP in HEK293TSA cells with *GFPT1* siRNA
HEK293TSA cells were co-transfected with GFAT1-L-EGFP- and mCherry-encoding plasmids, and specific or scrambled siRNA against *GFPT1* and *GFPT1-L*. Transfections without siRNA were also performed. 48 hours after the co-transfection, the cells were imaged using fluorescence microscopy. Example panels are shown.

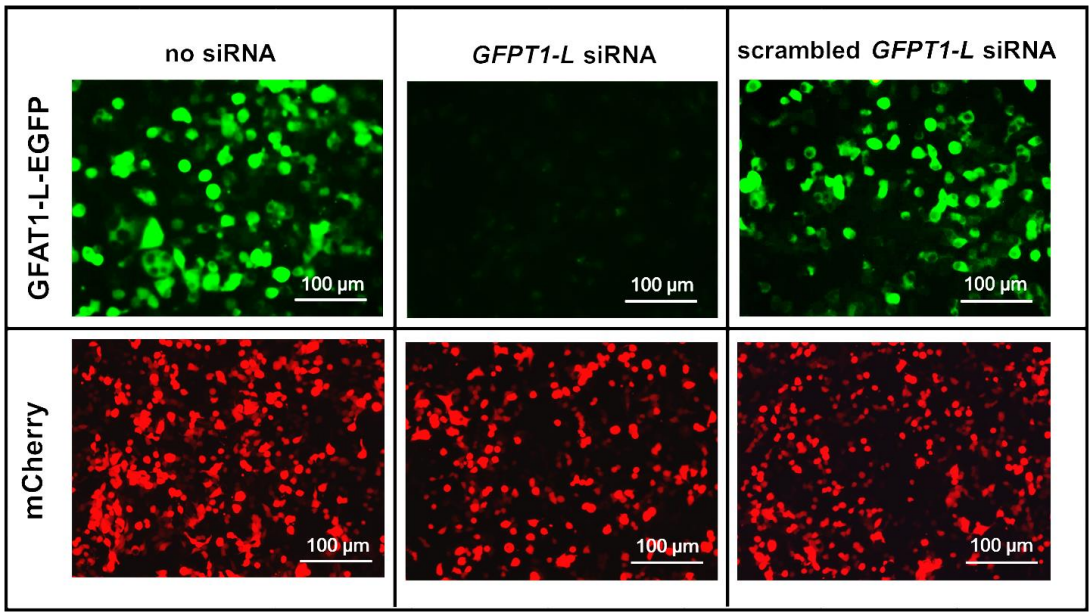

Fig.5.5. Knock-down of exogenous GFAT1-L-EGFP in HEK293TSA cells with *GFPT1-L* siRNA HEK293TSA cells were co-transfected with GFAT1-L-EGFP- and mCherry-encoding plasmids, and specific or scrambled siRNA against *GFPT1-L*. Transfections without siRNA were also performed. 48 hours after the co-transfection, the cells were imaged using fluorescence microscopy. Example panels are shown.

Green fluorescence, corresponding to GFAT1-EGFP and GFAT1-L-EGFP, was markedly reduced when the cells were co-transfected with respective DNA constructs and siRNA targeting *GFPT1* or *GFPT1-L*, respectively. No major reduction was detected when the scrambled sequences were used. Such results indicate that an efficient knock-down of exogenously expressed GFAT1-EGFP and GFAT1-L-EGFP can be achieved with the designed siRNA.

The silencing properties of siRNA were further analysed by immunoblotting the cell lysates with an anti-GFAT1 antibody. Equal amounts of protein were loaded into each lane and α-tubulin was used as a loading control (Figure 5.6.). This method allowed the effects of the siRNA on the expression of the exogenous EGFP-tagged molecules as well as endogenous GFAT1 to be analysed.

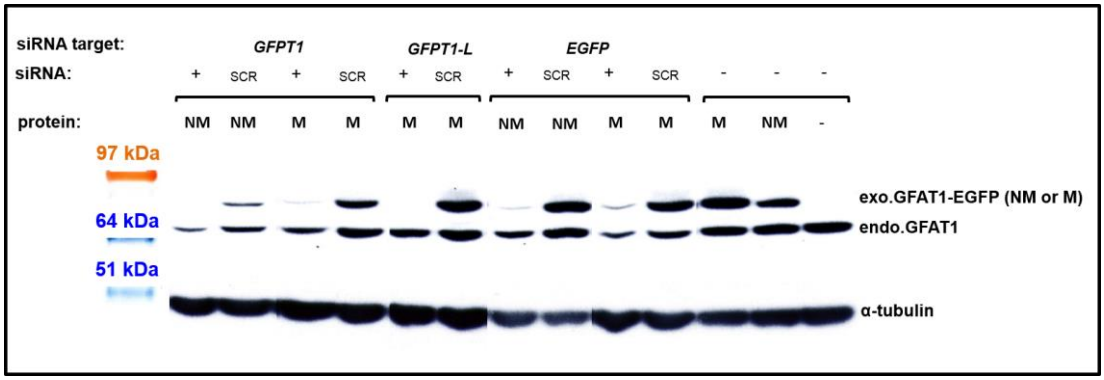

Fig.5.6. Silencing of exogenous GFAT1-EGFP (NM) and GFAT1-L-EGFP (M), and endogenous GFAT1 in HEK293TSA cells
HEK293TSA cells were transfected with GFAT1-EGFP (NM)- or GFAT1-L-EGFP (M)-encoding plasmids, and specific or scrambled siRNA against *GFPT1* and *GFPT1-L*, *GFPT1-L* or *EGFP*. Transfections without siRNA were also performed. Cell lysates were immunoblotted with anti-GFAT1 and anti-α-tubulin antibodies, and the appropriate HRP-conjugated secondary antibodies.

The western blotting experiments showed a reduction of intensity of the bands corresponding to exogenously expressed non-muscle (NM) and muscle (M) GFAT1-EGFP isoforms when the cells were co-transfected with specific siRNA (lanes 1, 3, 5, 7 and 9). This confirmed silencing of expression of human GFAT1-EGFP and GFAT1-L-EGFP, respectively. A reduction in the expression of endogenous GFAT1 was also observed in the cells transfected with the siRNA complementary to both *GFPT1* isoforms (lanes 1 and 3), though it was much less marked. This might suggest that the endogenous protein requires more time to break down or that an increased concentration of siRNA is needed for efficient knock-down. A minor decrease in the levels of endogenous GFAT1 was also recorded in cells co-transfected with *GFPT1-L* and *EGFP* siRNA (lanes 5, 7 and 9), indicating possible off-target effects of these molecules.

5.2.2.2. Silencing endogenous *GFPT1* expression in the HEK293TSA cell line

Several different conditions were tested to achieve efficient down-regulation of endogenously expressed GFAT1 in HEK293TSA cells. These included increased siRNA concentrations (25 nM and 50 nM vs. 2.5 nM used in the previous experiments) and prolonged incubation times (2, 4 or 6 days) following the transfection with siRNA. Only siRNA designed against both *GFPT1* isoforms was used in this experiment since HEK293TSA cells do not express *GFPT1-L*.

The efficiency of the silencing of endogenous GFAT1 was analysed by immunoblotting protein lysates with anti-GFAT1, anti-α-tubulin and anti-EGFP antibodies (Figure 5.7.).

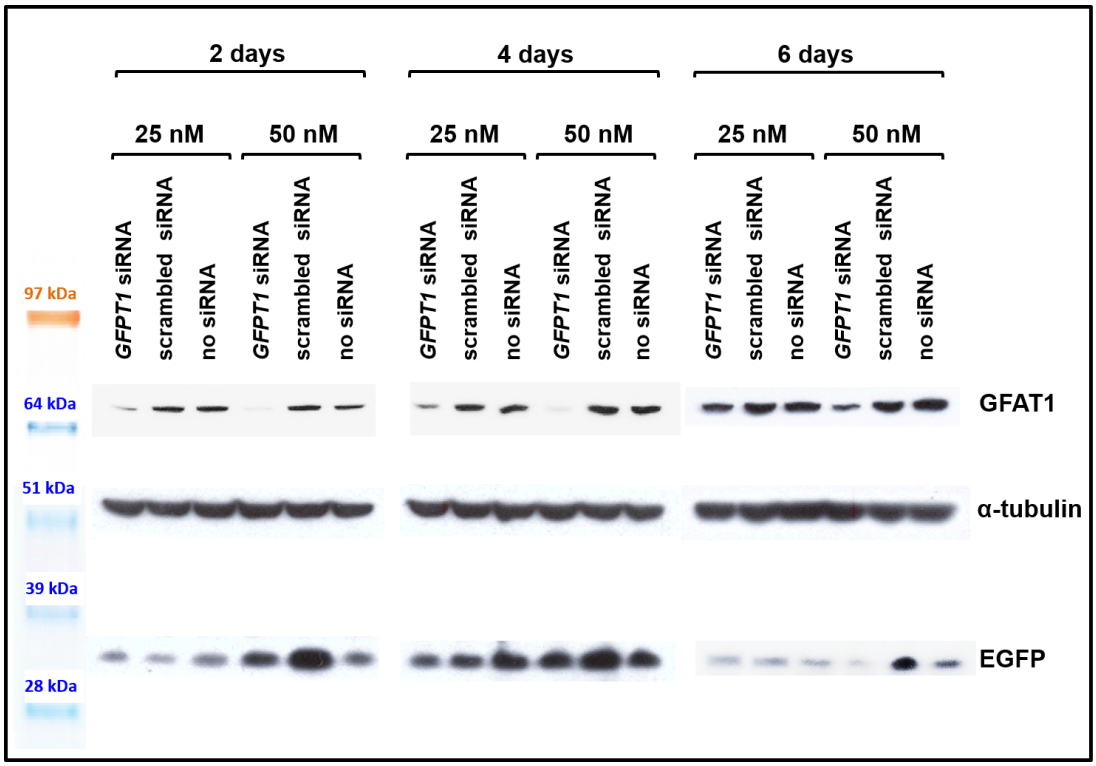

Fig.5.7. Knock-down of endogenous GFAT1 in HEK293TSA cells
HEK293TSA cells were co-transfected with 25 nM or 50 nM *GFPT1* specific or scrambled siRNA and pEGFP-N1. Transfections without siRNA were also performed. The cells were incubated for 2, 4 or 6 days, collected and analysed by immunoblotting with anti-GFAT1, anti-α-tubulin and anti-EGFP antibodies, and the appropriate HRP-conjugated secondary antibodies.

Figure 5.7. demonstrates that the decrease in intensity of the signal corresponding to GFAT1 was more apparent in the cells transfected with 50 nM siRNA (lanes 4, 10 and 16) compared to the ones transfected with 25 nM siRNA (lanes 1, 7 and 13). This shows that relatively high siRNA concentrations are needed to knock down the expression of endogenous GFAT1. Differences between the silencing efficiency in the cells incubated for 2, 4 or 6 days were also observed. The greatest knock-down was present after 2 and 4 days. Based on these findings, 50 nM siRNA and 72-hour incubation were used in subsequent investigations.

5.2.2.3. Silencing endogenous *GFPT1* expression in the rhabdomyosarcoma TE671 cell line

Tissue specificity of glycosylation might suggest that a muscle cell line, TE671, would better replicate the pathogenic mechanism of *GFPT1* CMS. This cell line is easy to culture and expresses muscle-specific proteins (Luther et al., 1989, Schoepfer et al., 1988).

The levels of the differentially spliced *GFPT1* isoforms were analysed in the TE671 cells. Total RNA was extracted, reverse transcribed into cDNA and the fragment of *GFPT1* cDNA, encompassing the muscle-specific exon, was amplified in a polymerase chain reaction (PCR). The same fragment was also amplified from the cDNA derived from human skeletal myotubes, which express both *GFPT1* isoforms and served as a positive control, and from HEK293TSA cells, expressing a non-muscle *GFPT1* isoform only, as a negative control. The PCR products were resolved by electrophoresis on agarose gels (Figure 5.8.).

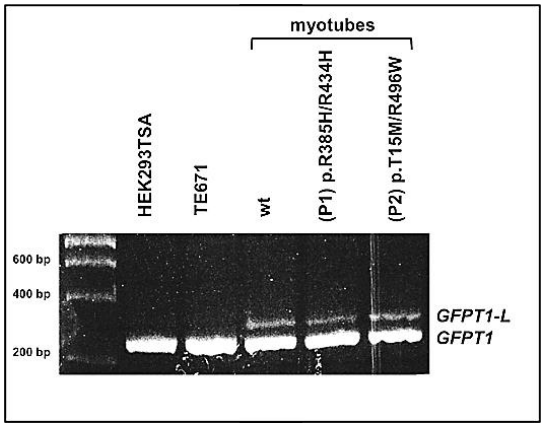

Fig.5.8. *GFPT1* isoforms in HEK293TSA and TE671 cell lines, and in human skeletal myotubes Total RNA was extracted from the cells, transcribed into cDNA and the *GFPT1* fragment adjacent to the muscle-specific exon was amplified using PCR.

A bright signal corresponding to *GFPT1* PCR products was detected in all lanes, irrespective of the cell type. By contrast, PCR products corresponding to *GFPT1-L* were observed only in the reactions where cDNA from myotubes was used (lanes 3, 4 and 5). This indicates that HEK293TSA and TE671 cells do not express *GFPT1-L* at sufficient levels to be detected on the ethidium bromide-stained agarose gel.

Only the siRNA specific for a non-muscle *GFPT1* isoform was used in subsequent experiments using TE671 cells. Down-regulation of GFAT1 expression in the cell line was achieved using a similar protocol to the one used for HEK293TSA cells, but lipofectamine®RNAiMAX was used instead of polyethylenimine (PEI). In initial experiments the siRNA molecules were also labelled with rhodamine to enable visualisation of the nucleic acid particles in the cells.

Conjugating nucleic acids with various fluorophores allows the molecules to be visualised in the cells, but labelling could affect the silencing efficacy of the siRNA. Therefore, HEK293TSA cells were co-transfected with 2.5 nM labelled or unlabelled siRNA, and EGFP-tagged GFAT1- or GFAT1-L-encoding plasmids. As a control, the cells were co-transfected with labelled or unlabelled scrambled siRNA, and DNA encoding GFAT1-EGFP or GFAT1-L-EGFP, respectively (Figures 5.9. and 5.10.)

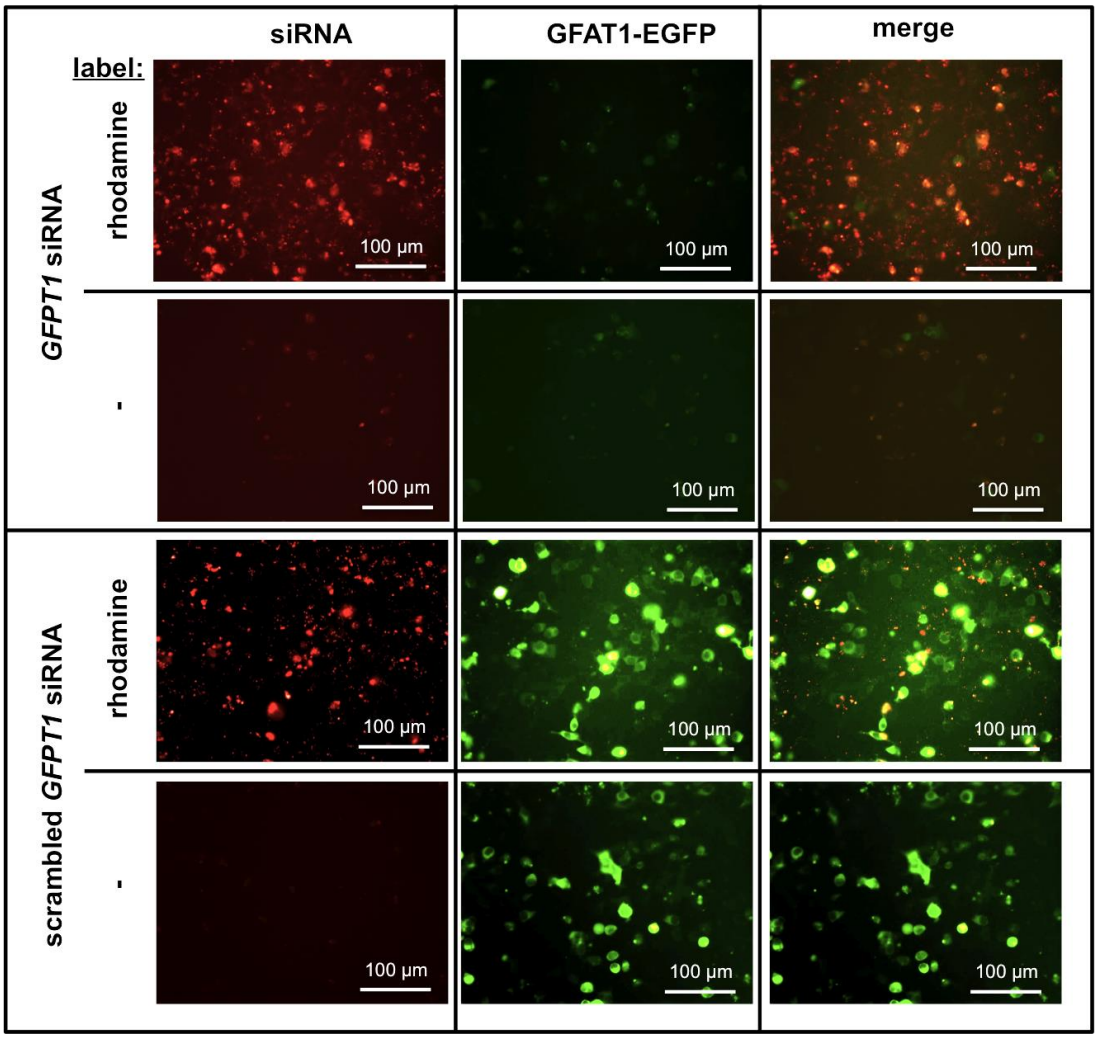

Fig.5.9. Comparison of the silencing efficacy of rhodamine-labelled and unlabelled *GFPT1* siRNA on the expression of GFAT1-EGFP

HEK293TSA cells were co-transfected with GFAT1-EGFP-encoding plasmid, and specific or scrambled labelled or unlabelled *GFPT1* siRNA, respectively. 48 hours after the co-transfection, the cells were visualised using fluorescence microscopy. Example panels are shown.

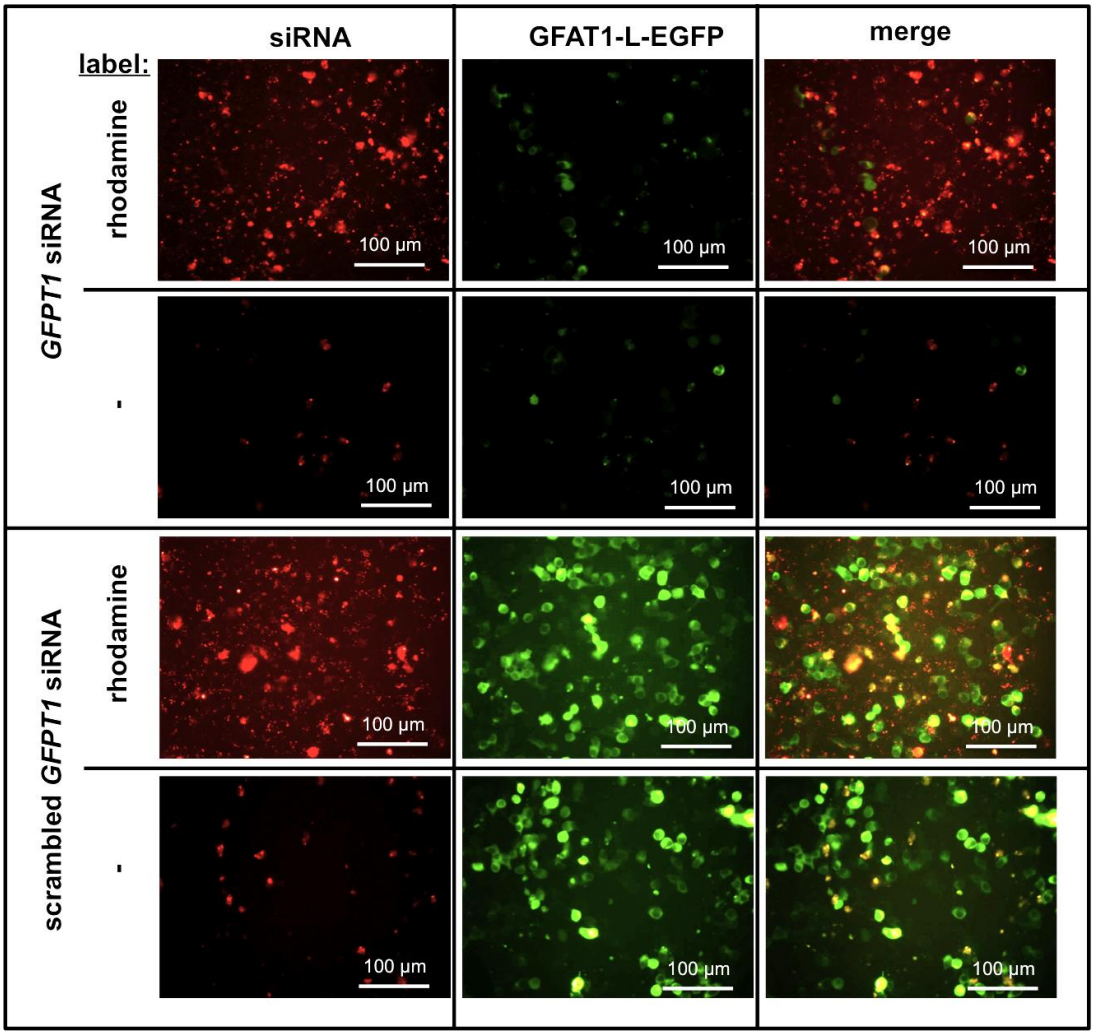

Fig.5.10. Comparison of the silencing efficacy of rhodamine-labelled and unlabelled *GFPT1* siRNA on the expression of GFAT1-L-EGFP
HEK293TSA cells were co-transfected with GFAT1-L-EGFP-encoding plasmid, and specific or scrambled labelled or unlabelled *GFPT1* siRNA, respectively. 48 hours after the co-transfection, the cells were visualised using fluorescence microscopy. Example panels are shown.

Presence of red fluorescence in the rhodamine-siRNA-transfected cells and substantial reduction in the GFAT1-EGFP and GFAT1-L-EGFP green fluorescence in both the rhodamine-labelled and the unlabelled *GFPT1* siRNA-transfected cells was observed. This indicated that the siRNA molecules were successfully delivered into the target cell line and retained their silencing efficacy.

Expression of GFAT1 was further assessed by immunoblotting the cell lysates with an anti-GFAT1 antibody (Figure 5.11.).

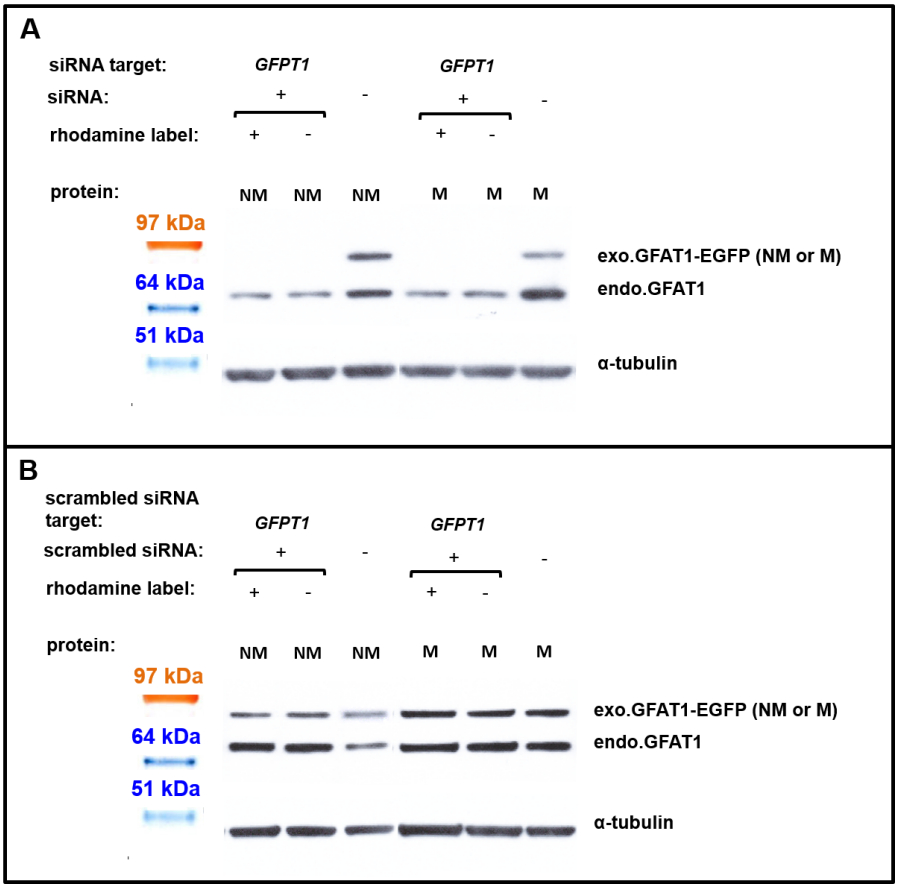

Fig.5.11. Comparison of the silencing efficacy of rhodamine-labelled and unlabelled *GFPT1* siRNA analysed by western blotting
HEK293TSA cells were co-transfected with GFAT1-EGFP (NM)- or GFAT1-L-EGFP (M)-encoding plasmids, and specific or scrambled labelled or unlabelled siRNA against *GFPT1*, respectively. Transfections without siRNA were also performed. Cell lysates were immunoblotted with anti-GFAT1 and anti-α-tubulin antibodies, and the appropriate HRP-conjugated secondary antibodies.

Reduced intensity of the bands corresponding to non-muscle (NM) and muscle (M) isoforms of GFAT1-EGFP was observed in cells co-transfected with *GFPT1*-specific siRNA (A: lanes 1, 2, 4 and 5), irrespective of the presence of the rhodamine label. A similar reduction was not seen when the scrambled sequences were used (B: lanes 1, 2, 4 and 5). This confirmed the initial microscopy observations that the labelling did not affect the silencing efficacy of siRNA. Modest down-regulation of the expression of endogenous GFAT1 in these cells was also seen. This only small reduction in the expression of endogenous GFAT1 was possibly due to the low concentrations of the siRNA (2.5 nM) used in these experiments.

The rhodamine-labelled siRNA, at a final concentration of 50 nM, was used to optimise the delivery of small nucleic acids into the TE671 cell line. Lipofectamine®RNAiMAX was used as a transfection reagent (Figure 5.12.).

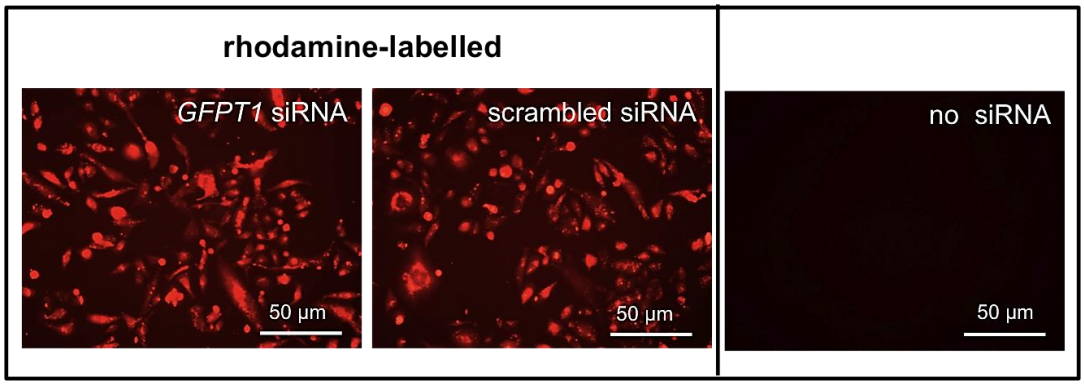

Fig.5.12. Delivery of rhodamine-labelled siRNA into TE671 cells
TE671 cells were transfected with *GFPT1* or scrambled siRNA labelled with rhodamine, and the transfection efficiency was visually assessed using fluorescence microscopy.

The transfected cells exhibited bright red fluorescence, corresponding to the labelled siRNA. This indicated an efficient transfection.

GFAT1 expression was analysed in these cells by immunoblotting extracted protein with an anti-GFAT1 antibody. The intensities of the bands corresponding to GFAT1 were measured, and normalised to the intensities of the bands corresponding to α-tubulin (Figure 5.13.).

A **B**

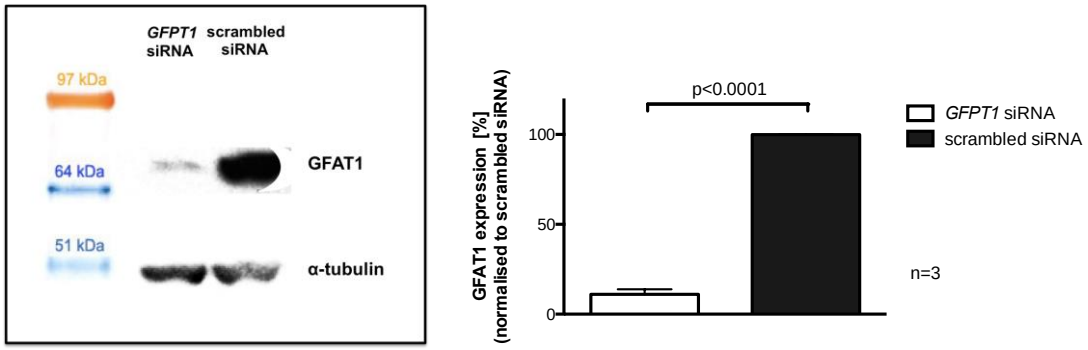

Fig.5.13. GFAT1 expression in *GFPT1*-silenced and wild type TE671 cells (Zoltowska et al., 2013)
(A) Protein extracts from *GFPT1*-silenced and wild type TE671 cells were immunoblotted with anti-GFAT1 and anti-α-tubulin antibodies, and the appropriate HRP-conjugated secondary antibodies.
(B) The intensities of the bands were measured by densitometry and GFAT1 expression was normalised to the α-tubulin levels. Each bar represents the mean±SEM GFAT1 protein levels, recorded in n=3 independent experiments, in *GFPT1*-silenced and wild type TE671 cells, respectively. All the data are expressed relative to the levels of GFAT1 in the wild type cells. p value was obtained using a student t-test.

The results from 3 experiments showed a reduction in GFAT1 protein levels to 11.03±2.86%, ($p<0.0001$, n=3) in *GFPT1* siRNA-transfected cells (lane 1) compared to the cells transfected with scrambled nucleic acids (lane 2). Thus the siRNA molecules could effectively down-regulate the expression of GFAT1 in TE671 cells.

Despite the high efficiency of the lipid-based siRNA delivery into TE671 cells, this method could not be used for the co-transfection of siRNA and DNA since it did not work efficiently for plasmid DNA delivery into TE671 cells. Electroporation was found to be a better approach. Co-delivery of siRNA and plasmid DNA was tested by electroporating the cells with the target siRNA molecules and pEGFP-N1 plasmid, as a marker of transfection efficiency. The concentration of the siRNA was increased up to 100 nM. GFAT1 protein levels were estimated in the electroporated cells by immunoblotting the cell lysates with anti-GFAT1, anti-EGFP and anti-α-tubulin antibodies (Figure 5.14.).

A **B**

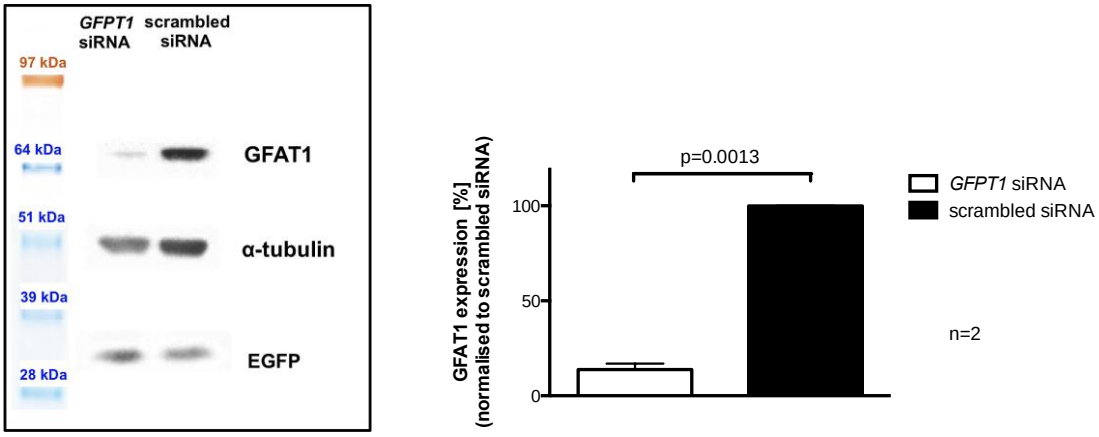

Fig.5.14. GFAT1 expression in *GFPT1*-silenced and wild type TE671 cells transfected by electroporation
(A) Protein extracts from *GFPT1*-silenced and wild type TE671 cells were immunoblotted with anti-GFAT1, anti-α-tubulin and anti-EGFP antibodies, and the appropriate HRP-conjugated secondary antibodies.
(B) The intensities of the bands were measured by densitometry and GFAT1 expression was normalised to the EGFP levels. Each bar represents the mean±SEM GFAT1 protein levels, recorded in n=2 independent experiments, in *GFPT1*-silenced and wild type TE671 cells, respectively. All the data are expressed relative to the levels of GFAT1 in the wild type cells. p value was obtained using a student t-test.

GFAT1 exhibited reduced expression (to 13.75±3.15%, p=0.0013, n=2) in TE671 cells transfected with specific siRNA (lane 1). This suggested that electroporation was an efficient method for DNA and siRNA co-delivery into TE671 cells.

5.2.3. Is GFAT1 required for the efficient cell surface expression and function of AChR?

Analyses of muscle biopsies from *GFPT1* patients and preliminary observations made in patient cell lines suggested that the main receptor at the NMJ, the AChR, might be a potential target affected by *GFPT1* deficiency. In this section the expression and the electrophysiological properties of the receptor in HEK293TSA, TE671 and TE671 DB40 cell lines, all exhibiting reduced GFAT1 protein levels or activity, were studied.

5.2.3.1. AChR cell surface expression in *GFPT1*-silenced, AChR-transfected HEK293TSA cells

HEK293TSA cells were transfected with cDNA encoding the four AChR subunits (α, β, δ, and ε) and siRNA designed against *GFPT1* mRNA. Cell surface expression of the AChR was measured with ^{125}I-α-bungarotoxin (^{125}I-α-BuTx) (Figure 5.15.).

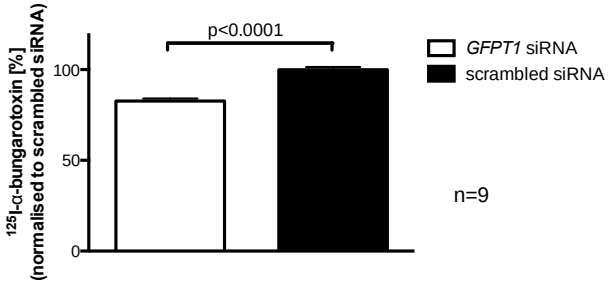

Fig.5.15. Cell surface ^{125}I-α-BuTx binding to *GFPT1*-silenced and wild type HEK293TSA cells transfected with AChR
Each bar represents the mean±SEM cell surface ^{125}I-α-BuTx binding, recorded in n=9 independent experiments, to *GFPT1*-silenced and wild type AChR-transfected HEK293TSA cells. The data are expressed relative to the cell surface ^{125}I-α-BuTx binding to the wild type cells. p value was obtained using a student t-test.

A modest, but reproducible, reduction to 82.53±1.39%, p<0.0001, n=9 was observed in the cell surface ^{125}I-α-BuTx binding to the *GFPT1*-silenced cells compared to the controls, which suggests that GFAT1 is essential for efficient expression of the AChR at the cell surface.

5.2.3.2. Identification of a suitable muscle cell line to study AChR cell surface expression

Preliminary experiments were performed to measure ^{125}I-α-BuTx binding to the surface of TE671 and TE671 DB40 (TE671 cells stably transfected with AChR β, δ and ε subunits (Beeson et al., 1996a)). Background binding was determined by preincubation with unlabelled (cold) α-BuTx (Figure 5.16.).

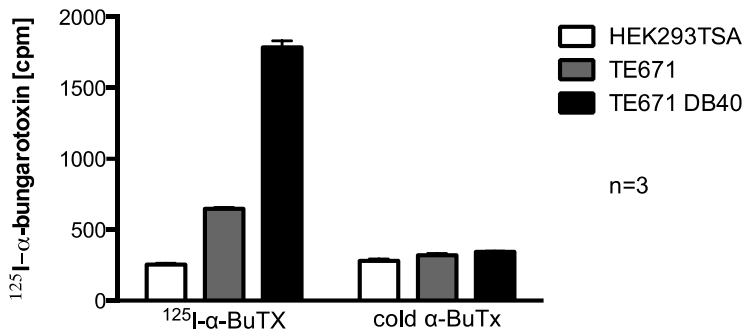

Fig.5.16. Cell surface ^{125}I-α-BuTx binding to HEK293TSA, TE671 and TE671 DB40 cells
Each bar represents the mean±SEM cell surface ^{125}I-α-BuTx binding, recorded in n=3 independent experiments, to HEK293TSA, TE671 and TE671 DB40 cells or the cells preincubated with cold α-BuTx. The radiolabelled toxin used in the experiment exhibited relatively low specific activity.

Both TE671 and TE671 DB40 cells expressed detectable amounts of AChR at the cell surface, whereas the HEK293TSA cell line did not express these receptors. The highest counts per minute (cpm) value, which corresponded to the AChR cell surface levels, were recorded in the TE671 DB40 cells. This dictated the choice of TE671 DB40 cells for the next series of experiments.

5.2.3.3. Does the inhibition of GFAT1 activity affect AChR cell surface expression in TE671 DB40 cells?

Reduced GFAT1 activity was first simulated in TE671 DB40 cells using a GFAT1 chemical inhibitor, a Gln analogue, DON. Cell surface expression of AChR was measured with ^{125}I-α-BuTx (Figure 5.17.).

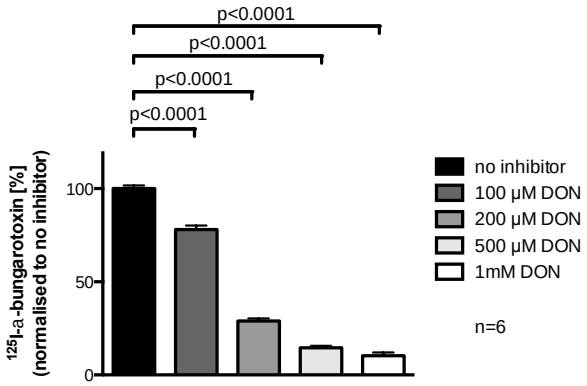

Fig.5.17. Cell surface ^{125}I-α-BuTx binding to TE671 DB40 cells following the inhibition of GFAT1 enzymatic activity with DON (Zoltowska et al., 2013)
Each bar represents the mean±SEM cell surface ^{125}I-α-BuTx binding, recorded in n=6 independent experiments, to TE671 DB40 cells treated with increasing concentrations of DON. The data are expressed relative to the cell surface ^{125}I-α-BuTx binding to the control (no inhibitor) cells. p values were obtained using a student t-test.

Figure 5.17. shows that the binding of toxin to the cell surface was reduced in a concentration-dependent manner in the DON-treated cells. This may indicate that GFAT1 activity is important for efficient cell surface expression of AChR in muscle cells, but non-specific off-target effects of the inhibitor cannot be ruled out.

5.2.3.4. Does silencing of *GFPT1* by siRNA affect AChR cell surface expression in TE671 DB40 cells?

Off-target effects of chemical inhibitors can be reduced by using an RNAi technique, and so GFAT1 deficiency was modelled in TE671 DB40 with siRNA (Figure 5.18.).

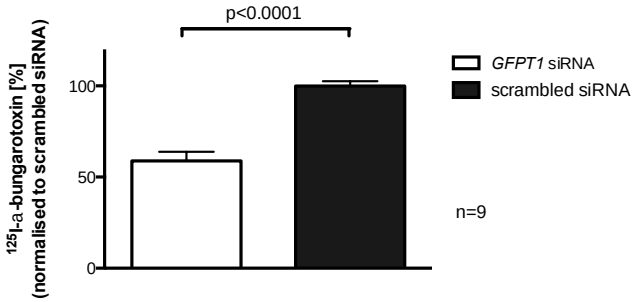

Fig.5.18. Cell surface ^{125}I-α-BuTx binding to *GFPT1*-silenced and wild type TE671 DB40 cells (Zoltowska et al., 2013)
Each bar represents the mean±SEM cell surface ^{125}I-α-BuTx binding, recorded in n=9 independent experiments, to *GFPT1*-silenced and wild type TE671 DB40 cells. The data are expressed relative to the cell surface ^{125}I-α-BuTx binding to the wild type cells. p value was obtained using a student t-test.

Figure 5.18. presents that the expression of AChR at the cell surface of the *GFPT1*-silenced TE671 DB40 cells was reduced to 58.85±4.97%, $p<0.0001$, $n=9$ compared to the control. This is consistent with the data from the investigations when DON was used to inhibit GFAT1 activity, and further indicates the importance of GFAT1 to AChR cell surface expression.

5.2.3.5. Investigating the underlying mechanism for the reduced AChR cell surface expression

Steady-state levels of the AChR subunits following *GFPT1* silencing were analysed. Total protein was extracted from the cells, deglycosylated using protein N-glycosidase F (PNGaseF) and immunoblotted with respective anti-AChR subunit antibodies. The specificity of the antibodies and lack of cross-reactivity with other subunits were first confirmed. The enzymatic deglycosylation of the protein was performed to ensure that any potential differences in the intensities of the bands were caused by variations in the protein levels of individual subunits, and not by differences in glycosylation. The intensity of signals corresponding to the receptor subunits was measured and their expression was normalised to α-tubulin (Figure 5.19.).

A

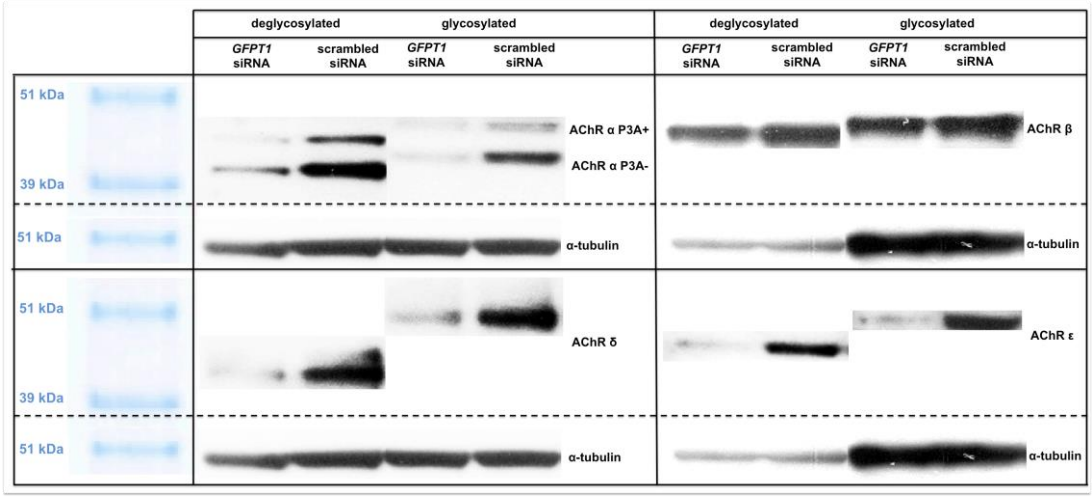

B

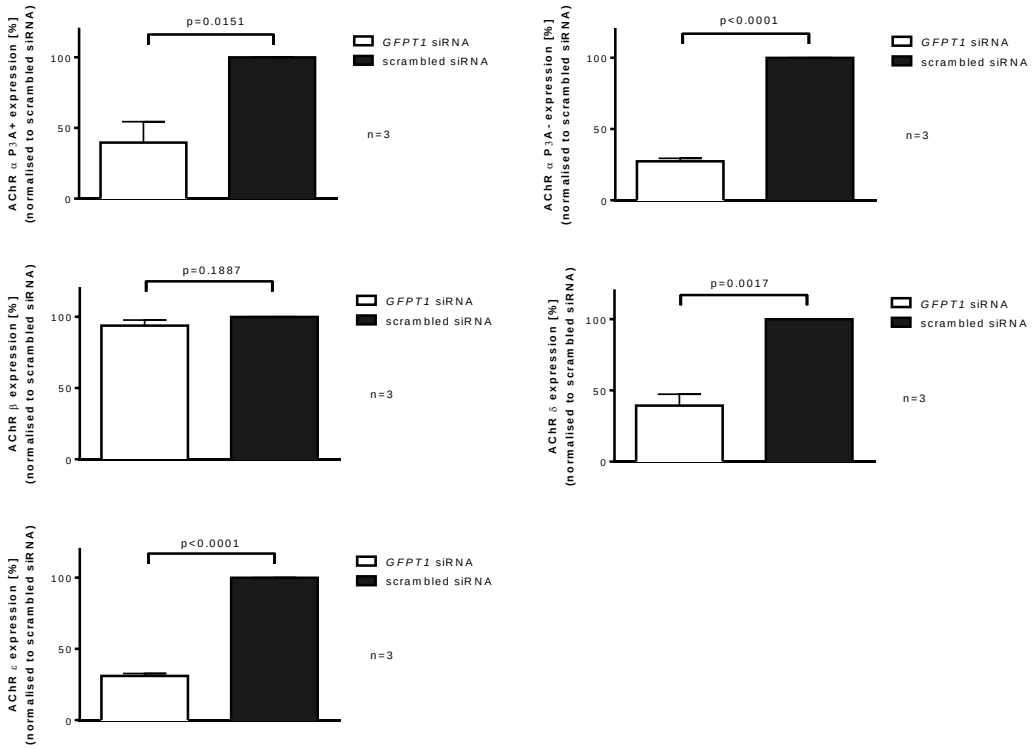

Fig.5.19. Expression of individual AChR subunits in *GFPT1*-silenced and wild type TE671 DB40 cells (Zoltowska et al., 2013)
(A) Protein lysates from *GFPT1*-silenced and wild type TE671 DB40 cells were immunoblotted with antibodies specific for individual AChR subunits and an anti-α-tubulin antibody, and the appropriate HRP-conjugated secondary antibodies. AChR α and δ subunits, and AChR β and ε subunits were detected on the same membranes, respectively.
(B) The intensities of the bands were measured by densitometry and AChR subunit expression was normalised to α-tubulin levels. Each bar represents the mean±SEM protein levels of the individual AChR subunit, recorded in n=3 independent experiments, in *GFPT1*-silenced and wild type TE671 DB40 cells. All the data are expressed relative to the levels of the respective AChR subunit in the wild type cells. p values were obtained using a student t-test.

Cells in which *GFPT1* was knocked down exhibited reduced levels of AChR α, both P3A+ and P3A- isoforms, δ and ε subunits (to 39.68±14.79%, p=0.0151, n=3; 27.4±2.01%, p<0.0001, n=3; 39.34±8.05%, p=0.0017, n=3 and 31.08±1.69%, p<0.0001, n=3, respectively) relative to the scrambled siRNA-transfected cells. By contrast, total protein levels of AChR β appeared not to be affected by the reduction in GFAT1 expression. Thus, the reduced levels of the receptor at the cell surface in *GFPT1*-silenced cells could be a consequence of diminished steady-state levels of individual AChR α, δ and ε subunits.

We also considered a second possibility that the reduced protein levels of AChR resulted from the down-regulated expression of AChR mRNA in *GFPT1*-silenced cells. The experiments focused on the expression of AChR α subunit since this is the only subunit expressed at relatively high levels endogenously by TE671 cells. No exogenous plasmid DNA encoding the protein was introduced during the establishment of the stable AChR-transfected TE671 DB40 cell line (Beeson et al., 1996a).

To analyse the *CHRNA1* mRNA levels, total RNA was extracted from wild type and *GFPT1*-silenced TE671 DB40 cells and reverse transcribed into cDNA. Fragments of the cDNA encoding AChR α and glyceraldehyde-3-phosphate dehydrogenase (GAPDH), as an endogenous reference, were amplified by quantitative polymerase chain reaction (qPCR). The *CHRNA1* expression was normalised to the *GAPDH* levels (Figure 5.20.). qPCR primers were designed in a way that enabled simultaneous analysis of the expression of both AChR α isoforms (P3A+ and P3A-) since the protein levels of both were similarly reduced in the TE671 DB40 *GFPT1*-silenced cells. The sequences of the primers are shown in Chapter 2, section 2.2.1.4.

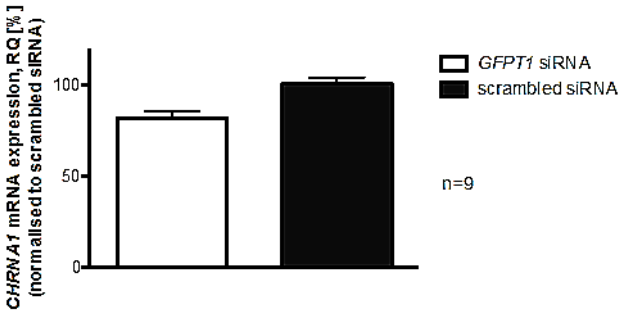

Fig.5.20. Relative quantification (RQ) of the expression of *CHRNA1* mRNA in *GFPT1*-silenced and wild type TE671 DB40 cells (Zoltowska et al., 2013)
TE671 DB40 cells were transfected with *GFPT1* or scrambled siRNA. Total RNA was extracted, reverse transcribed into cDNA and the expression of *CHRNA1* mRNA was analysed using qPCR. The levels of the *CHRNA1* mRNA were normalised to the expression of *GAPDH*. Each bar represents the mean±SEM of the expression of *CHRNA1* mRNA, recorded in n=9 independent experiments, in *GFPT1*-silenced and wild type TE671 DB40 cells.

Analysis of the reverse transcription quantitative polymerase chain reaction (RT-qPCR) data revealed a modest reduction in the mRNA levels of the target gene to 82.19±3.50%, n=9 in the *GFPT1*-silenced cells compared to the wild type. This modest reduction in the mRNA levels is unlikely to cause the severely reduced protein levels of AChR α P3A+ and P3A-, to 39.68±14.79%, p=0.0151, n=3 and 27.4±2.01%, p<0.0001, n=3, respectively. The data suggest that GFAT1 activity is required for the efficient translation and/or the stability of the receptor subunits, but not for the transcription of the mRNA from the AChR-encoding genes.

5.2.3.6. Does GFAT1 deficiency affect cell surface expression of MuSK?

GFAT1 is essential for AChR expression at the cell surface, but other NMJ proteins may also be affected by *GFPT1* mutations. Another target analysed was MuSK, which is modified with carbohydrate moieties and plays an important role in the formation of the synapse (Glass et al., 1996, Watty and Burden, 2002).

MuSK cell surface expression was analysed by immunoprecipitation, in *GFPT1*-silenced HEK293TSA cells transfected with MuSK-mCherry-encoding vectors. MuSK tagged with mCherry on its C-terminus was chosen for this experiment

since the tag allowed immunoprecipitation of the target from the cell surface using an anti-MuSK antibody and subsequent analysis of its levels by immunoblotting with an anti-mCherry antibody. In the first experiment, the optimal dilution of the anti-MuSK antibody was determined (Figure 5.21.).

A

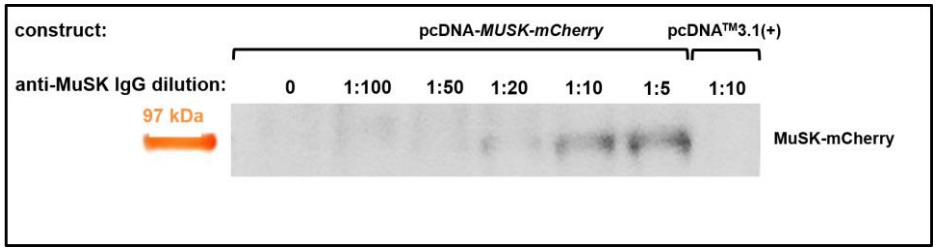

B

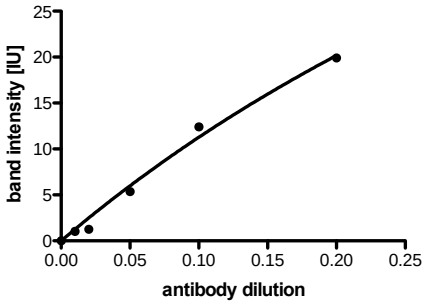

Fig.5.21. Determination of an appropriate dilution of an anti-MuSK antibody for immunoprecipitation
HEK293TSA cells were transfected with scrambled siRNA and MuSK-mCherry-encoding plasmid or pcDNA™3.1(+), as a negative control, and cell surface MuSK-mCherry was immunoprecipitated with an anti-MuSK antibody.
(A) The amounts of immunoprecipitated protein were analysed by western blotting with an anti-mCherry antibody and the appropriate HRP-conjugated secondary antibody.
(B) The intensities of the bands corresponding to MuSK-mCherry were measured by densitometry.

The western blot showed that the higher the dilution of the antibody, the lower the amount of MuSK-mCherry that was immunoprecipitated from the cell surface. The intensities of the bands corresponding to MuSK-mCherry were measured and plotted on the graph. Out of five tested dilutions of the anti-MuSK antibody (1:100, 1:50, 1:20, 1:10, 1:5), 1:10 was found to be in the middle of the linear range of the graph and therefore was suitable for the immunoprecipitation of MuSK-mCherry from the cell surface.

Subsequently, cell surface MuSK-mCherry was immunoprecipitated from HEK293TSA cells co-transfected with *GFPT1* siRNA or scrambled siRNA, and MuSK-mCherry-encoding plasmid. The immunoprecipitates were analysed by immunoblotting with an anti-mCherry antibody (Figure 5.22.).

A **B**

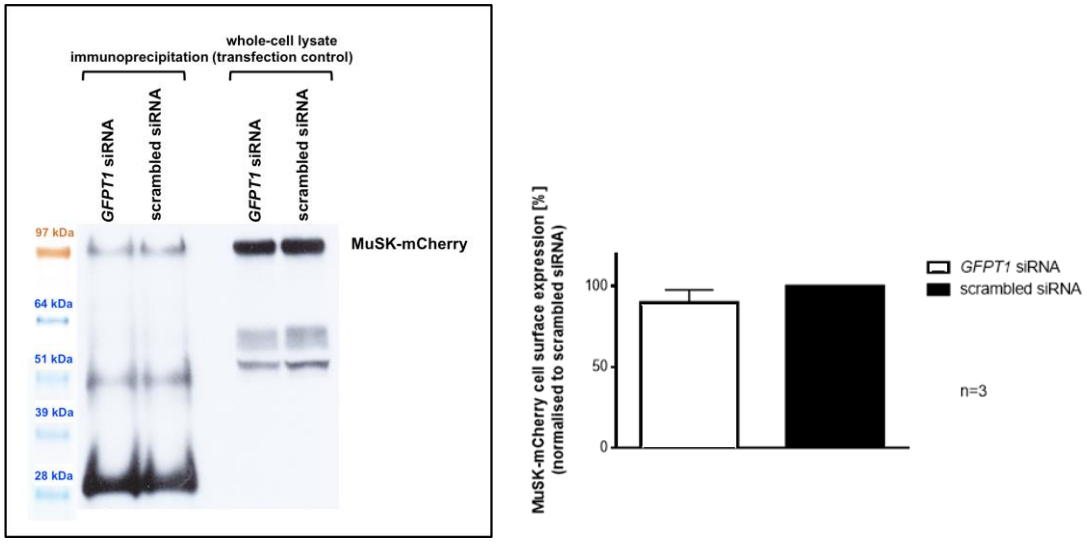

Fig.5.22. MuSK-mCherry cell surface expression in *GFPT1*-silenced and wild type HEK293TSA cells
(A) HEK293TSA cells were transfected with *GFPT1* or scrambled siRNA, respectively, and MuSK-mCherry-encoding vector. MuSK-mCherry was immunoprecipitated from the cell surface with an anti-MuSK antibody. The immunoprecipitated protein was analysed by immunoblotting with an anti-mCherry antibody. Whole cell lysates obtained from the same wells were also analysed, as a transfection control.
(B) The intensities of the bands corresponding to the immunoprecipitated MuSK-mCherry were measured by densitometry. Each bar represents the mean±SEM MuSK-mCherry cell surface expression, recorded in n=3 independent experiments, in *GFPT1*-silenced and wild type HEK293TSA cells.

Quantification of the intensities of the bands corresponding to MuSK-mCherry immunoprecipitated from the cell surface showed no clear-cut changes in the levels of MuSK-mCherry cell surface expression in *GFPT1*-silenced cells compared to the scrambled siRNA-transfected ones. This result suggests no gross effect of *GFPT1* mutations on MuSK cell surface expression, but cannot exclude subtle effects.

5.3. Discussion

Mutations in *GFPT1* have been identified in a group of patients presenting with a characteristic limb-girdle pattern of muscle weakness, but molecular mechanisms underlying impaired neurotransmission in these individuals remain elusive. In this chapter the role of GFAT1 was investigated in the expression of NMJ proteins. The preliminary experiments in patient muscle cell lines demonstrated that *GFPT1* mutations may impair neuromuscular transmission by reducing the levels of the AChR expressed at the cell surface, thus provided a possible link between this ubiquitously expressed enzyme and the NMJ.

To gain greater insight into the pathomechanism of the *GFPT1* CMS, we have studied a model, which could mirror the impaired GFAT1 activity. Reduction of the enzyme activity was achieved by the application of chemical inhibitors, such as DON, and silencing of *GFPT1* expression by using specific siRNA in a human-derived muscle cell line. The use of the human muscle cells was important because there is tissue and species specificity of the modification with carbohydrate structures. For example, it has been reported that AChR in *Xenopus* oocytes is not modified with complex glycans because these cells cannot produce this class of sugars (Buller and White, 1990). Trimming carbohydrate cores and synthesis of complex sugars is essential for stability and cell surface expression of the receptor subunits in BC3H-1 muscle cells (Smith et al., 1986), and for assembly of the complex in mouse fibroblasts L (Wanamaker and Green, 2005).

The cell line TE671 DB40 was chosen for its high expression of the receptor at the cell surface, and GFAT1 activity was reduced, using both, chemical inhibitors and siRNA. The findings were in line with the data recorded in *in vitro* cultured myotubes derived from the *GFPT1* CMS patient muscle biopsies and showed that the reduction

in AChR cell surface expression was, at least, one of the consequences of both diminished GFAT1 enzymatic activity and reduced GFAT1 protein levels. Further studies demonstrated substantially reduced steady-state levels of individual AChR α, δ and ε subunits, but not β subunit, in the *GFPT1*-silenced cells. The *CHRNA1* mRNA levels were decreased only modestly. This suggested that the reduction in the protein levels of AChR subunits was probably caused by a rapid degradation of the subunits rather than a decreased expression or stability of the mRNA encoding the molecules.

The increased degradation of the AChR subunits, resulting in their reduced steady-state levels, might be potentially caused by a number of factors. Based on the current knowledge of the expression, structure and function of the AChR, and genetics of CMS, the alterations in the AChR expression in *GFPT1*-deficient cells are most likely to result from aberrant N-glycosylation of individual subunits since the final product of the hexosamine biosynthetic pathway (UDP-GlcNAc) is used in the N-glycosylation pathway. Clinical features of *GFPT1* CMS patients (Guergueltcheva et al., 2011) are clearly similar to those observed in the individuals diagnosed with a CMS resulting from mutations in UDP-N-acetylglucosamine-dolichyl-phosphate N-acetylglucosaminephosphotransferase (DPAGT1) (Belaya et al., 2012), and asparagine-linked glycosylation 2 and 14 (ALG2 and ALG14) (Cossins et al., 2013b), that are all involved in early steps of the N-glycosylation pathway. Altered glycosylation of the AChR as a disease mechanism is in line with studies which reported that modification of receptor subunits with carbohydrate structures is essential for the assembly and expression of the AChR at the cell surface (Blount and Merlie, 1990, Prives and Bar-Sagi, 1983, Prives and Olden, 1980). In addition, studies of the role of the sugars attached to AChR subunits have demonstrated that glycosylation is a prerequisite for efficient expression of the AChR α and γ subunits

(Blount and Merlie, 1990, Gehle and Sumikawa, 1991), but not the AChR β subunit (Gehle et al., 1997, Gehle and Sumikawa, 1991). This is consistent with the data obtained from our experiments where *GFPT1* expression was knocked down in TE671 DB40 cells. The lack of increased degradation of the AChR β subunit might result from distinct glycosylation patterns of the protein or from the assembly mechanism of mature AChR (Figure 5.23.).

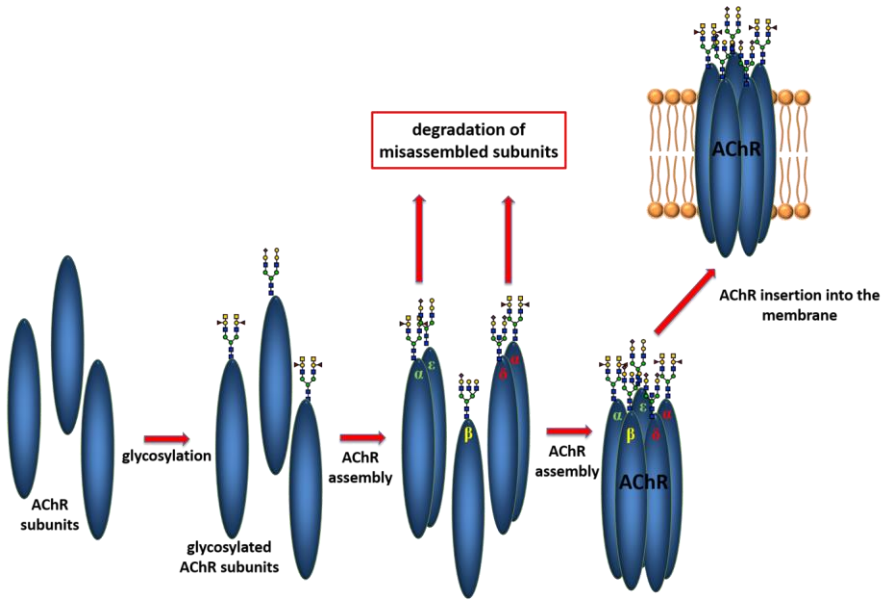

Fig.5.23. Schematic representation of the assembly of AChR subunits and their insertion into the membrane
The individual AChR subunits are synthesised in the cytoplasm, then modified with carbohydrate structures in the endoplasmic reticulum and in the Golgi apparatus, where the formation of AChR αδ and αε dimers and their assembly with the AChR β subunit occur. It is possible that in *GFPT1*-mutated cells an aberrant glycosylation impairs the formation of the dimers, and that the individual AChR α, δ and ε subunits or their misassembled dimers are targeted for degradation.

During AChR assembly the addition of AChR β to the pentamer is thought to occur separately and follow the initial assembly of the AChR αε and the AChR αδ dimers (Blount et al., 1990, Gu et al., 1991, Millar and Harkness, 2008). The glycosylation might be of particular importance for the assembly of the two dimers, and perhaps misglycosylated AChR α, δ and ε subunits fail to form these correct dimers. As a result the individual unassembled subunits or the misassembled dimers might be targeted for degradation.

The investigations presented also demonstrated that GFAT1 deficiency resulted in decreased protein levels of AChR δ subunit. Some previous reports have found that glycosylation is not required for an efficient expression of the AChR δ subunit (Gehle et al., 1997, Ramanathan and Hall, 1999). Differences with the present result might be explained through methodology. In those experiments glycosylation was investigated by site-directed mutagenesis, usually by mutating a single glycosylation site at a time (Gehle et al., 1997, Ramanathan and Hall, 1999), whereas *GFPT1* deficiency is likely to impair glycosylation at all three potential sites.

We also considered a possibility that the *GFPT1* mutations lead to the alteration in the functional properties of AChR. This aspect was investigated by AChR single channel recordings conducted by Dr Richard Webster in TE671 cells following down-regulation of *GFPT1* expression with siRNA. TE671 cells were chosen because this cell line expresses a single population of AChR (foetal form), as opposed to the TE671 DB40 cells, which express both foetal and adult AChR. The cells were co-transfected with *GFPT1* or scrambled siRNA and the pEGFP-N1 vector. The EGFP-encoding plasmid was added to the transfection mixes to enable selection of transfected cells during single channel recordings (Table 5.2. and Figure 5.24.).

Table 5.2. Burst duration characteristics of AChR single channel function recorded from *GFPT1*-silenced and wild type TE671 cells (Zoltowska et al., 2013)

	area$_1$ [%]	τau$_1$ [ms]	a$_2$	τ$_2$	a$_3$	τ$_3$	N
control TE671	39.00±1.00	0.09±0.01	23.60±2.10	1.65±0.10	37.4±1.50	11.62±0.92	4
***GFPT1* siRNA-transfected TE671**	37.70±2.00	0.10±0.02	25.60±3.20	1.77±0.30	36.4±2.00	12.53±1.09	5

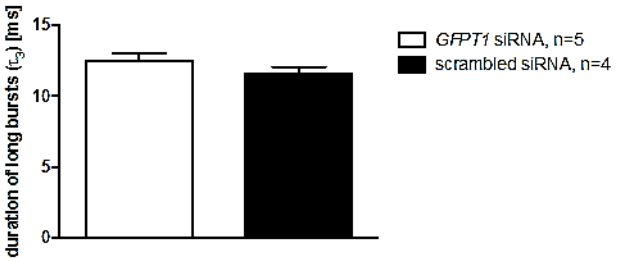

Fig.5.24. Duration of long bursts in *GFPT1*-silenced and control TE671 cells
TE671 cells were co-transfected with *GFPT1* or scrambled siRNA and pEGFP-N1. 72 hours after the transfection, single channel recordings were conducted from EGFP-expressing cells. Each bar represents the mean±SEM duration of long bursts (τ$_3$), recorded in n=5 or n=4 patches, on *GFPT1*-silenced and control TE671 cells, respectively.

No significant changes were recorded in duration of the functionally most important population of long bursts (τ_3) between the *GFPT1*-silenced and control TE671 cells (12.53±1.09 ms in *GFPT1*-silenced TE671 and 11.61±0.92 ms in control cells (n= 5 & 4 patches, respectively)). This would indicate that the small number of AChR, which despite *GFPT1* deficiency, reach the cell surface, is fully functional, and hence the disease results from the reduced levels of AChR at the NMJ but not their altered function.

The severely decreased levels of AChR at the NMJ can on its own lead to myasthenic weakness in *GFPT1* patients but it cannot be excluded that expression and function of other synapse-specific or ubiquitously expressed molecules are also affected by mutations in GFAT1, and thus MuSK cell surface expression was studied. Preliminary investigations indicated that GFAT1 deficiency did not affect MuSK levels at the cell surface. This is consistent with the observations made in *GFPT1* patients' cells, in

which the AChR clustering pathway does not appear to be impaired (Zoltowska et al., 2013).

The different consequences of GFAT1 deficiency on the expression of different molecules might be the result of distinct molecular functions of glycosylation, potentially depending on the modified target and/or on the structure of the attached sugar chains. However, it remains to be determined why AChR expression is particularly sensitive to GFAT1 deficiency and why 'limb-girdle' muscles are predominantly affected in *GFPT1* patients. Nevertheless, the experiments in this chapter show a link between *GFPT1* mutations and AChR expression, and thus provide a potential molecular mechanism for the impaired neuromuscular transmission seen in *GFPT1* CMS patients.

Chapter 6

Therapeutic approaches in myasthenic disorders

6.1. Introduction

Congenital myasthenic syndrome (CMS) and myasthenia gravis (MG) comprise a group of disorders caused by aberrant neuromuscular transmission that manifests as fatiguable muscle weakness affecting different groups of skeletal muscles: limb, trunk, bulbar, respiratory, facial or extraocular. Severity of the clinical symptoms and the group of muscles affected vary between individuals (Engel, 2011, Finlayson et al., 2013). In some cases, especially when respiratory muscles are affected, the disorders are life-threatening (Romaneli et al., 2013).

Symptoms can be partially alleviated using standard therapeutic approaches. The choice of treatment depends on the underlying molecular cause of the disease, i.e. a genetic defect or an antibody target, hence a precise diagnosis is essential for rational therapy. Of note is that treatments which show positive effects for a given CMS or MG subtype can show negative effects in others (Schara and Lochmuller, 2008, Abicht et al., 2012).

Current standard therapeutic approaches improve neuromuscular transmission and thus increase muscle strength in affected individuals (Finlayson et al., 2013), but often the beneficial effects of the drugs are not sustained during the disease course. Further studies into the therapy of myasthenic disorders would be helpful to improve benefit for the patients. Potential strategies would be, either to optimise the current treatments to prolong the beneficial action of the medicines used, or to design novel therapeutic approaches.

The most commonly administered drugs, which generate a rapid, but often unsustained

positive response, are carbamate acetylcholinesterase (AChE) inhibitors, such as pyridostigmine bromide and neostigmine. These show minimal transfer across the blood-brain barrier (Pohanka, 2012). They have been shown to be effective in many CMS and MG cases (Maselli et al., 2003, Muller et al., 2006, Webster et al., 2004, Belaya et al., 2012, Cossins et al., 2013b, Palace et al., 2012, Guergueltcheva et al., 2011, Senderek et al., 2011), but should not be used in AChE deficiency (Mihaylova et al., 2008, Wargon et al., 2012), downstream of tyrosine kinase 7 (*DOK7*) (Palace et al., 2007) and slow-channel CMS (Chaouch et al., 2012). The drugs act by AChE inhibition, and a consequent increase in the concentration of the neurotransmitter, acetylcholine (ACh), in the synaptic cleft. This facilitates transmission of the signal between a motor nerve and a muscle fibre at the neuromuscular junction (NMJ) (Pohanka, 2012). There are, however, three major disadvantages of this group of medicines. First, their benefits may not be fully sustained and the beneficial effects may reduce over time. Second, the therapy is only symptomatic and the drugs need to be administered regularly throughout life. Finally, the patients may suffer from side effects (Hood, 1990), which may result from the fact that the expression of AChE is not restricted to the NMJ (Massoulie, 2002).

Another major group of medications, which has been found to be effective in the therapy of myasthenic disorders, are the agonists of β_2-adrenergic receptor (ADRB2), such as ephedrine and salbutamol (Lefkowitz, 1974). These medicines are especially useful for the treatment of CMS resulting from mutations in *DOK7* (Liewluck et al., 2011, Burke et al., 2013), collagen Q (*COLQ*) (Chan et al., 2012, Yeung et al., 2010) and acetylcholine receptor (AChR) deficiency (Sadeh et al., 2011).

ADRB2 belongs to the superfamily of G-protein-coupled receptors (GPCR). The canonical pathway of its agonist-dependent signalling involves a G_s protein, which

upon the activation of the receptor, dissociates into the α and βγ subunits. The $G_{\alpha s}$ activates adenylyl cyclase, catalysing the conversion of adenosine triphosphate (ATP) to cyclic adenosine monophosphate (cAMP), which in turns activates cAMP-regulated proteins, including cAMP-dependent protein kinase (PKA) (Benovic, 2002). It is not known how this mechanism contributes to the improvement in the neuromuscular transmission in CMS and MG patients. The small number of patients with CMS limits an effective clinical trial. However, it may be possible to use animal models to give insight into the optimisation of the therapy.

6.2. *In vivo* trial of the combined treatment with pyridostigmine bromide and salbutamol sulphate

AChE inhibitors are the first-choice medicines for the treatment of many CMS and MG. However, the immediate beneficial effect of these drugs may reduce over time and become less striking. It has been observed (unpublished data) that addition of ADRB2 agonists (ephedrine or salbutamol sulphate) to the therapy may alleviate the attenuation of AChE inhibitors after prolonged treatment. This observation has not been confirmed experimentally and its molecular basis has not been analysed.

6.2.1. Muscle strength upon the administration of pyridostigmine bromide and salbutamol sulphate

The presented study was set up to investigate the response to pyridostigmine bromide and salbutamol sulphate *in vivo* in an AChR deficiency CMS mouse model ($ms\varepsilon^{-/-}$ $neo^{+/+}$ $h\gamma^{+}$). In these animals the expression of AChR ε subunit is knocked out and a single copy of cDNA encoding human AChR γ subunit is introduced. The introduction of the AChR γ enables to prolong the lifespan of the $Chrne^{-/-}$ mice, which otherwise die prematurely, 10-14 weeks after birth. The described genetic modifications result in decreased levels of AChR at the NMJ and disruption of the structure of the synapse. These manifest with aberrant neuromuscular transmission and myasthenic weakness (Cossins et al., 2004).

The efficacies of two different treatment regimens were tested. One group of animals (n=8) was treated with pyridostigmine bromide (7 mg/kg/day) for 4 weeks and then the treatment was changed to a combination of pyridostigmine bromide (7 mg/kg/day) and salbutamol sulphate (45 mg/kg/day) administered for the next 6 weeks. The second group (n=8) received pyridostigmine bromide alone (7 mg/kg/day) for the entire

10-week experiment. Muscle strength of the animals was monitored weekly using an inverted screen test. The data were normalised to the performance in the inverted screen test after the 4-week treatment with AChE inhibitor (Figure 6.1.).

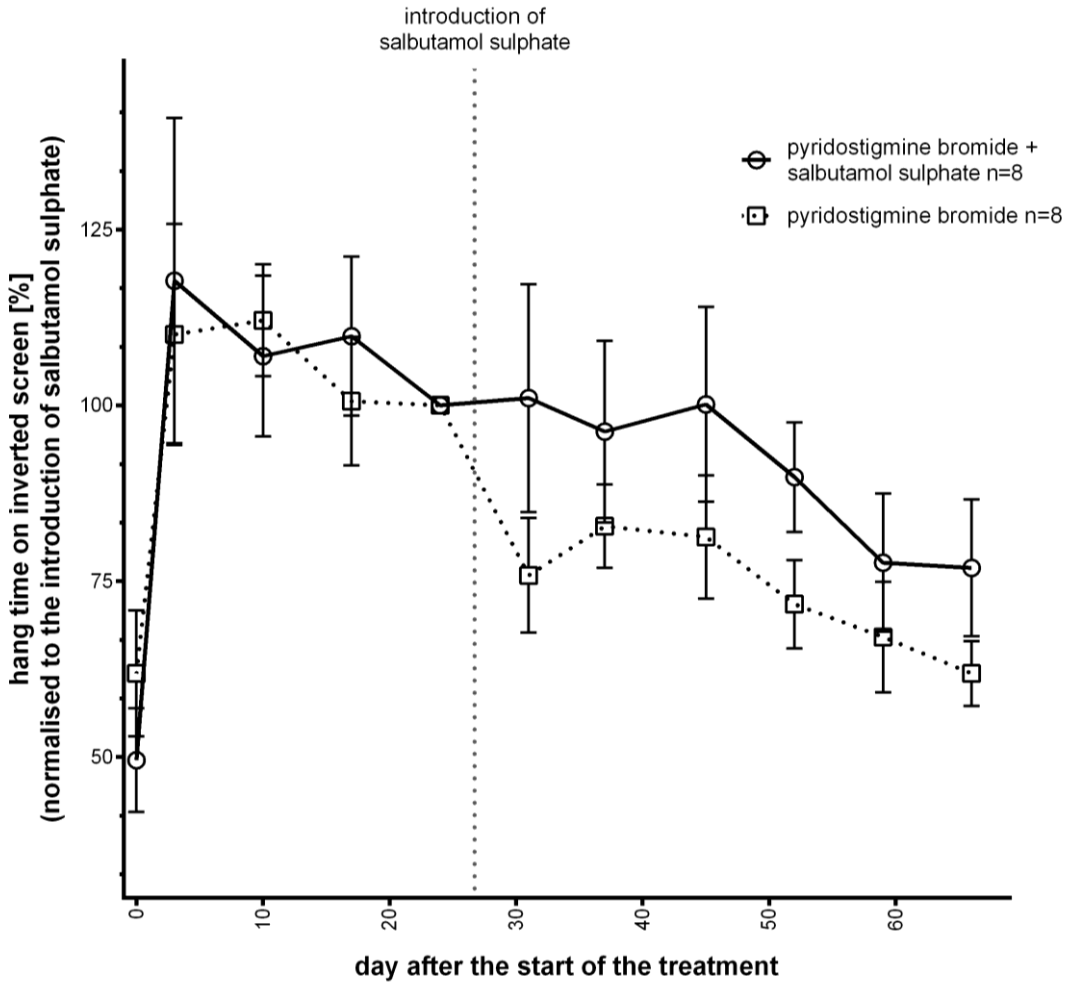

Fig.6.1. Performance in the inverted screen test of CMS mouse models treated for 4 weeks with pyridostigmine bromide, and then for 6 weeks with pyridostigmine bromide and salbutamol sulphate, or for the entire 10-week period with pyridostigmine bromide only
Each point represents the mean±SEM performance of n=8 animals receiving respective drugs. The data are normalised to the performance in the inverted screen test before the addition of salbutamol sulphate to the therapy.

The CMS mouse models showed a positive immediate response to treatment with pyridostigmine bromide, but a gradual loss of time on the inverted screen was observed during the subsequent weeks of the experiment. The addition of salbutamol sulphate on the 28th day appeared to prevent the worsening of myasthenic symptoms. The muscle strength in the group receiving pyridostigmine bromide and salbutamol

sulphate remained stable until the 45th day of the study. In the group treated with pyridostigmine bromide only, the hang time on the inverted screen decreased markedly from 100% on the 24th day to 81.31±8.75%, n=8 on the 45th day of the experiment. After the 45th day, progressive worsening of the symptoms was observed in both groups and continued until the 59th day in the group receiving pyridostigmine bromide and salbutamol sulphate, or until the end of the study (66th day) in the group treated with pyridostigmine bromide only. The inverted screen test performed on the final day of the experiment demonstrated that the efficacy of pyridostigmine bromide decreased from 100% to 61.88±4.59%, n=8 for animals receiving pyridostigmine bromide alone, and to 76.90±9.72%, n=8 for these treated with the combination of pyridostigmine bromide with salbutamol sulphate. Comparing the two treatment regimens using 2-way ANOVA statistics indicated that the addition of the ADRB2 agonist to the therapy with AChE inhibitor significantly ($p=0.0032$, n=8) reduced the progressive decrease in effectiveness of pyridostigmine bromide.

6.2.2. Does the treatment with salbutamol sulphate alter the proportion of slow- and fast-twitch fibres in skeletal muscle?

Salbutamol sulphate is well known for its anabolic effects (Clarkson and Thompson, 1997), which might at least partially mediate the improvement in the muscle strength in the animals treated with this drug. The anabolic effects can become apparent in the analysis of the proportions of slow- and fast-twitch muscle fibres.

Extensor digitorum longus, soleus and tibialis anterior muscles were dissected from the animals receiving medications (salbutamol sulphate and pyridostigmine bromide or pyridostigmine bromide alone) and from untreated ms$\varepsilon^{-/-}$ neo$^{+/+}$ hγ^{+} mice. The muscles were sectioned and immunolabelled with an anti-myosin antibody specific for

distinct myosin heavy chain isoforms, expressed differentially in slow- and fast-twitch muscle fibres, and horseradish peroxidase (HRP)-conjugated secondary antibodies. The HRP activity was developed and the stained sections were analysed by light microscopy (Figures 6.2. and 6.3.). Twenty representative images per condition were taken and the numbers of slow- and fast-twitch muscle fibres per optical field were counted (Figure 6.4.).

Fig.6.2. Slow-twitch muscle fibres in (EDL) extensor digitorum longus, soleus and (TA) tibialis anterior muscles dissected from the CMS mouse models receiving pyridostigmine bromide and salbutamol sulphate, pyridostigmine bromide alone or not receiving any medication
The EDL, soleus and TA muscles were dissected from the animals receiving trial medications, sectioned and labelled with an anti-myosin heavy chain slow isoform antibody and the appropriate HRP-conjugated secondary antibody. The HRP activity was developed and the sections were analysed by light microscopy. The panel shows an example staining.

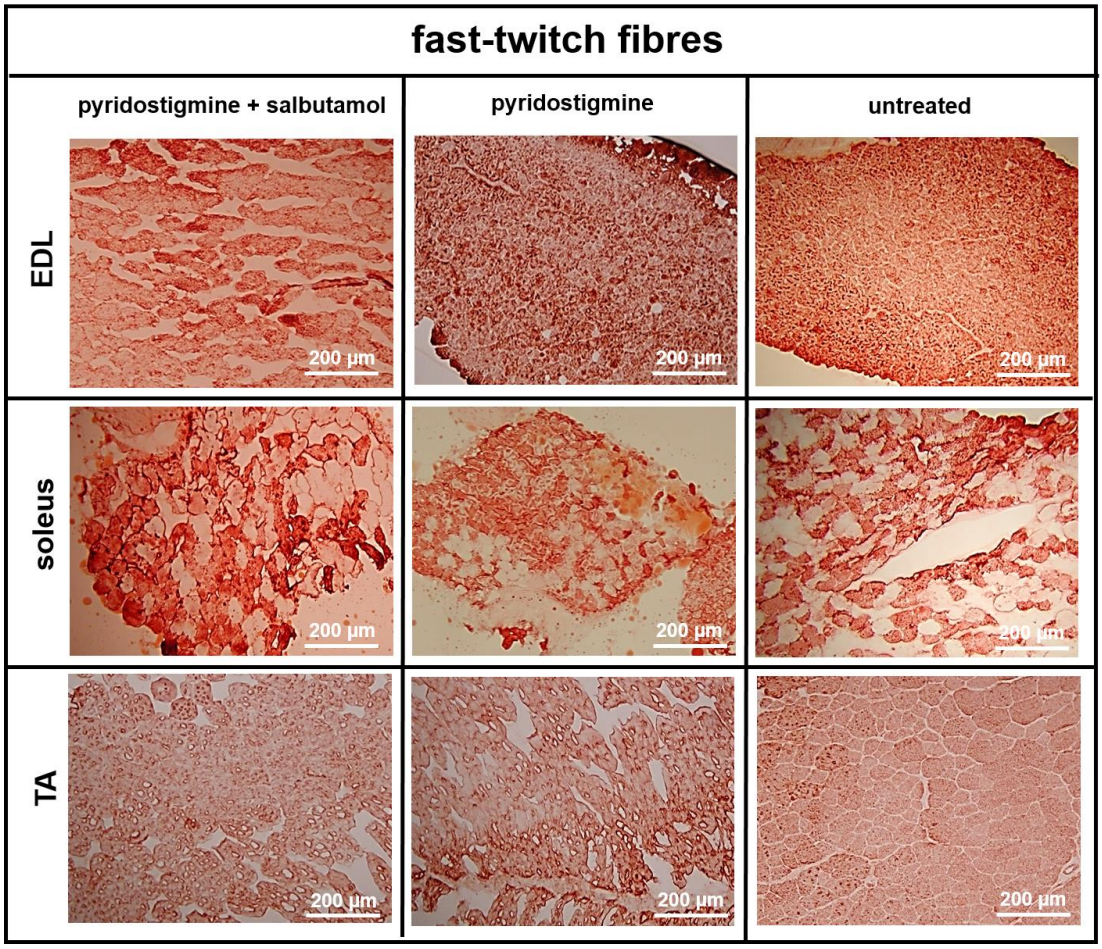

Fig.6.3. Fast-twitch muscle fibres in (EDL) extensor digitorum longus, soleus and (TA) tibialis anterior muscles dissected from the CMS mouse models receiving pyridostigmine bromide and salbutamol sulphate, pyridostigmine bromide alone or not receiving any medication
The EDL, soleus and TA muscles were dissected from the animals receiving trial medications, sectioned and labelled with an anti-myosin heavy chain fast isoform antibody and the appropriate HRP-conjugated secondary antibody. The HRP activity was developed and the sections were analysed by light microscopy. The panel shows an example staining.

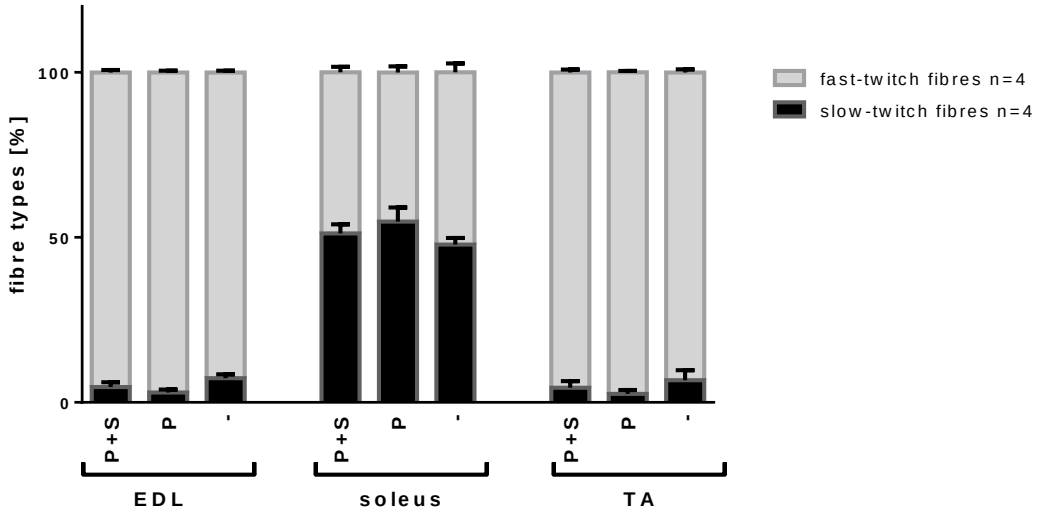

Fig.6.4. Proportion of slow- and fast-twitch muscle fibres in (EDL) extensor digitorum longus, soleus and (TA) tibialis anterior muscles dissected from the CMS mouse models receiving (P+S) pyridostigmine bromide and salbutamol sulphate, (P) pyridostigmine bromide alone or (-) not receiving any medication
The EDL, soleus and TA muscles were dissected from the animals receiving trial medications, sectioned and labelled with anti-myosin heavy chain fast or slow isoform, respectively, antibodies and the appropriate HRP-conjugated secondary antibodies. The HRP activity was developed and the sections were analysed by light microscopy. Fibres labelled with each antibody were counted. Each bar represents the mean±SEM of the slow- and fast-twitch fibres in n=4 analysed muscles from each group. The total number of fibres counted in a respective muscle section was considered as 100%. The data were analysed by 2-way ANOVA statistics and Bonferroni multiple comparison post-test.

Figure 6.4. shows the percentage of slow- and fast-twitch muscle fibres in the skeletal muscles dissected from the animals receiving treatment and from the untreated mice. The results confirmed the fact that both extensor digitorum longus and tibialis anterior muscles are predominantly composed of fast-twitch fibres, while the soleus comprises similar amounts of both fibre types. The patterns remained unchanged irrespective of the treatment regimen. This indicated that salbutamol sulphate did not cause changes in the proportion of fast- and slow-twitch fibres in skeletal muscles, and hence this experiment provided no evidence for the anabolic effect of the drug. The lack of fibre type switching following the salbutamol sulphate treatment may suggest that the beneficial effects of the drug may result from its local, NMJ-specific, action.

6.2.3. Structure of the NMJ after treatment with pyridostigmine bromide and salbutamol sulphate

Preliminary analysis of the structure of the endplates was performed. Extensor digitorum longus muscles were dissected from the mice, the muscle fibres were teased and the NMJ were stained with Alexa Fluor 594 α-BuTx. The labelled muscles were analysed by confocal fluorescence microscopy and the images processed using ZEN 2012 Black Edition software (Figure 6.5.).

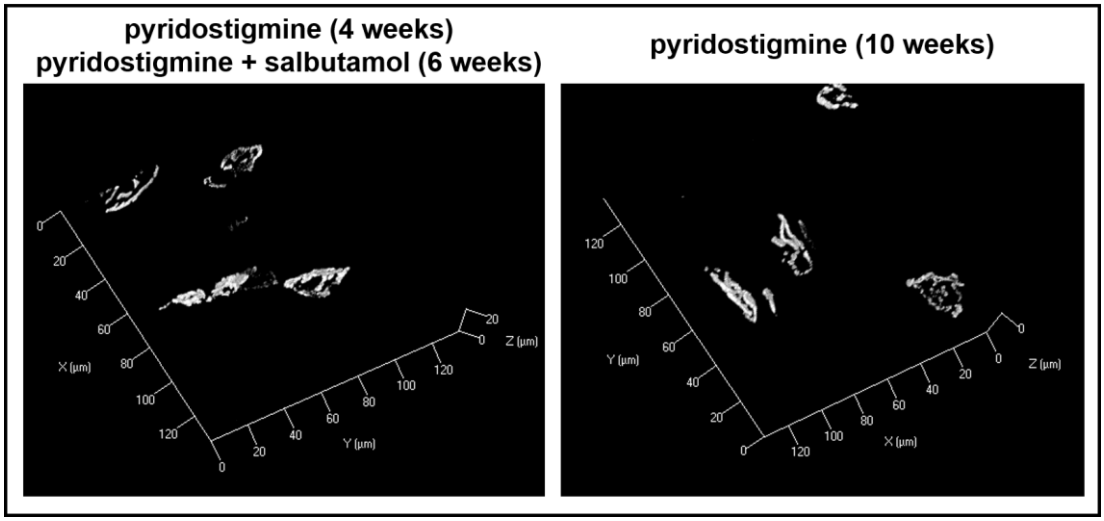

Fig.6.5. Structure of the NMJ in CMS mouse models treated with the combination of pyridostigmine bromide and salbutamol sulphate, or pyridostigmine bromide only
Extensor digitorum longus muscles were dissected from the animals, the fibres were teased, and the NMJ were labelled with Alexa Fluor 594 α-BuTx. The stained muscles were analysed by confocal fluorescence microscopy and the acquired images were processed using ZEN 2012 Black Edition software. Each image presents a representative group of the neuromuscular endplates observed in the animals receiving the respective treatments.

The NMJ had similar shapes, sizes and fluorescence intensity, corresponding to AChR levels, in the two groups (not quantified). Their structure appeared to be disrupted in both cases, which is a typical feature of the mouse model used in the study (Cossins et al., 2004). This may point to the lack of major differences between the endplates of the mice that received the combination of pyridostigmine bromide and salbutamol sulphate and those treated with pyridostigmine bromide only, but subtle changes cannot be excluded.

The structure of the NMJ was also studied in the diaphragms. These muscles were also dissected, labelled with Alexa Fluor 594 α-BuTx and analysed by widefield fluorescence microscopy (Figure 6.6.).

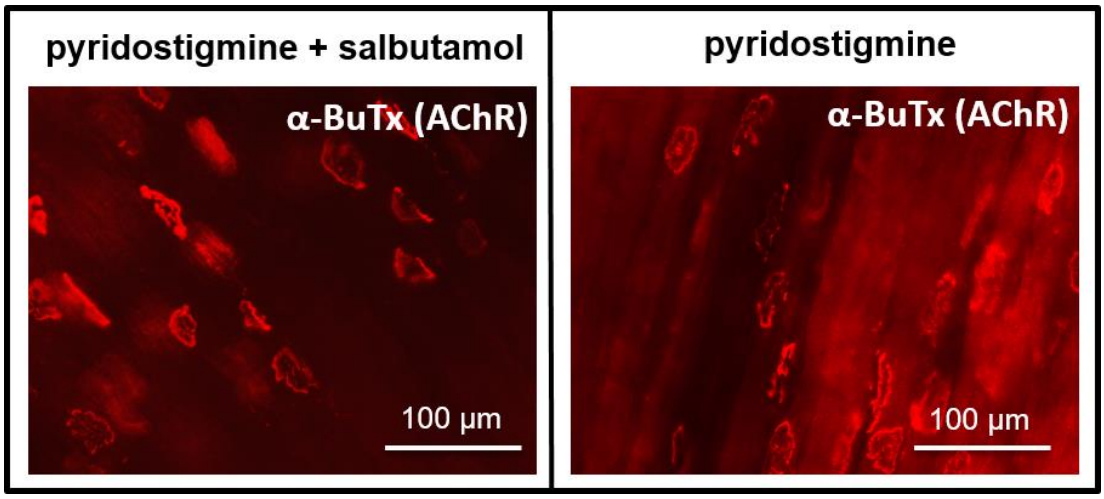

Fig.6.6. Neuromuscular endplates in the diaphragms dissected from mice treated with the combination of pyridostigmine bromide and salbutamol sulphate, or with pyridostigmine bromide alone
Diaphragms were dissected from the CMS mouse models receiving pyridostigmine bromide and salbutamol sulphate, or pyridostigmine bromide only. AChR were labelled with Alexa Fluor 594 α-BuTx and visualised by widefield fluorescence microscopy. Representative images of the labelled diaphragms dissected from the animals treated with the distinct medications are presented.

Again, preliminary observations did not detect any obvious differences in the intensity of red fluorescence, corresponding to AChR expression, and in the structures of the neuromuscular endplates between the animals receiving the medications. The structures of the endplates were disrupted in both groups, irrespective of the treatment regimen. Similar disruption is also apparent in the untreated animals since this is a standard feature of the AChR deficiency animal model used (Cossins et al., 2004). The preliminary observations may reaffirm the previous suggestion that salbutamol sulphate has no major effect on NMJ morphology, or the changes are so subtle that they cannot be detected with standard widefield and confocal microscopy techniques. The variability of the endplate structures in this disease model meant it was impractical to look for such small changes in the endplates.

6.3. *In vitro* model systems to study the mechanisms of the action of salbutamol sulphate at the NMJ

To investigate effects of salbutamol sulphate in greater detail, we used *in vitro*-cultured C2C12 myotubes to compare the AChR cell surface expression and the formation of AChR clusters between untreated and salbutamol sulphate-treated cells.

6.3.1. Determination of the optimal concentration of salbutamol sulphate for *in vitro* experiments

Salbutamol sulphate, acting via ADRB2, leads to an increase in the intracellular cAMP levels in treated cells. This increase can be monitored with a cAMP response element (CRE) reporter assay, which involves transfection of cells with a vector containing CRE that drives the transcription of a luciferase reporter gene (*luc2P*). Activity of the luciferase, corresponding to the intracellular cAMP levels and the transcription of *luc2P* gene, can be measured by luminometry.

The method was used to estimate the optimal concentration of salbutamol sulphate for *in vitro* research. Human embryonic kidney cells (HEK293TSA) were chosen for the study because they are easier to transfect than the C2C12 muscle cell line. The cells were transfected with pGL4.29[*luc2P*/CRE/Hygro] vector, incubated for 6 hours with varying salbutamol sulphate concentrations and the luciferase activity was measured by luminometry (Figure 6.7.).

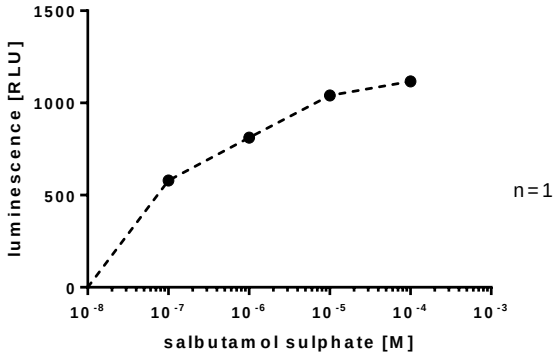

Fig.6.7. CRE reporter assay in HEK293TSA cells treated with salbutamol sulphate
HEK293TSA cells were transfected with pGL4.29[*luc2P*/CRE/Hygro], incubated for 6 hours with 0, 0.1, 1, 10 or 100 µM salbutamol sulphate, and the luciferase activity was measured by luminometry.

Figure 6.7. shows a dose response effect between the concentration of salbutamol sulphate in the medium and the activity of the luciferase. The highest luminescence was recorded in the cells incubated at the higher concentrations of 10 µM (1040 RLU) and 100 µM (1117 RLU) salbutamol sulphate, but the difference between these two was modest despite the 10-fold difference in concentration. Therefore, a 10 µM concentration of the drug was used in the next experiments.

6.3.2. Does salbutamol sulphate have an effect on the AChR cell surface expression?

Treatment with salbutamol sulphate may result in increased expression of AChR at the cell surface. Such potential increase in AChR expression is unlikely to be detectable by fluorescence microscopy methods.

The AChR cell surface expression was measured *in vitro* in untreated or salbutamol sulphate-treated C2C12 myotubes using a cell surface ^{125}I-α-BuTx binding assay (Figure 6.8.).

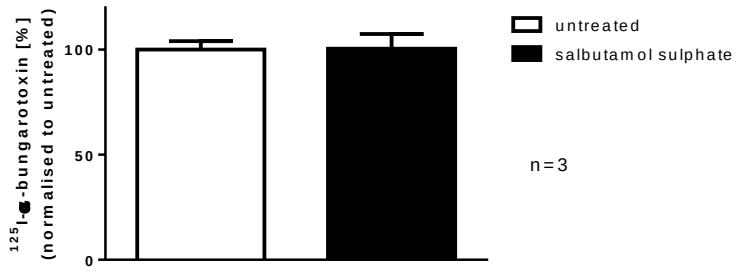

Fig.6.8. Cell surface ^{125}I-α-BuTx binding to untreated and salbutamol sulphate-treated C2C12 myotubes
Each bar represents the mean±SEM cell surface ^{125}I-α-BuTx binding to untreated C2C12 myotubes or these cells treated for 12 hours with 10 µM salbutamol sulphate, respectively, recorded in n=3 independent experiments. All the data are expressed relative to levels of cell surface ^{125}I-α-BuTx binding to the untreated cells.

No differences in the levels of ^{125}I-α-BuTx bound to the cell surface were recorded between untreated and salbutamol sulphate-treated cells. Therefore, salbutamol sulphate does not appear to affect AChR expression.

6.3.3. Does salbutamol sulphate have an effect on the stability of AChR clusters?

Another possibility is that treatment with salbutamol sulphate stabilises AChR clusters at the NMJ. This would be consistent with clinical observations of a positive response to treatment by patients with mutations in the proteins implicated in the formation and maintenance of the AChR clusters, such as DOK7.

Phosphorylation of the AChR β subunit can be used as a marker for the AChR cluster stability (Figure 6.9.). Phosphorylation of this subunit is triggered by agrin (AGRN) and is essential for the interaction of AChR with 43 kDa receptor-associated protein of the synapse (RAPSN), and thus the formation and stabilisation of the AChR clusters (Borges et al., 2008).

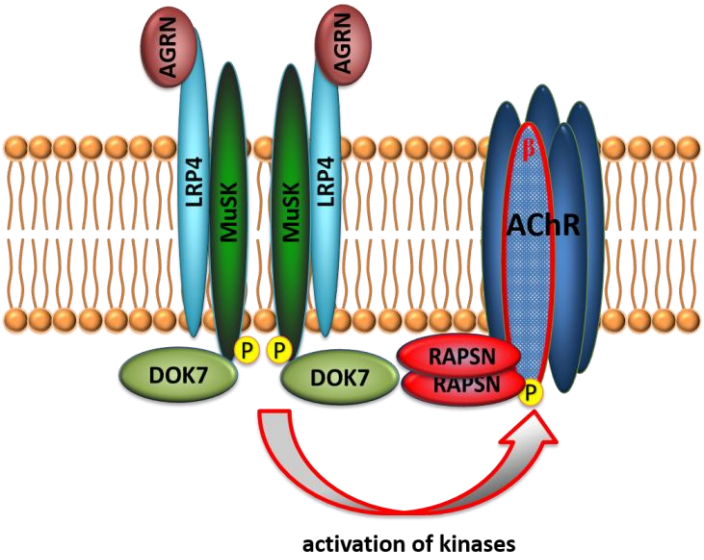

Fig.6.9. Schematic representation of the AGRN-mediated AChR clustering pathway
AChR – acetylcholine receptor; AGRN – agrin; DOK7 – downstream of tyrosine kinase 7; LRP4 – low-density lipoprotein receptor-related protein 4; P – phosphate group; RAPSN – 43 kDa receptor-associated protein of the synapse

6.3.3.1. Does salbutamol sulphate influence phosphorylation of the AChR β subunit and RAPSN binding to the AChR?

It is possible that treatment with salbutamol sulphate influences the levels of the phosphorylation of AChR β subunit and this was tested using C2C12 myotubes treated with AGRN to induce the formation of AChR clusters. After 12 hours, AGRN was removed from the system and salbutamol sulphate was added to the medium. Following a 6-hour treatment, AChR were extracted from the cell surface using biotin-XX α-BuTx and streptavidin-coated magnetic beads. The extracted protein was resolved by electrophoresis and immunoblotted with anti-AChR β and anti-phosphotyrosine antibodies (Figure 6.10.).

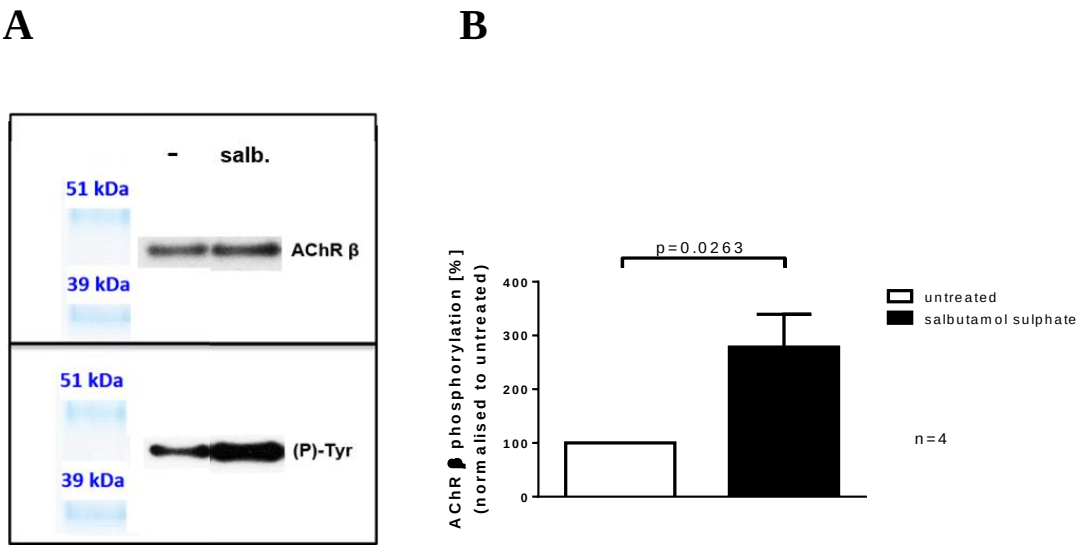

Fig.6.10. Phosphorylation of AChR β subunit in (-) untreated and (salb.) salbutamol sulphate-treated C2C12 myotubes
C2C12 myotubes were treated with AGRN for 12 hours, then AGRN was removed from the system and salbutamol sulphate was added to the medium to a final concentration of 10 µM. After a 6-hour treatment, AChR were extracted from the cell surface using biotin-XX α-BuTx and streptavidin-coated magnetic beads, and the protein extracts were resolved by electrophoresis.
(A) The extracted protein was analysed by immunoblotting with anti-AChR β and anti-phosphotyrosine antibodies, and the appropriate HRP-conjugated secondary antibodies.
(B) The intensities of the bands corresponding to the phosphorylated AChR β subunits were measured by densitometry and normalised to the total levels of AChR β subunits in the extracts. Each bar represents the mean±SEM levels of the phosphorylation of AChR β subunit, recorded in n=4 independent experiments, in untreated or salbutamol sulphate-treated C2C12 myotubes. All the data are expressed relative to the levels of the phosphorylation of the AChR β subunit in the untreated cells. p value was obtained using a student t-test.

The C2C12 myotubes treated with salbutamol sulphate (lane 2) exhibited increased to 278.51±60.94%, p=0.0263, n=4 levels of the phosphorylation of AChR β subunit when compared to the control cells (lane 1).

Since phosphorylation of AChR β subunit has been shown to be essential for the association of the AChR with RAPSN, crucial for the formation and stability of AChR clusters at the NMJ (Borges et al., 2008), the western blot membranes were reprobed with an anti-RAPSN antibody to look at the levels of RAPSN bound to the AChR in the untreated and the salbutamol sulphate-treated cells (Figure 6.11.).

A **B**

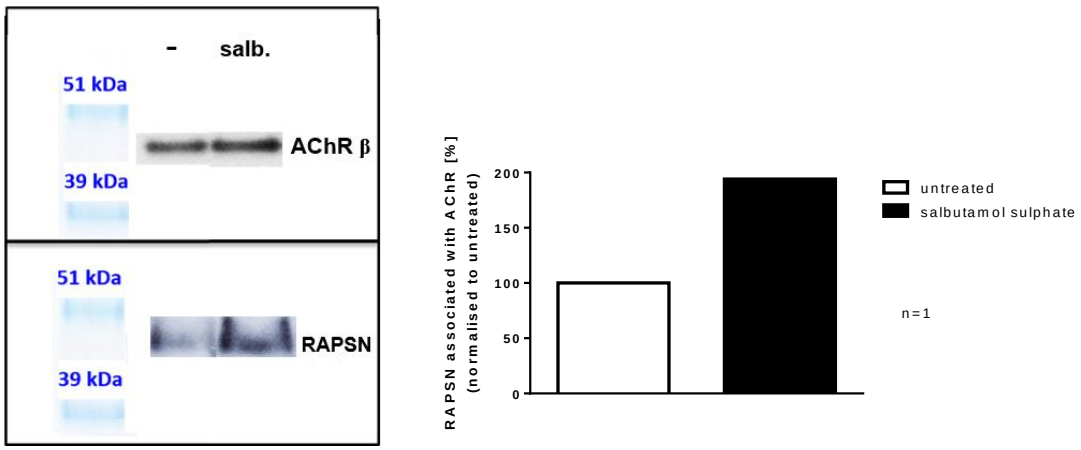

Fig.6.11. RAPSN interactions with cell surface AChR in (-) untreated and (salb.) salbutamol sulphate-treated C2C12 myotubes
C2C12 myotubes were treated with AGRN for 12 hours, then AGRN was removed from the system and salbutamol sulphate was added to the medium to a final concentration of 10 µM. After a 6-hour treatment, AChR were extracted from the cell surface using biotin-XX α-BuTx and streptavidin-coated magnetic beads, and the protein extracts were resolved by electrophoresis.
(A) The extracted protein was analysed by immunoblotting with anti-AChR β subunit and anti-RAPSN antibodies, and the appropriate HRP-conjugated secondary antibodies.
(B) The intensities of the bands corresponding to RAPSN were measured by densitometry and normalised to the total levels of AChR β subunits in the extracts. Each bar represents the levels of RAPSN bound to AChR, recorded in n=1 experiment, in untreated or salbutamol sulphate-treated C2C12 myotubes. All the data are expressed relative to the levels of RAPSN bound to AChR in the untreated cells.

The intensity of the band corresponding to RAPSN interacting with the AChR expressed at the cell surface was increased in the cells treated with salbutamol sulphate (lane 2) to 194%, n=1 compared to the untreated cells (lane 1). Due to the time constraints only one experiment was performed.

In summary, the results of these two studies suggest that salbutamol sulphate has the potential to elevate AChR β phosphorylation, which in turn may increase binding of RAPSN to the AChR and stabilisation of the AChR clusters at the synapse.

6.3.3.2. Stability of AChR clusters in C2C12 cells treated with salbutamol sulphate

The stability of the AChR clusters following treatment with salbutamol sulphate was further analysed in C2C12 myotubes using the AChR cluster assay. The cells were incubated for 12 hours with AGRN, then the AGRN was removed from the system and salbutamol sulphate was added to the medium. The cells were fixed at 0, 2, 4 or 6 hours after the addition of the drug, and the AChR clusters were stained with Alexa Fluor 594 α-BuTx. Ten representative images per condition were taken at each time point and the numbers of AChR clusters were counted in every optical field (Figure 6.12.).

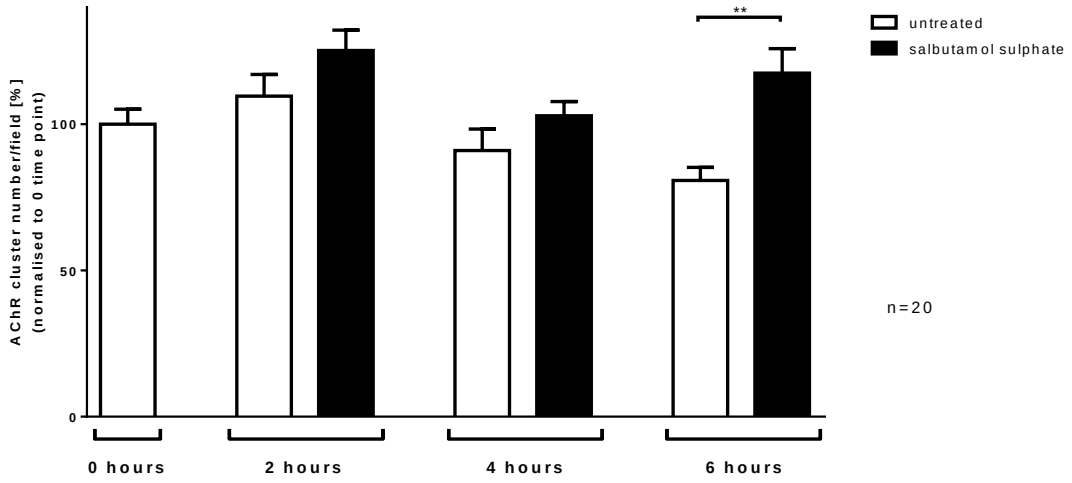

Fig.6.12. Stability of AChR clusters in untreated and salbutamol sulphate-treated C2C12 myotubes
C2C12 myotubes were incubated for 12 hours with AGRN, then AGRN was removed from the system and salbutamol sulphate was added to the medium to a final concentration of 10 µM. In 0, 2, 4 and 6 hours after the addition of the drug the cells were fixed and stained with Alexa Fluor 594 α-BuTx. 10 representative images per condition were taken at each time point and the numbers of AChR clusters per optical field were counted.
Each bar represents the mean±SEM number of AChR clusters counted on 10 optical fields in n=2 independent experiments. All the data are presented relative to the number of the AChR clusters in the cells at 0 time point, and were analysed using ANOVA statistics with Bonferroni multiple comparison post-test.

A reduction in numbers of AChR clusters was observed over time in the untreated C2C12 myotubes. This decrease appeared to be less profound in the cells treated with salbutamol sulphate. There was no further reduction in AChR clusters between the 4- and 6-hour time points in these cells. When the number of the AChR clusters was compared between the untreated and the salbutamol sulphate-treated cells at the 6-hour time point, a significant ($p<0.05$, $n=20$) difference was observed. The number of the AChR clusters in the untreated cells at 6 hours was reduced to 80.78±4.45%, n=20 of the zero time point number, whereas in the salbutamol sulphate-treated cells the number of the AChR clusters was higher (117.50±8.32%, n=20) than at the start of the experiment. An increase in the number of AChR clusters between 0 and 2 hours was also observed in both groups although it was more marked in the salbutamol sulphate-treated cells. This increase, however, did not reach statistical significance, and might be due to a variability in the number of AChR clusters detected from each optical field in the assay. Another possibility is that the full-length AGRN, due to its high glycosylation, was still having a stimulatory effect. Nevertheless, the data emerging from the AChR cluster assay points to salbutamol sulphate having the ability to potentiate and/or stabilise AChR clustering at the NMJ. This warrants further investigations.

6.4. Discussion

In this chapter an animal model of AChR deficiency syndrome was used to assess a therapy that has been reported anecdotally to benefit patients. This animal model expresses human *CHRNG* cDNA in the *Chrne*$^{-/-}$ background (Cossins et al., 2004) and was used to study treatment with a combination of AChE inhibitors and ADRB2 agonists. The hypothesis was that ADRB2 agonists would prevent the decrease over time in response to AChE inhibitors. The data demonstrated that the addition of salbutamol sulphate to treatment with pyridostigmine bromide improved the condition of the animals, compared to the ones treated with pyridostigmine bromide alone. However, the molecular basis of this improvement has not been identified. Preliminary morphological studies showed that the structure of the neuromuscular endplates in extensor digitorum longus and diaphragm muscles, and the proportion of slow- and fast-twitch fibres in extensor digitorum longus, soleus and tibialis anterior muscles were not altered in the animals, irrespective of the treatment regimen. The lack of difference in the proportions of slow- and fast-twitch muscle fibres between the animals receiving either therapy accords with recent studies conducted in C2C12 myotubes, which demonstrated no effect of ADRB2 agonists on the expression of hypertrophy markers, including slow and fast myosin and myogenin (Wannenes et al., 2012). It could also suggest that salbutamol sulphate may act at the NMJ, rather than through a general anabolic effect.

A potential mechanism through which the ADRB2 agonists could act is by increasing the AChR cell surface expression at the NMJ, which would be in line with the reports that muscle cell cultures treated with this group of agents exhibit higher levels of the receptor at the cell surface compared to controls (Blosser, 1983). However, here and in the research reported by (Li et al., 1996), ADRB2 agonists had no effect on the

AChR cell surface expression. This result agrees with Dr Georgina Burke's DPhil thesis, which studied the response to ephedrine administered on its own in the AChR deficiency CMS mouse model. She reported no improvement in the muscle strength, which should have occurred if the drug had increased AChR at the endplates (Figure 6.13.).

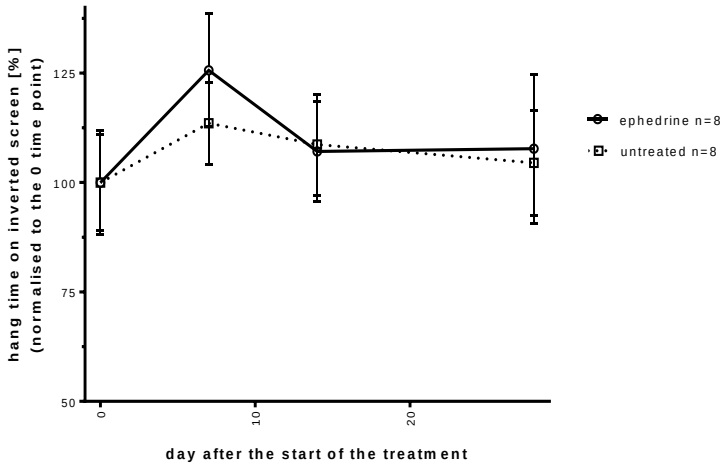

Fig.6.13. Performance in the inverted screen test of the animals treated for 4 weeks with ephedrine or not receiving any medication
Each point represents the mean±SEM performance of n=8 animals receiving respective treatment. The data are normalised to the performance in the inverted screen test before the start of the experiment.

Based on the data collected by Dr Burke and the results presented in this thesis one can conclude that administration of the drugs acting through ADRB2 improves muscle strength of AChR deficiency mice only when the medicines are administered with pyridostigmine bromide, which agrees with clinical observations in AChR deficiency patients. The beneficial effect of salbutamol sulphate only in the presence of pyridostigmine bromide suggests that a possible mechanism may involve counteracting disruption of the NMJ that follows prolonged treatment with pyridostigmine bromide. Similar disruption is observed at the endplates in AChE deficiency CMS cases (Wargon et al., 2012). Our preliminary data confirmed this hypothesis. Incubation of C2C12 cells with salbutamol sulphate increased the levels

of the phosphorylation of AChR β subunit and (from one experiment) the amounts of RAPSN bound to AChR, suggesting potential mechanism. These events appeared to have a stabilising effect on the AGRN-induced AChR clusters in the cells.

Further research is needed to establish a link between the ADRB2 activation and the phosphorylation of the AChR β subunit. A potential explanation might be that β_2-agonists activate the downstream cAMP-dependent protein kinase (PKA) type I signalling pathway. The activated PKA could play a role by activating the proto-oncogene tyrosine kinase SRC (Armaiz-Pena et al., 2013), which has been implicated in the phosphorylation of the AChR β subunit and the stabilisation of the AChR clusters (Smith et al., 2001, Sadasivam et al., 2005). The latter effect might be mediated by enhanced binding of RAPSN to AChR since the phosphorylation of the AChR β subunit is essential for this interaction (Borges et al., 2008), or by cytoskeletal rearrangements triggered by SRC-mediated phosphorylation events at the NMJ (Sadasivam et al., 2005). Another possibility is a direct interaction of PKA with RAPSN (Choi et al., 2012), which may stabilise self-association of RAPSN and its interactions with AChR (Maimone and Enigk, 1999, Ramarao et al., 2001). Finally, the ADRB2 agonists may influence transcription at the NMJ by increasing intracellular cAMP levels since the expression of several genes encoding NMJ-specific proteins is regulated by cAMP due to the presence of CRE in their promoters (Kim et al., 2005, Choi et al., 2007). All the described potential molecular events might result in stabilising the structure of the NMJ (Figure 6.14.). The proposed mechanism is supported by a positive response to the ADRB2 agonists in AChE deficiency and *DOK7* CMS, which both are thought to result from synaptic instability and the disruption of the AChR clusters (Liewluck et al., 2011, Cossins et al., 2012b, Wargon et al., 2012).

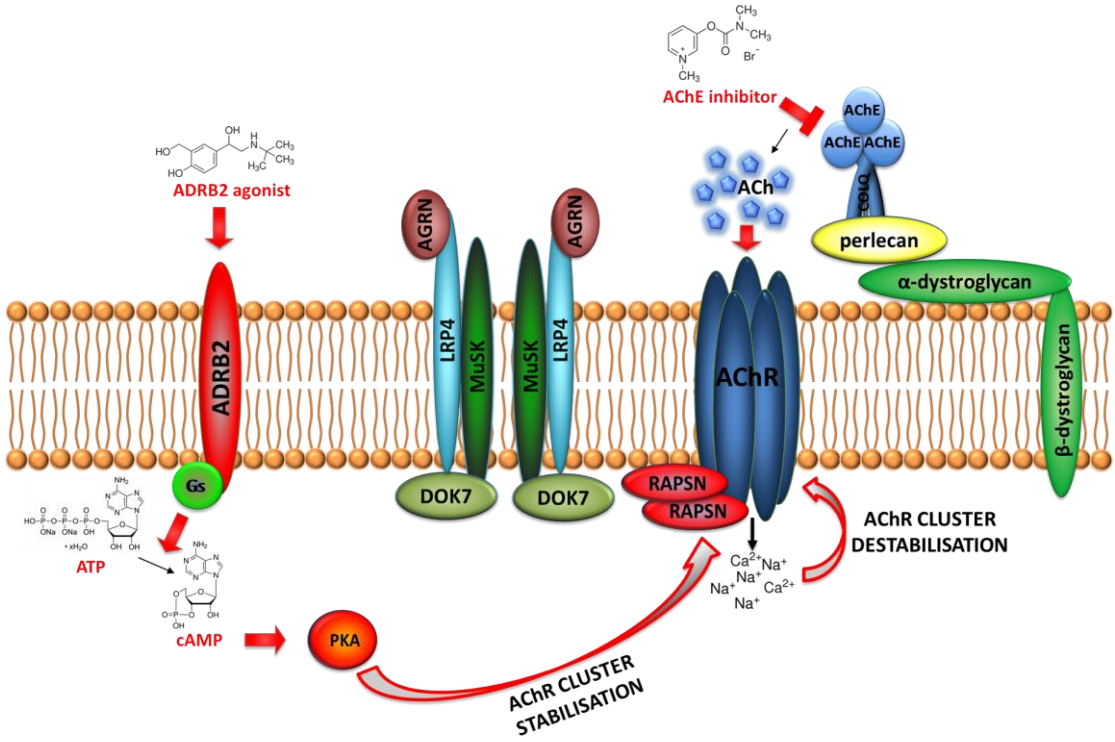

Fig.6.14. Potential proposed mechanism of the action of ADRB2 agonists and AChE inhibitors at the NMJ
ACh – acetylcholine; AChE – acetylcholinesterase; AChR – acetylcholine receptor; ADRB2 – β_2-adrenergic receptor; AGRN – agrin; ATP – adenosine triphosphate; cAMP – cyclic adenosine monophosphate; COLQ – collagen Q; DOK7 – downstream of tyrosine kinase 7; LRP4 – low-density lipoprotein receptor-related protein 4; MuSK – muscle-specific tyrosine kinase; PKA – cAMP-dependent protein kinase; RAPSN – 43 kDa receptor-associated protein of the synapse

An alternative mechanism might be desensitisation of the AChR from prolonged exposure of the receptor to ACh at the synapse. The desensitisation might be theoretically at least partially reversed by salbutamol acting via cAMP-dependent downstream signalling. However, it has been shown that the cAMP-dependent phosphorylation of the receptor subunits actually increases the AChR desensitisation rate (Mulle et al., 1988).

Further investigations are needed to establish the molecular action of the ADRB2 agonists at the synapse, but this preliminary study suggests that a combination of pyridostigmine bromide and salbutamol sulphate is likely to be helpful. The next steps should be to determine the optimum levels of pyridostigmine bromide and salbutamol

sulphate for maximum benefit, and to gain a greater insight into the molecular mechanisms linking the salbutamol sulphate treatment with the increased phosphorylation of AChR β subunit and the stabilisation or even potentiation of the AChR clustering.

Chapter 7

Autoimmunological causes of muscle weakness

7.1. Introduction

Neuromuscular transmission can be disrupted by inherited defects in synaptic proteins and also by autoantibodies targeting molecules expressed specifically at the neuromuscular junction (NMJ). Myasthenia gravis (MG) is a classical autoimmune disorder affecting the NMJ. In most cases the antibodies recognise acetylcholine receptor (AChR) or muscle-specific tyrosine kinase (MuSK) (Hoch et al., 2001), but there are many patients, referred to as seronegative MG (SNMG), in whom anti-AChR and anti-MuSK autoantibodies are not detected by present assays. Additional antibody targets proposed include: low-density lipoprotein receptor-related protein 4 (LRP4) (Higuchi et al., 2011, Pevzner et al., 2012, Zhang et al., 2012), agrin (AGRN) (Cossins et al., 2012a) and acetylcholinesterase (AChE) (Wang et al., 2010). Despite identifying a number of candidates, there is still a group of patients presenting with an autoimmune myasthenic weakness with an unknown underlying mechanism.

One possible novel antibody target might be collagen Q (COLQ) – a protein highly expressed at the NMJ, and crucial for anchoring and concentrating AChE at the synapse. It is expressed on the cell surface of the NMJ and therefore is easily accessible to the autoantibodies. Moreover, mutations in *COLQ* can underlie an inherited myasthenic disorder – congenital myasthenic syndrome (CMS) (Donger et al., 1998, Ohno et al., 1998). Although COLQ possesses many features that make it a target for autoantibodies in MG, immunoglobulins directed against the molecule have not yet been reported in patients.

Autoantibodies are detected traditionally by enzyme-linked immunosorbent assays

(ELISA) and radioimmunoprecipitation assays (RIA), and occasionally by fluorescence immunoprecipitation assays (FIPA). The ELISA method involves immobilisation of target epitopes on a plate and incubation of the plate with patient serum, and an enzyme-linked secondary antibody directed against the human antibodies. In RIA and FIPA the target radio- or fluorescently-labelled molecule is immunoprecipitated from solution using patient serum. The detection of radioactivity or fluorescence in the precipitate indicates the presence of target-specific antibodies in the sample. The intensity of the signal correlates with the antibody titre. Although commonly used in diagnostic laboratories, these assays do not always recognise pathogenic antibodies (Vincent et al., 2012, Yang et al., 2011).

Some disadvantages of ELISA, RIA and FIPA have been partially overcome by the design of a cell-based assay (CBA). In this method, a target protein is over-expressed at the cell surface, often in human embryonic kidney cells (HEK293TSA). The cells are incubated with patient serum and the autoantibodies, bound to the cell surface, are detected by a fluorescent secondary antibody. The intensity of the fluorescence, corresponding to the presence of a specific autoantibody, can be determined by fluorescence microscopy or flow cytometry (Cossins et al., 2012a, Leite et al., 2008). The sensitivity of the assay may be further improved to detect anti-AChR autoantibodies by co-transfection of HEK293TSA cells with DNA encoding AChR subunits and 43 kDa receptor-associated protein of the synapse (RAPSN) (Leite et al., 2008). RAPSN interacts with the receptor and induces the formation of AChR clusters at the NMJ (Porter and Froehner, 1985). The co-transfection of AChR with RAPSN results in the formation of ‘artificial’ AChR clusters at the surface of the transfected HEK293TSA cells.

Many potential antibody targets can be expressed easily at the surface of HEK293TSA

cells. However, proteins that are secreted or associated with other cell surface molecules, and do not possess a transmembrane domain (TM), may need to be modified. The cell surface expression of secreted proteins can be achieved by fusion with a TM originating from a different molecule, such as TM from contactin-associated protein-like 2 (CASPR2TM) (Irani et al., 2010).

The detection of antibodies directed against novel targets may act as a pointer to the mechanism of an autoimmune disease. However, they do not necessarily contribute to either the pathological process or to the clinical symptoms. Therefore, their pathogenicity needs to be determined first. In MG, there are several pathways by which the autoantibodies may lead to muscle weakness. These include complement activation, competition with ligand binding sites, steric hindrance affecting interactions between molecules at the NMJ or endocytosis. The molecular mechanism of action of immunoglobulins depends on their subclass and the recognised target (Gomez et al., 2010).

7.2. A cell-based assay for the detection of anti-COLQ antibodies

COLQ is a potential target for autoantibodies in SNMG patients, but it has not been demonstrated that antibodies directed against this molecule are present in MG patient sera. This could be tested by CBA in which COLQ is over-expressed at the surface of HEK293TSA cells. Expression of COLQ anchored to the cell surface was achieved by making a construct encoding COLQ fused with a TM originating from CASPR2. A Myc tag was introduced immediately downstream of a COLQ-CASPR2TM N-terminal signal peptide since there were no commercial antibodies for immunofluorescence detection of COLQ and there was a need for a positive control for the cell surface expression of COLQ-CASPR2TM (Figure 7.1.).

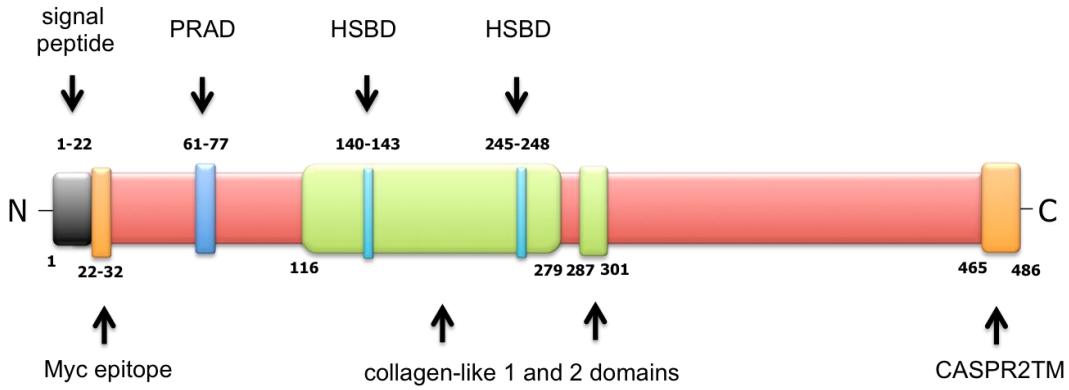

Fig.7.1. Schematic representation of Myc-COLQ-CASPR2TM applied in the CBA
The COLQ structure was based on the data stored in the UniProt database [Q9Y215].
PRAD – proline-rich attachment domain; HSBD – heparan sulphate binding domain
CASPR2TM – transmembrane domain of contactin-associated protein-like 2

A CBA for the detection of anti-COLQ antibodies was tested by over-expressing Myc-COLQ-CASPR2TM at the surface of HEK293TSA cells and detecting the target with an anti-Myc antibody, and an Alexa Fluor 594 secondary antibody (Figure 7.2.).

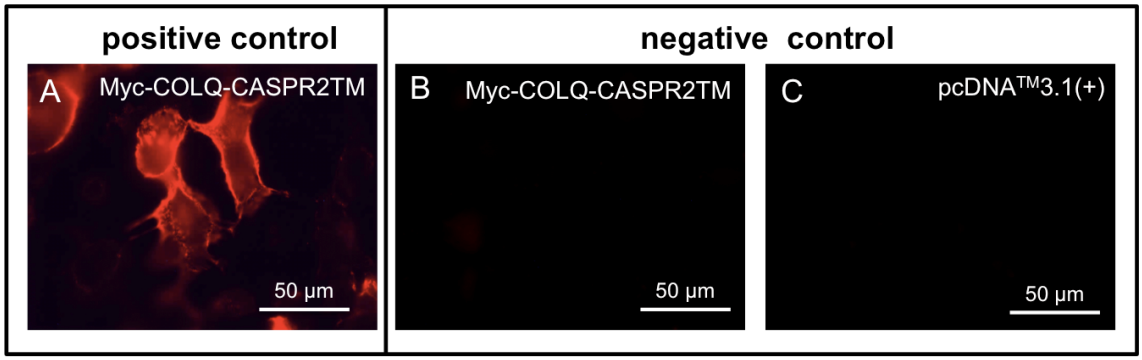

Fig.7.2. Cell surface expression of Myc-COLQ-CASPR2TM in transfected HEK293TSA cells
HEK293TSA cells were transfected with constructs encoding (A, B) Myc-COLQ-CASPR2TM or (C) an empty pcDNA™3.1 vector, and stained with (A, C) a mouse monoclonal anti-Myc antibody and the appropriate Alexa Fluor 594 secondary antibody or (B) the secondary antibody only.

Fluorescence microscopy imaging of the transfected cells revealed a bright red signal corresponding to Myc-COLQ-CASPR2TM at the cell surface. Thus the target exhibited an efficient cell surface expression.

7.3. Anti-COLQ antibodies in MG patient sera

Two cohorts of MG patients (selected by Prof. Angela Vincent) were analysed for the presence of anti-COLQ immunoglobulins in the sera. The first comprised 182, and the second 236 samples. The groups will be defined in greater detail later in this section.

The assay protocol involved a series of steps. First, all samples were tested on HEK293TSA cells co-transfected with plasmids encoding Myc-COLQ-CASPR2TM and enhanced green fluorescent protein (EGFP), as a marker of transfection efficiency. The patient sera, diluted 1:20, were incubated with the transfected HEK293TSA cells for one hour and the antibody binding was detected using an Alexa Fluor 568 anti-human IgG secondary antibody (Figure 7.3.).

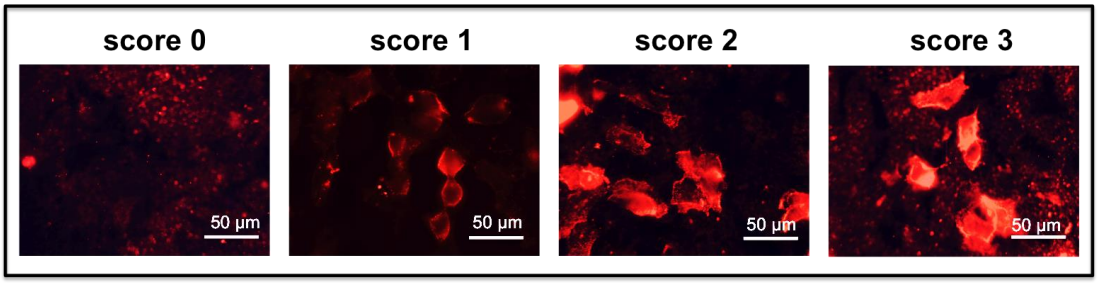

Fig.7.3. Anti-COLQ autoantibodies in patient sera
HEK293TSA cells over-expressing COLQ-CASPR2TM at the surface were stained with serum samples and an Alexa Fluor 568 anti-human IgG secondary antibody, and analysed by fluorescence microscopy. The intensity of red fluorescence was visually assessed and scored from 0 (no signal) to 3 (bright red fluorescence).

The intensity of red fluorescence, corresponding to the levels of anti-COLQ antibodies, varied between the analysed samples. The differences were assessed visually and a score ranging from 0 to 3 was assigned to each sample. The samples were considered positive if they received a score ≥1. The threshold was based on the mean±3xSD of the scores assigned to the control samples.

If positive in the first experiment (i.e. score ≥1), the sera were retested using the same system. Subsequently, samples positive (i.e. score ≥1) in the two assays were tested on HEK293TSA cells co-transfected with constructs encoding COLQ-CASPR2TM and EGFP. This was done in order to confirm that the autoantibodies recognised COLQ specifically and did not bind to the Myc tag. Finally, the sera which were positive (i.e. score ≥1) in all three assays were tested on HEK293TSA cells co-transfected with pcDNA™3.1(+) and pEGFP-N1 vectors to exclude the possibility that the antibodies exhibited a non-specific binding to the surface of HEK293TSA cells. The final result of the assay was determined by the performance in the four experiments (Figure 7.4.).

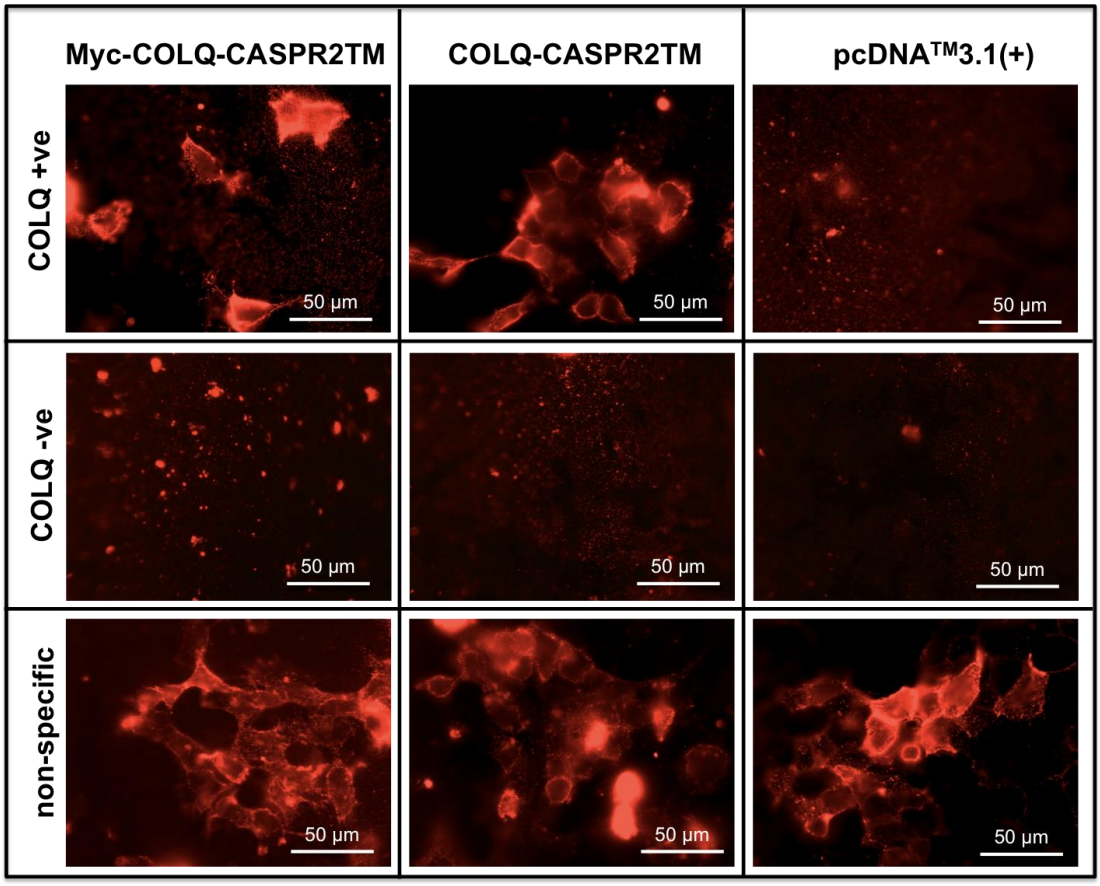

Fig.7.4. CBA for the presence of anti-COLQ autoantibodies in patient sera
HEK293TSA cells were transfected with pcDNA-Myc-*COLQ-CASPR2TM*, pcDNA-*COLQ-CASPR2TM* or pcDNA™3.1(+) vectors, respectively, and stained with patient sera, which potentially contained anti-COLQ autoantibodies, and an Alexa Fluor 568 anti-human IgG secondary antibody.

Samples which stained both Myc-COLQ-CASPR2TM- and COLQ-CASPR2TM-expressing cells, with all scores equal to or greater than 1, and did not stain mock-transfected cells were considered positive for the presence of anti-COLQ antibodies (COLQ+ve). If no red fluorescence was detected, or if it was observed in all subsequent tests, irrespective of the DNA construct used, the samples were considered as COLQ-ve or as presenting non-specific binding to the cell surface, respectively.

The protocol for the specific detection of anti-COLQ autoimmunoglobulins was used to screen the two cohorts of MG patients. The analysis of the first cohort was part of a screen for a series of novel antibody targets in MG patients. The cohort was subdivided

into three categories: (1) AChR+ve or (2) MuSK+ve by RIA and (3) both AChR-ve and MuSK-ve, each of which was analysed for the presence of the autoantibodies targeting AGRN, COLQ and LRP4 (Table 7.1. and Figure 7.5.).

Table.7.1. The prevalence of the antibodies targeting AGRN, COLQ and LRP4 in AChR+ve, MuSK+ve and both AChR-ve and MuSK-ve MG patients

	AGRN	COLQ	LRP4	AGRN + COLQ	AGRN + LRP4	COLQ + LRP4	N/K	total
AChR+ve	13	0	1	0	0	0	42	56
MuSK+ve	0	2	6	0	0	0	24	32
AChR-ve and MuSK-ve	11	6	6	0	1	1	69	94
								182

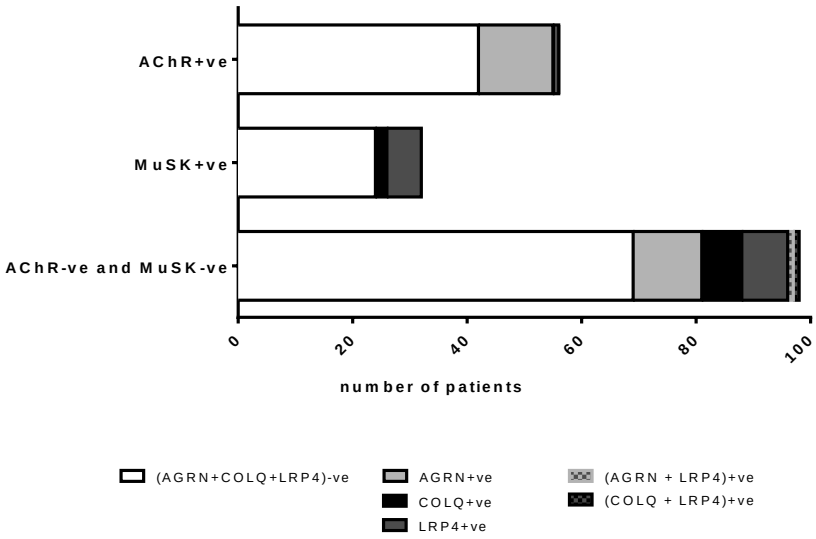

Fig.7.5. The prevalence of the antibodies targeting AGRN, COLQ and LRP4 in AChR+ve, MuSK+ve and both AChR-ve and MuSK-ve MG patients
Each bar represents a number of analysed cases subdivided into subclasses positive for the antibodies against the analysed targets.

Among the 56 AChR+ve patients analysed, 14 possessed antibodies to additional targets: 13 anti-AGRN and one anti-LRP4, but none had anti-COLQ. By contrast, in the group of 32 MuSK+ve patients, 2 were also COLQ+ve and 6 LRP4+ve, but none

had anti-AGRN antibodies. Thus there was a lower prevalence of anti-COLQ antibodies among AChR+ve (0.00%) when compared to MuSK+ve (6.25%) patients. The largest subgroup comprised 94 sera from individuals without detectable anti-AChR or anti-MuSK antibodies by RIA. After screening, target biding was detected in 25 patients. 11 were found to be AGRN+ve (11.70%), 6 COLQ+ve (6.38%), 6 LRP4+ve (6.38%), one was both AGRN+ve and LRP4+ve (1.06%) and one both COLQ+ve and LRP4+ve (1.06%). The antibody targets remained unknown in 69 out of 94 AChR-ve and MuSK-ve samples (73.42%).

The COLQ CBA scores were assigned to the analysed sera (Figure 7.6.).

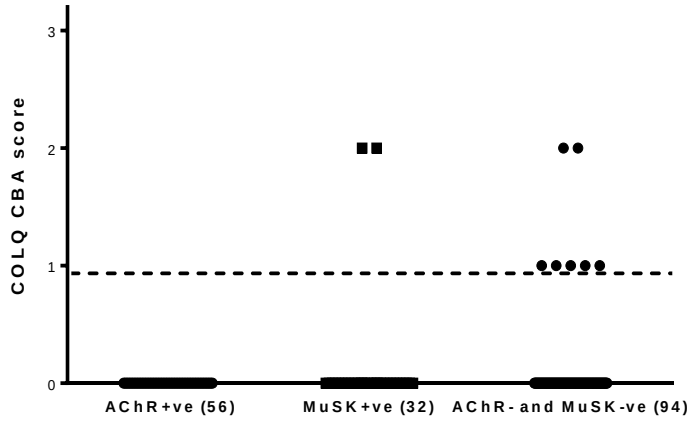

Fig.7.6. COLQ CBA scores in the first cohort of serum samples
The dot plot presents the scores, reflecting the intensity of the fluorescence corresponding to the titre of anti-COLQ antibodies in patient sera. The numbers in brackets indicate the number of individuals in a particular subgroup. The dashed line indicates the threshold of the CBA (score≥1).

A score=2 was assigned to 2 out of 32 MuSK+ve (6.25%) and 2 out of 94 both AChR-ve and MuSK-ve (2.13%) samples, and score=1 to 5 out of 94 both AChR-ve and MuSK-ve (5.32%) patient sera.

Some clinical data, such as ethnic origin, gender, age, Myasthenia Gravis Foundation of America Clinical Classification (MGFACC) score and treatment details, were available for 6 out of the 9 COLQ+ve patients (Table 7.2.).

Table.7.2. Clinical data of COLQ+ve patients from the first cohort
F/M – female/male; MGFACC – Myasthenia Gravis Foundation of America Clinical Classification score; N/K – not known; RIA-radioimmunoprecipitation assay

	country	ethnic origin	gender	age	MGFACC at clinic	MGFACC max	MGFACC final	treatment	other autoantibodies	COLQ CBA score
1	Maryland	AfroCarribean	F			IIIa	IIa	prednisolone azathioprine	MuSK (RIA 5574)	2
2	Holland	Caucasian/NL	F		I	IIIb			MuSK (RIA 2643)	2
3	Cyprus								N/K	1
4	Maryland								N/K	2
5	Maryland	AfroCarribean	F	65		IIa	IIa	methotrexate prednisolone	N/K	2
6	Maryland								AGRN (CBA score 1.5)	1
7	Holland	Caucasian/NL	F	22	I	V			N/K	1
8	Japan		F	6	I			steroids	LRP4 (CBA score 1.0)	1
9	Norway		F	7	II	II	II	pyridostigmine	N/K	1

All the patients were females, despite the equal numbers of males and females in the analysed cohort. Three of them presented in clinic at the relatively early ages of 6, 7 and 22 (average in the cohort=39.9). The severity of the disease was scored using the MGFACC score, which is commonly used for the general assessment of severity of MG. The score ranges from I-V, where I indicates the weakness of ocular muscles only, II – mild weakness, III – moderate weakness, IV – severe weakness, V – intubation. The subclass *a* points towards weakness predominantly affecting limb or axial muscles, while the subclass *b* indicates predominant involvement of oropharyngeal or respiratory muscles. Most of the patients were on immunosuppressive medication, such as azathioprine, methotrexate, prednisolone and steroids. One was also treated with AChE inhibitor (pyridostigmine), but based on the MGFACC score, no improvement was observed in that patient. However, the results of the study need to be interpreted with caution due to the small number of COLQ+ve patients and the lack of a detailed clinical picture of the disease. No firm conclusions can be drawn about age, ethnicity, gender, disease severity and the treatment response in the COLQ+ve individuals compared to other MG patients. A crucial aspect to be analysed in the COLQ+ve group would be the response of the patients to AChE inhibitors, such as pyridostigmine, but details about the treatment with this drug were not available.

The second cohort comprised 236 serum samples collected from MG patients in Glasgow, Oxford and Portugal. Many of the samples were archived in other countries and send to Oxford only for analysis. All samples were screened for the presence of anti-COLQ, anti-AGRN, anti-AChR and anti-MuSK antibodies (Table 7.3. and Figure 7.7.).

Table.7.3. The prevalence of the anti-COLQ autoantibodies in serum samples collected in Glasgow, Oxford and Portugal
The samples were screened for anti-COLQ, anti-AGRN, anti-AChR and anti-MuSK antibodies.

	COLQ	COLQ + AChR	COLQ + MuSK	COLQ + AGRN	N/K	total
Glasgow, Oxford, Portugal	8	5	1	1	221	236

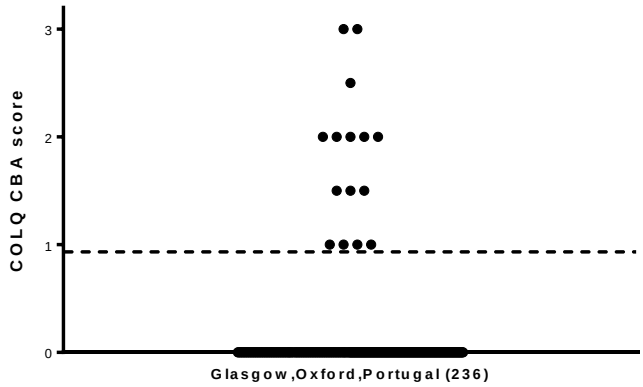

Fig.7.7. COLQ CBA scores in the cohort of serum samples collected in Oxford, Glasgow and Portugal
The dot plot presents the scores, reflecting the intensity of the fluorescence corresponding to the titre of anti-COLQ antibodies. The number in brackets indicates the number of individuals in the group. The dashed line indicates the threshold of the CBA (score≥1).

15 out of 236 (6.35%) sera were found to be COLQ+ve. Five of them were additionally AChR+ve, one MuSK+ve and one AGRN+ve. The CBA scores assigned to the COLQ+ve samples ranged from 1 to 3, with the highest number of samples being assigned a score=2.

A partial disease history was available for the COLQ+ve individuals (Table 7.4.).

Table.7.4. Clinical data of COLQ+ve patients from the second cohort
Abn – abnormal; F/M – female\male; ND – not diagnosed; N/K – not known; SFEMG – single fibre electromyography

	country	gender	onset age	form of MG	decrement	SFEMG	response to AChE	response to steroids	outcome	other autoantibodies	COLQ CBA score
1	UK	F	15	generalised (oculobulbar)	normal	Abn	yes	yes	stable	N/K	3
2	Germany	F	38	ocular	normal	ND	yes	ND	mild symptoms	N/K	1
3	UK	F	23	ocular	normal	Abn	poor	yes	mild symptoms	clustered AChR	2
4	UK	F	6	generalised (limbs, trunk)	decrement	ND	poor	ND	progressively worse	N/K	1
5	UK	M								N/K	2.5
6	UK	F	6	generalised	normal	Abn	yes	yes	better	N/K	1.5
7	UK	F	45	generalised	normal	Abn	poor	yes	better	MuSK	1.5
8	UK	F	23	generalised	normal	Abn	poor	ND	stable	N/K	3
9	Israel	F	33	generalised	decrement	ND	poor	ND	unchanged	clustered AChR	2
10	Portugal	F	31	ocular	normal	Abn	yes	ND	remission	clustered AChR	2
11	Portugal	F	20	generalised	decrement	ND	yes	yes	mild symptoms	AChR	2
12	Portugal	F	39	ocular	decrement	ND	yes	yes	mild symptoms	clustered AChR	2
13	UK	F	25	generalised	normal	normal	yes	ND	stable	N/K	1
14	UK	F								N/K	1.5
15	UK	M	60	ocular	normal	normal	ND	ND	stable	AGRN	1

The collected data were similar to the previous findings, with a high prevalence of the anti-COLQ antibodies among females compared to males. Similar to the previous cohort, anti-COLQ antibodies were present relatively frequently in young-onset MG patients, with seven of the individuals developing the disease under the age of 30. Finally, as in the previous study, some patients responded to anti-AChE medication, which is surprising.

In addition to the MG serum samples, 21 epilepsy patients (disease controls) and 23 healthy individuals were screened for the presence of anti-COLQ autoantibodies (Figure 7.8.).

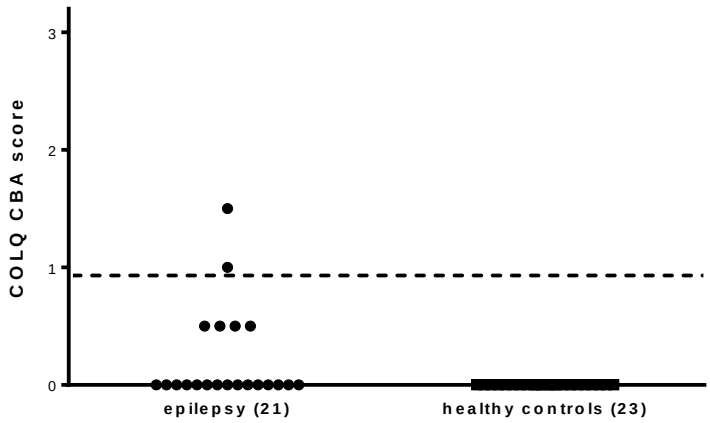

Fig.7.8. COLQ CBA scores in the cohort of epilepsy patients and healthy individuals
The dot plot presents the scores, reflecting the intensity of the fluorescence corresponding to the titre of anti-COLQ antibodies. The numbers in brackets indicate the number of individuals in a particular subgroup. The dashed line indicates the threshold of the CBA (score≥1).

2 out of 21 patients from the epilepsy group (9.52%) and none of the healthy controls were found to be COLQ+ve. Although the percentage may appear relatively high, the number of the available control samples was very limited and therefore no firm conclusions should be made based on these findings. However, the results could suggest the assay is not absolutely specific or that the anti-COLQ antibodies are not pathogenic. There were insufficient amounts of serum samples from COLQ+ve epilepsy-affected individuals to investigate COLQ binding in these sera any further.

7.4. Case study of COLQ+ve patient

One case (number 1 in Table 7.4.), chosen because a number of serum samples could be taken during subsequent visits in clinic, was studied in detail (Figure 7.9.). The patient was a 40-year-old female who presented with a severe muscle weakness, which was likely to be due to the presence of autoantibodies, but their target remained unknown. She appeared not to respond well to any standard therapeutic approaches.

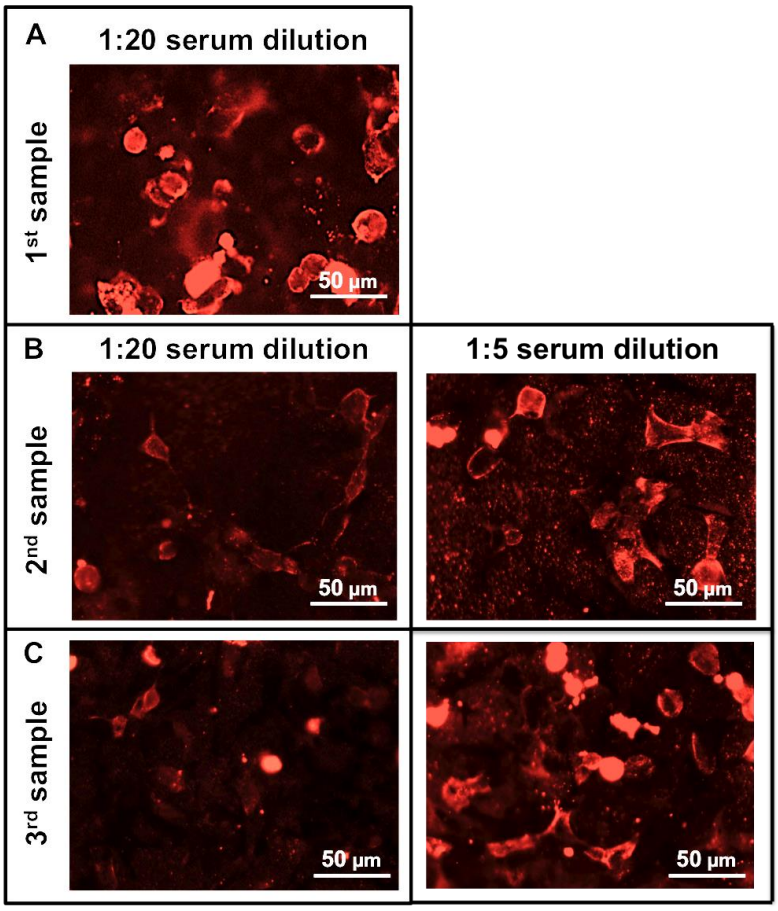

Fig.7.9. Analysis of three serum samples from COLQ+ve patient taken during subsequent visits in clinic
Three subsequent serum samples were tested for the presence of anti-COLQ antibodies. HEK293TSA cells were transfected with the construct encoding COLQ-CASPR2TM and incubated with a respective serum sample. Primary antibodies bound to the cell surface were detected with an Alexa Fluor 568 anti-human IgG secondary antibody.

The CBA performed on the serum sample taken during the first visit showed a high level of anti-COLQ binding (score=3, 3, 2 in repeated independent experiments). The patient was prescribed high doses of immunosuppressive drugs, which resulted in a

notable improvement in muscle strength and a substantial reduction in the titre of anti-COLQ autoantibodies in the serum (score=0.5 and 0.5 in repeated independent experiments, conducted using standard 1:20 serum dilution). A third serum sample was collected after 6 months in order to follow the changes in the titres of the anti-COLQ antibodies. The analysis of this sample showed that the anti-COLQ immunoglobulins remained at very low levels (score=0.5, 0.5 in repeated independent experiments conducted using standard 1:20 serum dilution).

The 0.5 score might indicate the presence of low levels of the anti-COLQ antibodies in the serum or could be potentially non-specific. To reinvestigate this, the assay was repeated at four times higher serum concentrations (1:5). Red fluorescence corresponding to anti-COLQ autoantibodies was detected at the cell surface in HEK293TSA cells over-expressing the target protein (score=2, 2 for both samples in repeated independent experiments), but not in mock-transfected cells. Such a result confirms the presence of low levels of antibodies targeting COLQ in these samples. It remains uncertain whether they underlie a myasthenic weakness and whether they are specific to COLQ, and do not cross-react with other collagens, which are common antigens in arthritis (Rowley et al., 2008).

For the third sample a detailed description of the clinical symptoms of the patient was available. On the day she was seen in clinic, the patient showed relatively mild symptoms of disease. She reported bulbar symptoms and general tiredness. On examination, she had a full range of eye movements, a fatiguable weakness of the uvula, tongue, lip and neck flexion, but no weakness of limb muscles. The treatment was anticholinesterase medication and immunosuppression.

7.5. Titration of the COLQ+ve sera

Four samples, which were found to be positive for the presence of anti-COLQ antibodies and where sufficient serum was available, were titrated to investigate specificity of the binding. HEK293TSA cells transfected with COLQ-CASPR2TM-encoding plasmid were incubated with sera diluted 1:20, 1:50, 1:100, 1:200 and 1:500, respectively, and an Alexa Fluor 568 anti-human IgG secondary antibody (Figure 7.10.). CBA scores, corresponding to the staining intensity, were assigned and plotted on the graph (Figure 7.11.).

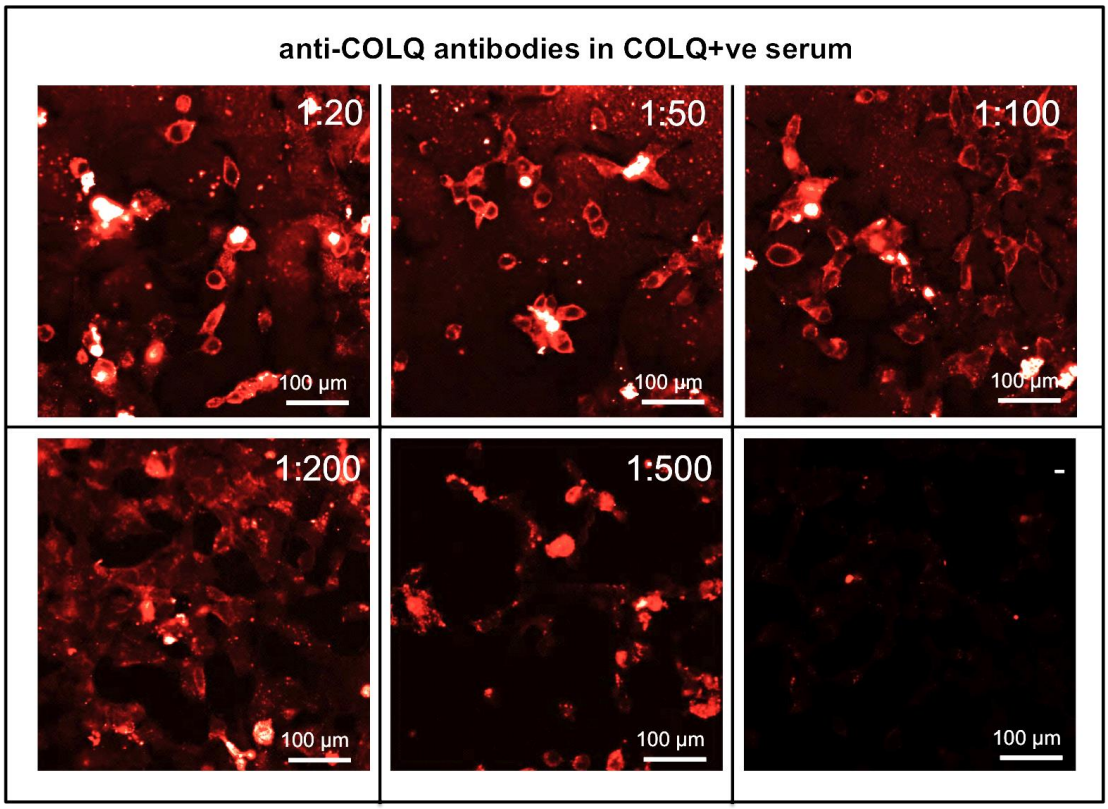

Fig.7.10. Fluorescence images of the titration of a COLQ+ve serum
HEK293TSA cells were transfected with pcDNA-*COLQ-CASPR2TM* vector, stained with patient serum, diluted 1:20, 1:50, 1:100, 1:200 and 1:500, which contained anti-COLQ antibodies, and an Alexa Fluor 568 anti-human IgG secondary antibody. The panel shows example staining.

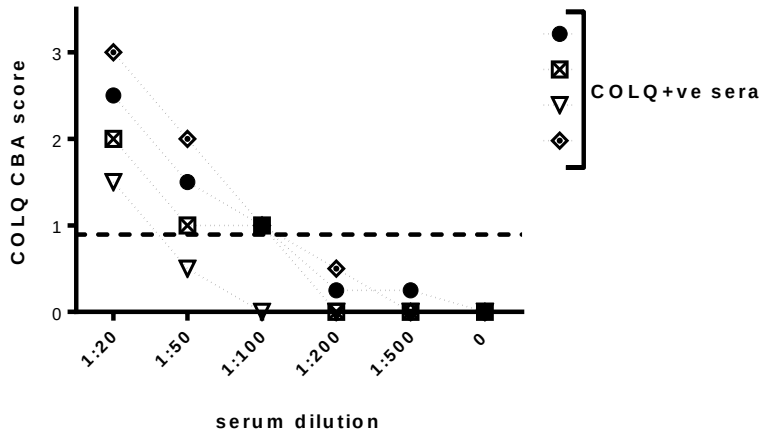

Fig.7.11. Titration of COLQ+ve sera
HEK293TSA cells were transfected with pcDNA-*COLQ-CASPR2TM* vector, stained with COLQ+ve sera diluted 1:20, 1:50, 1:100, 1:200, and 1:500, and an Alexa Fluor 568 anti-human IgG secondary antibody. The intensity of the fluorescence was visually assessed and scored (0-3). The assigned values were plotted on the graph. Different symbols represent serum samples from different individuals. The dashed line indicates the threshold of the CBA (score≥1).

The intensity of fluorescence signal, corresponding to the levels of the immunoglobulins bound to the cell surface, was reduced in all samples tested with higher serum dilutions. This favours specificity of the COLQ binding.

7.6. Binding of COLQ+ve sera to the neuromuscular junctions

To investigate whether anti-COLQ sera also bind to the COLQ expressed at the NMJ, wild type mouse muscle sections were stained with COLQ+ve or healthy control sera diluted 1:500, and an Alexa Fluor 568 anti-human IgG secondary antibody. Endplates were labelled with Alexa Fluor 488 fasciculin and the slides were analysed by confocal fluorescence microscopy (Figure 7.12.).

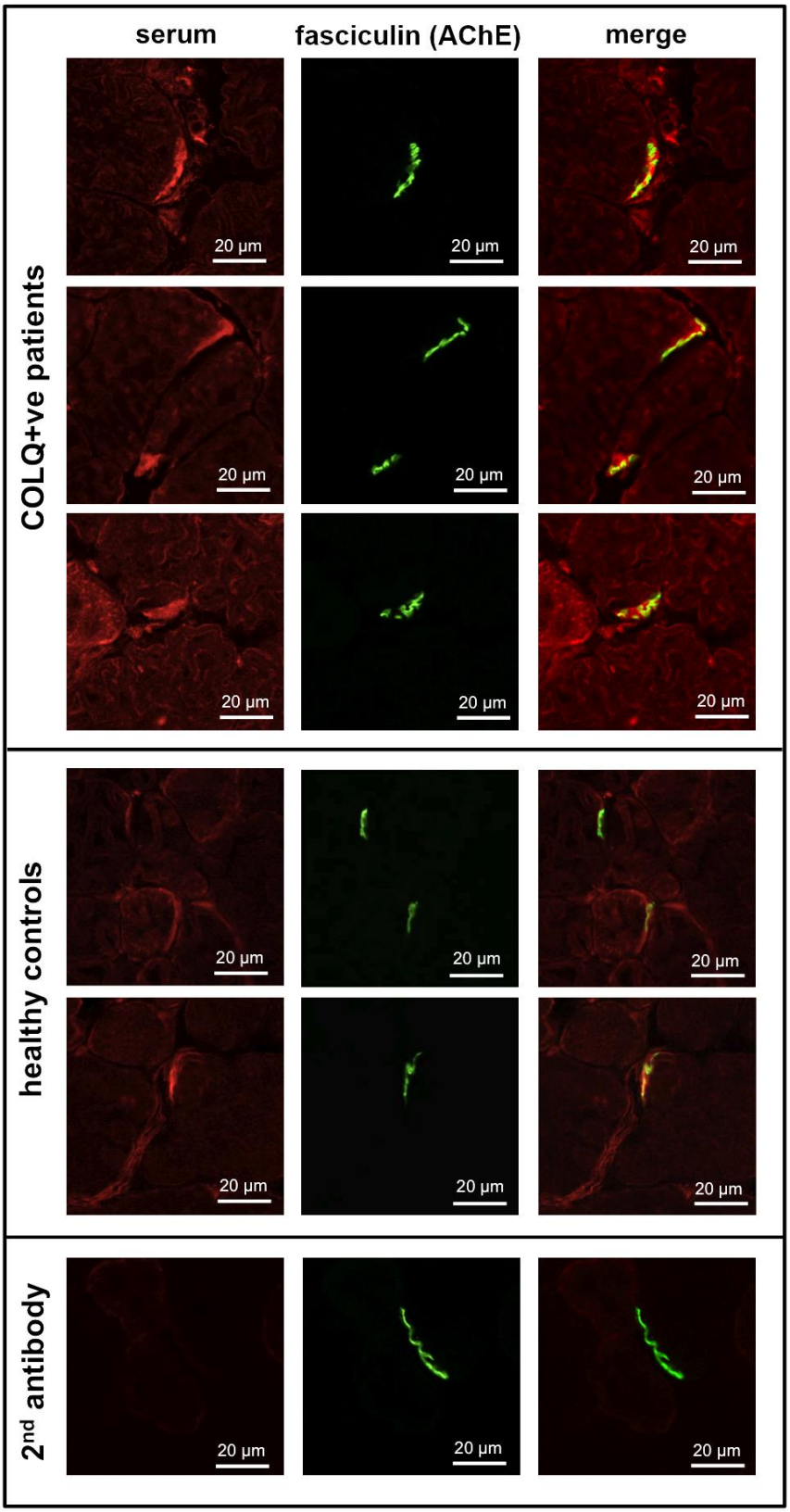

Fig.7.12. Labelling of the NMJ on mouse muscle sections with COLQ+ve and healthy control serum samples

Wild type mouse muscle sections were labelled with COLQ+ve and healthy control sera, and an Alexa Fluor 568 anti-human IgG secondary antibody. Neuromuscular endplates were stained with Alexa Fluor 488 fasciculin. The stained tissue sections were analysed by confocal fluorescence microscopy. The panel shows example staining.

Increased fluorescence signal at the NMJ was observed when the tissue was incubated with the COLQ+ve sera. However, healthy control sera were also found to stain some of the NMJ on muscle sections. This might be due to the high levels of membrane folding occurring at the endplate, causing a misleading increase in the fluorescence signal, irrespective of the primary antibody.

7.7. Preadsorption of anti-COLQ autoantibodies from COLQ+ve sera

To determine further the specificity of COLQ binding detected in MG sera, the samples were preadsorbed against COLQ. The sera were incubated for one hour with HEK293TSA cells transfected with COLQ-CASPR2TM-encoding vector. The process was repeated 6 times to ensure an effective preadsorption of the anti-COLQ antibodies. As a control, the sera were incubated with HEK293TSA cells over-expressing MuSK at their surface. The samples were then applied in CBA using HEK293TSA cells transfected with the COLQ-CASPR2TM-encoding plasmid (Figure 7.13.).

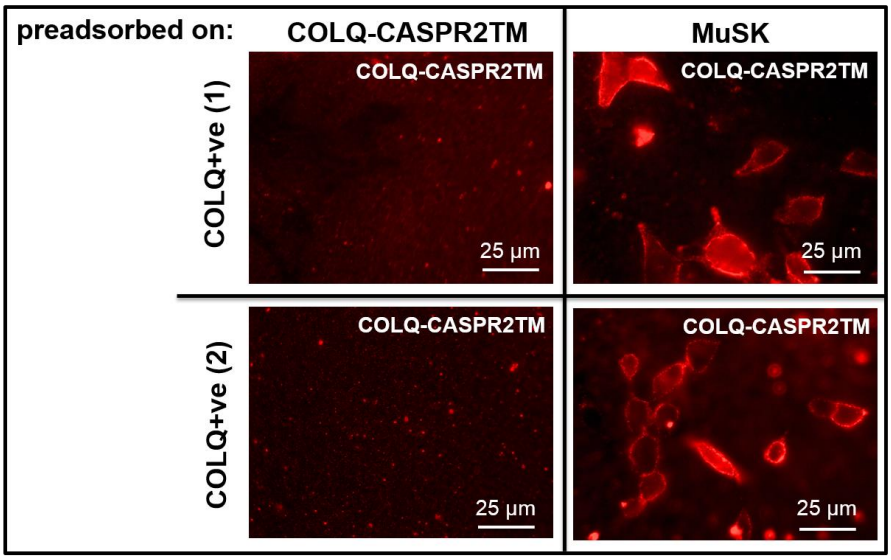

Fig.7.13. Preadsorption of anti-COLQ antibodies from COLQ+ve sera
HEK293TSA cells were transfected with COLQ-CASPR2TM-encoding plasmid and immunolabelled with two different COLQ+ve serum samples (1 and 2) preadsorbed against COLQ-CASPR2TM or MuSK, respectively. The human antibodies bound to the cell surface were detected using an Alexa Fluor 568 anti-human IgG secondary antibody.

Bright red fluorescence signal, corresponding to the human antibodies bound to the cell surface, was only observed at the surface of the cells labelled with samples preadsorbed against MuSK. This indicated that the incubation of the sera with the cells over-expressing COLQ-CASPR2TM resulted in the removal of the COLQ binding, and thus provided additional evidence for a specific binding of the sera to COLQ-CASPR2TM over-expressing cells.

The preadsorbed sera were also applied in the staining of mouse tibialis anterior muscle sections. The sections were incubated with COLQ+ve and healthy control serum samples preadsorbed against MuSK or COLQ-CASPR2TM, respectively. Binding of human antibodies to the tissue was detected using an Alexa Fluor 568 anti-human IgG secondary antibody. Neuromuscular endplates were stained with Alexa Fluor 488 fasciculin and the slides were analysed by confocal fluorescence microscopy (Figure 7.14.).

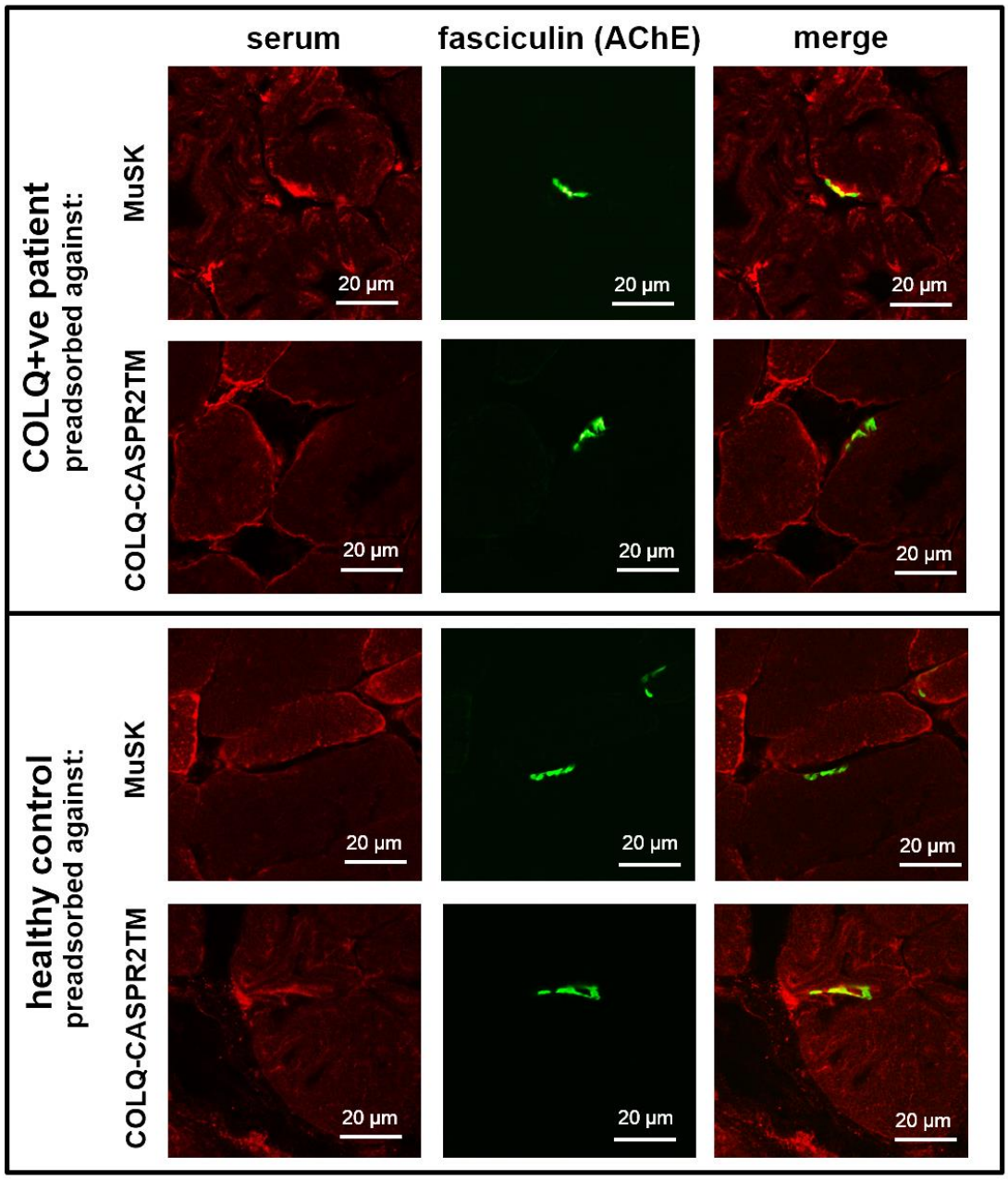

Fig.7.14. Labelling of the NMJ with COLQ+ve and healthy control sera preadsorbed against MuSK or COLQ-CASPR2TM, respectively
Mouse tibialis anterior muscle sections were labelled with COLQ+ve and healthy control serum samples preadsorbed against MuSK and COLQ-CASPR2TM, respectively. The binding of the antibodies was detected with an Alexa Fluor 568 anti-human IgG secondary antibody. Neuromuscular endplates were labelled using Alexa Fluor 488 fasciculin. The slides were analysed by confocal microscopy. The panel shows example staining.

When COLQ+ve sera preadsorbed against MuSK were applied, bright red fluorescence, corresponding to human antibodies, co-localised with green fluorescence of labelled AChE at most of the neuromuscular endplates. Preadsorption of the COLQ+ve sera against COLQ-CASPR2TM resulted in a mild reduction of the

red fluorescence at a number of, but not all, synapses. This was not observed in healthy control sera, which labelled some of the NMJ weakly, irrespective of the target used for the preadsorption. The results might suggest a specificity of the anti-COLQ antibodies detected in the serum samples to COLQ expressed at the NMJ. However, the presence of binding of healthy control sera to the synapses, and the lack of reduction in levels of the red fluorescence at some neuromuscular endplates labelled with the COLQ+ve sera preadsorbed against COLQ-CASPR2TM, make the data difficult to interpret.

7.8. Western blotting with COLQ+ve serum samples

To determine whether COLQ+ve samples can also recognise the target antigen on western blots, protein lysates obtained from HEK293TSA cells transfected with Myc-COLQ-CASPR2TM- or COLQ-CASPR2TM-encoding vectors, and pcDNA^{TM}3.1(+), as a negative control, were resolved on polyacrylamide gels and immunoblotted with the COLQ+ve serum samples. Immunoblotting with an anti-Myc antibody was also performed as a control for an efficient expression of the target protein (Figure 7.15.).

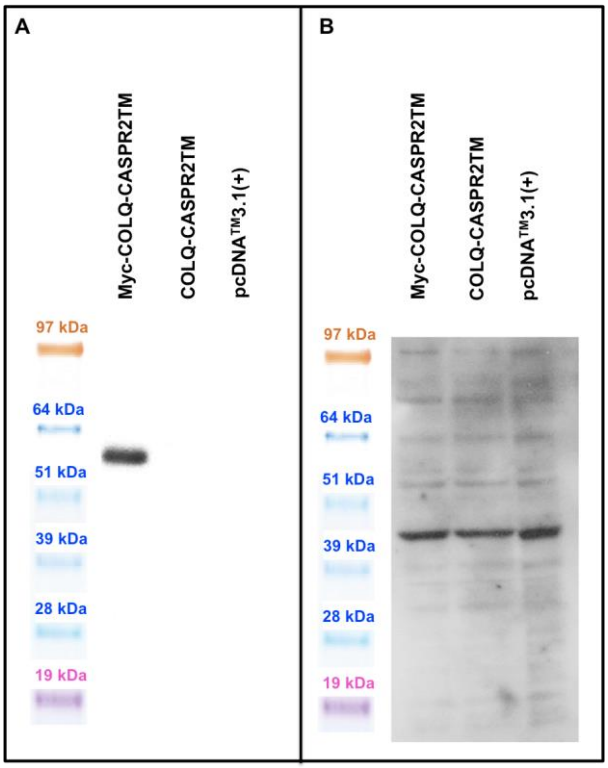

Fig.7.15. Western blotting with COLQ+ve serum
Protein lysates obtained from HEK293TSA transfected with Myc-COLQ-CASPR2TM- or COLQ-CASPR2TM-encoding vectors, or pcDNA™3.1(+) were immunoblotted with (A) an anti-Myc antibody or (B) a COLQ+ve serum sample, and the appropriate HRP-conjugated secondary antibodies. An example western blot is shown.

The serum samples did not exhibit specific binding to proteins migrating as 60 kDa molecules, which corresponded to Myc-COLQ-CASPR2TM and COLQ-CASPR2TM. A possible explanation for these observations is that the autoimmunoglobulins present in the COLQ+ve sera recognise only native epitopes.

7.9. Investigations into potential pathogenicity of anti-COLQ autoantibodies

The CBA showed some anti-COLQ binding in the sera obtained from MG patients. However, we have not established whether the antibodies are pathogenic and if so, what the mechanism is that could lead to abnormal neuromuscular transmission.

7.9.1. Interactions between MuSK and COLQ

One possible consequence of the presence of anti-COLQ binding in SNMG patient sera is an impaired MuSK-COLQ interaction (Cartaud et al., 2004).

First, an attempt was made to reproduce evidence of binding between the molecules, as previously described by (Cartaud et al., 2004). Myc-COLQ, which did not possess a TM domain, and MuSK were co-expressed in HEK293TSA cells. The cells were stained with anti-MuSK and anti-Myc antibodies, and the appropriate Alexa Fluor 594 and Alexa Fluor 488 secondary antibodies, respectively. If interaction between the two molecules occurred, then MuSK would anchor Myc-COLQ to the cell surface (Figure 7.16.). As a control, the cells were co-transfected with Myc-COLQ- and LRP4-encoding vectors (Figure 7.17.). The choice of LRP4 was determined by the fact that it is known to interact with MuSK, but is not expected to bind to COLQ (Zhang et al., 2008, Kim et al., 2008).

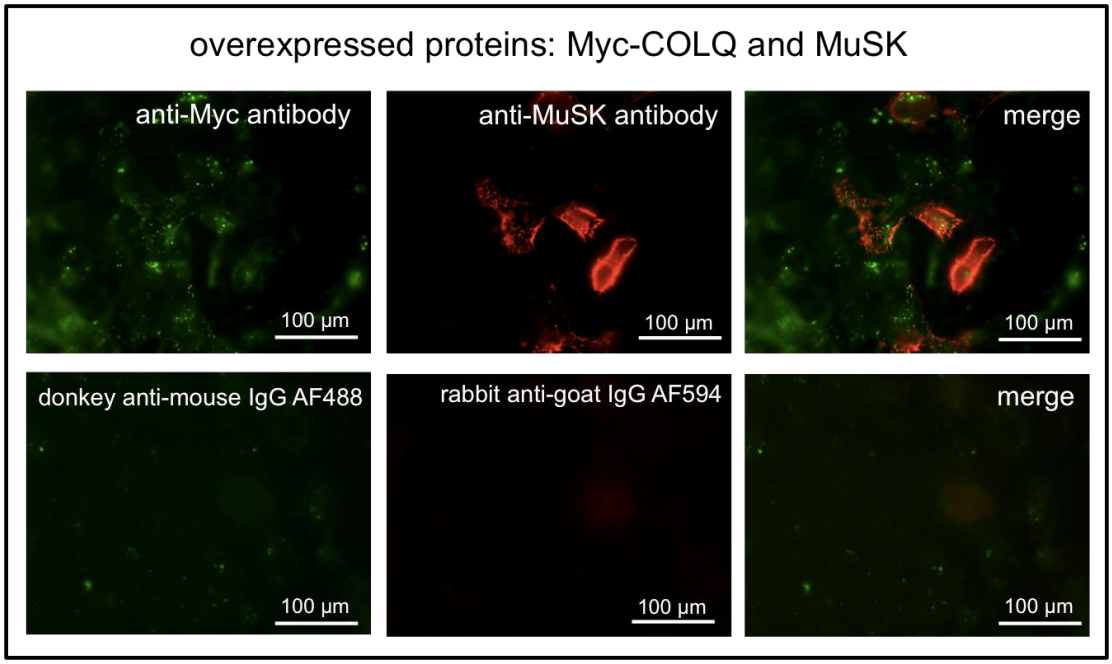

Fig.7.16. Expression of Myc-COLQ and MuSK at the cell surface
HEK293TSA cells were co-transfected with Myc-COLQ- and MuSK-encoding plasmids. The cell surface proteins were immunostained with a mouse monoclonal anti-Myc antibody and a goat polyclonal anti-MuSK antibody, and the appropriate Alexa Fluor 488 and 594 secondary antibodies, respectively. As a negative control, the cells were labelled with the secondary antibodies only.

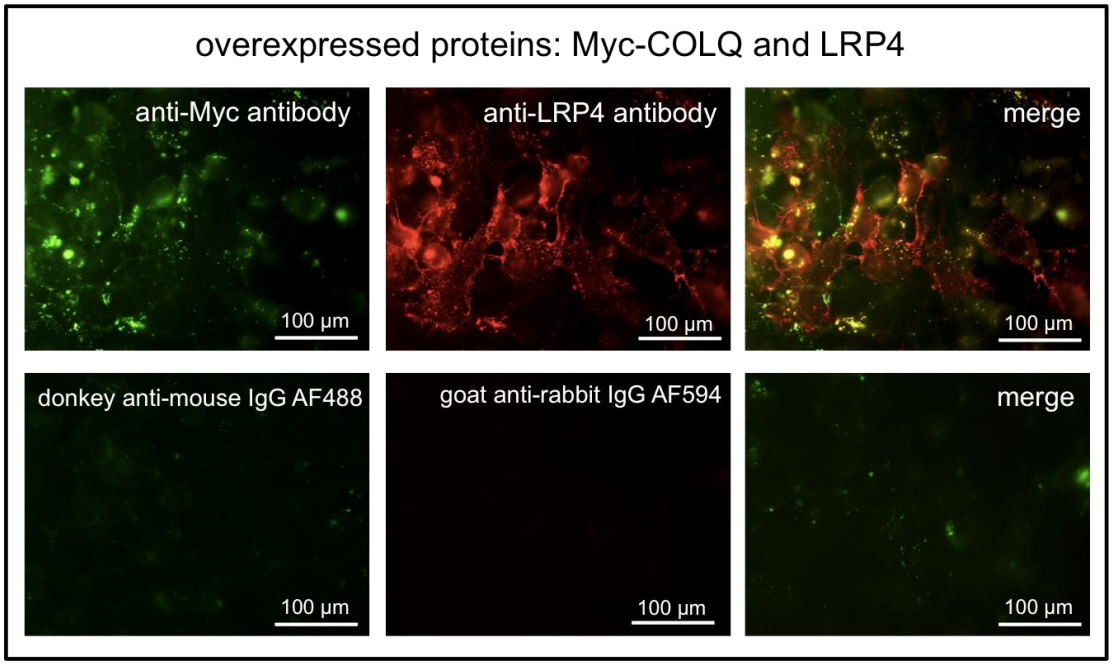

Fig.7.17. Expression of Myc-COLQ and LRP4 at the cell surface
HEK293TSA cells were co-transfected with Myc-COLQ- and LRP4-encoding plasmids. The cell surface proteins were immunostained with a mouse monoclonal anti-Myc antibody and a rabbit polyclonal anti-LRP4 antibody, and the appropriate Alexa Fluor 488 and 594 secondary antibodies, respectively. As a negative control, the cells were labelled with the secondary antibodies only.

Fluorescence microscopy analyses did not show any co-localisation of red fluorescence, corresponding to MuSK or LRP4, and green fluorescence, corresponding to Myc-COLQ. The observations might indicate the lack of influence of either MuSK or LRP4 on the Myc-COLQ cell surface expression.

To look further for interactions between MuSK and COLQ, co-immunoprecipitation experiments were performed. HEK293TSA cells were co-transfected with MuSK- and Myc-COLQ-encoding vectors. The over-expressed MuSK or Myc-COLQ was then immunoprecipitated from the cell surface with anti-MuSK or anti-Myc antibodies. The immunoprecipitates were analysed by western blotting with the antibodies recognising the potential partner molecule (Figure 7.18.).

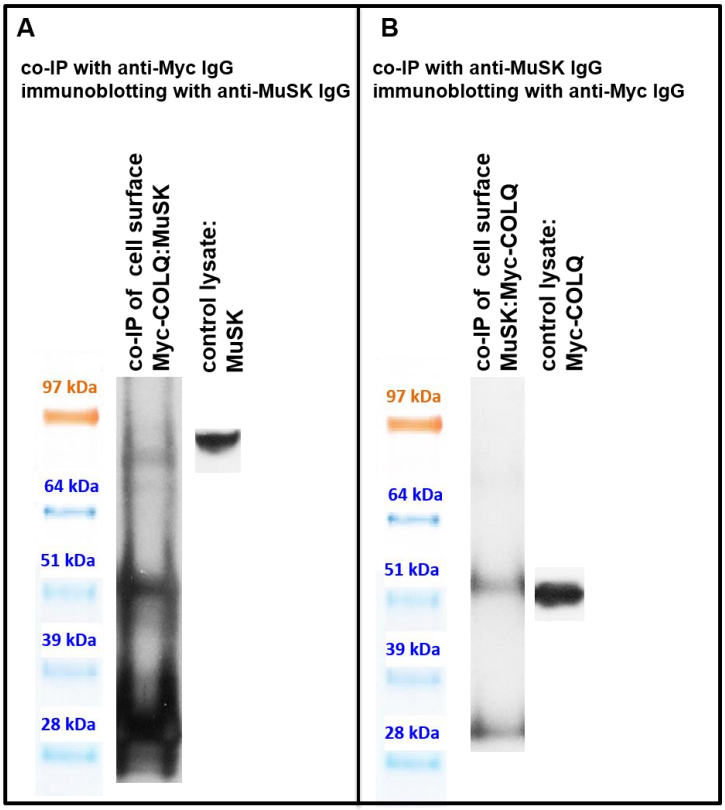

Fig.7.18. Co-immunoprecipitation of Myc-COLQ and MuSK from the surface of HEK293TSA cells

HEK293TSA cells were transfected with plasmids encoding Myc-COLQ and MuSK. (A) Myc-COLQ or (B) MuSK were immunoprecipitated from the cell surface with anti-Myc and anti-MuSK antibodies, respectively. The immunoprecipitates were immunoblotted with (A) anti-MuSK and (B) anti-Myc antibodies, and the appropriate HRP-conjugated secondary antibodies. Whole protein lysates extracted from the cells were also analysed to control for the expression of the target proteins and to serve as molecular weight markers.

When Myc-COLQ was immunoprecipitated from the cell surface using the anti-Myc antibody and the immunoprecipitates were analysed by immunoblotting with the anti-MuSK antibody, no bands were observed migrating at the same level as MuSK over-expressed in HEK293TSA cells. When the approach was reversed, so the cell surface MuSK was immunoprecipitated and the immunoprecipitates were immunoblotted with the anti-Myc IgG, there was a cross-reaction of the secondary antibody used in western blotting with an IgG heavy chain, which migrated at the similar level (50 kDa) as Myc-COLQ. This considerably hindered the analysis. Nevertheless, the data obtained in the co-immunoprecipitation experiments were consistent with fluorescence microscopy imaging and did not indicate any specific interactions between MuSK and Myc-COLQ over-expressed at the surface of HEK293TSA cells.

7.9.2. Do COLQ+ve sera affect the formation of AChR clusters?

Serum samples obtained from MG patients, containing antibodies targeting proteins involved in the formation of AChR clusters, such as MuSK (Hoch et al., 2001) or LRP4 (Pevzner et al., 2012), affect the formation of AChR clusters *in vitro* in C2C12 myotubes. The incubation of the cells with patient sera and the analysis of the formation of the AChR clusters can be used to assess the pathogenicity of antibodies in MG serum samples.

C2C12 myotubes were co-incubated overnight with AGRN and serum samples obtained from two healthy individuals or two COLQ+ve patients, and AChR clusters were visualised using Alexa Fluor 594 α-BuTx. The cells were imaged and the number of clusters per microscopic field (20x) was quantified out of 20 images per condition using a Volocity 4.3.1. software. The number of AChR clusters in the cells not treated

with any serum was considered as 100% (Figure 7.19.).

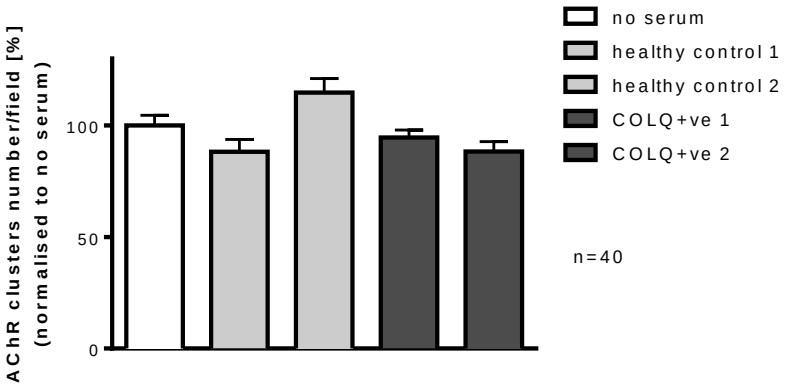

Fig.7.19. Effects of COLQ+ve serum samples on the formation of AChR clusters *in vitro* in C2C12 myotubes
C2C12 myotubes were co-incubated with AGRN and serum samples obtained from two healthy individuals or two COLQ+ve patients, respectively. AChR clusters were labelled with Alexa Fluor 594 α-BuTx. The number of clusters per microscopic field (20x) was quantified out of 20 images per condition using a Volocity 4.3.1. software. Each bar represents the mean±SEM of the number of AChR clusters observed in C2C12 cells co-incubated with AGRN and various serum samples. The presented data are normalised to the number of AChR clusters in the cells incubated with AGRN only.

The analyses showed that in the cells incubated with the sera obtained from two healthy individuals and two COLQ+ve patients: 88.23±5.58%, 114.8±6.29%, 94.65±3.39% and 88.37±4.45%, n=40 AChR clusters were formed compared to untreated cells. This suggests that formation of AChR clusters is not affected by the incubation of the C2C12 cells with the serum samples containing anti-COLQ autoantibodies.

7.10. Discussion

A CBA was developed to detect COLQ binding in patient sera. When the assay was used in the screening of two cohorts of MG patients, it detected the presence of antibodies binding to COLQ in the sera. In a number of cases the autoantibodies were not the only ones present in the samples. Some individuals were found to be AChR, MuSK, LRP4 or AGRN positive in addition. Other targets were not investigated. Despite the detection of the COLQ binding in the sera, it is not clear if the immunoglobulins are disease-specific and whether they play a direct role in impaired neuromuscular transmission. An experimental demonstration of pathogenicity of the antibodies might point to their potential role in the disease mechanism. Several aspects were investigated that could be potentially affected by the antibodies.

One possibility, suggested by Cartaud et al., was impaired formation of the MuSK-COLQ complex (Cartaud et al., 2004). This has been reported as pathogenic in some *COLQ* CMS cases (Nakata et al., 2013) and in MuSK+ve MG patients (Kawakami et al., 2011). Initial experiments aimed to reproduce the results reported by Cartaud et al. that indicated the presence of specific interactions between COLQ and MuSK (Cartaud et al., 2004). We attempted this using two different approaches. The first involved the co-expression of MuSK and Myc-COLQ in HEK293TSA cells, and subsequent fluorescence microscopy analyses of the potential influence of MuSK on levels and localisation of Myc-COLQ at the cell surface. As a control, HEK293TSA cells over-expressing Myc-COLQ and LRP4 were used. The second approach was to co-immunoprecipitate MuSK and Myc-COLQ from the surface of the co-transfected HEK293TSA cells. Neither method showed binding between the molecules, and thus we failed to reproduce the reported results (Cartaud et al., 2004). There are several possible reasons for the discrepancies. Firstly, COLQ tagged N-terminally with green

fluorescent protein (GFP) and MuSK tagged with hemagglutinin (HA) epitope at the N-terminus were used by Cartaud et al. The use of this large GFP tag in COLQ may have impaired the ability of the protein to acquire a correct tertiary structure. The HA epitope at the MuSK N-terminus, which might be involved in the MuSK-COLQ interactions, may have also affected their results. The lack of reproducibility of the MuSK and COLQ binding in our system hindered further investigations.

Another potential pathogenic mechanism analysed was the effect of the COLQ+ve sera on the formation and maintenance of the NMJ. Such a mechanism may underlie myasthenic weakness in a number of MuSK+ve (Hoch et al., 2001) and LRP4+ve (Pevzner et al., 2012) MG cases. Analysis of the formation of AChR clusters in C2C12 myotubes *in vitro* did not indicate any impairment of the process. This accords with our previous results, where no interactions between MuSK and COLQ were detected. If such interactions are indeed present, then potentially anti-COLQ sera could impair the formation of AChR clusters in the same way as MuSK+ve sera. However, the results may also suggest lack of pathogenicity for anti-COLQ antibodies.

Indirect evidence for the potential pathogenicity of antibodies detected in some myasthenic patients could also be provided by a comprehensive analysis of the clinical data of COLQ+ve cases. This was hindered by the lack of sufficient clinical details for many of the patients. COLQ+ve patients may share many clinical features with AChE deficiency (*COLQ*) CMS-affected individuals (Donger et al., 1998, Mihaylova et al., 2008, Ohno et al., 1998, Wargon et al., 2012). A proposed mechanism for this type of CMS is impaired formation of AChE-COLQ complexes or disrupted attachment to the cell surface at the NMJ. Since the complexes are formed intracellularly in the Golgi apparatus and then transported to the cell surface (Rotundo, 1984), it is unlikely that the COLQ+ve sera affect this process, but it is possible that they disrupt attachment

and concentration of asymmetric AChE complexes at the synapse (Rotundo et al., 2005, Ohno et al., 2000), and so potentially reduce the amounts of AChE in this region. This would lead to a prolonged exposure to the neurotransmitter – acetylcholine (ACh) – in the synaptic cleft, increased duration of endplate currents and an increased ion flux, resulting in an endplate myopathy and compromised neuromuscular transmission (Muller et al., 2007). The endplate myopathy would be apparent in the histological examination of patient muscle biopsies. Prolonged exposure to ACh might also manifest itself during the neurophysiological studies of endplate currents in the patients by way of a double response to a single stimulus for the compound muscle action potential (CMAP) (Mihaylova et al., 2008).

Another important clinical aspect worth analysing would be the treatment response of the COLQ+ve patients. Patients would not be expected to present a prolonged beneficial response to AChE inhibitors, such as pyridostigmine. Symptoms might even become worse (Mihaylova et al., 2008). A short-lasting response would not exclude a possible role of anti-COLQ antibodies in the disease process since this also occurs sometimes in the AChE deficiency CMS (Mihaylova et al., 2008).

Another interesting feature is the slow pupillary response to light, which is observed more frequently in *COLQ* CMS patients compared to those with other forms of the disease (Mihaylova et al., 2008). However, there was insufficient clinical data available to draw any conclusions on pupillary reaction.

Finally, since antibodies targeting collagen type II have been reported to be one of the underlying mechanisms of arthritis (Rowley et al., 2008, Strollo et al., 2013), it would be important to see if this was not a possible co-existing disease in the patients, and thus eliminate a potential for cross-reactivity.

The number of clinical features that might indicate a disease modifying mechanism of

anti-COLQ antibodies points to the vital importance of a detailed clinical history from the patients. Our current efforts are directed towards that. Greater volumes of COLQ+ve plasma or serum samples would also facilitate passive transfer experiments and the studies of the induced symptoms, and of the endplate structures.

In summary, the presented research resulted in the development of a diagnostic assay for the anti-COLQ antibodies in serum samples and the detection of COLQ binding in cohorts of MG patients. The novel, although relatively rare, antibodies targeting COLQ, even if not pathogenic on their own, have the potential to influence clinical presentation and modify the response to treatment in patients and thus warrant further investigation.

Chapter 8

Discussion

8.1. A novel group of congenital myasthenic syndromes

A new group of congenital myasthenic syndromes (CMS) has recently been identified due to mutations in a number of genes encoding proteins involved in glycosylation processes (Belaya et al., 2012, Cossins et al., 2013a, Senderek et al., 2011). The first enzyme from this group was L-glutamine:D-fructose-6-phosphate amidotransferase 1 (GFAT1), but the role of the protein in the CMS pathology was not explained. The finding that the mutations in *GFPT1* result in reduced levels or diminished catalytic activity of the enzyme, which consequently lead to a substantial decrease in cell surface expression of acetylcholine receptor (AChR) in muscle cells, provides a major insight into these myasthenic disorders. It suggests a pathogenic mechanism for the group of CMS caused by glycosylation defects and indicates particular importance of glycosylation for the stable expression of AChR α, δ and ε subunits. This should provide a rational basis for treatment of patients, and point towards additional novel candidate proteins, which when mutated may lead to myasthenic weakness. The next step should be identifying patients, who present similar phenotypes to the *GFPT1* CMS-affected individuals, but who do not harbour mutations in any of the known CMS causative glycosylation genes, and then sequencing their genomes or exomes for the presence of pathogenic variants using next generation sequencing (NGS) platforms.

Both whole genome and whole exome sequencing (WGS and WES) are well-justified, cost- and time-effective strategies for discovering rare alleles underlying Mendelian and complex phenotypes, but they still present several challenges. A key challenge

remains the identification of the causal alleles among a large amount of data. This can be facilitated by filtering the data against a set of polymorphisms available in public databases, such as dbSNP and 1000 Genomes Project, and by further stratifying the candidates on the basis of their predicted deleteriousness. However, the use of the bioinformatics prediction tools is limited since approximately 2.3% of the identified changes in each genome are predicted to impair the structure or function of the proteins according to the prediction software (Tennessen et al., 2012). A better approach is to select candidate alleles based on information about function of encoded proteins and their roles in the molecular pathways that are already associated with similar phenotypes (Bamshad et al., 2011, Marian, 2012). This additionally emphasizes the importance of the presented findings for future identification of novel pathogenic variants in CMS and the development of more effective treatments.

8.2. Novel therapeutic approaches for congenital myasthenic syndrome and myasthenia gravis

Current practice for CMS-affected individuals aims to tailor the treatment to the patient. In some cases this can be best achieved by combining therapies that act in different ways on the neuromuscular synapse. The presented research tested novel therapeutic approach in an animal model of AChR deficiency. The treatment focused on the combined administration of pyridostigmine bromide and salbutamol sulphate. The *in vivo* trials in the AChR deficiency CMS mouse model indicated that the combination of the medicines significantly improved muscle strength in the affected animals. This beneficial effect might be explained by opposing influences (destabilising vs. stabilising) of the two drugs on the AChR clusters at the NMJ. This

has yet to be confirmed fully by experiment, and therefore warrants further investigations.

These studies might be greatly facilitated by the ability to generate patient derived induced pluripotent stem cells (iPSCs) and the capacity to differentiate these into disease relevant cell types, including motor neurons and muscle cells, which are of a particular importance for the design of the tailored treatments for CMS-affected individuals (Salani et al., 2012, Umbach et al., 2012, Lopez-Gonzalez and Velasco, 2012). IPSC technology may enable recapitulating the disease phenotype *in vitro,* serve as a platform for drug discovery and potentially reduce the staggeringly high attrition rate of the compounds reaching clinical trials (Ellis and Bhatia, 2011, Grskovic et al., 2011). The failure in the clinical tests is usually caused by the inefficacy or the unanticipated toxicity of the medicines and might be attributed to the fact that genetically inbred animal models or highly contrived cell lines, often used in the preclinical research, do not faithfully replicate human diseases.

IPSCs have several advantages over the aforementioned approaches. First and foremost, they carry the precise constellation of genetic variants in a given individual, allowing the influence of genetic background to be explored and enabling broader evaluation of the use of potential therapeutics for a particular patient. Secondly, the skin biopsies, which may serve as a fibroblast source for iPSCs generation, are relatively easy to obtain and iPSCs can be expanded and differentiated into a number of cell types, including those affected by a disease process and those most commonly affected by drug side effects (cardiac myocytes and hepatocytes) (Rubin and Haston, 2011). Thirdly, iPSCs enable inter species differences between humans and rodents, which are most commonly used as disease models, to be overcome. Finally, the iPSC strategy avoids ethical issues of using animals for drug testing. Recent reports of the

formation of a functional NMJ *in vitro* using iPSCs offer a potential for the application of the system for the drug screening for myasthenic disorders (Umbach et al., 2012, Thomson et al., 2012).

Despite the great promise shown by the iPSC technology, there are still several challenges to be overcome before it can be routinely used for the design of the tailored therapies (Ellis and Bhatia, 2011). This may suggest that the current approaches should combine both, standard strategies, using established cell lines and animal models, as well as patient derived iPSCs differentiated into disease-relevant cell types.

Another scientific advancement, which may facilitate understanding of the disease mechanisms and the drug discovery, is the design of state-of-the-art imaging techniques, such as super resolution microscopy that enables resolution of a few nanometres, while keeping most advantages of standard fluorescence microscopy methods, such as simple sample preparation, molecular-specific labelling and live cell imaging. High resolution structural reconstruction of molecular assemblies is offered by stochastic optical reconstruction microscopy (STORM) and photoactivated localisation microscopy (PALM). The development of these powerful techniques, coupled with rapid improvements in the production of live cell-friendly dye labelling approaches, unlocks the possibility of studying nanoscale structures (Herbert et al., 2012). This may shed new light on the molecular structure and function of the NMJ and provide insight into the pathogenesis of CMS and the mechanisms of action of therapeutic agents in the synaptic region.

8.3. The search for new antibody targets in myasthenia gravis

Another finding emerging from the presented research is identification of anti-collagen Q (COLQ) autoantibodies in a number of seronegative myasthenia

gravis (SNMG) patients. Although the pathogenicity of these antibodies has not been confirmed, they may influence the disease course and treatment response of individuals, and thus should potentially be monitored in myasthenia gravis (MG) patients whose disease is difficult to manage. This will be possible following the development of the sensitive cell-based assay for the detection of the COLQ binding in patient sera. At the same time, studies should continue to determine pathogenicity of the antibodies using *in vivo* model, replicating the human disease by passive transfer of anti-COLQ IgG. It would be interesting to see whether the features of these mice would be similar to those of the already established *Colq*$^{-/-}$ genetic mouse model (Feng et al., 1999), and whether they would also resemble the phenotype of COLQ+ve MG and acetylcholinesterase (AChE) deficiency CMS patients (Wargon et al., 2012).

8.4. Concluding remarks

A great deal is known about the complex structure and function of neuromuscular synapses, but there are still substantial gaps in our knowledge. Recent advances in molecular biology, resulting in the development of novel tools, such as NGS platforms, iPSC technologies and super resolution microscopy, should contribute to filling these gaps, and should eventually lead to more effective treatments for CMS and MG patients.

References

ABDELGANY, A., WOOD, M. & BEESON, D. 2003. Allele-specific silencing of a pathogenic mutant acetylcholine receptor subunit by RNA interference. *Human molecular genetics,* 12**,** 2637-44.

ABICHT, A., DUSL, M., GALLENMULLER, C., GUERGUELTCHEVA, V., SCHARA, U., DELLA MARINA, A., WIBBELER, E., ALMARAS, S., MIHAYLOVA, V., VON DER HAGEN, M., HUEBNER, A., CHAOUCH, A., MULLER, J. S. & LOCHMULLER, H. 2012. Congenital myasthenic syndromes: achievements and limitations of phenotype-guided gene-after-gene sequencing in diagnostic practice: a study of 680 patients. *Human mutation,* 33**,** 1474-84.

ADZHUBEI, I. A., SCHMIDT, S., PESHKIN, L., RAMENSKY, V. E., GERASIMOVA, A., BORK, P., KONDRASHOV, A. S. & SUNYAEV, S. R. 2010. A method and server for predicting damaging missense mutations. *Nature methods,* 7**,** 248-9.

AIHARA, H. & MIYAZAKI, J. 1998. Gene transfer into muscle by electroporation in vivo. *Nature biotechnology,* 16**,** 867-70.

ANTOLIK, C., CATINO, D. H., RESNECK, W. G. & BLOCH, R. J. 2006. The tetratricopeptide repeat domains of rapsyn bind directly to cytoplasmic sequences of the muscle-specific kinase. *Neuroscience,* 141**,** 87-100.

ARMAIZ-PENA, G. N., ALLEN, J. K., CRUZ, A., STONE, R. L., NICK, A. M., LIN, Y. G., HAN, L. Y., MANGALA, L. S., VILLARES, G. J., VIVAS-MEJIA, P., RODRIGUEZ-AGUAYO, C., NAGARAJA, A. S., GHARPURE, K. M., WU, Z., ENGLISH, R. D., SOMAN, K. V., SHAHZAD, M. M., ZIGLER, M., DEAVERS, M. T., ZIEN, A., SOLDATOS, T. G., JACKSON, D. B., WIKTOROWICZ, J. E., TORRES-LUGO, M., YOUNG, T., DE GEEST, K., GALLICK, G. E., BAR-ELI, M., LOPEZ-BERESTEIN, G., COLE, S. W., LOPEZ, G. E., LUTGENDORF, S. K. & SOOD, A. K. 2013. Src activation by beta-adrenoreceptors is a key switch for tumour metastasis. *Nat Commun,* 4**,** 1403.

BAMSHAD, M. J., NG, S. B., BIGHAM, A. W., TABOR, H. K., EMOND, M. J., NICKERSON, D. A. & SHENDURE, J. 2011. Exome sequencing as a tool for Mendelian disease gene discovery. *Nat Rev Genet,* 12**,** 745-55.

BARISIC, N., MULLER, J. S., PAUCIC-KIRINCIC, E., GAZDIK, M., LAH-TOMULIC, K., PERTL, A., SERTIC, J., ZURAK, N., LOCHMULLER, H. & ABICHT, A. 2005. Clinical variability of CMS-EA (congenital myasthenic syndrome with episodic apnea) due to identical CHAT mutations in two infants. *European journal of paediatric neurology : EJPN : official journal of the European Paediatric Neurology Society,* 9**,** 7-12.

BEESON, D., AMAR, M., BERMUDEZ, I., VINCENT, A. & NEWSOM-DAVIS, J. 1996a. Stable functional expression of the adult subtype of human muscle acetylcholine receptor following transfection of the human rhabdomyosarcoma cell line TE671 with cDNA encoding the epsilon subunit. *Neuroscience letters,* 207**,** 57-60.

BEESON, D., HIGUCHI, O., PALACE, J., COSSINS, J., SPEARMAN, H., MAXWELL, S., NEWSOM-DAVIS, J., BURKE, G., FAWCETT, P., MOTOMURA, M., MULLER, J. S., LOCHMULLER, H., SLATER, C., VINCENT, A. & YAMANASHI, Y. 2006. Dok-7 mutations underlie a neuromuscular junction synaptopathy. *Science,* 313**,** 1975-8.

BEESON, D., JACOBSON, L., NEWSOM-DAVIS, J. & VINCENT, A. 1996b. A transfected human muscle cell line expressing the adult subtype of the human muscle acetylcholine receptor for diagnostic assays in myasthenia gravis. *Neurology,* 47**,** 1552-5.

BEESON, D., MORRIS, A., VINCENT, A. & NEWSOM-DAVIS, J. 1990. The human muscle nicotinic acetylcholine receptor alpha-subunit exist as two isoforms: a novel exon. *The EMBO journal,* 9**,** 2101-6.

BELAYA, K., FINLAYSON, S., SLATER, C. R., COSSINS, J., LIU, W. W., MAXWELL, S., MCGOWAN, S. J., MASLAU, S., TWIGG, S. R., WALLS, T. J., PASCUAL PASCUAL, S. I., PALACE, J. & BEESON, D. 2012. Mutations in DPAGT1 cause a limb-girdle congenital myasthenic syndrome with tubular aggregates. *American journal of human genetics,* 91**,** 193-201.

BELTRAN-VALERO DE BERNABE, D., CURRIER, S., STEINBRECHER, A., CELLI, J., VAN BEUSEKOM, E., VAN DER ZWAAG, B., KAYSERILI, H., MERLINI, L., CHITAYAT, D., DOBYNS, W. B., CORMAND, B., LEHESJOKI, A. E., CRUCES, J., VOIT, T., WALSH, C. A., VAN BOKHOVEN, H. & BRUNNER, H. G. 2002. Mutations in the O-mannosyltransferase gene POMT1 give rise to the severe neuronal migration disorder Walker-Warburg syndrome. *American journal of human genetics,* 71**,** 1033-43.

BENOVIC, J. L. 2002. Novel beta2-adrenergic receptor signaling pathways. *J Allergy Clin Immunol,* 110**,** S229-35.

BERGAMIN, E., HALLOCK, P. T., BURDEN, S. J. & HUBBARD, S. R. 2010. The cytoplasmic adaptor protein Dok7 activates the receptor tyrosine kinase MuSK via dimerization. *Molecular cell,* 39**,** 100-9.

BERTOZZI, C. R. & RABUKA, D. 2009. Structural Basis of Glycan Diversity. *In:* VARKI, A., CUMMINGS, R. D., ESKO, J. D., FREEZE, H. H., STANLEY, P., BERTOZZI, C. R., HART, G. W. & ETZLER, M. E. (eds.) *Essentials of Glycobiology.* 2nd ed. Cold Spring Harbor (NY).

BEZAKOVA, G., HELM, J. P., FRANCOLINI, M. & LOMO, T. 2001. Effects of purified recombinant neural and muscle agrin on skeletal muscle fibers in vivo. *The Journal of cell biology,* 153**,** 1441-52.

BEZAKOVA, G. & RUEGG, M. A. 2003. New insights into the roles of agrin. *Nature reviews. Molecular cell biology,* 4**,** 295-308.

BLOOM, J. W., MADANAT, M. S. & RAY, M. K. 1996. Cell line and site specific comparative analysis of the N-linked oligosaccharides on human ICAM-1des454-532 by electrospray ionization mass spectrometry. *Biochemistry,* 35**,** 1856-64.

BLOSSER, J. C. 1983. beta-Adrenergic receptor activation increases acetylcholine receptor number in cultured skeletal muscle myotubes. *Journal of neurochemistry,* 40**,** 1144-9.

BLOUNT, P. & MERLIE, J. P. 1989. Molecular basis of the two nonequivalent ligand binding sites of the muscle nicotinic acetylcholine receptor. *Neuron,* 3**,** 349-57.

BLOUNT, P. & MERLIE, J. P. 1990. Mutational analysis of muscle nicotinic acetylcholine receptor subunit assembly. *The Journal of cell biology,* 111**,** 2613-22.

BLOUNT, P., SMITH, M. M. & MERLIE, J. P. 1990. Assembly intermediates of the mouse muscle nicotinic acetylcholine receptor in stably transfected fibroblasts. *J Cell Biol,* 111**,** 2601-11.

BON, S., AYON, A., LEROY, J. & MASSOULIE, J. 2003. Trimerization domain of the collagen tail of acetylcholinesterase. *Neurochemical research,* 28**,** 523-35.

BON, S., COUSSEN, F. & MASSOULIE, J. 1997. Quaternary associations of acetylcholinesterase. II. The polyproline attachment domain of the collagen tail. *The Journal of biological chemistry,* 272**,** 3016-21.

BON, S., DUFOURCQ, J., LEROY, J., CORNUT, I. & MASSOULIE, J. 2004. The C-terminal t peptide of acetylcholinesterase forms an alpha helix that supports homomeric and heteromeric interactions. *European journal of biochemistry / FEBS,* 271**,** 33-47.

BON, S., VIGNY, M. & MASSOULIE, J. 1979. Asymmetric and globular forms of acetylcholinesterase in mammals and birds. *Proceedings of the National Academy of Sciences of the United States of America,* 76**,** 2546-50.

BORGES, L. S. & FERNS, M. 2001. Agrin-induced phosphorylation of the acetylcholine receptor regulates cytoskeletal anchoring and clustering. *The Journal of cell biology,* 153**,** 1-12.

BORGES, L. S., YECHIKHOV, S., LEE, Y. I., RUDELL, J. B., FRIESE, M. B., BURDEN, S. J. & FERNS, M. J. 2008. Identification of a motif in the acetylcholine receptor beta subunit whose phosphorylation regulates rapsyn association and postsynaptic receptor localization. *The Journal of neuroscience : the official journal of the Society for Neuroscience,* 28**,** 11468-76.

BRENNAN, C. M. & STEITZ, J. A. 2001. HuR and mRNA stability. *Cellular and molecular life sciences : CMLS,* 58**,** 266-77.

BROCKHAUSEN, I., SCHACHTER, H. & STANLEY, P. 2009. O-GalNAc Glycans. *In:* VARKI, A., CUMMINGS, R. D., ESKO, J. D., FREEZE, H. H., STANLEY, P., BERTOZZI, C. R., HART, G. W. & ETZLER, M. E. (eds.) *Essentials of Glycobiology.* 2nd ed. Cold Spring Harbor (NY).

BROSCHAT, K. O., GORKA, C., PAGE, J. D., MARTIN-BERGER, C. L., DAVIES, M. S., HUANG HC, H. C., GULVE, E. A., SALSGIVER, W. J. & KASTEN, T. P. 2002. Kinetic characterization of human glutamine-fructose-6-phosphate amidotransferase I: potent feedback inhibition by glucosamine 6-phosphate. *The Journal of biological chemistry,* 277**,** 14764-70.

BRUNNGRABER, E. G., BROWN, B. D. & HOF, H. 1971. Determination of gangliosides, glycoproteins, and glycosaminoglycans in brain tissue. *Clinica chimica acta; international journal of clinical chemistry,* 32**,** 159-70.

BULLENS, R. W., O'HANLON, G. M., WAGNER, E., MOLENAAR, P. C., FURUKAWA, K., PLOMP, J. J. & WILLISON, H. J. 2002. Complex gangliosides at the neuromuscular junction are membrane receptors for autoantibodies and botulinum neurotoxin but redundant for normal synaptic function. *The Journal of neuroscience : the official journal of the Society for Neuroscience,* 22**,** 6876-84.

BULLER, A. L. & WHITE, M. M. 1990. Altered patterns of N-linked glycosylation of the Torpedo acetylcholine receptor expressed in Xenopus oocytes. *The Journal of membrane biology,* 115**,** 179-89.

BURKE, G., HISCOCK, A., KLEIN, A., NIKS, E. H., MAIN, M., MANZUR, A. Y., NG, J., DE VILE, C., MUNTONI, F., BEESON, D. & ROBB, S. 2012. Salbutamol benefits children with congenital myasthenic syndrome due to DOK7 mutations. *Neuromuscular disorders : NMD.*

BURKE, G., HISCOCK, A., KLEIN, A., NIKS, E. H., MAIN, M., MANZUR, A. Y., NG, J., DE VILE, C., MUNTONI, F., BEESON, D. & ROBB, S. 2013. Salbutamol benefits children with congenital myasthenic syndrome due to DOK7 mutations. *Neuromuscular disorders : NMD,* 23**,** 170-5.

BURT, D., BRODBECK, K., HARING, H. U., SCHLEICHER, E. D. & WEIGERT, C. 2005. Partial characterisation of the human GFAT promoter: effect of single nucleotide polymorphisms on promoter function. *Biochimica et biophysica acta,* 1740**,** 85-90.

CARRERA, I. A., MATTHIJS, G., PEREZ, B. & CERDA, C. P. 2012. DPAGT1-CDG: report of a patient with fetal hypokinesia phenotype. *American journal of medical genetics. Part A,* 158A**,** 2027-30.

CARTAUD, A., COUTANT, S., PETRUCCI, T. C. & CARTAUD, J. 1998. Evidence for in situ and in vitro association between beta-dystroglycan and the subsynaptic 43K rapsyn protein. Consequence for acetylcholine receptor clustering at the synapse. *The Journal of biological chemistry,* 273**,** 11321-6.

CARTAUD, A., STROCHLIC, L., GUERRA, M., BLANCHARD, B., LAMBERGEON, M., KREJCI, E., CARTAUD, J. & LEGAY, C. 2004. MuSK is required for anchoring acetylcholinesterase at the neuromuscular junction. *The Journal of cell biology,* 165**,** 505-15.

CHAN, S. H., WONG, V. C. & ENGEL, A. G. 2012. Neuromuscular junction acetylcholinesterase deficiency responsive to albuterol. *Pediatric neurology,* 47**,** 137-40.

CHANG, Q., SU, K., BAKER, J. R., YANG, X., PATERSON, A. J. & KUDLOW, J. E. 2000. Phosphorylation of human glutamine:fructose-6-phosphate amidotransferase by cAMP-dependent protein kinase at serine 205 blocks the enzyme activity. *The Journal of biological chemistry,* 275**,** 21981-7.

CHAOUCH, A., MULLER, J. S., GUERGUELTCHEVA, V., DUSL, M., SCHARA, U., RAKOCEVIC-STOJANOVIC, V., LINDBERG, C., SCOLA, R. H., WERNECK, L. C., COLOMER, J., NASCIMENTO, A., VILCHEZ, J. J., MUELAS, N., ARGOV, Z., ABICHT, A. & LOCHMULLER, H. 2012. A retrospective clinical study of the treatment of slow-channel congenital myasthenic syndrome. *Journal of neurology,* 259**,** 474-81.

CHEN, C. Y. & SHYU, A. B. 1995. AU-rich elements: characterization and importance in mRNA degradation. *Trends in biochemical sciences,* 20**,** 465-70.

CHEN, V. P., LUK, W. K., CHAN, W. K., LEUNG, K. W., GUO, A. J., CHAN, G. K., XU, S. L., CHOI, R. C. & TSIM, K. W. 2011. Molecular Assembly and Biosynthesis of Acetylcholinesterase in Brain and Muscle: the Roles of t-peptide, FHB Domain, and N-linked Glycosylation. *Frontiers in molecular neuroscience,* 4**,** 36.

CHESTER, M. A. 1998. IUPAC-IUB Joint Commission on Biochemical Nomenclature (JCBN). Nomenclature of glycolipids--recommendations 1997. *European journal of biochemistry / FEBS,* 257**,** 293-8.

CHEVESSIER, F., FARAUT, B., RAVEL-CHAPUIS, A., RICHARD, P., GAUDON, K., BAUCHE, S., PRIOLEAU, C., HERBST, R., GOILLOT, E., IOOS, C., AZULAY, J. P., ATTARIAN, S., LEROY, J. P., FOURNIER, E., LEGAY, C., SCHAEFFER, L., KOENIG, J., FARDEAU, M., EYMARD, B., POUGET, J. & HANTAI, D. 2004. MUSK, a new target for mutations causing congenital myasthenic syndrome. *Human molecular genetics,* 13**,** 3229-40.

CHOI, K. R., BERRERA, M., REISCHL, M., STRACK, S., ALBRIZIO, M., RODER, I. V., WAGNER, A., PETERSEN, Y., HAFNER, M., ZACCOLO, M. & RUDOLF, R. 2012. Rapsyn mediates subsynaptic anchoring of PKA type I and stabilisation of acetylcholine receptor in vivo. *Journal of cell science,* 125**,** 714-23.

CHOI, R. C., TING, A. K., LAU, F. T., XIE, H. Q., LEUNG, K. W., CHEN, V. P., SIOW, N. L. & TSIM, K. W. 2007. Calcitonin gene-related peptide induces the expression of acetylcholinesterase-associated collagen ColQ in muscle: a distinction in driving two different promoters between fast- and slow-twitch muscle fibers. *Journal of neurochemistry,* 102**,** 1316-28.

CIENIEWSKI-BERNARD, C., BASTIDE, B., LEFEBVRE, T., LEMOINE, J., MOUNIER, Y. & MICHALSKI, J. C. 2004. Identification of O-linked N-acetylglucosamine proteins in rat skeletal muscle using two-dimensional gel electrophoresis and mass spectrometry. *Molecular & cellular proteomics : MCP,* 3**,** 577-85.

CIENIEWSKI-BERNARD, C., MONTEL, V., STEVENS, L. & BASTIDE, B. 2009. O-GlcNAcylation, an original modulator of contractile activity in striated muscle. *Journal of muscle research and cell motility,* 30**,** 281-7.

CLARKSON, P. M. & THOMPSON, H. S. 1997. Drugs and sport. Research findings and limitations. *Sports Med,* 24**,** 366-84.

CLEMENTI, F. & SHER, E. 1985. Antibody induced internalization of acetylcholine nicotinic receptor: kinetics, mechanism and selectivity. *European journal of cell biology,* 37**,** 220-8.

COETZEE, T., FUJITA, N., DUPREE, J., SHI, R., BLIGHT, A., SUZUKI, K. & POPKO, B. 1996. Myelination in the absence of galactocerebroside and sulfatide: normal structure with abnormal function and regional instability. *Cell,* 86**,** 209-19.

COLOMER, J., MULLER, J. S., VERNET, A., NASCIMENTO, A., PONS, M., GONZALEZ, V., ABICHT, A. & LOCHMULLER, H. 2006. Long-term improvement of slow-channel congenital myasthenic syndrome with fluoxetine. *Neuromuscular disorders : NMD,* 16**,** 329-33.

CONTI-FINE, B. M., MILANI, M. & KAMINSKI, H. J. 2006. Myasthenia gravis: past, present, and future. *The Journal of clinical investigation,* 116**,** 2843-54.

COSSINS, J., BELAYA, K., HICKS, D., SALIH, M. A., FINLAYSON, S., CARBONI, N., LIU, W. W., MAXWELL, S., ZOLTOWSKA, K., FARSANI, G. T., LAVAL, S., SEIDHAMED, M. Z., DONNELLY, P., BENTLEY, D., MCGOWAN, S. J., MULLER, J., PALACE, J., LOCHMULLER, H. & BEESON, D. 2013a. Congenital myasthenic syndromes due to mutations in ALG2 and ALG14. *Brain : a journal of neurology,* 136**,** 944-56.

COSSINS, J., BELAYA, K., HICKS, D., SALIH, M. A., FINLAYSON, S., CARBONI, N., LIU, W. W., MAXWELL, S., ZOLTOWSKA, K., FARSANI, G. T., LAVAL, S., SEIDHAMED, M. Z., DONNELLY, P., BENTLEY, D., MCGOWAN, S. J., MULLER, J., PALACE, J., LOCHMULLER, H. & BEESON, D. 2013b. Congenital myasthenic syndromes due to mutations in ALG2 and ALG14. *Brain : a journal of neurology*.

COSSINS, J., BELAYA, K., ZOLTOWSKA, K., KONECZNY, I., MAXWELL, S., JACOBSON, L., LEITE, M. I., WATERS, P., VINCENT, A. & BEESON, D. 2012a. The search for new antigenic targets in myasthenia gravis. *Annals of the New York Academy of Sciences,* 1275**,** 123-8.

COSSINS, J., LIU, W. W., BELAYA, K., MAXWELL, S., OLDRIDGE, M., LESTER, T., ROBB, S. & BEESON, D. 2012b. The spectrum of mutations that underlie the neuromuscular junction synaptopathy in DOK7 congenital myasthenic syndrome. *Human molecular genetics,* 21**,** 3765-75.

COSSINS, J., WEBSTER, R., MAXWELL, S., BURKE, G., VINCENT, A. & BEESON, D. 2004. A mouse model of AChR deficiency syndrome with a phenotype reflecting the human condition. *Human molecular genetics,* 13**,** 2947-57.

COTMAN, S. L., HALFTER, W. & COLE, G. J. 1999. Identification of extracellular matrix ligands for the heparan sulfate proteoglycan agrin. *Experimental cell research,* 249**,** 54-64.

CROXEN, R., HATTON, C., SHELLEY, C., BRYDSON, M., CHAUPLANNAZ, G., OOSTERHUIS, H., VINCENT, A., NEWSOM-DAVIS, J., COLQUHOUN, D. & BEESON, D. 2002. Recessive inheritance and variable penetrance of slow-channel congenital myasthenic syndromes. *Neurology,* 59**,** 162-8.

DE CONTI, L., BARALLE, M. & BURATTI, E. 2013. Exon and intron definition in pre-mRNA splicing. *Wiley interdisciplinary reviews. RNA,* 4**,** 49-60.

DEHAVEN, J. E., ROBINSON, K. A., NELSON, B. A. & BUSE, M. G. 2001. A novel variant of glutamine: fructose-6-phosphate amidotransferase-1 (GFAT1) mRNA is selectively expressed in striated muscle. *Diabetes,* 50**,** 2419-24.

DENISOT, M. A., LE GOFFIC, F. & BADET, B. 1991. Glucosamine-6-phosphate synthase from Escherichia coli yields two proteins upon limited proteolysis: identification of the glutamine amidohydrolase and 2R ketose/aldose isomerase-bearing domains based on their biochemical properties. *Archives of biochemistry and biophysics,* 288**,** 225-30.

DENNISSEN, M. A., JENNISKENS, G. J., PIEFFERS, M., VERSTEEG, E. M., PETITOU, M., VEERKAMP, J. H. & VAN KUPPEVELT, T. H. 2002. Large, tissue-regulated domain diversity of heparan sulfates demonstrated by phage display antibodies. *The Journal of biological chemistry,* 277**,** 10982-6.

DENZER, A. J., HAUSER, D. M., GESEMANN, M. & RUEGG, M. A. 1997. Synaptic differentiation: the role of agrin in the formation and maintenance of the neuromuscular junction. *Cell and tissue research,* 290**,** 357-65.

DILL, K. A. & MACCALLUM, J. L. 2012. The protein-folding problem, 50 years on. *Science,* 338**,** 1042-6.

DOBBINS, G. C., LUO, S., YANG, Z., XIONG, W. C. & MEI, L. 2008. alpha-Actinin interacts with rapsyn in agrin-stimulated AChR clustering. *Molecular brain,* 1**,** 18.

DONGER, C., KREJCI, E., SERRADELL, A. P., EYMARD, B., BON, S., NICOLE, S., CHATEAU, D., GARY, F., FARDEAU, M., MASSOULIE, J. & GUICHENEY, P. 1998. Mutation in the human acetylcholinesterase-associated collagen gene, COLQ, is responsible for congenital myasthenic syndrome with end-plate acetylcholinesterase deficiency (Type Ic). *American journal of human genetics,* 63**,** 967-75.

DVIR, H., HAREL, M., BON, S., LIU, W. Q., VIDAL, M., GARBAY, C., SUSSMAN, J. L., MASSOULIE, J. & SILMAN, I. 2004. The synaptic acetylcholinesterase tetramer assembles around a polyproline II helix. *The EMBO journal,* 23**,** 4394-405.

DVIR, H., SILMAN, I., HAREL, M., ROSENBERRY, T. L. & SUSSMAN, J. L. 2010. Acetylcholinesterase: from 3D structure to function. *Chemico-biological interactions,* 187**,** 10-22.

EGUCHI, S., OSHIRO, N., MIYAMOTO, T., YOSHINO, K., OKAMOTO, S., ONO, T., KIKKAWA, U. & YONEZAWA, K. 2009. AMP-activated protein kinase phosphorylates glutamine : fructose-6-phosphate amidotransferase 1 at Ser243 to modulate its enzymatic activity. *Genes to cells : devoted to molecular & cellular mechanisms,* 14**,** 179-89.

ELBEIN, S. C., ZHENG, H., JIA, Y., CHU, W., COOPER, J. J., HALE, T. & ZHANG, Z. 2004. Molecular screening of the human glutamine-fructose-6-phosphate amidotransferase 1 (GFPT1) gene and association studies with diabetes and diabetic nephropathy. *Molecular genetics and metabolism,* 82**,** 321-8.

ELLIS, J. & BHATIA, M. 2011. iPSC technology: platform for drug discovery. Point. *Clin Pharmacol Ther,* 89**,** 639-41.

ELSON, L. A. & MORGAN, W. T. 1933. A colorimetric method for the determination of glucosamine and chondrosamine. *The Biochemical journal,* 27**,** 1824-8.

ENGEL, A. G. 2011. Congenital Myasthenic Syndromes in 2012. *Current neurology and neuroscience reports*.

ENGEL, A. G., SAHASHI, K. & FUMAGALLI, G. 1981. The immunopathology of acquired myasthenia gravis. *Annals of the New York Academy of Sciences,* 377**,** 158-74.

FENG, G., KREJCI, E., MOLGO, J., CUNNINGHAM, J. M., MASSOULIE, J. & SANES, J. R. 1999. Genetic analysis of collagen Q: roles in acetylcholinesterase and butyrylcholinesterase assembly and in synaptic structure and function. *The Journal of cell biology,* 144**,** 1349-60.

FERGUSON, M. A. J., KINOSHITA, T. & HART, G. W. 2009. Glycosylphosphatidylinositol Anchors. *In:* VARKI, A., CUMMINGS, R. D., ESKO, J. D., FREEZE, H. H., STANLEY, P., BERTOZZI, C. R., HART, G. W. & ETZLER, M. E. (eds.) *Essentials of Glycobiology.* 2nd ed. Cold Spring Harbor (NY).

FINLAYSON, S., BEESON, D. & PALACE, J. 2013. Congenital myasthenic syndromes: an update. *Pract Neurol,* 13**,** 80-91.

FINLAYSON, S., SPILLANE, J., KULLMANN, D. M., HOWARD, R., WEBSTER, R., PALACE, J. & BEESON, D. 2012. Slow channel congenital myasthenic syndrome responsive to a combination of fluoxetine and salbutamol. *Muscle & nerve*.

FLANAGAN, S. E., PATCH, A. M. & ELLARD, S. 2010. Using SIFT and PolyPhen to predict loss-of-function and gain-of-function mutations. *Genetic testing and molecular biomarkers,* 14**,** 533-7.

FLOQUET, N., MOUILLERON, S., DAHER, R., MAIGRET, B., BADET, B. & BADET-DENISOT, M. A. 2007. Ammonia channeling in bacterial glucosamine-6-phosphate synthase (Glms): molecular dynamics simulations and kinetic studies of protein mutants. *FEBS letters,* 581**,** 2981-7.

FLORINI, J. R. & ROBERTS, S. B. 1979. A serum-free medium for the growth of muscle cells in culture. *In vitro,* 15**,** 983-92.

FLUCHER, B. E. & DANIELS, M. P. 1989. Distribution of Na+ channels and ankyrin in neuromuscular junctions is complementary to that of acetylcholine receptors and the 43 kd protein. *Neuron,* 3**,** 163-75.

FRIEDRICH, M. V., GOHRING, W., MORGELIN, M., BRANCACCIO, A., DAVID, G. & TIMPL, R. 1999. Structural basis of glycosaminoglycan modification and of heterotypic interactions of perlecan domain V. *Journal of molecular biology,* 294**,** 259-70.

GAUTAM, M., NOAKES, P. G., MOSCOSO, L., RUPP, F., SCHELLER, R. H., MERLIE, J. P. & SANES, J. R. 1996. Defective neuromuscular synaptogenesis in agrin-deficient mutant mice. *Cell,* 85**,** 525-35.

GEHL, J. 2003. Electroporation: theory and methods, perspectives for drug delivery, gene therapy and research. *Acta physiologica Scandinavica,* 177**,** 437-47.

GEHLE, V. M. & SUMIKAWA, K. 1991. Site-directed mutagenesis of the conserved N-glycosylation site on the nicotinic acetylcholine receptor subunits. *Brain research. Molecular brain research,* 11**,** 17-25.

GEHLE, V. M., WALCOTT, E. C., NISHIZAKI, T. & SUMIKAWA, K. 1997. N-glycosylation at the conserved sites ensures the expression of properly folded functional ACh receptors. *Brain research. Molecular brain research,* 45**,** 219-29.

GESEMANN, M., DENZER, A. J. & RUEGG, M. A. 1995. Acetylcholine receptor-aggregating activity of agrin isoforms and mapping of the active site. *The Journal of cell biology,* 128**,** 625-36.

GHAZANFARI, N., FERNANDEZ, K. J., MURATA, Y., MORSCH, M., NGO, S. T., REDDEL, S. W., NOAKES, P. G. & PHILLIPS, W. D. 2011. Muscle specific kinase: organiser of synaptic membrane domains. *The international journal of biochemistry & cell biology,* 43**,** 295-8.

GILHUS, N. E., OWE, J. F., HOFF, J. M., ROMI, F., SKEIE, G. O. & AARLI, J. A. 2011. Myasthenia gravis: a review of available treatment approaches. *Autoimmune diseases,* 2011**,** 847393.

GLASS, D. J., DECHIARA, T. M., STITT, T. N., DISTEFANO, P. S., VALENZUELA, D. M. & YANCOPOULOS, G. D. 1996. The receptor tyrosine kinase MuSK is required for neuromuscular junction formation and is a functional receptor for agrin. *Cold Spring Harbor symposia on quantitative biology,* 61**,** 435-44.

GOMEZ, A. M., VAN DEN BROECK, J., VROLIX, K., JANSSEN, S. P., LEMMENS, M. A., VAN DER ESCH, E., DUIMEL, H., FREDERIK, P., MOLENAAR, P. C., MARTINEZ-MARTINEZ, P., DE BAETS, M. H. & LOSEN, M. 2010. Antibody effector mechanisms in myasthenia gravis-pathogenesis at the neuromuscular junction. *Autoimmunity,* 43**,** 353-70.

GOUJON, M., MCWILLIAM, H., LI, W., VALENTIN, F., SQUIZZATO, S., PAERN, J. & LOPEZ, R. 2010. A new bioinformatics analysis tools framework at EMBL-EBI. *Nucleic acids research,* 38**,** W695-9.

GOVINDASAMY, L., PEDERSEN, B., LIAN, W., KUKAR, T., GU, Y., JIN, S., AGBANDJE-MCKENNA, M., WU, D. & MCKENNA, R. 2004. Structural insights and functional implications of choline acetyltransferase. *Journal of structural biology,* 148**,** 226-35.

GROW, W. A., FERNS, M. & GORDON, H. 1999. A mechanism for acetylcholine receptor clustering distinct from agrin signaling. *Developmental neuroscience,* 21**,** 436-43.

GRSKOVIC, M., JAVAHERIAN, A., STRULOVICI, B. & DALEY, G. Q. 2011. Induced pluripotent stem cells--opportunities for disease modelling and drug discovery. *Nat Rev Drug Discov,* 10**,** 915-29.

GU, Y., FORSAYETH, J. R., VERRALL, S., YU, X. M. & HALL, Z. W. 1991. Assembly of the mammalian muscle acetylcholine receptor in transfected COS cells. *J Cell Biol,* 114**,** 799-807.

GUERGUELTCHEVA, V., MULLER, J. S., DUSL, M., SENDEREK, J., OLDFORS, A., LINDBERGH, C., MAXWELL, S., COLOMER, J., MALLEBRERA, C. J., NASCIMENTO, A., VILCHEZ, J. J., MUELAS, N., KIRSCHNER, J., NAFISSI, S., KARIMINEJAD, A., NILIPOUR, Y., BOZORGMEHR, B., NAJMABADI, H., RODOLICO, C., SIEB, J. P., SCHLOTTER, B., SCHOSER, B., HERRMANN, R., VOIT, T., STEINLEIN, O. K., NAJAFI, A., URTIZBEREA, A., SOLER, D. M., MUNTONI, F., HANNA, M. G., CHAOUCH, A., STRAUB, V., BUSHBY, K., PALACE, J., BEESON, D., ABICHT, A. & LOCHMULLER, H. 2011. Congenital myasthenic syndrome with tubular aggregates caused by GFPT1 mutations. *Journal of neurology*.

HAHNE, H., MOGHADDAS GHOLAMI, A. & KUSTER, B. 2012. Discovery of O-GlcNAc-modified proteins in published large-scale proteome data. *Molecular & cellular proteomics : MCP,* 11**,** 843-50.

HALILOGLU, G. & TOPALOGLU, H. 2004. Glycosylation defects in muscular dystrophies. *Current opinion in neurology,* 17**,** 521-7.

HAMILL, O. P., MARTY, A., NEHER, E., SAKMANN, B. & SIGWORTH, F. J. 1981. Improved patch-clamp techniques for high-resolution current recording from cells and cell-free membrane patches. *Pflugers Archiv : European journal of physiology,* 391**,** 85-100.

HAMURO, J., HISHIDA, Y., HIGUCHI, O. & YAMANASHI, Y. 2011. The transcription factor Sp1 plays a crucial role in dok-7 gene expression. *Biochemical and biophysical research communications,* 408**,** 293-9.

HARPER, C. M. & ENGEL, A. G. 1998. Safety and efficacy of quinidine sulfate in slow-channel congenital myasthenic syndrome. *Annals of the New York Academy of Sciences,* 841**,** 203-6.

HART, G. W. & AKIMOTO, Y. 2009. The O-GlcNAc Modification. *In:* VARKI, A., CUMMINGS, R. D., ESKO, J. D., FREEZE, H. H., STANLEY, P., BERTOZZI, C. R., HART, G. W. & ETZLER, M. E. (eds.) *Essentials of Glycobiology*. 2nd ed. Cold Spring Harbor (NY).

HART, G. W., SLAWSON, C., RAMIREZ-CORREA, G. & LAGERLOF, O. 2011. Cross talk between O-GlcNAcylation and phosphorylation: roles in signaling, transcription, and chronic disease. *Annual review of biochemistry,* 80**,** 825-58.

HARTZELL, H. C., KUFFLER, S. W. & YOSHIKAMI, D. 1976. The number of acetylcholine molecules in a quantum and the interaction between quanta at the subsynaptic membrane of the skeletal neuromuscular synapse. *Cold Spring Harbor symposia on quantitative biology,* 40**,** 175-86.

HE, P., NG, B. G., LOSFELD, M. E., ZHU, W. & FREEZE, H. H. 2012. Identification of intercellular cell adhesion molecule 1 (ICAM-1) as a hypoglycosylation marker in congenital disorders of glycosylation cells. *The Journal of biological chemistry,* 287**,** 18210-7.

HERBERT, S., SOARES, H., ZIMMER, C. & HENRIQUES, R. 2012. Single-molecule localization super-resolution microscopy: deeper and faster. *Microsc Microanal,* 18**,** 1419-29.

HERBST, R., ISKRATSCH, T., UNGER, E. & BITTNER, R. E. 2009. Aberrant development of neuromuscular junctions in glycosylation-defective Large(myd) mice. *Neuromuscular disorders : NMD,* 19**,** 366-78.

HIGUCHI, O., HAMURO, J., MOTOMURA, M. & YAMANASHI, Y. 2011. Autoantibodies to low-density lipoprotein receptor-related protein 4 in myasthenia gravis. *Annals of neurology,* 69**,** 418-22.

HOCH, W., MCCONVILLE, J., HELMS, S., NEWSOM-DAVIS, J., MELMS, A. & VINCENT, A. 2001. Auto-antibodies to the receptor tyrosine kinase MuSK in patients with myasthenia gravis without acetylcholine receptor antibodies. *Nature medicine,* 7**,** 365-8.

HOLZFEIND, P. J., GREWAL, P. K., REITSAMER, H. A., KECHVAR, J., LASSMANN, H., HOEGER, H., HEWITT, J. E. & BITTNER, R. E. 2002. Skeletal, cardiac and tongue muscle pathology, defective retinal transmission, and neuronal migration defects in the Large(myd) mouse defines a natural model for glycosylation-deficient muscle - eye - brain disorders. *Human molecular genetics,* 11**,** 2673-87.

HOOD, L. J. 1990. Myasthenia gravis: regimens and regimen-associated problems in adults. *J Neurosci Nurs,* 22**,** 358-64.

HOYTE, K., KANG, C. & MARTIN, P. T. 2002. Definition of pre- and postsynaptic forms of the CT carbohydrate antigen at the neuromuscular junction: ubiquitous expression of the CT antigens and the CT GalNAc transferase in mouse tissues. *Brain research. Molecular brain research,* 109**,** 146-60.

HU, Y., RIESLAND, L., PATERSON, A. J. & KUDLOW, J. E. 2004. Phosphorylation of mouse glutamine-fructose-6-phosphate amidotransferase 2 (GFAT2) by cAMP-dependent protein kinase increases the enzyme activity. *The Journal of biological chemistry,* 279**,** 29988-93.

HUGHES, R. A. & CORNBLATH, D. R. 2005. Guillain-Barre syndrome. *Lancet,* 366**,** 1653-66.

HUH, S. Y., KIM, H. S., JANG, H. J., PARK, Y. E. & KIM, D. S. 2012. Limb-girdle myasthenia with tubular aggregates associated with novel GFPT1 mutations. *Muscle & nerve,* 46**,** 600-4.

HUIJBERS, M. G., LIPKA, A. F., POTMAN, M., HENSBERGEN, P. J., TITULAER, M. J., NIKS, E. H., VAN DER MAAREL, S. M., KLOOSTER, R. & VERSCHUUREN, J. J. 2013. Antibodies to active zone protein ERC1 in Lambert-Eaton myasthenic syndrome. *Human immunology*.

HUYNH, Q. K., GULVE, E. A. & DIAN, T. 2000. Purification and characterization of glutamine:fructose 6-phosphate amidotransferase from rat liver. *Arch Biochem Biophys,* 379**,** 307-13.

HUZE, C., BAUCHE, S., RICHARD, P., CHEVESSIER, F., GOILLOT, E., GAUDON, K., BEN AMMAR, A., CHABOUD, A., GROSJEAN, I., LECUYER, H. A., BERNARD, V., ROUCHE, A., ALEXANDRI, N., KUNTZER, T., FARDEAU, M., FOURNIER, E., BRANCACCIO, A., RUEGG, M. A., KOENIG, J., EYMARD, B., SCHAEFFER, L. & HANTAI, D. 2009. Identification of an agrin mutation that causes congenital myasthenia and affects synapse function. *American journal of human genetics,* 85**,** 155-67.

IQBAL, Z., SHAHZAD, M., VISSERS, L. E., VAN SCHERPENZEEL, M., GILISSEN, C., RAZZAQ, A., ZAHOOR, M. Y., KHAN, S. N., KLEEFSTRA, T., VELTMAN, J. A., DE BROUWER, A. P., LEFEBER, D. J., VAN BOKHOVEN, H. & RIAZUDDIN, S. 2012. A compound heterozygous mutation in DPAGT1 results in a congenital disorder of glycosylation with a relatively mild phenotype. *European journal of human genetics : EJHG*.

IRANI, S. R., ALEXANDER, S., WATERS, P., KLEOPA, K. A., PETTINGILL, P., ZULIANI, L., PELES, E., BUCKLEY, C., LANG, B. & VINCENT, A. 2010. Antibodies to Kv1 potassium channel-complex proteins leucine-rich, glioma inactivated 1 protein and contactin-associated protein-2 in limbic encephalitis, Morvan's syndrome and acquired neuromyotonia. *Brain : a journal of neurology,* 133**,** 2734-48.

ISUPOV, M. N., OBMOLOVA, G., BUTTERWORTH, S., BADET-DENISOT, M. A., BADET, B., POLIKARPOV, I., LITTLECHILD, J. A. & TEPLYAKOV, A. 1996. Substrate binding is required for assembly of the active conformation of the catalytic site in Ntn amidotransferases: evidence from the 1.8 A crystal structure of the glutaminase domain of glucosamine 6-phosphate synthase. *Structure,* 4**,** 801-10.

JACKSON, S. P. & TJIAN, R. 1988. O-glycosylation of eukaryotic transcription factors: implications for mechanisms of transcriptional regulation. *Cell,* 55**,** 125-33.

JACOB, S., VIEGAS, S., LEITE, M. I., WEBSTER, R., COSSINS, J., KENNETT, R., HILTON-JONES, D., MORGAN, B. P. & VINCENT, A. 2012. Presence and pathogenic relevance of antibodies to clustered acetylcholine receptor in ocular and generalized myasthenia gravis. *Archives of neurology,* 69**,** 994-1001.

JACOBSON, C., COTE, P. D., ROSSI, S. G., ROTUNDO, R. L. & CARBONETTO, S. 2001. The dystroglycan complex is necessary for stabilization of acetylcholine receptor clusters at neuromuscular junctions and formation of the synaptic basement membrane. *The Journal of cell biology,* 152**,** 435-50.

JAHN, K., FRANKE, C. & BUFLER, J. 2000. Mechanism of block of nicotinic acetylcholine receptor channels by purified IgG from seropositive patients with myasthenia gravis. *Neurology,* 54**,** 474-9.

JONES, M. A., NG, B. G., BHIDE, S., CHIN, E., RHODENIZER, D., HE, P., LOSFELD, M. E., HE, M., RAYMOND, K., BERRY, G., FREEZE, H. H. & HEGDE, M. R. 2012. DDOST mutations identified by whole-exome sequencing are implicated in congenital disorders of glycosylation. *American journal of human genetics,* 90**,** 363-8.

KAUFER, D., FRIEDMAN, A., SEIDMAN, S. & SOREQ, H. 1998. Acute stress facilitates long-lasting changes in cholinergic gene expression. *Nature,* 393**,** 373-7.

KAWAKAMI, Y., ITO, M., HIRAYAMA, M., SAHASHI, K., OHKAWARA, B., MASUDA, A., NISHIDA, H., MABUCHI, N., ENGEL, A. G. & OHNO, K. 2011. Anti-MuSK autoantibodies block binding of collagen Q to MuSK. *Neurology,* 77**,** 1819-26.

KEMP, G., MORLEY, B., DWYER, D. & BRADLEY, R. J. 1980. Purification and characterization of nicotinic acetylcholine receptors from muscle. *Membr Biochem,* 3**,** 229-57.

KIM, C. H., XIONG, W. C. & MEI, L. 2005. Inhibition of MuSK expression by CREB interacting with a CRE-like element and MyoD. *Mol Cell Biol,* 25**,** 5329-38.

KIM, N., STIEGLER, A. L., CAMERON, T. O., HALLOCK, P. T., GOMEZ, A. M., HUANG, J. H., HUBBARD, S. R., DUSTIN, M. L. & BURDEN, S. J. 2008. Lrp4 is a receptor for Agrin and forms a complex with MuSK. *Cell,* 135**,** 334-42.

KIMBELL, L. M., OHNO, K., ENGEL, A. G. & ROTUNDO, R. L. 2004. C-terminal and heparin-binding domains of collagenic tail subunit are both essential for anchoring acetylcholinesterase at the synapse. *The Journal of biological chemistry,* 279**,** 10997-1005.

KOBAYASHI, K., NAKAHORI, Y., MIYAKE, M., MATSUMURA, K., KONDO-IIDA, E., NOMURA, Y., SEGAWA, M., YOSHIOKA, M., SAITO, K., OSAWA, M., HAMANO, K., SAKAKIHARA, Y., NONAKA, I., NAKAGOME, Y., KANAZAWA, I., NAKAMURA, Y., TOKUNAGA, K. & TODA, T. 1998. An ancient retrotransposal insertion causes Fukuyama-type congenital muscular dystrophy. *Nature,* 394**,** 388-92.

KORNFELD, R. 1967. Studies on L-glutamine D-fructose 6-phosphate amidotransferase. I. Feedback inhibition by uridine diphosphate-N-acetylglucosamine. *The Journal of biological chemistry,* 242**,** 3135-41.

KOSTELIDOU, K., TRAKAS, N., ZOURIDAKIS, M., BITZOPOULOU, K., SOTIRIADIS, A., GAVRA, I. & TZARTOS, S. J. 2006. Expression and characterization of soluble forms of the extracellular domains of the beta, gamma and epsilon subunits of the human muscle acetylcholine receptor. *The FEBS journal,* 273**,** 3557-68.

KREJCI, E., COUSSEN, F., DUVAL, N., CHATEL, J. M., LEGAY, C., PUYPE, M., VANDEKERCKHOVE, J., CARTAUD, J., BON, S. & MASSOULIE, J. 1991. Primary structure of a collagenic tail peptide of Torpedo acetylcholinesterase: co-expression with catalytic subunit induces the production of collagen-tailed forms in transfected cells. *The EMBO journal,* 10**,** 1285-93.

KREJCI, E., LEGAY, C., THOMINE, S., SKETELJ, J. & MASSOULIE, J. 1999. Differences in expression of acetylcholinesterase and collagen Q control the distribution and oligomerization of the collagen-tailed forms in fast and slow muscles. *The Journal of neuroscience : the official journal of the Society for Neuroscience,* 19**,** 10672-9.

KREJCI, E., THOMINE, S., BOSCHETTI, N., LEGAY, C., SKETELJ, J. & MASSOULIE, J. 1997. The mammalian gene of acetylcholinesterase-associated collagen. *The Journal of biological chemistry,* 272**,** 22840-7.

KRISSINEL, E. & HENRICK, K. 2007. Inference of macromolecular assemblies from crystalline state. *Journal of molecular biology,* 372**,** 774-97.

KUNIKA, K., TANAHASHI, T., KUDO, E., MIZUSAWA, N., ICHIISHI, E., NAKAMURA, N., YOSHIKAWA, T., YAMAOKA, T., YASUMO, H., TSUGAWA, K., MORITANI, M., INOUE, H. & ITAKURA, M. 2006. Effect of +36T>C in intron 1 on the glutamine: fructose-6-phosphate amidotransferase 1 gene and its contribution to type 2 diabetes in different populations. *Journal of human genetics,* 51**,** 1100-9.

LAHIRI, S. & FUTERMAN, A. H. 2007. The metabolism and function of sphingolipids and glycosphingolipids. *Cellular and molecular life sciences : CMLS,* 64**,** 2270-84.

LARKIN, M. A., BLACKSHIELDS, G., BROWN, N. P., CHENNA, R., MCGETTIGAN, P. A., MCWILLIAM, H., VALENTIN, F., WALLACE, I. M., WILM, A., LOPEZ, R., THOMPSON, J. D., GIBSON, T. J. & HIGGINS, D. G. 2007. Clustal W and Clustal X version 2.0. *Bioinformatics,* 23**,** 2947-8.

LASHLEY, D., PALACE, J., JAYAWANT, S., ROBB, S. & BEESON, D. 2010. Ephedrine treatment in congenital myasthenic syndrome due to mutations in DOK7. *Neurology,* 74**,** 1517-23.

LAU, F. T., CHOI, R. C., XIE, H. Q., LEUNG, K. W., CHEN, V. P., ZHU, J. T., BI, C. W., CHU, G. K. & TSIM, K. W. 2008. Myocyte enhancer factor 2 mediates acetylcholine-induced expression of acetylcholinesterase-associated collagen ColQ in cultured myotubes. *Molecular and cellular neurosciences,* 39**,** 429-38.

LEE, H. H., CHOI, R. C., TING, A. K., SIOW, N. L., JIANG, J. X., MASSOULIE, J. & TSIM, K. W. 2004. Transcriptional regulation of acetylcholinesterase-associated collagen ColQ: differential expression in fast and slow twitch muscle fibers is driven by distinct promoters. *The Journal of biological chemistry,* 279**,** 27098-107.

LEE, Y., RUDELL, J., YECHIKHOV, S., TAYLOR, R., SWOPE, S. & FERNS, M. 2008. Rapsyn carboxyl terminal domains mediate muscle specific kinase-induced phosphorylation of the muscle acetylcholine receptor. *Neuroscience,* 153**,** 997-1007.

LEFKOWITZ, R. J. 1974. Editorial: Selectivity in beta-adrenergic responses: clinical implications. *Circulation,* 49**,** 783-6.

LEITE, M. I., JACOB, S., VIEGAS, S., COSSINS, J., CLOVER, L., MORGAN, B. P., BEESON, D., WILLCOX, N. & VINCENT, A. 2008. IgG1 antibodies to acetylcholine receptors in 'seronegative' myasthenia gravis. *Brain : a journal of neurology,* 131**,** 1940-52.

LENNON, V. A., KRYZER, T. J., GRIESMANN, G. E., O'SUILLEABHAIN, P. E., WINDEBANK, A. J., WOPPMANN, A., MILJANICH, G. P. & LAMBERT, E. H. 1995. Calcium-channel antibodies in the Lambert-Eaton syndrome and other paraneoplastic syndromes. *The New England journal of medicine,* 332**,** 1467-74.

LI, Y., CAMP, S., RACHINSKY, T. L., GETMAN, D. & TAYLOR, P. 1991. Gene structure of mammalian acetylcholinesterase. Alternative exons dictate tissue-specific expression. *The Journal of biological chemistry,* 266**,** 23083-90.

LI, Y., ROUX, C., LAZEREG, S., LECAER, J. P., LAPREVOTE, O., BADET, B. & BADET-DENISOT, M. A. 2007. Identification of a novel serine phosphorylation site in human glutamine:fructose-6-phosphate amidotransferase isoform 1. *Biochemistry,* 46**,** 13163-9.

LI, Z., FORESTER, N. & VINCENT, A. 1996. Modulation of acetylcholine receptor function in TE671 (rhabdomyosarcoma) cells by non-AChR ligands: possible relevance to seronegative myasthenia gravis. *Journal of neuroimmunology,* 64**,** 179-83.

LIEWLUCK, T., SELCEN, D. & ENGEL, A. G. 2011. Beneficial effects of albuterol in congenital endplate acetylcholinesterase deficiency and Dok-7 myasthenia. *Muscle & nerve,* 44**,** 789-94.

LIM, K. H. & FAIRBROTHER, W. G. 2012. Spliceman--a computational web server that predicts sequence variations in pre-mRNA splicing. *Bioinformatics,* 28**,** 1031-2.

LIM, K. H., FERRARIS, L., FILLOUX, M. E., RAPHAEL, B. J. & FAIRBROTHER, W. G. 2011. Using positional distribution to identify splicing elements and predict pre-mRNA processing defects in human genes. *Proceedings of the National Academy of Sciences of the United States of America,* 108**,** 11093-8.

LONGMAN, C., BROCKINGTON, M., TORELLI, S., JIMENEZ-MALLEBRERA, C., KENNEDY, C., KHALIL, N., FENG, L., SARAN, R. K., VOIT, T., MERLINI, L., SEWRY, C. A., BROWN, S. C. & MUNTONI, F. 2003. Mutations in the human LARGE gene cause MDC1D, a novel form of congenital muscular dystrophy with severe mental retardation and abnormal glycosylation of alpha-dystroglycan. *Human molecular genetics,* 12**,** 2853-61.

LOPEZ-GONZALEZ, R. & VELASCO, I. 2012. Therapeutic potential of motor neurons differentiated from embryonic stem cells and induced pluripotent stem cells. *Arch Med Res,* 43**,** 1-10.

LOSFELD, M. E., SONCIN, F., NG, B. G., SINGEC, I. & FREEZE, H. H. 2012. A sensitive green fluorescent protein biomarker of N-glycosylation site occupancy. *FASEB journal : official publication of the Federation of American Societies for Experimental Biology,* 26**,** 4210-7.

LU, Q. L., BOU-GHARIOS, G. & PARTRIDGE, T. A. 2003. Non-viral gene delivery in skeletal muscle: a protein factory. *Gene therapy,* 10**,** 131-42.

LUTHER, M. A., SCHOEPFER, R., WHITING, P., CASEY, B., BLATT, Y., MONTAL, M. S., MONTAL, M. & LINSTROM, J. 1989. A muscle acetylcholine receptor is expressed in the human cerebellar medulloblastoma cell line TE671. *The Journal of neuroscience : the official journal of the Society for Neuroscience,* 9**,** 1082-96.

MAIMONE, M. M. & ENIGK, R. E. 1999. The intracellular domain of the nicotinic acetylcholine receptor alpha subunit mediates its coclustering with rapsyn. *Molecular and cellular neurosciences,* 14**,** 340-54.

MAIMONE, M. M. & MERLIE, J. P. 1993. Interaction of the 43 kd postsynaptic protein with all subunits of the muscle nicotinic acetylcholine receptor. *Neuron,* 11**,** 53-66.

MARIAN, A. J. 2012. Challenges in medical applications of whole exome/genome sequencing discoveries. *Trends Cardiovasc Med,* 22**,** 219-23.

MARTIN, A. R. 1994. Amplification of neuromuscular transmission by postjunctional folds. *Proceedings. Biological sciences / The Royal Society,* 258**,** 321-6.

MARTIN, P. T. 2003. Glycobiology of the neuromuscular junction. *Journal of neurocytology,* 32**,** 915-29.

MARTIN, P. T. & SANES, J. R. 1995. Role for a synapse-specific carbohydrate in agrin-induced clustering of acetylcholine receptors. *Neuron,* 14**,** 743-54.

MARTIN, P. T., SCOTT, L. J., PORTER, B. E. & SANES, J. R. 1999. Distinct structures and functions of related pre- and postsynaptic carbohydrates at the mammalian neuromuscular junction. *Molecular and cellular neurosciences,* 13**,** 105-18.

MASELLI, R., ARREDONDO, J., NGUYEN, J., LARA, M., NG, F., NGO, M., PHAM, J., YI, Q., STAJICH, J., MCDONALD, K., HAUSER, M. & WOLLMANN, R. 2013. Exome sequencing detection of two untranslated GFPT1 mutations in a family with limb-girdle myasthenia. *Clin Genet*.

MASELLI, R. A., ARREDONDO, J., CAGNEY, O., MOZAFFAR, T., SKINNER, S., YOUSIF, S., DAVIS, R. R., GREGG, J. P., SIVAK, M., KONIA, T. H., THOMAS, K. & WOLLMANN, R. L. 2011. Congenital myasthenic syndrome associated with epidermolysis bullosa caused by homozygous mutations in PLEC1 and CHRNE. *Clinical genetics,* 80**,** 444-51.

MASELLI, R. A., DUNNE, V., PASCUAL-PASCUAL, S. I., BOWE, C., AGIUS, M., FRANK, R. & WOLLMANN, R. L. 2003. Rapsyn mutations in myasthenic syndrome due to impaired receptor clustering. *Muscle & nerve,* 28**,** 293-301.

MASELLI, R. A., NG, J. J., ANDERSON, J. A., CAGNEY, O., ARREDONDO, J., WILLIAMS, C., WESSEL, H. B., ABDEL-HAMID, H. & WOLLMANN, R. L. 2009. Mutations in LAMB2 causing a severe form of synaptic congenital myasthenic syndrome. *Journal of medical genetics,* 46**,** 203-8.

MASSOULIE, J. 2002. The origin of the molecular diversity and functional anchoring of cholinesterases. *Neuro-Signals,* 11**,** 130-43.

MASSOULIE, J., BON, S., PERRIER, N. & FALASCA, C. 2005. The C-terminal peptides of acetylcholinesterase: cellular trafficking, oligomerization and functional anchoring. *Chemico-biological interactions,* 157-158**,** 3-14.

MCDEARMON, E. L., COMBS, A. C. & ERVASTI, J. M. 2001. Differential Vicia villosa agglutinin reactivity identifies three distinct dystroglycan complexes in skeletal muscle. *The Journal of biological chemistry,* 276**,** 35078-86.

MERLIE, J. P., SEBBANE, R., TZARTOS, S. & LINDSTROM, J. 1982. Inhibition of glycosylation with tunicamycin blocks assembly of newly synthesized acetylcholine receptor subunits in muscle cells. *The Journal of biological chemistry,* 257**,** 2694-701.

MERRILL, A. H., JR. 2011. Sphingolipid and glycosphingolipid metabolic pathways in the era of sphingolipidomics. *Chemical reviews,* 111**,** 6387-422.

METCALF, R. H. & BOEGMAN, R. J. 1989. Release of acetylcholine from tissue slices of the rat nucleus basalis magnocellularis. *Journal of neurochemistry,* 52**,** 1143-8.

MIHAYLOVA, V., MULLER, J. S., VILCHEZ, J. J., SALIH, M. A., KABIRAJ, M. M., D'AMICO, A., BERTINI, E., WOLFLE, J., SCHREINER, F., KURLEMANN, G., RASIC, V. M., SISKOVA, D., COLOMER, J., HERCZEGFALVI, A., FABRICIOVA, K., WESCHKE, B., SCOLA, R., HOELLEN, F., SCHARA, U., ABICHT, A. & LOCHMULLER, H. 2008. Clinical and molecular genetic findings in COLQ-mutant congenital myasthenic syndromes. *Brain : a journal of neurology,* 131**,** 747-59.

MILEWSKI, S. 1993. Chemical modification studies of the active site of glucosamine-6-phosphate synthase from baker's yeast. *Biochimica et biophysica acta,* 1161**,** 279-84.

MILEWSKI, S. 2002. Glucosamine-6-phosphate synthase--the multi-facets enzyme. *Biochimica et biophysica acta,* 1597**,** 173-92.

MILLAR, N. S. & HARKNESS, P. C. 2008. Assembly and trafficking of nicotinic acetylcholine receptors (Review). *Mol Membr Biol,* 25**,** 279-92.

MILONE, M., SHEN, X. M., SELCEN, D., OHNO, K., BRENGMAN, J., IANNACCONE, S. T., HARPER, C. M. & ENGEL, A. G. 2009. Myasthenic syndrome due to defects in rapsyn: Clinical and molecular findings in 39 patients. *Neurology,* 73**,** 228-35.

MOREMEN, K. W., TIEMEYER, M. & NAIRN, A. V. 2012. Vertebrate protein glycosylation: diversity, synthesis and function. *Nature reviews. Molecular cell biology,* 13**,** 448-62.

MORGAN, W. T. & ELSON, L. A. 1934. A colorimetric method for the determination of N-acetylglucosamine and N-acetylchrondrosamine. *Biochem J,* 28**,** 988-95.

MOUILLERON, S., BADET-DENISOT, M. A., BADET, B. & GOLINELLI-PIMPANEAU, B. 2011. Dynamics of glucosamine-6-phosphate synthase catalysis. *Archives of biochemistry and biophysics,* 505**,** 1-12.

MOUILLERON, S., BADET-DENISOT, M. A. & GOLINELLI-PIMPANEAU, B. 2006. Glutamine binding opens the ammonia channel and activates glucosamine-6P synthase. *The Journal of biological chemistry,* 281**,** 4404-12.

MOUILLERON, S., BADET-DENISOT, M. A. & GOLINELLI-PIMPANEAU, B. 2008. Ordering of C-terminal loop and glutaminase domains of glucosamine-6-phosphate synthase promotes sugar ring opening and formation of the ammonia channel. *Journal of molecular biology,* 377**,** 1174-85.

MUCKENSCHNABEL, I., BERNHARDT, G., SPRUSS, T., DIETL, B. & BUSCHAUER, A. 1998. Quantitation of hyaluronidases by the Morgan-Elson reaction: comparison of the enzyme activities in the plasma of tumor patients and healthy volunteers. *Cancer Lett,* 131**,** 13-20.

MULLE, C., BENOIT, P., PINSET, C., ROA, M. & CHANGEUX, J. P. 1988. Calcitonin gene-related peptide enhances the rate of desensitization of the nicotinic acetylcholine receptor in cultured mouse muscle cells. *Proc Natl Acad Sci U S A,* 85**,** 5728-32.

MULLER, J. S., BAUMEISTER, S. K., SCHARA, U., COSSINS, J., KRAUSE, S., VON DER HAGEN, M., HUEBNER, A., WEBSTER, R., BEESON, D., LOCHMULLER, H. & ABICHT, A. 2006. CHRND mutation causes a congenital myasthenic syndrome by impairing co-clustering of the acetylcholine receptor with rapsyn. *Brain : a journal of neurology,* 129**,** 2784-93.

MULLER, J. S., MIHAYLOVA, V., ABICHT, A. & LOCHMULLER, H. 2007. Congenital myasthenic syndromes: spotlight on genetic defects of neuromuscular transmission. *Expert reviews in molecular medicine,* 9**,** 1-20.

MUTHING, J. & CACIC, M. 1997. Glycosphingolipid expression in human skeletal and heart muscle assessed by immunostaining thin-layer chromatography. *Glycoconjugate journal,* 14**,** 19-28.

NAKAISHI, Y., BANDO, M., SHIMIZU, H., WATANABE, K., GOTO, F., TSUGE, H., KONDO, K. & KOMATSU, M. 2009. Structural analysis of human glutamine:fructose-6-phosphate amidotransferase, a key regulator in type 2 diabetes. *FEBS letters,* 583**,** 163-7.

NAKATA, T., ITO, M., AZUMA, Y., OTSUKA, K., NOGUCHI, Y., KOMAKI, H., OKUMURA, A., SHIRAISHI, K., MASUDA, A., NATSUME, J., KOJIMA, S. & OHNO, K. 2013. Mutations in the C-Terminal Domain of ColQ in Endplate Acetylcholinesterase Deficiency Compromise ColQ-MuSK Interaction. *Human mutation.*

NAQVI, A. R., ISLAM, M. N., CHOUDHURY, N. R. & HAQ, Q. M. 2009a. The fascinating world of RNA interference. *Int J Biol Sci,* 5**,** 97-117.

NAQVI, A. R., ISLAM, M. N., CHOUDHURY, N. R. & HAQ, Q. M. 2009b. The fascinating world of RNA interference. *International journal of biological sciences,* 5**,** 97-117.

NEVILLE, D. C., COQUARD, V., PRIESTMAN, D. A., TE VRUCHTE, D. J., SILLENCE, D. J., DWEK, R. A., PLATT, F. M. & BUTTERS, T. D. 2004. Analysis of fluorescently labeled glycosphingolipid-derived oligosaccharides following ceramide glycanase digestion and anthranilic acid labeling. *Analytical biochemistry,* 331**,** 275-82.

NEWLAND, C. F., BEESON, D., VINCENT, A. & NEWSOM-DAVIS, J. 1995. Functional and non-functional isoforms of the human muscle acetylcholine receptor. *The Journal of physiology,* 489 (Pt 3)**,** 767-78.

NIIMI, M., OGAWARA, T., YAMASHITA, T., YAMAMOTO, Y., UEYAMA, A., KAMBE, T., OKAMOTO, T., BAN, T., TAMANOI, H., OZAKI, K., FUJIWARA, T., FUKUI, H., TAKAHASHI, E. I., KYUSHIKI, H. & TANIGAMI, A. 2001. Identification of GFAT1-L, a novel splice variant of human glutamine: fructose-6-phosphate amidotransferase (GFAT1) that is expressed abundantly in skeletal muscle. *Journal of human genetics,* 46**,** 566-71.

NISHIMUNE, H. 2012. Molecular mechanism of active zone organization at vertebrate neuromuscular junctions. *Molecular neurobiology,* 45**,** 1-16.

NOMOTO, H., TAKAHASHI, N., NAGAKI, Y., ENDO, S., ARATA, Y. & HAYASHI, K. 1986. Carbohydrate structures of acetylcholine receptor from Torpedo californica and distribution of oligosaccharides among the subunits. *European journal of biochemistry / FEBS,* 157**,** 233-42.

NOONAN, D. M., FULLE, A., VALENTE, P., CAI, S., HORIGAN, E., SASAKI, M., YAMADA, Y. & HASSELL, J. R. 1991. The complete sequence of perlecan, a basement membrane heparan sulfate proteoglycan, reveals extensive similarity with laminin A chain, low density lipoprotein-receptor, and the neural cell adhesion molecule. *The Journal of biological chemistry,* 266**,** 22939-47.

NORTH, S. J., HITCHEN, P. G., HASLAM, S. M. & DELL, A. 2009. Mass spectrometry in the analysis of N-linked and O-linked glycans. *Current opinion in structural biology,* 19**,** 498-506.

NYS, M., KESTERS, D. & ULENS, C. 2013. Structural insights into Cys-loop receptor function and ligand recognition. *Biochem Pharmacol,* 86**,** 1042-1053.

OGAWA-GOTO, K., FUNAMOTO, N., OHTA, Y., ABE, T. & NAGASHIMA, K. 1992. Myelin gangliosides of human peripheral nervous system: an enrichment of GM1 in the motor nerve myelin isolated from cauda equina. *Journal of neurochemistry,* 59**,** 1844-9.

OGAWA, M., MIZOFUCHI, H., KOBAYASHI, Y., TSUZUKI, G., YAMAMOTO, M., WADA, S. & KAMEMURA, K. 2012. Terminal differentiation program of skeletal myogenesis is negatively regulated by O-GlcNAc glycosylation. *Biochimica et biophysica acta,* 1820**,** 24-32.

OHNO, K. 2012. Anti-MuSK antibodies in myasthenia gravis block binding of collagen Q to MuSK. *Rinsho shinkeigaku = Clinical neurology,* 52**,** 1306-8.

OHNO, K. 2013. Glycosylation defects as an emerging novel cause leading to a limb-girdle type of congenital myasthenic syndromes. *Journal of neurology, neurosurgery, and psychiatry*.

OHNO, K., BRENGMAN, J., TSUJINO, A. & ENGEL, A. G. 1998. Human endplate acetylcholinesterase deficiency caused by mutations in the collagen-like tail subunit (ColQ) of the asymmetric enzyme. *Proceedings of the National Academy of Sciences of the United States of America,* 95**,** 9654-9.

OHNO, K., ENGEL, A. G., BRENGMAN, J. M., SHEN, X. M., HEIDENREICH, F., VINCENT, A., MILONE, M., TAN, E., DEMIRCI, M., WALSH, P., NAKANO, S. & AKIGUCHI, I. 2000. The spectrum of mutations causing end-plate acetylcholinesterase deficiency. *Annals of neurology,* 47**,** 162-70.

OHNO, K., ENGEL, A. G., SHEN, X. M., SELCEN, D., BRENGMAN, J., HARPER, C. M., TSUJINO, A. & MILONE, M. 2002. Rapsyn mutations in humans cause endplate acetylcholine-receptor deficiency and myasthenic syndrome. *American journal of human genetics,* 70**,** 875-85.

OHNO, K., ITO, M., KAWAKAMI, Y., KREJCI, E. & ENGEL, A. G. 2012. Specific binding of collagen Q to the neuromuscular junction is exploited to cure congenital myasthenia and to explore bases of myasthenia gravis. *Chemico-biological interactions*.

OHNO, K., QUIRAM, P. A., MILONE, M., WANG, H. L., HARPER, M. C., PRUITT, J. N., 2ND, BRENGMAN, J. M., PAO, L., FISCHBECK, K. H., CRAWFORD, T. O., SINE, S. M. & ENGEL, A. G. 1997. Congenital myasthenic syndromes due to heteroallelic nonsense/missense mutations in the acetylcholine receptor epsilon subunit gene: identification and functional characterization of six new mutations. *Human molecular genetics,* 6**,** 753-66.

OKI, T., YAMAZAKI, K., KUROMITSU, J., OKADA, M. & TANAKA, I. 1999. cDNA cloning and mapping of a novel subtype of glutamine:fructose-6-phosphate amidotransferase (GFAT2) in human and mouse. *Genomics,* 57**,** 227-34.

OVERELL, J. R. & WILLISON, H. J. 2005. Recent developments in Miller Fisher syndrome and related disorders. *Current opinion in neurology,* 18**,** 562-6.

OZCAN, S., ANDRALI, S. S. & CANTRELL, J. E. 2010. Modulation of transcription factor function by O-GlcNAc modification. *Biochimica et biophysica acta,* 1799**,** 353-64.

PAL, J., ROZSA, C., KOMOLY, S. & ILLES, Z. 2011. Clinical and biological heterogeneity of autoimmune myasthenia gravis. *Journal of neuroimmunology,* 231**,** 43-54.

PALACE, J., LASHLEY, D., BAILEY, S., JAYAWANT, S., CARR, A., MCCONVILLE, J., ROBB, S. & BEESON, D. 2012. Clinical features in a series of fast channel congenital myasthenia syndrome. *Neuromuscular disorders : NMD,* 22**,** 112-7.

PALACE, J., LASHLEY, D., NEWSOM-DAVIS, J., COSSINS, J., MAXWELL, S., KENNETT, R., JAYAWANT, S., YAMANASHI, Y. & BEESON, D. 2007. Clinical features of the DOK7 neuromuscular junction synaptopathy. *Brain : a journal of neurology,* 130**,** 1507-15.

PAULICK, M. G. & BERTOZZI, C. R. 2008. The glycosylphosphatidylinositol anchor: a complex membrane-anchoring structure for proteins. *Biochemistry,* 47**,** 6991-7000.

PENG, H. B., ALI, A. A., DAGGETT, D. F., RAUVALA, H., HASSELL, J. R. & SMALHEISER, N. R. 1998. The relationship between perlecan and dystroglycan and its implication in the formation of the neuromuscular junction. *Cell adhesion and communication,* 5**,** 475-89.

PENG, H. B., XIE, H., ROSSI, S. G. & ROTUNDO, R. L. 1999. Acetylcholinesterase clustering at the neuromuscular junction involves perlecan and dystroglycan. *The Journal of cell biology,* 145**,** 911-21.

PERRIER, A. L., MASSOULIE, J. & KREJCI, E. 2002. PRiMA: the membrane anchor of acetylcholinesterase in the brain. *Neuron,* 33**,** 275-85.

PEVZNER, A., SCHOSER, B., PETERS, K., COSMA, N. C., KARAKATSANI, A., SCHALKE, B., MELMS, A. & KROGER, S. 2012. Anti-LRP4 autoantibodies in AChR- and MuSK-antibody-negative myasthenia gravis. *Journal of neurology,* 259**,** 427-35.

POHANKA, M. 2012. Acetylcholinesterase inhibitors: a patent review (2008 - present). *Expert Opin Ther Pat,* 22**,** 871-86.

PONTIER, S. M. & SCHWEISGUTH, F. 2012. Glycosphingolipids in signaling and development: from liposomes to model organisms. *Developmental dynamics : an official publication of the American Association of Anatomists,* 241**,** 92-106.

PORTER, S. & FROEHNER, S. C. 1985. Interaction of the 43K protein with components of Torpedo postsynaptic membranes. *Biochemistry,* 24**,** 425-32.

POULTER, L., EARNEST, J. P., STROUD, R. M. & BURLINGAME, A. L. 1989. Structure, oligosaccharide structures, and posttranslationally modified sites of the nicotinic acetylcholine receptor. *Proceedings of the National Academy of Sciences of the United States of America,* 86**,** 6645-9.

PRIVES, J. & BAR-SAGI, D. 1983. Effect of tunicamycin, an inhibitor of protein glycosylation, on the biological properties of acetylcholine receptor in cultured muscle cells. *The Journal of biological chemistry,* 258**,** 1775-80.

PRIVES, J., SILMAN, I. & AMSTERDAM, A. 1975. Proceedings: Appearance and disappearance of acetylcholine receptor during differentiation of embryonic chick skeletal muscle in vitro. *Israel journal of medical sciences,* 11**,** 1192.

PRIVES, J. M. & OLDEN, K. 1980. Carbohydrate requirement for expression and stability of acetylcholine receptor on the surface of embryonic muscle cells in culture. *Proceedings of the National Academy of Sciences of the United States of America,* 77**,** 5263-7.

PURI, K. D., GOPALAKRISHNAN, B. & SUROLIA, A. 1992. Carbohydrate binding specificity of the Tn-antigen binding lectin from Vicia villosa seeds (VVLB4). *FEBS letters,* 312**,** 208-12.

QUIRAM, P. A., OHNO, K., MILONE, M., PATTERSON, M. C., PRUITT, N. J., BRENGMAN, J. M., SINE, S. M. & ENGEL, A. G. 1999. Mutation causing congenital myasthenia reveals acetylcholine receptor beta/delta subunit interaction essential for assembly. *The Journal of clinical investigation,* 104**,** 1403-10.

RACZYNSKA, J., OLCHOWY, J., KONARIEV, P. V., SVERGUN, D. I., MILEWSKI, S. & RYPNIEWSKI, W. 2007. The crystal and solution studies of glucosamine-6-phosphate synthase from Candida albicans. *Journal of molecular biology,* 372**,** 672-88.

RAMANATHAN, V. K. & HALL, Z. W. 1999. Altered glycosylation sites of the delta subunit of the acetylcholine receptor (AChR) reduce alpha delta association and receptor assembly. *The Journal of biological chemistry,* 274**,** 20513-20.

RAMARAO, M. K., BIANCHETTA, M. J., LANKEN, J. & COHEN, J. B. 2001. Role of rapsyn tetratricopeptide repeat and coiled-coil domains in self-association and nicotinic acetylcholine receptor clustering. *The Journal of biological chemistry,* 276**,** 7475-83.

REISSIG, J. L., STORMINGER, J. L. & LELOIR, L. F. 1955. A modified colorimetric method for the estimation of N-acetylamino sugars. *J Biol Chem,* 217**,** 959-66.

RICHEZ, C., BOETZEL, J., FLOQUET, N., KOTESHWAR, K., STEVENS, J., BADET, B. & BADET-DENISOT, M. A. 2007. Expression and purification of active human internal His(6)-tagged L-glutamine: D-Fructose-6P amidotransferase I. *Protein expression and purification,* 54**,** 45-53.

RODER, I. V., CHOI, K. R., REISCHL, M., PETERSEN, Y., DIEFENBACHER, M. E., ZACCOLO, M., POZZAN, T. & RUDOLF, R. 2010. Myosin Va cooperates with PKA RIalpha to mediate maintenance of the endplate in vivo. *Proceedings of the National Academy of Sciences of the United States of America,* 107**,** 2031-6.

ROMANELI, M. T., CASTRO, C. C., FRAGA, A. D., LOMAZI, E. A., NUCCI, A. & TRESOLDI, A. T. 2013. Recurrent apparent life-threatening event as the first manifestation of congenital myasthenia. *Rev Paul Pediatr,* 31**,** 121-123.

ROMI, F., SKEIE, G. O., VEDELER, C., AARLI, J. A., ZORZATO, F. & GILHUS, N. E. 2000. Complement activation by titin and ryanodine receptor autoantibodies in myasthenia gravis. A study of IgG subclasses and clinical correlations. *Journal of neuroimmunology,* 111**,** 169-76.

ROMI, F., SUZUKI, S., SUZUKI, N., PETZOLD, A., PLANT, G. T. & GILHUS, N. E. 2012. Anti-voltage-gated potassium channel Kv1.4 antibodies in myasthenia gravis. *Journal of neurology,* 259**,** 1312-6.

ROTUNDO, R. L. 1984. Asymmetric acetylcholinesterase is assembled in the Golgi apparatus. *Proceedings of the National Academy of Sciences of the United States of America,* 81**,** 479-83.

ROTUNDO, R. L., ROSSI, S. G., KIMBELL, L. M., RUIZ, C. & MARRERO, E. 2005. Targeting acetylcholinesterase to the neuromuscular synapse. *Chemico-biological interactions,* 157-158**,** 15-21.

ROWLEY, M. J., NANDAKUMAR, K. S. & HOLMDAHL, R. 2008. The role of collagen antibodies in mediating arthritis. *Modern rheumatology / the Japan Rheumatism Association,* 18**,** 429-41.

RUBIN, L. L. & HASTON, K. M. 2011. Stem cell biology and drug discovery. *BMC Biol,* 9**,** 42.

RUFF, R. L. 2011. Endplate contributions to the safety factor for neuromuscular transmission. *Muscle & nerve,* 44**,** 854-61.

SADASIVAM, G., WILLMANN, R., LIN, S., ERB-VOGTLI, S., KONG, X. C., RUEGG, M. A. & FUHRER, C. 2005. Src-family kinases stabilize the neuromuscular synapse in vivo via protein interactions, phosphorylation, and cytoskeletal linkage of acetylcholine receptors. *J Neurosci,* 25**,** 10479-93.

SADEH, M., SHEN, X. M. & ENGEL, A. G. 2011. Beneficial effect of albuterol in congenital myasthenic syndrome with epsilon-subunit mutations. *Muscle & nerve,* 44**,** 289-91.

SALANI, S., DONADONI, C., RIZZO, F., BRESOLIN, N., COMI, G. P. & CORTI, S. 2012. Generation of skeletal muscle cells from embryonic and induced pluripotent stem cells as an in vitro model and for therapy of muscular dystrophies. *J Cell Mol Med,* 16**,** 1353-64.

SCHARA, U., CHRISTEN, H. J., DURMUS, H., HIETALA, M., KRABETZ, K., RODOLICO, C., SCHREIBER, G., TOPALOGLU, H., TALIM, B., VOSS, W., PIHKO, H., ABICHT, A., MULLER, J. S. & LOCHMULLER, H. 2010. Long-term follow-up in patients with congenital myasthenic syndrome due to CHAT mutations. *European journal of paediatric neurology : EJPN : official journal of the European Paediatric Neurology Society,* 14**,** 326-33.

SCHARA, U. & LOCHMULLER, H. 2008. Therapeutic strategies in congenital myasthenic syndromes. *Neurotherapeutics : the journal of the American Society for Experimental NeuroTherapeutics,* 5**,** 542-7.

SCHNAAR, R. L., SUZUKI, A. & STANLEY, P. 2009. Glycosphingolipids. *In:* VARKI, A., CUMMINGS, R. D., ESKO, J. D., FREEZE, H. H., STANLEY, P., BERTOZZI, C. R., HART, G. W. & ETZLER, M. E. (eds.) *Essentials of Glycobiology*. 2nd ed. Cold Spring Harbor (NY).

SCHOEPFER, R., LUTHER, M. & LINDSTROM, J. 1988. The human medulloblastoma cell line TE671 expresses a muscle-like acetylcholine receptor. Cloning of the alpha-subunit cDNA. *FEBS letters,* 226**,** 235-40.

SCHRODINGER, LLC 2010. The PyMOL Molecular Graphics System, Version 1.3r1.

SCOTT, L. J., BACOU, F. & SANES, J. R. 1988. A synapse-specific carbohydrate at the neuromuscular junction: association with both acetylcholinesterase and a glycolipid. *The Journal of neuroscience : the official journal of the Society for Neuroscience,* 8**,** 932-44.

SENDEREK, J., MULLER, J. S., DUSL, M., STROM, T. M., GUERGUELTCHEVA, V., DIEPOLDER, I., LAVAL, S. H., MAXWELL, S., COSSINS, J., KRAUSE, S., MUELAS, N., VILCHEZ, J. J., COLOMER, J., MALLEBRERA, C. J., NASCIMENTO, A., NAFISSI, S., KARIMINEJAD, A., NILIPOUR, Y., BOZORGMEHR, B., NAJMABADI, H., RODOLICO, C., SIEB, J. P., STEINLEIN, O. K., SCHLOTTER, B., SCHOSER, B., KIRSCHNER, J., HERRMANN, R., VOIT, T., OLDFORS, A., LINDBERGH, C., URTIZBEREA, A., VON DER HAGEN, M., HUBNER, A., PALACE, J., BUSHBY, K., STRAUB, V., BEESON, D., ABICHT, A. & LOCHMULLER, H. 2011. Hexosamine biosynthetic pathway mutations cause neuromuscular transmission defect. *American journal of human genetics,* 88**,** 162-72.

SHEIKH, K. A., SUN, J., LIU, Y., KAWAI, H., CRAWFORD, T. O., PROIA, R. L., GRIFFIN, J. W. & SCHNAAR, R. L. 1999. Mice lacking complex gangliosides develop Wallerian degeneration and myelination defects. *Proceedings of the National Academy of Sciences of the United States of America,* 96**,** 7532-7.

SHEN, X. M., DEYMEER, F., SINE, S. M. & ENGEL, A. G. 2006. Slow-channel mutation in acetylcholine receptor alphaM4 domain and its efficient knockdown. *Annals of neurology,* 60**,** 128-36.

SHI, L., FU, A. K. & IP, N. Y. 2012. Molecular mechanisms underlying maturation and maintenance of the vertebrate neuromuscular junction. *Trends in neurosciences,* 35**,** 441-53.

SINGHAL, N. & MARTIN, P. T. 2011. Role of extracellular matrix proteins and their receptors in the development of the vertebrate neuromuscular junction. *Developmental neurobiology,* 71**,** 982-1005.

SINGHAL, N., XU, R. & MARTIN, P. T. 2012. Distinct contributions of Galgt1 and Galgt2 to carbohydrate expression and function at the mouse neuromuscular junction. *Molecular and cellular neurosciences,* 51**,** 112-26.

SMITH, C. L., MITTAUD, P., PRESCOTT, E. D., FUHRER, C. & BURDEN, S. J. 2001. Src, Fyn, and Yes are not required for neuromuscular synapse formation but are necessary for stabilization of agrin-induced clusters of acetylcholine receptors. *J Neurosci,* 21**,** 3151-60.

SMITH, M. M., SCHLESINGER, S., LINDSTROM, J. & MERLIE, J. P. 1986. The effects of inhibiting oligosaccharide trimming by 1-deoxynojirimycin on the nicotinic acetylcholine receptor. *The Journal of biological chemistry,* 261**,** 14825-32.

SOHN, A., KAIDOH, T. & INOUE, T. 1999. Three-dimensional structure of the synaptic contact of the neuromuscular junction in the rat lumbrical muscle. *Archives of histology and cytology,* 62**,** 237-47.

STANLEY, P., SCHACHTER, H. & TANIGUCHI, N. 2009. N-Glycans. *In:* VARKI, A., CUMMINGS, R. D., ESKO, J. D., FREEZE, H. H., STANLEY, P., BERTOZZI, C. R., HART, G. W. & ETZLER, M. E. (eds.) *Essentials of Glycobiology*. 2nd ed. Cold Spring Harbor (NY).

STILES, G. L., CARON, M. G. & LEFKOWITZ, R. J. 1984. Beta-adrenergic receptors: biochemical mechanisms of physiological regulation. *Physiological reviews,* 64**,** 661-743.

STORMS, S. D., KIM, A. C., TRAN, B. H., COLE, G. J. & MURRAY, B. A. 1996. NCAM-mediated adhesion of transfected cells to agrin. *Cell adhesion and communication,* 3**,** 497-509.

STROLLO, R., PONCHEL, F., MALMSTROM, V., RIZZO, P., BOMBARDIERI, M., WENHAM, C. Y., LANDY, R., PERRET, D., WATT, F., CORRIGALL, V. M., WINYARD, P. G., POZZILLI, P., CONAGHAN, P. G., PANAYI, G. S., KLARESKOG, L., EMERY, P. & NISSIM, A. 2013. Auto-antibodies to post translationally modified type II collagen as potential biomarkers for rheumatoid arthritis. *Arthritis and rheumatism*.

SVENNERHOLM, L. 1964. The Gangliosides. *Journal of lipid research,* 5**,** 145-55.

TAJIMA, O., EGASHIRA, N., OHMI, Y., FUKUE, Y., MISHIMA, K., IWASAKI, K., FUJIWARA, M., INOKUCHI, J., SUGIURA, Y. & FURUKAWA, K. 2009. Reduced motor and sensory functions and emotional response in GM3-only mice: emergence from early stage of life and exacerbation with aging. *Behavioural brain research,* 198**,** 74-82.

TAKAMIYA, K., YAMAMOTO, A., FURUKAWA, K., YAMASHIRO, S., SHIN, M., OKADA, M., FUKUMOTO, S., HARAGUCHI, M., TAKEDA, N., FUJIMURA, K., SAKAE, M., KISHIKAWA, M., SHIKU, H. & AIZAWA, S. 1996. Mice with disrupted GM2/GD2 synthase gene lack complex gangliosides but exhibit only subtle defects in their nervous system. *Proceedings of the National Academy of Sciences of the United States of America,* 93**,** 10662-7.

TANIGUCHI, M., KURAHASHI, H., NOGUCHI, S., FUKUDOME, T., OKINAGA, T., TSUKAHARA, T., TAJIMA, Y., OZONO, K., NISHINO, I., NONAKA, I. & TODA, T. 2006. Aberrant neuromuscular junctions and delayed terminal muscle fiber maturation in alpha-dystroglycanopathies. *Human molecular genetics,* 15**,** 1279-89.

TAYLOR, P., LI, Y., CAMP, S., RACHINSKY, T. L., EKSTROM, T., GETMAN, D., FUENTES, M. E., VELLOM, D. C. & RADIC, Z. 1993. Structure and regulation of expression of the acetylcholinesterase gene. *Chemico-biological interactions,* 87**,** 199-207.

TENNESSEN, J. A., BIGHAM, A. W., O'CONNOR, T. D., FU, W., KENNY, E. E., GRAVEL, S., MCGEE, S., DO, R., LIU, X., JUN, G., KANG, H. M., JORDAN, D., LEAL, S. M., GABRIEL, S., RIEDER, M. J., ABECASIS, G., ALTSHULER, D., NICKERSON, D. A., BOERWINKLE, E., SUNYAEV, S., BUSTAMANTE, C. D., BAMSHAD, M. J., AKEY, J. M., BROAD, G. O., SEATTLE, G. O. & PROJECT, N. E. S. 2012. Evolution and functional impact of rare coding variation from deep sequencing of human exomes. *Science,* 337**,** 64-9.

TEPLYAKOV, A., OBMOLOVA, G., BADET, B. & BADET-DENISOT, M. A. 2001. Channeling of ammonia in glucosamine-6-phosphate synthase. *Journal of molecular biology,* 313**,** 1093-102.

THEODORE, M. & MORAVA, E. 2011. Congenital disorders of glycosylation: sweet news. *Current opinion in pediatrics,* 23**,** 581-7.

THIEL, C., SCHWARZ, M., PENG, J., GRZMIL, M., HASILIK, M., BRAULKE, T., KOHLSCHUTTER, A., VON FIGURA, K., LEHLE, L. & KORNER, C. 2003. A new type of congenital disorders of glycosylation (CDG-Ii) provides new insights into the early steps of dolichol-linked oligosaccharide biosynthesis. *The Journal of biological chemistry,* 278**,** 22498-505.

THOMSON, S. R., WISHART, T. M., PATANI, R., CHANDRAN, S. & GILLINGWATER, T. H. 2012. Using induced pluripotent stem cells (iPSC) to model human neuromuscular connectivity: promise or reality? *J Anat,* 220**,** 122-30.

THUSBERG, J. & VIHINEN, M. 2009. Pathogenic or not? And if so, then how? Studying the effects of missense mutations using bioinformatics methods. *Human mutation,* 30**,** 703-14.

TOMASSINI, J. E., MAXSON, T. R. & COLONNO, R. J. 1989. Biochemical characterization of a glycoprotein required for rhinovirus attachment. *The Journal of biological chemistry,* 264**,** 1656-62.

TSUJINO, A., MAERTENS, C., OHNO, K., SHEN, X. M., FUKUDA, T., HARPER, C. M., CANNON, S. C. & ENGEL, A. G. 2003. Myasthenic syndrome caused by mutation of the SCN4A sodium channel. *Proceedings of the National Academy of Sciences of the United States of America,* 100**,** 7377-82.

UMBACH, J. A., ADAMS, K. L., GUNDERSEN, C. B. & NOVITCH, B. G. 2012. Functional neuromuscular junctions formed by embryonic stem cell-derived motor neurons. *PLoS One,* 7**,** e36049.

UNWIN, N. 2005. Refined structure of the nicotinic acetylcholine receptor at 4A resolution. *Journal of molecular biology,* 346**,** 967-89.

USDIN, T. B., EIDEN, L. E., BONNER, T. I. & ERICKSON, J. D. 1995. Molecular biology of the vesicular ACh transporter. *Trends in neurosciences,* 18**,** 218-24.

VAN REEUWIJK, J., JANSSEN, M., VAN DEN ELZEN, C., BELTRAN-VALERO DE BERNABE, D., SABATELLI, P., MERLINI, L., BOON, M., SCHEFFER, H., BROCKINGTON, M., MUNTONI, F., HUYNEN, M. A., VERRIPS, A., WALSH, C. A., BARTH, P. G., BRUNNER, H. G. & VAN BOKHOVEN, H. 2005. POMT2 mutations cause alpha-dystroglycan hypoglycosylation and Walker-Warburg syndrome. *Journal of medical genetics,* 42**,** 907-12.

VARKI, A. 1993. Biological roles of oligosaccharides: all of the theories are correct. *Glycobiology,* 3**,** 97-130.

VARKI, A. & SHARON, N. 2009. Historical Background and Overview. *In:* VARKI, A., CUMMINGS, R. D., ESKO, J. D., FREEZE, H. H., STANLEY, P., BERTOZZI, C. R., HART, G. W. & ETZLER, M. E. (eds.) *Essentials of Glycobiology*. 2nd ed. Cold Spring Harbor (NY).

VINCENT, A., JACOBSON, L. & CURRAN, L. 1998. Alpha-Bungarotoxin binding to human muscle acetylcholine receptor: measurement of affinity, delineation of AChR subunit residues crucial to binding, and protection of AChR function by synthetic peptides. *Neurochemistry international,* 32**,** 427-33.

VINCENT, A., WATERS, P., LEITE, M. I., JACOBSON, L., KONECZNY, I., COSSINS, J. & BEESON, D. 2012. Antibodies identified by cell-based assays in myasthenia gravis and associated diseases. *Annals of the New York Academy of Sciences,* 1274**,** 92-8.

WANAMAKER, C. P. & GREEN, W. N. 2005. N-linked glycosylation is required for nicotinic receptor assembly but not for subunit associations with calnexin. *The Journal of biological chemistry,* 280**,** 33800-10.

WANG, W. W., HAO, H. J. & GAO, F. 2010. Detection of multiple antibodies in myasthenia gravis and its clinical significance. *Chinese medical journal,* 123**,** 2555-8.

WANNENES, F., MAGNI, L., BONINI, M., DIMAURO, I., CAPOROSSI, D., MORETTI, C. & BONINI, S. 2012. In vitro effects of Beta-2 agonists on skeletal muscle differentiation, hypertrophy, and atrophy. *World Allergy Organ J,* 5**,** 66-72.

WARGON, I., RICHARD, P., KUNTZER, T., STERNBERG, D., NAFISSI, S., GAUDON, K., LEBAIL, A., BAUCHE, S., HANTAI, D., FOURNIER, E., EYMARD, B. & STOJKOVIC, T. 2012. Long-term follow-up of patients with congenital myasthenic syndrome caused by COLQ mutations. *Neuromuscular disorders : NMD,* 22**,** 318-24.

WATTY, A. & BURDEN, S. J. 2002. MuSK glycosylation restrains MuSK activation and acetylcholine receptor clustering. *The Journal of biological chemistry,* 277**,** 50457-62.

WATTY, A., NEUBAUER, G., DREGER, M., ZIMMER, M., WILM, M. & BURDEN, S. J. 2000. The in vitro and in vivo phosphotyrosine map of activated MuSK. *Proceedings of the National Academy of Sciences of the United States of America,* 97**,** 4585-90.

WEBSTER, R., BRYDSON, M., CROXEN, R., NEWSOM-DAVIS, J., VINCENT, A. & BEESON, D. 2004. Mutation in the AChR ion channel gate underlies a fast channel congenital myasthenic syndrome. *Neurology,* 62**,** 1090-6.

WEIGERT, C., THAMER, C., BRODBECK, K., GUIRGUIS, A., MACHICAO, F., MACHANN, J., SCHICK, F., STUMVOLL, M., FRITSCHE, A., HARING, H. U. & SCHLEICHER, E. D. 2005. The -913 G/A glutamine:fructose-6-phosphate aminotransferase gene polymorphism is associated with measures of obesity and intramyocellular lipid content in nondiabetic subjects. *The Journal of clinical endocrinology and metabolism,* 90**,** 1639-43.

WESTON, C., YEE, B., HOD, E. & PRIVES, J. 2000. Agrin-induced acetylcholine receptor clustering is mediated by the small guanosine triphosphatases Rac and Cdc42. *The Journal of cell biology,* 150**,** 205-12.

WHITMORE, T. E., MUDRI, S. L. & MCKNIGHT, G. L. 1995. Physical mapping of the human glutamine:fructose-6-phosphate amidotransferase gene (GFPT) to chromosome 2p13. *Genomics,* 26**,** 422-3.

WILCOX, G. 2005. Insulin and insulin resistance. *The Clinical biochemist. Reviews / Australian Association of Clinical Biochemists,* 26**,** 19-39.

WILLISON, H. J. 2005. The immunobiology of Guillain-Barre syndromes. *Journal of the peripheral nervous system : JPNS,* 10**,** 94-112.

WILLISON, H. J., HALSTEAD, S. K., BEVERIDGE, E., ZITMAN, F. M., GREENSHIELDS, K. N., MORGAN, B. P. & PLOMP, J. J. 2008. The role of complement and complement regulators in mediating motor nerve terminal injury in murine models of Guillain-Barre syndrome. *Journal of neuroimmunology,* 201-202**,** 172-82.

WINTERBURN, P. J. & PHELPS, C. F. 1971. Studies on the control of hexosamine biosynthesis by glucosamine synthetase. *The Biochemical journal,* 121**,** 711-20.

WINZEN, U., COLE, G. J. & HALFTER, W. 2003. Agrin is a chimeric proteoglycan with the attachment sites for heparan sulfate/chondroitin sulfate located in two multiple serine-glycine clusters. *The Journal of biological chemistry,* 278**,** 30106-14.

WITZEMANN, V., STEIN, E., BARG, B., KONNO, T., KOENEN, M., KUES, W., CRIADO, M., HOFMANN, M. & SAKMANN, B. 1990. Primary structure and functional expression of the alpha-, beta-, gamma-, delta- and epsilon-subunits of the acetylcholine receptor from rat muscle. *European journal of biochemistry / FEBS,* 194**,** 437-48.

WU, X., RUSH, J. S., KARAOGLU, D., KRASNEWICH, D., LUBINSKY, M. S., WAECHTER, C. J., GILMORE, R. & FREEZE, H. H. 2003. Deficiency of UDP-GlcNAc:Dolichol Phosphate N-Acetylglucosamine-1 Phosphate Transferase (DPAGT1) causes a novel congenital disorder of Glycosylation Type Ij. *Human mutation,* 22**,** 144-50.

WURDE, A. E., REUNERT, J., RUST, S., HERTZBERG, C., HAVERKAMPER, S., NURNBERG, G., NURNBERG, P., LEHLE, L., ROSSI, R. & MARQUARDT, T. 2012. Congenital disorder of glycosylation type Ij (CDG-Ij, DPAGT1-CDG): extending the clinical and molecular spectrum of a rare disease. *Molecular genetics and metabolism,* 105**,** 634-41.

XIA, B., HOYTE, K., KAMMESHEIDT, A., DEERINCK, T., ELLISMAN, M. & MARTIN, P. T. 2002. Overexpression of the CT GalNAc transferase in skeletal muscle alters myofiber growth, neuromuscular structure, and laminin expression. *Developmental biology,* 242**,** 58-73.

XIE, H. Q., LEUNG, K. W., CHEN, V. P., CHAN, G. K., XU, S. L., GUO, A. J., ZHU, K. Y., ZHENG, K. Y., BI, C. W., ZHAN, J. Y., CHAN, W. K., CHOI, R. C. & TSIM, K. W. 2010. PRiMA directs a restricted localization of tetrameric AChE at synapses. *Chemico-biological interactions,* 187**,** 78-83.

YANG, L., MAXWELL, S., LEITE, M. I., WATERS, P., CLOVER, L., FAN, X., ZHANG, D., YANG, C., BEESON, D. & VINCENT, A. 2011. Non-radioactive serological diagnosis of myasthenia gravis and clinical features of patients from Tianjin, China. *Journal of the neurological sciences,* 301**,** 71-6.

YANG, W. H., KIM, J. E., NAM, H. W., JU, J. W., KIM, H. S., KIM, Y. S. & CHO, J. W. 2006. Modification of p53 with O-linked N-acetylglucosamine regulates p53 activity and stability. *Nature cell biology,* 8**,** 1074-83.

YANG, X., SU, K., ROOS, M. D., CHANG, Q., PATERSON, A. J. & KUDLOW, J. E. 2001. O-linkage of N-acetylglucosamine to Sp1 activation domain inhibits its transcriptional capability. *Proceedings of the National Academy of Sciences of the United States of America,* 98**,** 6611-6.

YE, F., MAEGAWA, H., MORINO, K., KASHIWAGI, A., KIKKAWA, R., XIE, M. & SHEN, Z. 2004. A simple and sensitive method for glutamine:fructose-6-phosphate amidotransferase assay. *Journal of biochemical and biophysical methods,* 59**,** 201-8.

YEUNG, W. L., LAM, C. W. & NG, P. C. 2010. Intra-familial variation in clinical manifestations and response to ephedrine in siblings with congenital myasthenic syndrome caused by novel COLQ mutations. *Developmental medicine and child neurology,* 52**,** e243-4.

YOSHIDA, A., KOBAYASHI, K., MANYA, H., TANIGUCHI, K., KANO, H., MIZUNO, M., INAZU, T., MITSUHASHI, H., TAKAHASHI, S., TAKEUCHI, M., HERRMANN, R., STRAUB, V., TALIM, B., VOIT, T., TOPALOGLU, H., TODA, T. & ENDO, T. 2001. Muscular dystrophy and neuronal migration disorder caused by mutations in a glycosyltransferase, POMGnT1. *Developmental cell,* 1**,** 717-24.

ZACHARA, N. E. & HART, G. W. 2006. Cell signaling, the essential role of O-GlcNAc! *Biochimica et biophysica acta,* 1761**,** 599-617.

ZHANG, B., LUO, S., WANG, Q., SUZUKI, T., XIONG, W. C. & MEI, L. 2008. LRP4 serves as a coreceptor of agrin. *Neuron,* 60**,** 285-97.

ZHANG, B., TZARTOS, J. S., BELIMEZI, M., RAGHEB, S., BEALMEAR, B., LEWIS, R. A., XIONG, W. C., LISAK, R. P., TZARTOS, S. J. & MEI, L. 2012. Autoantibodies to lipoprotein-related protein 4 in patients with double-seronegative myasthenia gravis. *Archives of neurology,* 69**,** 445-51.

ZHANG, G., GURTU, V. & KAIN, S. R. 1996. An enhanced green fluorescent protein allows sensitive detection of gene transfer in mammalian cells. *Biochemical and biophysical research communications,* 227**,** 707-11.

ZHOU, J., NEIDIGH, J. L., ESPINOSA, R., 3RD, LEBEAU, M. M. & MCCLAIN, D. A. 1995. Human glutamine: fructose-6-phosphate amidotransferase: characterization of mRNA and chromosomal assignment to 2p13. *Human genetics,* 96**,** 99-101.

ZITMAN, F. M., TODOROV, B., FURUKAWA, K., WILLISON, H. J. & PLOMP, J. J. 2010. Total ganglioside ablation at mouse motor nerve terminals alters neurotransmitter release level. *Synapse,* 64**,** 335-8.

ZOLTOWSKA, K., WEBSTER, R., FINLAYSON, S., MAXWELL, S., COSSINS, J., MULLER, J., LOCHMULLER, H. & BEESON, D. 2013. Mutations in GFPT1 that underlie limb-girdle congenital myasthenic syndrome result in reduced cell-surface expression of muscle AChR. *Human molecular genetics*.

ZOURIDAKIS, M., ZISIMOPOULOU, P., POULAS, K. & TZARTOS, S. J. 2009. Recent advances in understanding the structure of nicotinic acetylcholine receptors. *IUBMB life,* 61**,** 407-23.

Appendix

I. Standard methods

I.1. DNA methods

I.1.1. DNA extraction from bacterial cultures

DNA was extracted from bacterial cell cultures on a small scale using QIAprep Spin Miniprep Kit (QIAGEN, 27106) or on a large scale with PureLink® HiPure Plasmid Filter Maxiprep Kit (Invitrogen, K2100-17) following the manufacturers' protocols.

I.1.2. DNA extraction from mammalian cells

DNA was isolated from mammalian cells using Nucleon BACC 2 Kit (GEN-PROBE, SL8502). The cells were collected, resuspended in 1 ml Reagent A and incubated on ice for 5 minutes. The samples were centrifuged at 1300xg for 5 minutes at 4^{o}C. The supernatants were discarded and the cell pellets were resuspended in 350 µl Reagent B. The samples were deproteinised by an addition of 100 µl sodium perchlorate solution, 600 µl chloroform and 150 µl Nucleon Resin and 1-minute centrifugation at 350xg. Upper phases were transferred to new eppendorf tubes. DNA was precipitated by an addition of 900 µl cold absolute ethanol and pelleted by centrifugation for 5 minutes at 4000xg. The DNA pellets were washed with 70% ethanol, air-dried and redissolved in 50 µl Tris-EDTA (TE) (10 mM Tris, 1 mM EDTA, pH8.0) buffer.

I.1.3. DNA extraction from tissue

DNA was extracted from tissue using DirectPCR® Extraction Reagent (ViagenBiotech, 401-E). The tissue fragments were incubated for 12 hours at 55^{o}C in 100 µl of the reagent supplemented with 1 µl proteinase K (bioWorld, 21560024-1). The proteinase K was heat-inactivated by a 45-minute incubation at 95^{o}C.

I.1.4. Resolution of DNA on agarose gels

DNA fragments were resolved on agarose gels. The concentrations of agarose varied according the size of the DNA fragments. For small fragments higher concentrations of agarose (1.5%-4.0%) were used while larger fragments were resolved on 0.8%-1.0% agarose gels. The gels were prepared by dissolving an appropriate amount of agarose in 1xTBE buffer (90 mM Trizma base, 90 mM boric acid, 2 mM EDTA) supplemented with ethidium bromide to enable visualisation of the DNA fragments with a UV transiluminator. To prevent diffusion on loading and provide a visual indicator while the gels were running, a loading buffer (4 mM bromophenol blue, 0.35 M EDTA, 30% glycerol) was added to the DNA samples. The gels were run in 1xTBE buffer at 50-80 V and analysed using a UV transiluminator. All chemicals were purchased from Sigma.

I.1.5. Extraction of DNA from agarose gels

Appropriate DNA bands were excised from agarose gels and the DNA was purified using QIAquick Gel Extraction Kit (QIAGEN, 28704). The gel slices were weighed and the agarose was disolved by an addition of 3 volumes of Buffer QG to 1 volume of the gel (100 mg ~ 100 µl) and incubation for 10 minutes at 50^{o}C. When the agarose slices had dissolved, 1 volume of isopropanol was added. The mixtures were transferred to QIAquick columns and the columns were centrifuged for 1 minute at 10000rpm. The column membranes were washed with 0.5 ml Buffer QG and 0.75 ml Buffer PE containing ethanol. The DNA was eluted by an addition of 50 µl of nuclease-free water to the columns and 1-minute centrifugation at 10000rpm. The purified DNA samples were stored at -20^{o}C.

I.1.6. DNA digestion

DNA was digested using restriction enzymes purchased from New England Biolabs. The digestions were performed according the manufacturer's recommendations.

I.1.7. Dephosphorylation of DNA fragments

To prevent reannealing of vectors digested with single restriction enzymes, the linearised plasmids were dephosphorylated using antarctic phosphatase (New England Biolabs, M0289). Reaction mixtures were prepared as specified in Table I.1. and incubated for 1 hour at 37°C. The enzyme was heat-inactivated by a 5-minute incubation at 65°C.

Table I.1. Components of DNA dephosphorylation reactions

Component	Amount
10x antarctic phosphatase reaction buffer	2 µl
DNA	1-5 µg
nuclease-free water	to 20 µl
antarctic phosphatase	1 µl (5U)

I.1.8. Purification of DNA fragments from enzymatic reactions

DNA fragments were purified from enzymatic reactions using QIAquick PCR Purification Kit (QIAGEN, 28104). 1 volume of samples was mixed with 5 volumes of Buffer PB. The mixtures were applied to QIAquick columns and the columns were centrifuged for 1 minute at 10000rpm. The column membranes were washed with 0.75 ml PE buffer containing ethanol. The DNA was eluted by an addition of 40 µl nuclease-free water to the centre of the membranes and 1-minute centrifugation at 10000rpm.

I.1.9. Annealing of oligonucleotides

In order to anneal oligonucleotides, equal volumes of both complementary oligonucleotides resuspended in an annealing buffer (10 mM Tris, 50 mM NaCl, 1 mM EDTA, pH7.5-8.0) were mixed at equimolar concentrations. The reactions were incubated at 90ºC for 5 minutes and cooled for 1 hour at room temperature. The sequences of the annealed oligonucleotides are specified in Table I.2.

Table I.2. Sequences of oligonucleotides used in annealing reaction

Construct name	Oligonucleotide name	Oligonucleotide sequence
Myc-COLQ	MycF	CCGGTCGAACAAAAACTTATTTCTGAAGAA GATCTA
Myc-COLQ	MycR	CCGGTAGATCTTCTTCAGAAATAAGTTTTT GTTCGA

I.1.10. DNA ligation

Ligations of DNA fragments were performed using T4 DNA ligase (Roche, 10481220001). The reactions were set up following manufacturer's recommendations, as specified in Table I.3., where x is a calculated amount of insert DNA. All ligations were carried using a molar ratio of 1:3 vector to insert.

Table I.3. Components of ligation reactions

Component	Amount
10x T4 DNA ligase buffer	2 µl
vector DNA	50 ng
insert DNA	x
T4 DNA ligase	2 µl
nuclease-free water	to 20 µl

The reaction mixtures were incubated overnight at 4ºC for cohesive ends and at 16ºC for blunt ends. Control ligations were performed in all experiments. They did not contain insert DNA, thus gave a measure of a background caused by vector

reannealing. 2 µl of the ligation mixes were used to transform 50 µl of competent bacterial cells (Appendix, section I.5.2.).

I.1.11. pGEM®-T Easy cloning

PCR products were cloned into pGEM®-T Easy vector using pGEM®-T Easy Vector System (Promega, A1380). The pGEM®-T Easy plasmid is supplied in a linearised form with single 3' terminal thymidines at both ends, which provide compatible overhangs for PCR products generated by a *Taq* polymerase. The vector also contains an α-peptide coding region of an enzyme β-galactosidase. This allows blue/white screening of recombinants. The ligations of the PCR products with the pGEM®-T Easy vectors were set up following manufacturer's recommendations. The reaction mixes were prepared as specified in Table I.4. and incubated for 1 hour at room temperature.

Table I.4. Components of ligation reactions for inserting PCR products into pGEM®-T-Easy vector

Component	Amount
2x Rapid Ligation Buffer for T4 DNA ligase	5 µl
pGEM®-T Easy vector (50 ng/µl)	1 µl
PCR product	x µl*
T4 DNA ligase	1 µl
nuclease-free water	to 10 µl

* 3:1 molar ratio of PCR product:vector was used

2 µl of the ligation reactions were used for the transformation of JM109 High Efficiency Competent Cells supplied with the kit (Appendix, section I.5.2.). The transformed cells were plated onto lysogeny broth / ampicillin / isopropyl β-D-1-thiogalactopyranoside / 5-bromo-4-chloro-3-indolyl-β-D-galactopyranoside (LB/Amp/IPTG/X-Gal) plates. The plates were incubated overnight at 37°C. A

successful cloning of PCR products into the pGEM®-T Easy vector should interrupt a coding sequence of β-galactosidase. Therefore, clones containing PCR products should produce white colonies.

I.1.12. pJET1.2/blunt cloning

PCR products with blunt ends produced by *PfuUltra* II Fusion HS polymerase (Agilent Technologies, 600670) were cloned into pJET1.2/blunt cloning vector using CloneJET™ PCR Cloning Kit (Fermentas, K1231). The vector was supplied in a linearised form, possessing phosphoryl groups at the 5' blunt ends of the cloning site for a direct ligation of the blunt-end PCR products. The vector also contains a lethal gene, which should be disrupted by the ligation of DNA inserts into the cloning site. As a result, only cells with recombinant plasmids should be able to propagate. The ligations were set up according the manufacturer's recommendations (Table I.5.). They were incubated at room temperature for 5 minutes and used directly for transformation of XL1-Blue *Escherichia coli* strain (Appendix, section I.5.2.).

Table I.5. Components of a ligation reaction for inserting PCR products into pJET1.2/blunt cloning vector

Component	Amount
2x reaction buffer	2 µl
pJET1.2/blunt cloning vector (50 ng/µl)	1 µl
purified PCR product	0.15 pmol ends
T4 DNA ligase	1 µl
nuclease-free water	to 20 µl

I.1.13. Sequencing

Standard sequencing was carried out by WIMM DNA Sequencing Facility.

Only miRNA inserts, which tend to form hairpin structures, were sequenced by Source BioScience LifeSciences, which offered a secondary structure resolution using dGTP BigDye Terminator Ready Reaction Cycle Sequencing Kit.

PCR products were sequenced with primers used in amplification reactions, specified in Chapter 2, section 2.2.1. Other targets were sequenced using primers summarised in Table I.6.

Table I.6. Sequences of the oligonucleotides used for sequencing
The sequences are shown from 5' to 3'.

Target	Primer name	Primer sequence
GFPT1(-L), GFPT1(-L)-EGFP	*GFPT1*cDNA F1	ATTCACAATGGAATCATCACCAACTA
GFPT1(-L), GFPT1(-L)-EGFP	*GFPT1*cDNA F2	GCAAGTGCTGTCATAGAACACACCAA
GFPT1(-L), GFPT1(-L)-EGFP	*GFPT1*cDNA F3	TCAGGTGAGACAGCAGATACTTTGAT
GFPT1(-L), GFPT1(-L)-EGFP	*GFPT1*cDNA F4	TATATGCACTCTGAAGGCATCCTTGC
GFPT1(-L), GFPT1(-L)-EGFP	*GFPT1*cDNA R1	GGATAACTCTCTCCACCAAGGTAGTA
GFPT1(-L)-EGFP	EGFP mid	GACCACATGAAGCAGCACGACTTC
Myc-COLQ-CASPR2TM, COLQ-CASPR2TM, Myc-COLQ	*COLQ*seq F1	GGTCCACCGGGGCTTCCTGGCAAGAC
Myc-COLQ-CASPR2TM, COLQ-CASPR2TM	*COLQ*seq F2	GGTCCAAAAGGTGAACCTGGGATAGC
Myc-COLQ-CASPR2TM, COLQ-CASPR2TM	*COLQ*seq F3	GCATGAGGGTGTGGAGGACTGTGACG
CMV promoter	CMVpcDNA3.1seq	GGCAAGGCTTGACCGACAATTGCATG
inserts cloned into pcDNA™3.1(+), pcDNA™3.1/Hygro(-), pET-22b(+)	T7 pGMT7	TAATACGACTCACTATAGGG
inserts cloned into pcDNA™3.1(+), pcDNA™3.1/Hygro(-), pET-22b(+)	BGHRev	TAGAAGGCACAGTCGAGG

I.2. RNA methods

I.2.1. RNA extraction from mammalian cells and animal tissue

RNA was extracted from mammalian cells and animal tissue using RNeasy Mini Kit (Qiagen, 74104). Pelleted cells were disrupted by an addition of 600 µl Buffer RLT supplemented with 6 µl β-mercaptoethanol and homogenised by passing several times through a blunt 20-gauge needle. Tissue was first disrupted in the same buffer using Precellys®24 and then passed through the needle. 700 µl 70% ethanol was added to the lysates and the mixtures were transferred to RNeasy spin columns, which were centrifuged for 15 seconds at 10000rpm. The columns were washed with 700 µl Buffer RW1, centrifuged and washed twice with 500 µl Buffer RPE. To elute the RNA, 40 µl RNase-free water was added to the column membranes and the columns were centrifuged for 1 minute at 10000rpm.

I.2.2. Removal of DNA from RNA preparations

DNA contamination was removed from RNA samples using TURBO DNA-*free*™ Kit (AM1907, Ambion). The samples were mixed with 0.1 volume of 10x TURBO DNase Buffer and 1 µl TURBO DNase, and incubated for 30 minutes at 37^{o}C. The DNase was inactivated by an addition of 0.1 volume of DNase Inactivation Reagent and a 5-minute incubation at room temperature. The samples were centrifuged for 1.5 minute at 10000xg to pellet the DNase Inactivation Reagent and the purified RNA was transferred to fresh tubes.

I.2.3. siRNA labelling

Small interfering RNA (siRNA) molecules were labelled using *Label* IT®siRNA Tracker Intracellular Localisation CX-Rhodamine kit (Mirus Bio, MIR 7214). The labelling reactions were prepared as specified in Table I.7. and incubated for 1 hour at 37ºC, with a quick spin performed after 30 minutes of the incubation.

Table I.7. Components of siRNA labelling reactions

Component	Amount
10x Labelling Buffer A	10 µl
siRNA duplex (~10 µg)	20 µl of 40 µM stock
***Label* IT®Tracker Reagent**	10 µl
nuclease-free water	to 100 µl

The unreacted *Label* IT® Tracker Reagent was removed from the labelled siRNA by ethanol precipitation. 0.1 volume of 5 M sodium chloride and 2.5 volumes of ice cold 100% ethanol were added to the reactions and the mixes were incubated for 30 minutes at -20ºC. To pellet the labelled siRNA, the reactions were centrifuged for 15 minutes at 15000rpm. The supernatants were removed and the siRNA was washed with 500 µl 70% ethanol. The samples were centrifuged again for 15 minutes at 15000rpm. Traces of ethanol were removed and the siRNA was resuspended in siRNA Dilution Buffer to the final concentration of 40 µM.

I.3. Protein methods

I.3.1. Protein extraction and determination of the protein concentration

Cell pellets were lysed in 100 µl lysis buffer (10 mM Tris, 100 mM NaCl, 1 mM EDTA, 1% Triton X-100, pH7.4) supplemented with 1 µl proteinase inhibitor cocktail (Sigma, P8340) for one hour at 4ºC. To remove cell debris, the samples were centrifuged for 15 minutes at 14000rpm at 4ºC. Supernatants, containing extracted proteins, were transferred to fresh eppendorf microcentrifuge tubes. Protein

concentration in each sample was estimated against bovine serum albumin (BSA) standards using Pierce™ BCA Protein Assay Kit (ThermoScientific, 23227).

I.3.2. Sodium dodecyl sulphate polyacrylamide gel electrophoresis

Proteins were resolved by sodium dodecyl sulphate polyacrylamide gel electrophoresis (SDS-PAGE). Samples containing 15-40 µg protein and SeeBlue® Plus2 Pre-Stained Standard (Invitrogen, LC5925) were loaded onto pre-cast NuPAGE® Novex 4-12% Bis-Tris 1.0 mm gels (Invitrogen, NP0322BOX). The samples were prepared according to the manufacturer's guidelines by the addition of 4xNuPAGE® LDS Sample Buffer (Invitrogen, NP0008) and 10xNuPAGE® Reducing Agent (Invitrogen, NP0004), and heated for 5 minutes at 95ºC before loading. The gels were run at 100 V in 1xNuPAGE® MOPS SDS Running Buffer, which was prepared by diluting 20xNuPAGE® MOPS SDS Running Buffer (Invitrogen, NP0001) in deionised water. Resolved proteins were transferred to Amersham Hybond-P polyvinylidene difluoride (PVDF) membranes (GE Healthcare, RPN303F) prewet in 100% methanol for 10 seconds, washed with distilled water for 5 minutes and preequilibrated for at least 10 minutes in protein transfer buffer prepared by mixing 50 ml 20xNuPAGE® Transfer Buffer (Invitrogen, NP0006), 200 ml 100% methanol and 750 ml deionised water. The blotting procedure was performed using an XCell *SureLock*™ Mini-Cell (Invitrogen, EI0002). The gels containing the protein samples and PVDF membranes were placed in the blot modules, as recommended by the manufacturer. The blot modules were filled with the protein transfer buffer. The blotting procedure was carried out at 30 V for 2 hours. Transfer efficiency was assessed by staining the PVDF membranes with Ponceau Red (Sigma, P7170).

I.3.3. Native polyacrylamide gel electrophoresis

Native proteins were resolved using NativePAGE™ Novex® Bis-Tris Gel System manufactured by Invitrogen. First, 100 µl buffer prepared by mixing 25 µl 4XNativePAGE™ Sample Buffer (Invitrogen, BN2003), 20 µl 5% digitonin (Invitrogen, BN2006), 1 µl proteinase inhibitor cocktail (Sigma, P8340) and 54 µl deionised water were added to pelleted cells and the samples were homogenised by pipetting up and down several times. The lysates were clarified by centrifugation for 30 minutes at 20000xg at 4ºC. Supernatants were collected and NativePAGE™ 5% G-250 Sample Additive (Invitrogen, BN2004) was added to the samples to a final concentration of 0.25%. The prepared samples and the NativeMark™ Unstained Protein Standard (Invitrogen, LC0725) were loaded onto pre-cast NativePAGE™ Novex® 4-16% Bis-Tris Gels (Invitrogen, BN1004BOX) placed in XCell *SureLock*™ Mini-Cell (Invitrogen, EI0002). An inner buffer chamber was filled with 200 ml Dark Blue 1xNativePAGE™ Cathode Buffer prepared by mixing 10 ml 20xNativePAGE™ Running Buffer (Invitrogen, BN2007), 10 ml NativePAGE™ Cathode Additive (Invitrogen, BN2002) and 180 ml deionised water. An outer buffer chamber was filled with 600 ml 1xAnode Buffer prepared by diluting 50 ml 20xNativePAGE™ Running Buffer in 950 ml deionised water. The electrophoresis was performed at 150 V until the dye migration front reached the bottom 1/3rd of the gel. Then the run was paused and the Dark Blue Cathode Buffer was replaced with a Light Blue Cathode Buffer prepared by mixing 10 ml 20xNativePAGE™ Running Buffer, 1 ml NativePAGE™ Cathode Additive and 189 ml deionised water. Further electrophoresis was performed at 150 V until the dye migration front reached the bottom of the gel. The resolved proteins were transferred to Amersham Hybond-P PVDF membranes (GE Healthcare, RPN303F) prewet in 100% methanol for 10 seconds, washed in deionised water for 5

minutes and preequilibrated for at least 10 minutes in a protein transfer buffer prepared by mixing 50 ml 20xNuPAGE® Transfer Buffer (Invitrogen, NP0006) and 950 ml deionised water. The gels and the PVDF membranes were placed in the XCell *SureLock*™ Mini-Cell and the inner buffer chamber was filled with the protein transfer buffer. The outer buffer chamber was filled with 650 ml deionised water. The transfer was performed at 25 V for 1 hour. The membranes were removed from the blot module and incubated for 15 minutes in 20 ml 8% acetic acid to fix the transferred proteins. Finally, they were stained with Ponceau Red (Sigma, P7170) to ensure an equal transfer of the proteins and to visualise the NativeMark™ Unstained Protein Standard.

I.3.4. Fluorescence plate reading

To quantify the expression of fluorescent proteins, total protein was extracted and equal amounts of protein were diluted in 100 µl phosphate buffered saline (PBS). The dilution factor was determined in each experiment to allow the protein fluorescence to be detected before saturation. The 100 µl samples were transferred to Thermo-Fast® 96 PCR Plates (Skirted, Low Profile, opaque black) (Abgene, AB-0800/k). Three wells per sample were used to ensure the reproducibility of the results. The fluorescence was read on a Molecular Devices Spectra Max Gemini XS Microplate Spectrofluorometer (Conquer Scientific) using the settings summarised in Table I.8.

Table I.8. Excitation and emission wavelengths used in fluorescence plate reader measurements

Protein	Excitation wavelength (nm)	Emission Wavelength (nm)
EGFP	472	512

I.3.5. Luciferase activity assay

Luciferase activity assay was used to estimate an increase in the intracellular levels of cyclic adenosine monophosphate (cAMP) upon salbutamol sulphate (Sigma, PHR1053) treatment. Human embryonic kidney cells (HEK293TSA), plated into 24-well Corning® Costar® Cell Culture plates (CLS3527-100EA) at the density of $6x10^4$/well, were transfected with pGL4.29[*luc2P*/CRE/Hygro] plasmid (Promega, E847A) containing cAMP-response element (CRE), which drives the transcription of the luciferase reporter gene *luc2P* (*Photinus pyralis*). 48 hours after the transfection, salbutamol sulphate was added to the medium and the cells were incubated for 6 hours. The luciferase activity following salbutamol sulphate treatment was measured using Bright-Glo™ luciferase assay system (Promega, E2610). The growth medium was exchanged to 100 µl PBS per well and 100 µl Bright-Glo™ Reagent were added into each well. After 5-minute incubation the supernatant was collected and transferred to glass tubes. The activity of the luciferase was measured using Turner Designs TD-20/20 luminometer.

I.4. Glycoprotein and glycolipid methods

I.4.1. PNGaseF treatment

Protein was deglycosylated using protein N-glycosidase F (PNGaseF) (New England Biolabs, P074), which is an endoglycosidase that cleaves N-acetylglucosamine (GlcNAc)-asparagine linkage of N-linked oligosaccharides in glycoproteins. 20 µg protein, 1 µl 10x glycoprotein denaturing buffer and deionised water were mixed to make a 10 µl reaction volume. The mixtures were heated for 10 minutes at 100°C. 2 µl 10x G7 Reaction Buffer (50 mM sodium phosphate, pH7.5 at 25°C), 2 µl 10% nonyl phenoxypolyethoxylethanol (NP40), 5 µl deionised water and 1 µl PNGaseF were

added to the mixtures and the reactions were incubated for 1 hour at 37ºC.

I.4.2. Glycoprotein analyses

Glycoproteins extracted from *in vitro* cultured cells were analysed in collaboration with Prof. Anne Dell and Dr Stuart Haslam at the Imperial College London in The Glycobiology Training, Research and Infrastructure Centre (GlycoTRIC).

To determine N-glycan profiles of wild type and *GFPT1*-mutated human skeletal myoblasts and dermal fibroblasts, the cells were grown in serum-free medium (Cell Progen, M36077-03S for myoblasts or ScienCell, 2311 for fibroblasts) in monolayer cultures until confluent. To collect the cells, the medium was removed and exchanged for a buffer (5 ml chilled PBS with 1 mM $CaCl_2$ and 1 mM $MgCl_2$). The cells were scraped into the buffer, centrifuged and washed 3 times. The cell pellets were resuspended in 1 ml of the buffer, transferred to microfuge tubes and pelleted at 800xg. The supernatants were aspirated and the cell pellets were stored at -80ºC.

To extract proteins, four volumes of ice-cold water were added to the cell pellets and the cells were sonicated on ice in a continuous mode at 40 Amps for 10 seconds. The process was repeated three times, pausing for 15 seconds between each sonication. 2.67 volumes of 100% methanol and 1.33 volumes of chloroform were added to the samples and they were centrifuged for 10 minutes at 3000rpm to pellet the proteins. The upper layers, containing glycolipids, were removed and discarded. 4 droplets of 0.6 M Tris buffer, pH8.5 were added to the pellets to prevent complete drying of the samples and the remaining chloroform was evaporated by placing the samples under a gentle stream of nitrogen for 20 seconds. The dried protein pellets were reduced and carboxymethylated. This was done by the addition of 0.5 ml of 2 mg/ml dithiothreitol (DTT) solution in degassed Tris 0.6 M, pH8.5 buffer and incubation of the samples

for 1 hour at 37°C. Following the incubation, 0.5 ml 12 mg/ml indole-3-acetic acid (IAA) solution was added to the samples and they were kept in the dark for 90 minutes at room temperature. Then they were transferred to dialysis cassettes and dialysed in 50 mM ambic buffer for 24 hours at 4°C, changing the buffer every 8 hours. The dialysed samples were transferred to fresh tubes and lyophilised. The glycoproteins were cleaved into a mixture of peptides and glycopeptides to facilitate efficient release of N-glycans. This was done by an addition of 50 µg trypsin for every 10^6 cells used in the experiment and an incubation of the samples for 14 hours at 37°C. The trypsin solution was prepared by dissolving the trypsin in the ambic buffer to the final concentration of 1 µg/µl. Following the 14-hour incubation, the tryptic digestion was terminated by a 2-minute incubation at 100°C. Peptides and glycopeptides were purified using Oasis®HLB Plus cartridges (Waters, 186000132), which were preconditioned by eluting successively with 5 ml methanol, 5 ml 5% acetic acid, 5 ml 100% propan-1-ol and 3 times with 5 ml 5% acetic acid. The samples were loaded on the prepared cartridges and eluted stepwise with 20 ml 5% acetic acid, 4 ml 20% propan-1-ol and 4 ml 40% propan-1-ol. The 5% acetic acid fraction, which should have contained hydrophilic contaminants was discarded and both propanol fractions were collected and lyophilised. The purified samples were dissolved in 150 µl ambic buffer. 5 U PNGase F were added to the solutions and the samples were incubated for 24 hours. N-glycans were separated from peptides by Sep-Pak purification using Sep-Pak®C_{18} cartridges, which were preconditioned by eluting successively with 5 ml 100% methanol, 5 ml 5% acetic acid, 5 ml 100% propan-1-ol and 3 times with 5 ml 5% acetic acid. The samples were loaded on the preconditioned cartridges and eluted stepwise with 5 ml 5% acetic acid, 3 ml 20% propan-1-ol and 3 ml 40% propan-1-ol. All fractions were collected and lyophilised. The 5% acetic acid fraction, containing

N-glycans, was NaOH permethylated. This was done by adding 1 ml NaOH slurry in anhydrous dimethyl sulphoxide (DMSO) and 600 µl methyl iodide to the samples and incubating for 30 minutes at room temperature on an automatic shaker. The reactions were terminated by the addition of ultra-pure water. The hydrophobic, permethylated N-glycans were extracted by adding 2 ml chloroform. The upper layers, containing DMSO, were removed and discarded, and the bottom layers were washed 4 times with ultra-pure water, dried under a gentle stream of nitrogen and dissolved in 200 µl 50% methanol. The dissolved samples were purified by Sep-Pak®C_{18} purification (Waters, WAT051910). The Sep-Pak®C_{18} cartridges were preconditioned by eluting successively with 3 ml 100% methanol, 3 ml ultra-pure water, 3 ml 100% acetonitrile and 2x3 ml ultra-pure water. The samples were loaded on the cartridges and eluted stepwise with 5 ml ultra-pure water and 3 ml of each 15%, 30%, 50% and 75% aqueous acetonitrile. The 30%, 50% and 75% fractions were collected and lyophilised. The purified N-glycans were resuspended in 10 µl 10% methanol and mixed in 1:1 ratio with a matrix prepared by diluting 3,4-diaminobenzophenone (DABP) in 75% aqueous acetonitrile to make 10 mg/ml solution. 2 µl of the mixtures were spotted on matrix-assisted laser desorption/ionisation-time-of-flight/time-of-flight (MALDI-TOF/TOF) plates and analysed using 4800 *Plus* MALDI TOF/TOF™ Analyser. All reagents, unless stated otherwise, were purchased from Sigma.

I.4.3. Glycolipid analyses

Glycosphingolipids (GSLs) from wild type and *GFPT1*-mutated human skeletal muscle cells were extracted and analysed in collaboration with Dr David Priestman. This was done by extracting GSLs from the cells using chloroform/methanol extraction and releasing glycans by ceramide glycanase digestion. The glycans were

labelled with anthranilic acid (2-amino-benzoic acid; 2-AA) and separated by normal-phase high-performance liquid chromatography (NP-HPLC). The detailed description of the method used can be found in (Neville et al., 2004).

I.5. Bacterial cell culture

I.5.1. Growth conditions

Escherichia coli (strains JM109, DH5α, DH5α™-T1R, XL1-Blue, TOP10) were grown at 37°C in a liquid culture of lysogeny broth (LB) medium (10 g/l NaCl, 10 g/l tryptone, 5 g/l yeast extract purchased from BD Bionutrients) in a shaking incubator or on LB-agar plates.

Antibiotic-resistant bacteria were selected by adding 100 µg/ml ampicillin, 40 µg/ml kanamycin, 25 µl/ml spectinomycin or 33 µg/ml chloramphenicol, respectively, to the medium or the plates. For blue/white screening the transformation mixtures were plated on LB-agar plates containing a respective antibiotic, 80 µg/ml IPTG and 0.5 mM X-Gal. All chemicals, unless stated otherwise, were purchased from Sigma.

I.5.2. Transformations

High efficiency competent bacterial cells, *Escherichia coli* strain JM109 (*end*A1, *rec*A1, *gyr*A96, *thi*, *hsd*R17 (r_k^-, m_k^+), *rel*A1, *sup*E44, Δ(*lac-pro*AB), [F´ *tra*D36, *pro*AB, *laq*$I^qZ\Delta$M15]), were purchased from Promega (Promega, L2001). These were later replaced by an alternative competent bacterial strain, *Escherichia coli* DH5α (*fhuA2*Δ*(argF-lacZ)U169 phoA glnV44* Φ*80* Δ*(lacZ)M15 gyrA96 recA1 relA1 endA1 thi-1 hsdR17*), supplied by New England BioLabs (New Englands BioLabs, C2987I). This was done to avoid the recombination of DNA, which occurred frequently in the JM109 cells. For mutagenesis using GeneArt® Site-Directed Mutagenesis System

(Invitrogen, A13282), One Shot® MAX Efficiency DH5α™-T1R chemically competent cells (*F- φ 80lac ZΔ M15 Δ(lacZYA-argF)U169 recA1 endA1 hsdR17(rk-, mk+) phoA supE44 thi-1 gyrA96 relA1 tonA*) were used. For cloning PCR products into pJET1.2/blunt, XL1-Blue *E.coli* strain (recA1 endA1 gyrA96 thi-1 hsdR17 supE44 relA1 lac [FÅL proAB lacIqZΔM15 Tn10 (Tetr)]) was used.

The appropriate bacterial cells were thawed on ice and 50 µl bacterial glycerol solutions were pipetted to microcentrifuge eppendorf tubes. 10 pg-100 ng DNA were added to the cells. The reactions were carried out according the suppliers' protocols (Table I.9.).

Table I.9. Transformation conditions for bacterial strains used in experiments

	JM109 and XL1-Blue	DH5α	One Shot® MAX Efficiency DH5α™-T1R
incubation on ice	30 minutes	30 minutes	12 minutes
heat shock	45 seconds at 42ºC	30 seconds at 42ºC	30 seconds at 42ºC
incubation on ice	2 minutes	5 minutes	2 minutes

After the final incubation on ice, 950 µl LB medium were added to the transformation mixes and the reactions were incubated at 37ºC for 1 hour with vigorous shaking (250rpm). Finally, the bacteria were spread onto antibiotic-selective plates and incubated overnight at 37ºC. 5-10 colonies were analysed for the presence of correct constructs.

I.6. Mammalian cell culture

I.6.1. Human embryonic kidney cells (HEK293TSA) culture

HEK293TSA cell line was obtained from European Collection of Cell Cultures (ECACC) (85120602).

I.6.1.1. Growth conditions

HEK293TSA were cultured in Corning® Cell Culture flasks in Dulbecco's Modified Eagle Medium (DMEM) (Sigma, D6429) supplemented with 10% foetal calf serum (FCS) (Sigma, F2442) and antibiotics (penicillin, streptomycin. amphotericin B) (Invitrogen, 15240-062) in a humidified 5% CO_2 incubator at 37^{o}C.

I.6.2. TE671 and TE671 DB40 cell culture

Rhabdomyosarcoma TE671 cell line was obtained from American Type Culture Collection (ATCC) (CRL-8805). These were stably transfected with plasmids encoding human AChR β, δ and ε subunits to establish a cell line (TE671 DB40) with high expression of adult subtype of AChR (Beeson et al., 1996a, Beeson et al., 1996b).

I.6.2.1. Growth conditions

TE671 and TE671 DB40 cells were cultured in Corning® Cell Culture flasks in DMEM (Sigma, D6429) supplemented with 10% FCS (Sigma, F2442) and antibiotics (penicillin, streptomycin. amphotericin B) (Invitrogen, 15240-062) in a humidified 5% CO_2 incubator at 37^{o}C.

I.6.3. C2C12 cell culture

Mouse C3H muscle cell line (C2C12) was obtained from ECACC (91031101).

I.6.3.1. Growth conditions

C2C12 myoblasts were grown in Corning® Cell Culture flasks in DMEM (Sigma, D6429) supplemented with 15% FCS (Sigma, F2442) and antibiotics (penicillin, streptomycin. amphotericin B) (Invitrogen, 15240-062) in a humidified 5% CO_2 incubator at 37ºC.

I.6.3.2. Differentiation conditions

Fusion of C2C12 myoblasts into multinucleated myotubes was induced by serum starvation. DMEM (Sigma, 6429) containing 15% FCS and antibiotics (penicillin, streptomycin. amphotericin B) (Invitrogen, 15240-062) was exchanged to DMEM supplemented with 2% horse serum (HS) (Sigma, H1138) and the antibiotics. Following that, the cells were cultured in a humidified 5% CO_2 incubator at 37ºC, replacing the medium every day, until the myotubes were formed (usually 5-7 days).

I.6.4. Transfections

I.6.4.1. Polyethylenamine transfections

$3x10^5$ HEK293TSA were seeded in each well of 6-well Corning® Costar® Cell Culture plates (Corning, CLS3516-50EA). Transfection mixes containing 2.5-100 nM siRNA or 1-4 µg DNA, 1.25 µl 20% glucose in nuclease-free water (filtered before use), 1.5 µl polyethylenamine (PEI) (45 mg PEI, 8 ml distilled water, pH7.2 with HCl, filtered before use), nuclease-free water up to 6.5 µl and 1 ml growth medium, were applied into each well. 12 hours after the transfection, the transfection mixes were

replaced with 2 ml fresh growth medium and the cells were cultured for 24, 48 or 72 hours. If necessary, the reactions were scaled down to a 24-well format.

I.6.4.2. Lipofectamine®LTX transfections

Lipofectamine®LTX & Plus Reagent (Invitrogen, 15338-030) were used for the delivery of DNA into human primary fibroblasts. $3x10^5$ cells were seeded in each well of 6-well Corning® Costar® Cell Culture plates (Corning, CLS3516-50EA). The medium was changed to 2 ml/well fresh FM-sf serum-free medium (ScienCell, 2311) and the DNA-lipofectamine mixes were prepared. This was done by diluting 3 µg DNA mixed with 3 µl Plus Reagent in 150 µl Opti-MEM® Reduced-Serum Medium (Gibco®, 11058-021) and incubating the mixtures for 5 minutes at room temperature. After the 5 minutes, 10 µl Lipofectamine®LTX diluted in 150 µl Opti-MEM® Reduced-Serum Medium were added to the mixtures, which were subsequently incubated for 30 minutes at room temperature. The complexes were added directly to the cells. After 6 hours, the transfection mixes were exchanged to fresh medium.

I.6.4.3. Lipofectamine®RNAiMAX transfections

Lipofectamine®RNAiMAX (Invitrogen, 13778030) was used for a delivery of siRNA into TE671 and TE671 DB40 cell line. $3x10^5$ cells were seeded in each well of 6-well Corning® Costar® Cell Culture plates (Corning, CLS3516-50EA). Growth medium was changed to 2.5 ml/well fresh growth medium not containing antibiotics and the transfection mixes, containing 1.5 µl 100 µM siRNA, 5 µl lipofectamine®RNAiMAX and 493.5 µl Opti-MEM® Reduced-Serum Medium (Gibco®, 11058-021) were prepared, incubated for 15 minutes at room temperature and added to the cells. If necessary, the reactions were scaled down to a 24-well format according to the

lipofectamine®RNAiMAX manufacturer's recommendations. 12 hours after the transfection, the transfection mixes were replaced with 2 ml fresh growth medium and the cells were cultured for 48 hours.

I.6.4.4. Electroporations

TE671 and TE671 DB40 cells were transfected with DNA and/or siRNA using Neon® Transfection System (Invitrogen, MPK5000). $6.25x10^5$ cells were transferred to eppendorf tubes and centrifuged at 1200rpm for 5 minutes, washed with PBS, pelleted using the same settings and resuspended in 125 µl Resuspension Buffer R. An appropriate amount of DNA (0.5-3 µg/well of 6-well plate) or siRNA (final concentration 100 nM) was added to the cells. 100 µl of the cells-DNA/siRNA mixture was aspirated into the Neon™ Tip attached to the Neon™ Pipette and the tip was inserted into the Neon™ tube filled with 3 ml Electrolytic Buffer E2. One 30-second pulse at 1100 V was applied and the cells were transferred into 2 ml prewarmed growth medium.

I.6.5. Single channel recordings

Single channel analysis was performed by Richard Webster using methods previously described (Hamill et al., 1981, Webster et al., 2004). Briefly, cells were subjected to cell-attached patch recordings with 100 nM acetylcholine (ACh) added to pipette solution to stimulate low levels of AChR activity. Channel burst activity was analysed and fit by 3 simultaneous exponential populations in pClamp 10 software (Molecular Devices).

I.7. *in vivo* techniques

I.7.1. Injections

I.7.1.1. Intramuscular injections

Tibialis anterior muscle, which lies close to the surface of a mouse leg, was the target for intramuscular injections of DNA because it is easily accessible for both injections and electroporations. After pretreatment with a non-steroidal anti-inflammatory drug (Meloxicam) at 0.3 mg/kg, the mice were anaesthetised with isofluorane and the DNA was injected into the muscle using a BD Micro-Fine 0.3 mm (30G) x 8 mm needle.

I.7.1.2. Intraperitoneal injections

An anaesthetic – hypnorm – was delivered via intraperitoneal injection. The injection was given in the lower left quadrant of the abdomen using a BD Micro-Fine 0.3 mm (30G) x 8 mm needle.

I.7.1.3. Subcutaneous injections

Subcutaneous injections containing an analgesic – metacam – were given into the scruff of the neck using a BD Micro-Fine 0.3 mm (30G) x 8 mm needle.

I.7.2. Electroporations

Electroporations were performed under isoflurane-maintained general anaesthesia, following injection of DNA into a tibialis anterior muscle. They were conducted using a BTX® ECM 830 generator and BTX® 1.0 cm x 1.0 cm caliper electrodes with the following settings: 225 V/cm, 8 pulses (after 4 pulses, the polarity across the electrodes was reversed), 20 ms duration, 1 second interval between pulses, 1 Hz frequency. To

ensure a good contact between the electrodes and the leg, the animal's fur was removed using hair removal cream and conductive gel was applied on the skin.

I.8. Bioinformatics predictions

The consequences of single base substitutions in *GFPT1*, identified in affected individuals, were predicted using web-based bioinformatics tools. The pathogenicity of the mutations were analysed using PolyPhen2.0 (http://genetics.bwh.harvard.edu/pph2/) (Adzhubei et al., 2010). Effects of the substitutions on the mRNA splicing were analysed with Spliceman web server (http://fairbrother.biomed.brown.edu/spliceman/index.cgi) (Lim and Fairbrother, 2012). Changes in the intramolecular interactions and effects of the mutations on the tertiary and the quaternary structures were analysed using PDBePisa (http://www.ebi.ac.uk/msd-srv/prot_int/) (Krissinel and Henrick, 2007) and PyMOL v1.5 software (Schrodinger, 2010).

I.9. Statistical analysis

Statistics were calculated with GraphPad® Prism 6 using a two-tailed unpaired student t-test, ANOVA or 2-way ANOVA with Bonferroni multiple comparison post-test. A p value of <0.05 was a predetermined threshold for statistical significance.

II. Standard buffers

II.1. Phosphate Buffered Saline (PBS)

Phosphate Buffered Saline (PBS) (3.2 mM Na_2HPO_4, 0.5 mM KH_2PO_4, 1.3 mM KCl, 135 mM NaCl) was prepared by dissolving phosphate buffered saline Dulbecco 'A' tablets (Fisher Scientific, BR014G) in deionised water according manufacturer's protocol.

II.2. Phosphate Buffered Saline – Tween 20 (PBST)

Phosphate Buffered Saline – Tween 20 (PBST) (3.2 mM Na_2HPO_4, 0.5 mM KH_2PO_4, 1.3 mM KCl, 135 mM NaCl, 0.05% Tween 20, pH 7.4) was prepared by dissolving phosphate buffered saline Dulbecco 'A' tablets (Fisher Scientific, BR014G) in deionised water according manufacturer's protocol and then supplementing the buffer with Tween 20 (Sigma, P9416) to a final concentration of 0.05%.

II.3. Tris/Borate/EDTA (TBE)

Tris/Borate/EDTA buffer (TBE) (90 mM Trizma base, 90 mM boric acid, 2 mM EDTA) was prepared as 5x concentrated stock by dissolving 54g Trizma base, 27.5 g boric acid and 20 ml 0.5 M EDTA in 1 l deionised water. All chemicals were purchased from Sigma.

III. Outline of cloning of *GFPT1* and *GFPT1-L* cDNA, and glycosylation markers

All constructs described in this section were sequenced to ensure the lack of any nucleotide changes. The primer sequences used in the sequencing reactions, site-directed mutagenesis and for cloning of specific inserts are specified in Chapter 2 and Appendix I.

III.1. Cloning of human *GFPT1* and *GFPT1-L*

L-glutamine:D-fructose-6-phosphate amidotransferase 1 (GFAT1) is the first and rate-limiting enzyme of a hexosamine biosynthetic pathway. It exists as two splice variants with alternatively spliced exon 9. The short isoform (*GFPT1*) is ubiquitously expressed in all tissues, while the long one, designated as *GFPT1-L*, is predominantly expressed in skeletal and heart muscle (DeHaven et al., 2001, Niimi et al., 2001). Both *GFPT1* isoforms were cloned into expression constructs.

III.1.1. Cloning of human *GFPT1-L*

Human *GFPT1* cDNA was commercially available in a pBluescript vector as an I.M.A.G.E clone (Unigene ID: Hs.580300, Source BioScience). This was a non-muscle *GFPT1* isoform, which additionally contained a long fragment of intronic DNA and a long 3' untranslated region (3'UTR) (Figure III.1.).

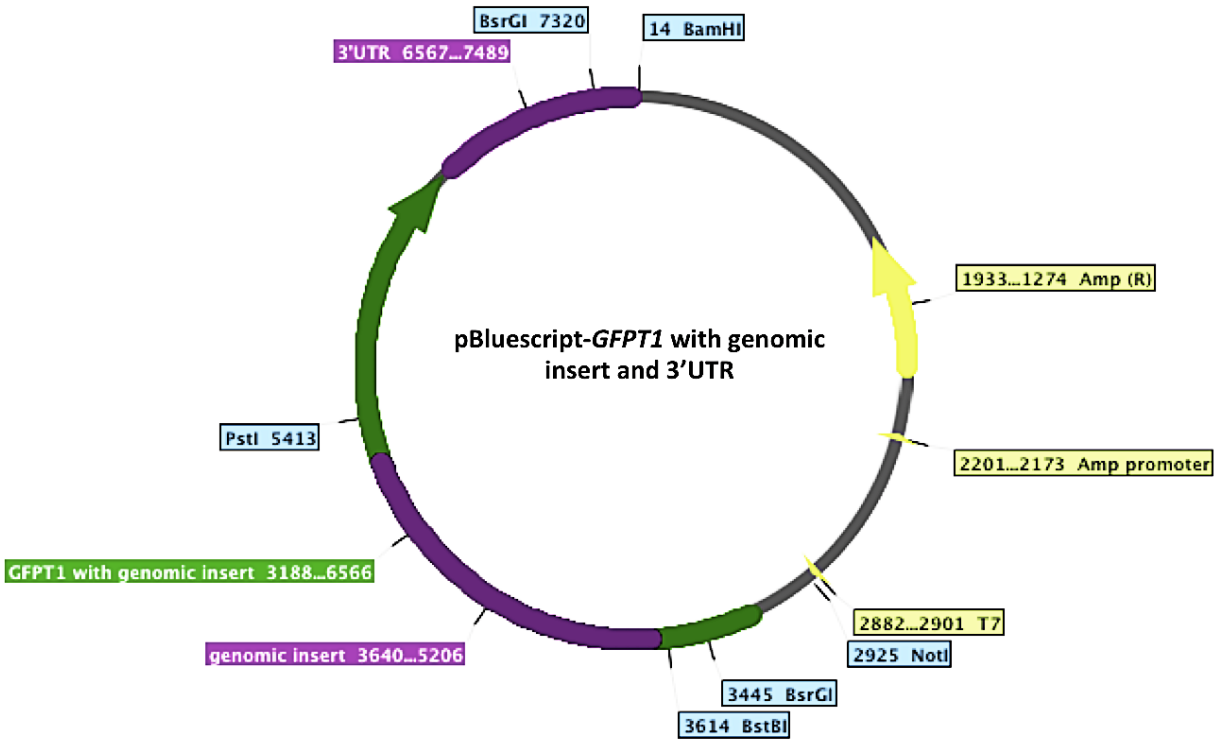

Fig.III.1. Schematic representation of a pBluescript plasmid encoding GFAT1 (dark green) with genomic insert (purple) and 3'UTR (purple)

To remove the intronic fragment and to introduce a muscle-specific exon into the construct, the alternatively spliced exon was first amplified from human cDNA using primers introducing *BstBI* and *PstI* restriction sites at 5' and 3' ends of the polymerase chain reaction (PCR) products, respectively. *Taq* polymerase was chosen for the amplification since it adds additional adenine (A) overhangs at the 3' ends of PCR products. This feature enabled direct cloning of the amplified fragments into pGEMT®-T-Easy vector (Promega, A1360), supplied in a linear form with thymine (T) 3' overhangs. Another feature of the vector is the location of a multiple cloning site (MCS) within an α-peptide coding region of β-galactosidase. The introduction of the target insert should lead to disruption of the α-peptide and allow blue/white screening of the recombinant clones on indicator plates (Figure III.2.).

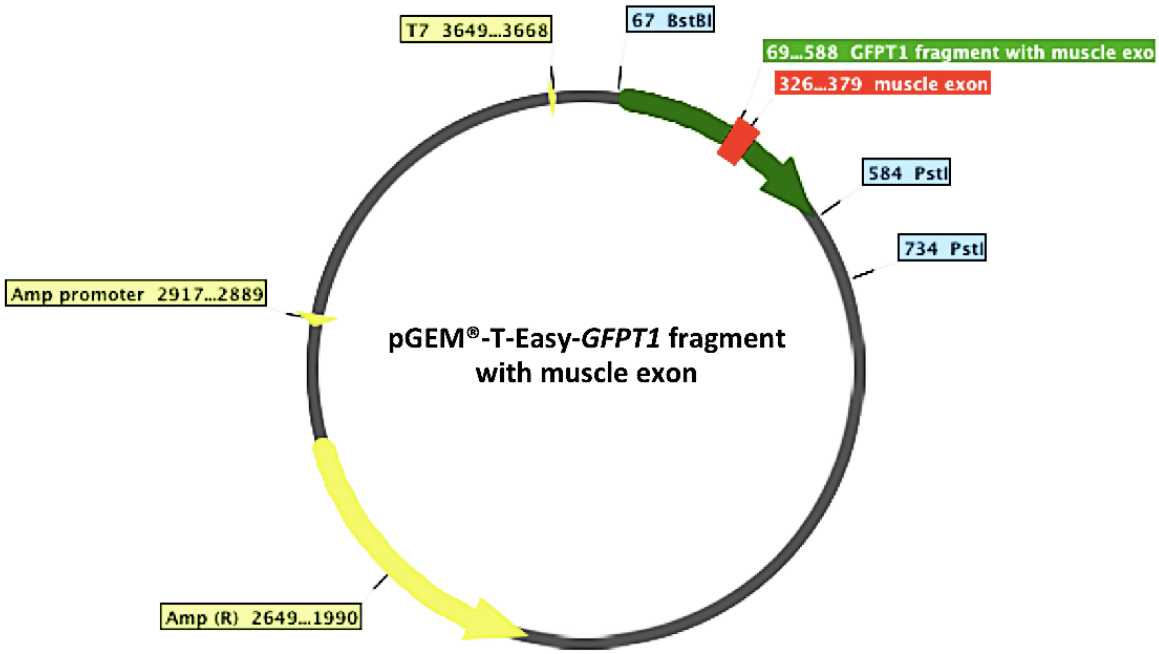

Fig.III.2. Schematic representation of a pGEM®-T-Easy plasmid encoding a fragment of GFAT1 (dark green) encompassing muscle-specific exon (red)

pBluescript-*GFPT1* and pGEM®-T-Easy with the insert encompassing the muscle-specific exon were digested with *BstBI* and *PstI* restriction enzymes. The backbone (pBluescript-*GFPT1*) and the insert (muscle-specific exon) were ligated. The ligation products were digested with *BsrGI* endonuclease to identify correct constructs.

To achieve a high expression of the target gene in mammalian cells, the *GFPT1-L* cDNA was subcloned to a mammalian expression vector pcDNA™3.1/Hygro(-) (Invitrogen, V87520) using *NotI* and *BamHI* restriction sites present in the MCS of both pcDNA™3.1/Hygro(-) and pBluescript vectors (Figure III.3.). Both plasmids were digested with the endonucleases and the appropriate DNA fragments were ligated. The ligation products were analysed by digestion with a *BsrGI* restriction enzyme.

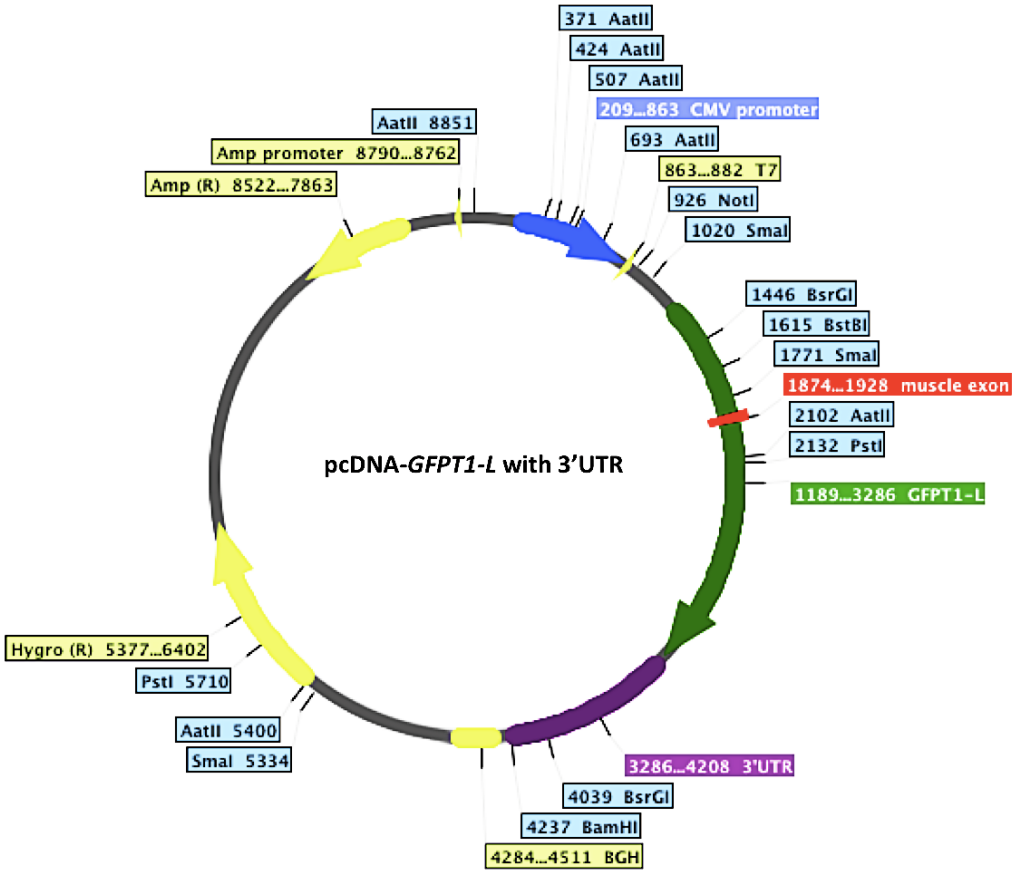

Fig.III.3. Schematic representation of pcDNA™3.1/Hygro(-) plasmid encoding GFAT1-L (dark green) with muscle exon (red) and 3'UTR (purple)

III.1.2. Cloning of human *GFPT1*

The next step was to clone a ubiquitously expressed *GFPT1* isoform, lacking the muscle-specific exon (Figure III.4.). This was done by removal of the additional exon using GeneArt® Site-Directed Mutagenesis System (Invitrogen, A13282) and a mutagenesis primer pair.

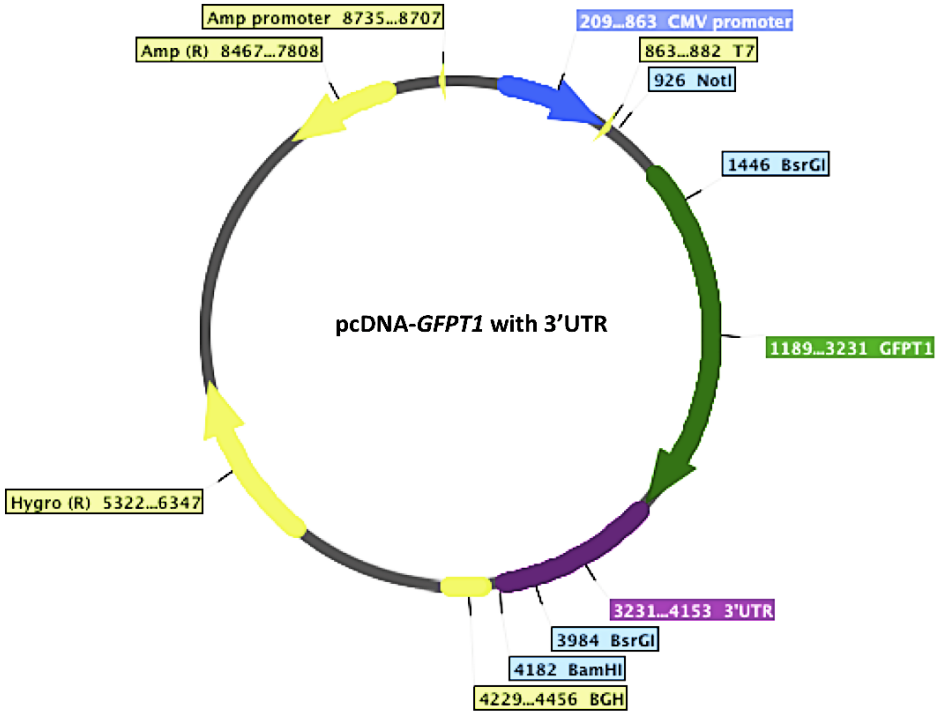

Fig.III.4. Schematic representation of pcDNA™3.1/Hygro(-) plasmid encoding GFAT1 (dark green) with 3'UTR (purple)

III.1.3. Introduction of the mutations identified in *GFPT1* patients into pcDNA-*GFPT1-L* and pcDNA-*GFPT1*

GFPT1 congenital myasthenic syndrome (CMS) is a myasthenic disorder affecting predominantly the transmission of the signal at the neuromuscular junction (NMJ). Therefore, the muscle-specific *GFPT1-L* isoform was chosen for most of the investigations and the amino acid substitutions identified in *GFPT1* patients (p.T15M, p.R385H, p.R434H and p.R496W) were introduced into pcDNA-*GFPT1-L*, respectively (Figure III.5.A). Only the variant p.T479N, which was identified in two related individuals who presented with a severe multisystem disorder, was introduced into the non-muscle *GFPT1* isoform (Figure III.5.B). The mutations were introduced using GeneArt® Site-Directed Mutagenesis System (Invitrogen, A13282) and respective primer pairs.

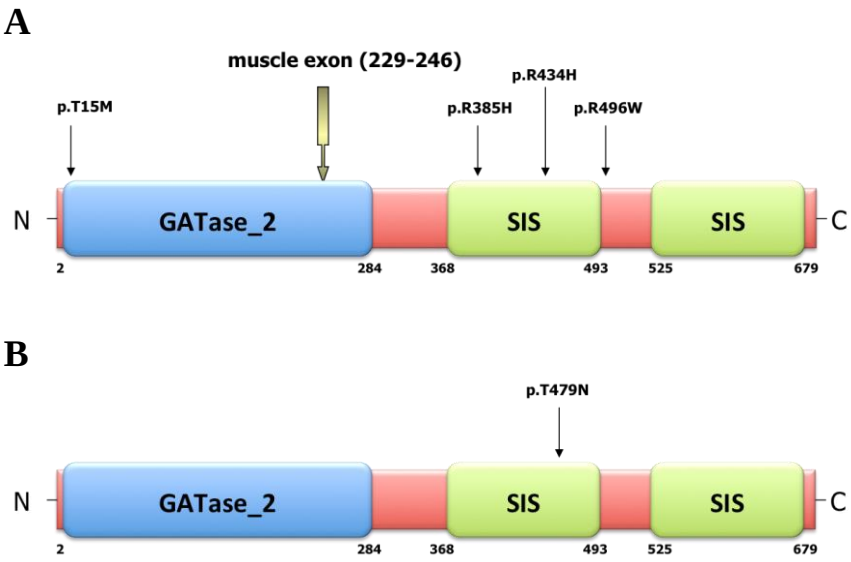

Fig.III.5. Schematic representation of (A) GFAT1-L and (B) GFAT1, and the mutations identified in the protein in (A) CMS patients or (B) individuals diagnosed with a multisystem disorder GATase_2 – glutaminase domain type 2; SIS – sugar isomerase domain

III.1.4. Cloning of *GFPT1-L-EGFP* (C-terminally tagged)

To follow expression and localisation of the over-expressed GFAT1-L *in vitro* and *in vivo*, an enhanced green fluorescent protein (EGFP) was fused to the C-terminus of GFAT1-L (Figure III.6.).

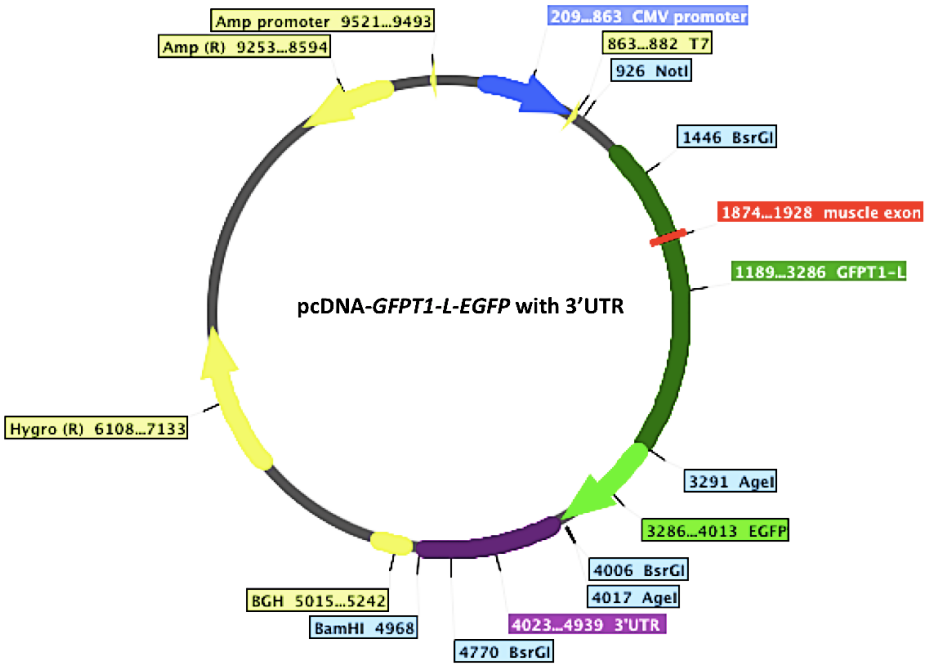

Fig.III.6. Schematic representation of a pcDNA™3.1/Hygro(-) plasmid encoding GFAT1-L (dark green) with muscle exon (red), C-terminal EGFP tag (fluorescent green) and 3'UTR (purple)

First, an appropriate restriction site – *AgeI*, which could have been used for the C-terminal fusion with EGFP was introduced into a pcDNA-*GFPT1-L* with 3'UTR construct. This was done using GeneArt® Site-Directed Mutagenesis System (Invitrogen, A13282) and mutagenesis primers.

Next, *EGFP* cDNA was amplified from the pEGFP-N1 vector (Clontech, 6085-1) using primers introducing *AgeI* restriction sites at both ends of the PCR products. *Taq* polymerase was used for amplification since it enabled a direct cloning of the PCR products into a pGEM®-T-Easy vector (Promega, A1360). The constructs containing the inserts were selected by blue/white screening and sequenced to identify correct plasmids.

The *AgeI*-mutated pcDNA-*GFPT1-L* and the pGEM®-T-Easy-*EGFP* were then digested with an *AgeI* restriction enzyme. The pcDNA-*GFPT1-L* backbone was also dephosphorylated to prevent self-ligation. Then it was ligated with an *EGFP* insert and orientation of the *EGFP* cDNA was confirmed by digestion with a *BsrGI* endonuclease.

III.1.5. Cloning of *GFPT1-EGFP* (C-terminally tagged)

Plasmid encoding GFAT1 tagged with EGFP at its C-terminus was created by a removal of an additional 54-base pair exon from pcDNA-*GFPT1-L-EGFP* in a mutagenesis reaction using GeneArt® Site-Directed Mutagenesis System (Invitrogen, A13282) and mutagenesis primers (Figure III.7.).

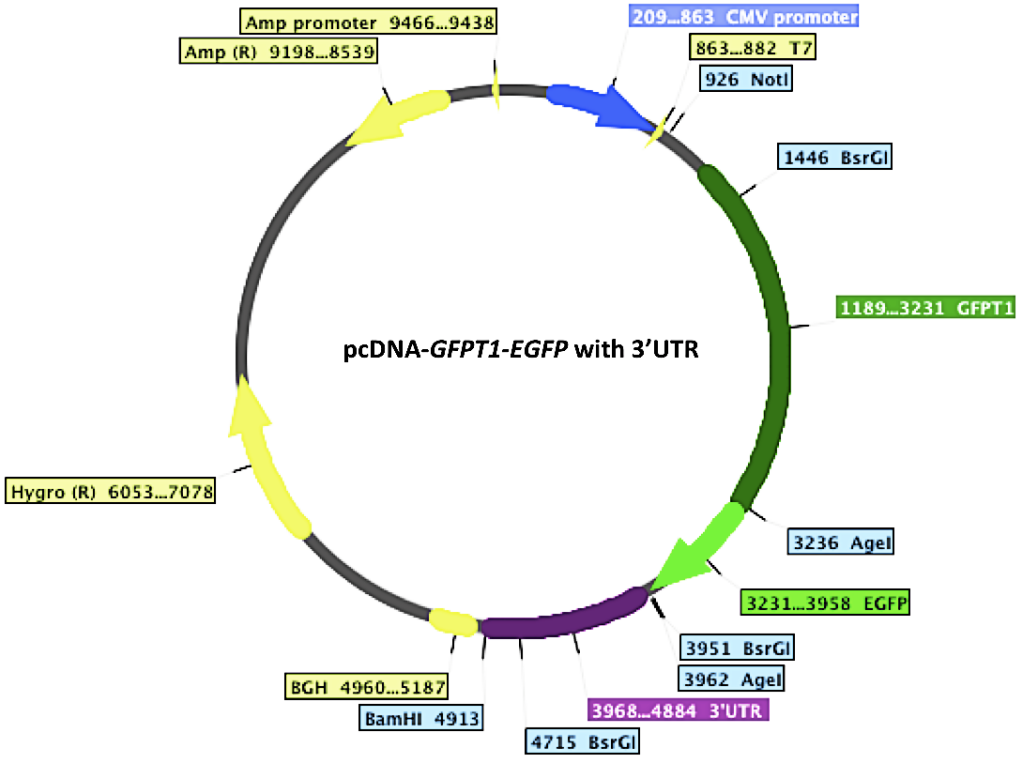

Fig.III.7. Schematic representation of pcDNA™3.1/Hygro(-) plasmid encoding human GFAT1 (dark green) with C-terminal EGFP tag (fluorescent green) and 3'UTR (purple)

III.1.6. Removal of 3'UTR from all plasmids encoding GFAT1-L, GFAT1, GFAT1-L-EGFP and GFAT1-EGFP

Despite cloning the cDNA encoding GFAT1-L, GFAT1, GFAT1-L-EGFP and GFAT1-EGFP into pcDNA™3.1/Hygro(-) (Invitrogen, V87520), which possesses a human cytomegalovirus (CMV) immediate-early promoter that drives high expression of the target gene in a wide range of mammalian cells, GFAT1 did not exhibit high expression in human embryonic kidney cells (HEK293TSA). One possible cause of a relatively low expression was the presence of a long 3'UTR in the constructs. Therefore, the fragment was removed from all the plasmids (Figures III.8., III.9., III.10. and III.11.).

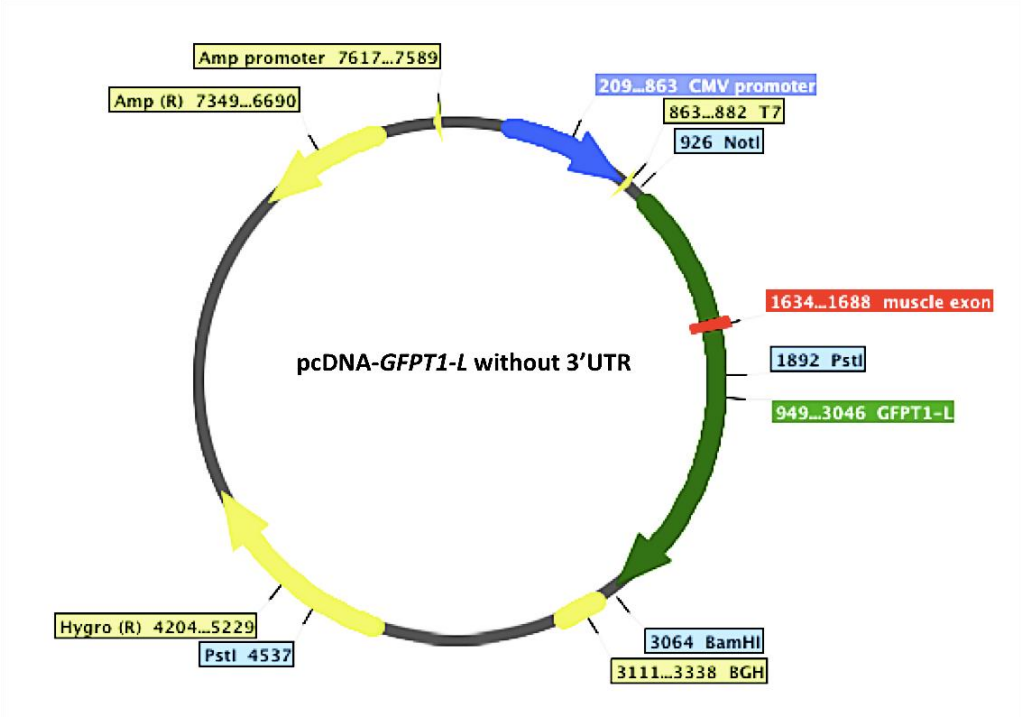

Fig.III.8. Schematic representation of pcDNA™3.1/Hygro(-) plasmid encoding GFAT1-L (dark green) with muscle exon (red)

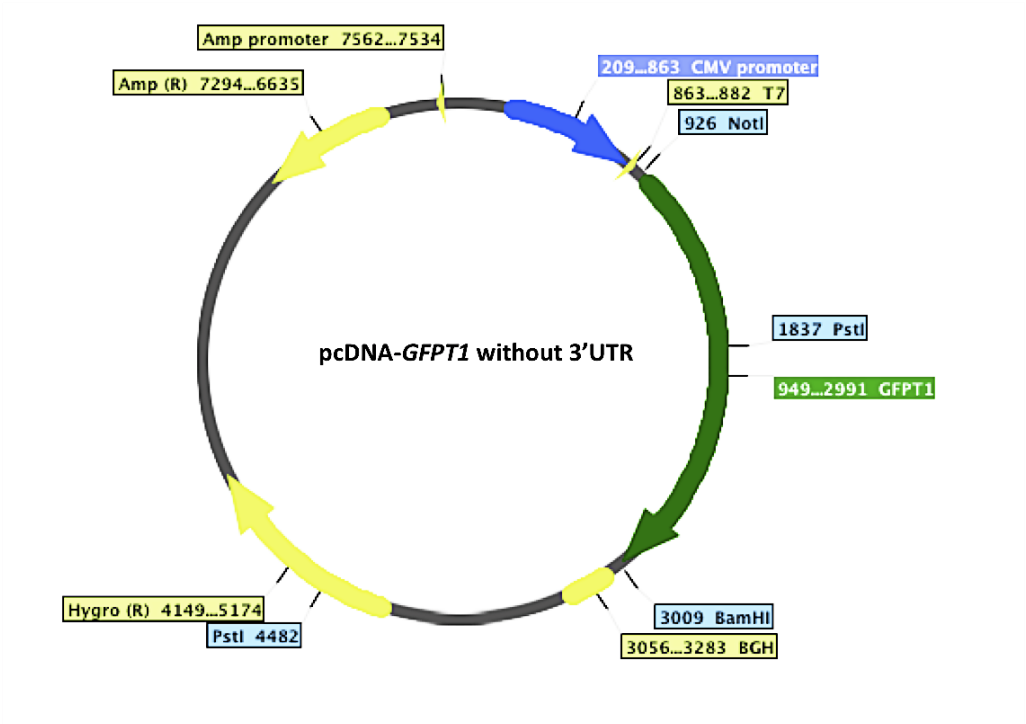

Fig.III.9. Schematic representation of pcDNA™3.1/Hygro(-) plasmid encoding GFAT1 (dark green)

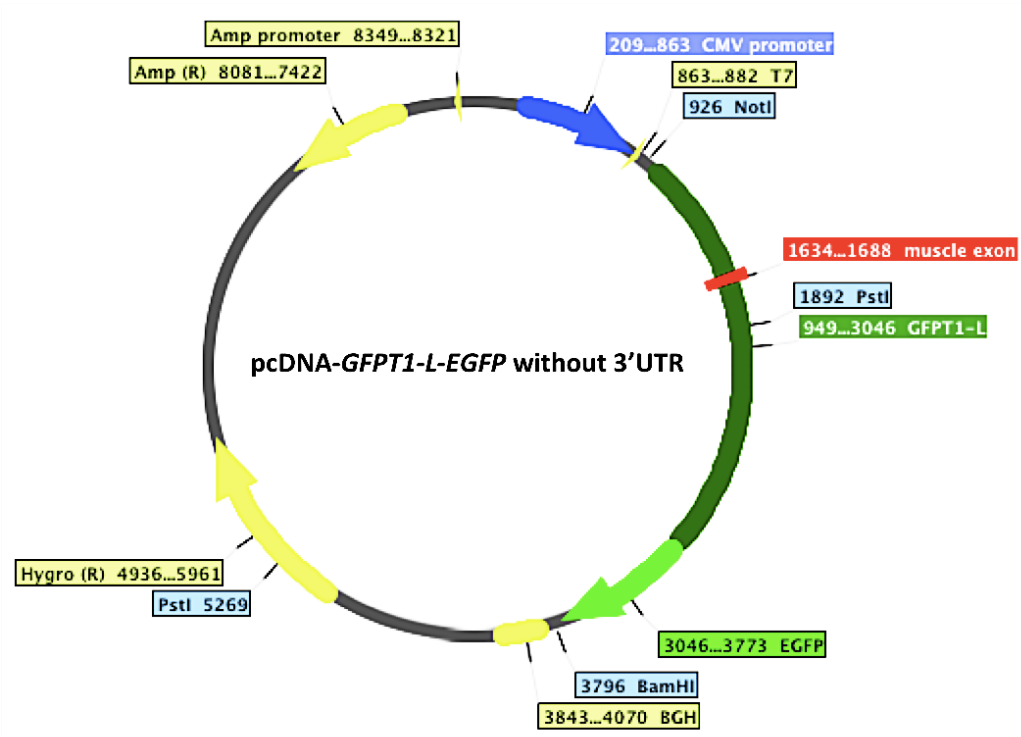

Fig.III.10. Schematic representation of pcDNA™3.1/Hygro(-) plasmid encoding GFAT1-L (dark green) with muscle exon (red) and a C-terminal EGFP tag (fluorescent green)

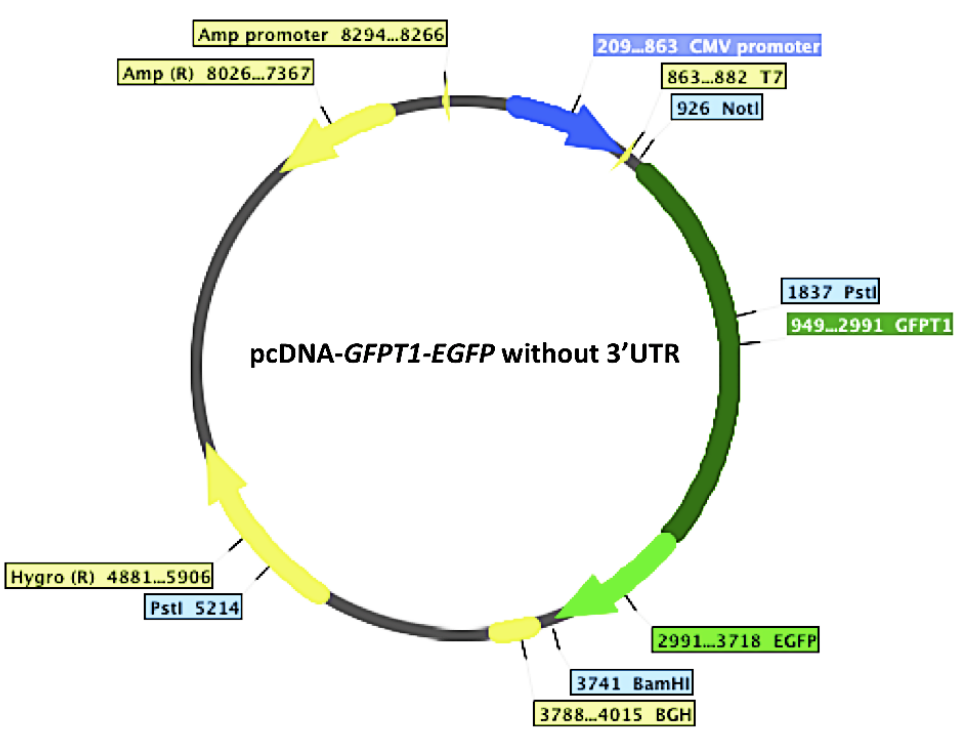

Fig.III.11. Schematic representation of pcDNA™3.1/Hygro(-) plasmid encoding GFAT1 (dark green) with a C-terminal EGFP tag (fluorescent green)

GFPT1-L, *GFPT1*, *GFPT1-L-EGFP* and *GFPT1-EGFP* cDNA were amplified from respective pcDNA™3.1/Hygro(-) plasmids using primers introducing *NotI* and *BamHI* restriction sites at the 5' and the 3' ends of the PCR products, respectively. The amplification reactions were performed using a proof-reading polymerase *PfuUltra* II Fusion HS (Agilent Technologies, 600670) to reduce the probability of PCR-induced mutations. This enzyme produced blunt-end PCR products, which were directly cloned into pJET1.2/blunt Cloning Vector (Fermentas, K1231), supplied as a digested blunt-end backbone. Presence of the desired inserts was confirmed by digestion of the ligation products with a *BlgI* endonuclease. The correct pJET1.2 plasmids, encoding respective GFAT1 proteins, and an empty pcDNA™3.1/Hygro(-) vector (Invitrogen, V87520) were then digested with *NotI* and *BamHI* restriction enzymes, and the appropriate DNA fragments were ligated. The constructs were confirmed by digestion with a *PstI* enzyme.

III.1.7. Cloning of *GFPT1* into pET-22b(+)

To achieve a high expression of GFAT1 in *Escherichia coli*, *GFPT1* cDNA was cloned into pET-22b(+) vector (Merck Millipore, 69744) (Figure III.12.). This was done by Dr Janet Kenyon.

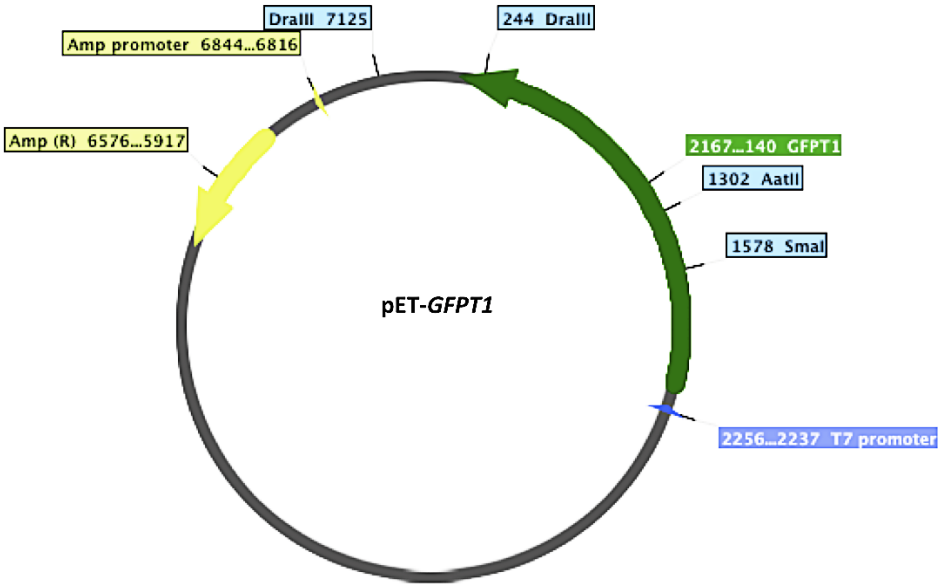

Fig.III.12. Schematic representation of pET-22b(+) plasmid encoding GFAT1 (dark green)

The pET system allows cloning of target genes under a control of a strong bacteriophage T7 promoter. Expression of the proteins can be then induced by providing the respective plasmid and a source of T7 RNA polymerase in the host cell.

III.1.8. Cloning of *GFPT1-L* into pET-22b(+)

The muscle-specific *GFPT1-L* isoform was also cloned into pET-22b(+) vector (Merck Millipore, 69744) for its efficient expression in a bacterial system (Figure III.13.).

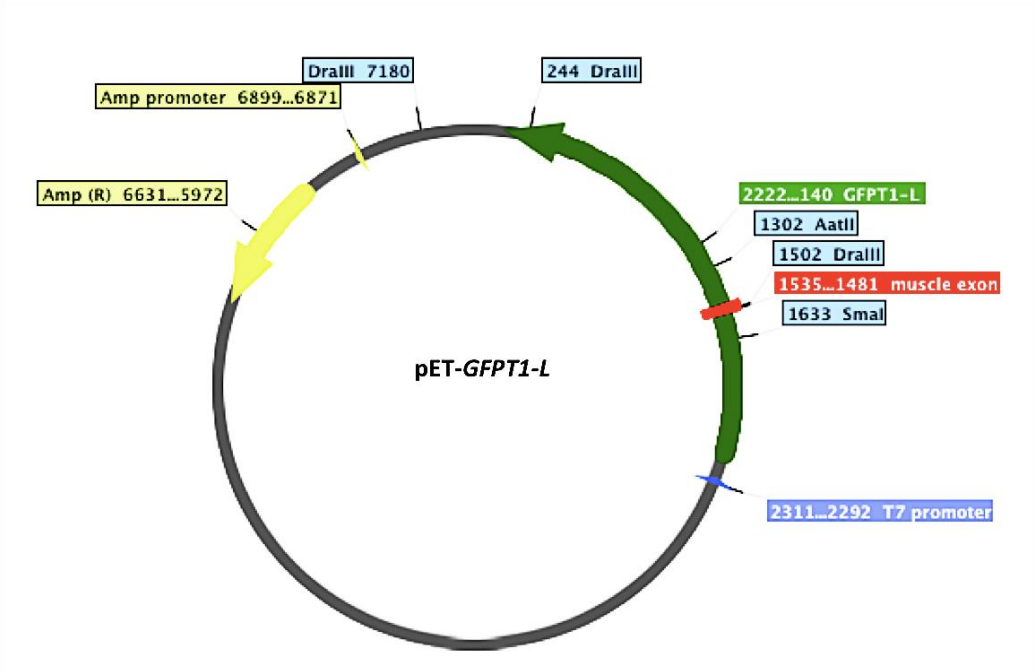

Fig.III.13. Schematic representation of pET-22b(+) plasmid encoding GFAT1-L (dark green) with muscle exon (red)

The cloning procedure was designed in a way to exchange a part of *GFPT1* cDNA to a fragment of *GFPT1-L* cDNA containing the muscle-specific exon. The restriction sites used are available in *GFPT1* and *GFPT1-L* sequences. Both pET-*GFPT1* and pcDNA-*GFPT1-L* with 3'UTR were digested with *AatII* and *SmaI* endonucleases. Additionally, the pcDNA-*GFPT1-L* with 3'UTR plasmid was digested with a *NotI* enzyme to facilitate the separation of the appropriate DNA fragment. The digested pET-*GFPT1* backbone was then ligated with the insert digested out of pcDNA-*GFPT1-L*. The success of the ligation was verified using a *DraIII* endonuclease.

III.2. Cloning of glycosylation markers

III.2.1. pcDNA-*EGFP-Glc-ER* and pcDNA-*EGFP-ER*

An endoplasmic reticulum (ER)-located EGFP with an introduced N-glycosylation site (EGFP-Glc-ER) has been recently reported as a sensitive fluorescent marker of an N-linked glycosylation (Losfeld et al., 2012) (Figure III.14.).

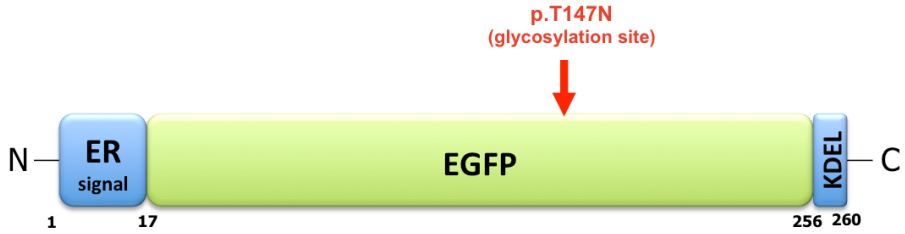

Fig.III.14. Schematic representation of the ER-retained enhanced green fluorescent protein with an introduced N-glycosylation site (EGFP-Glc-ER)
EGFP.p.T147N – enhanced green fluorescent protein with an introduced N-glycosylation site
ER signal – signal peptide from calreticulin, targeting to endoplasmic reticulum
KDEL – (lysine-aspartic acid-glutamic acid-leucine) endoplasmic reticulum retention signal

The EGFP-Glc-ER-encoding vector and a negative control, EGFP-ER-expressing plasmid were kindly provided by Prof. Hudson Freeze (Losfeld et al., 2012). Both constructs were based on a pcDNA™3.1 vector.

III.2.2. Cloning of pIRES2-DsRed2-*EGFP-ER* and pIRES2-DsRed2-*EGFP-Glc-ER*

For the application in flow cytometry experiments, *EGFP-Glc-ER* and *EGFP-ER* cDNA, respectively, were subcloned into pIRES2-DsRed2 vector (Clontech, 632420) (Figure III.15.).

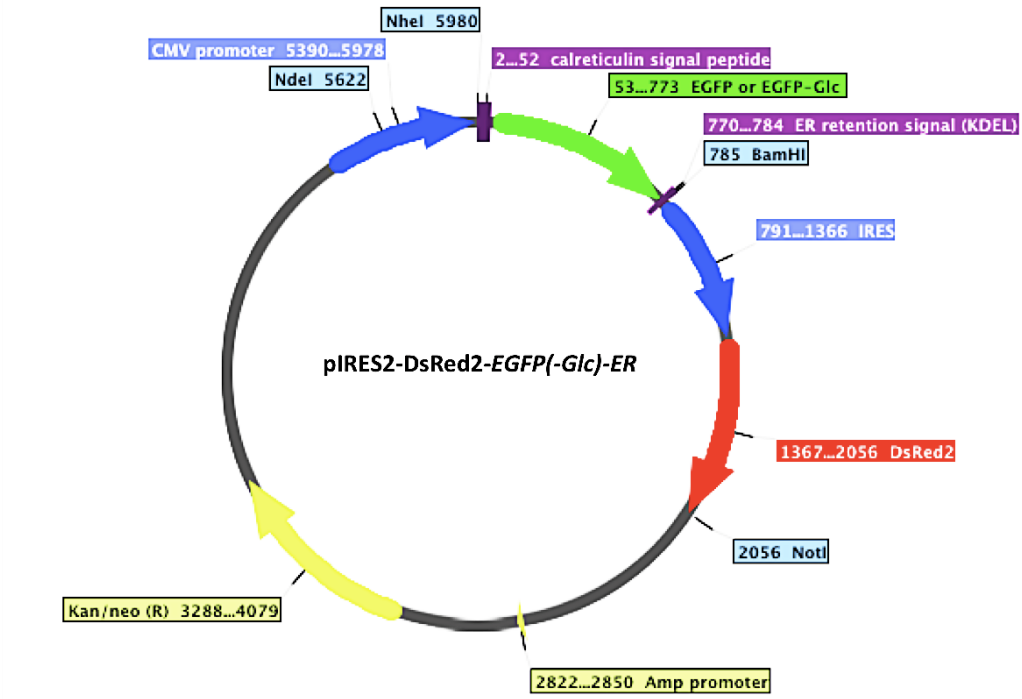

Fig.III.15. Schematic representation of pIRES2-DsRed2 plasmid encoding EGFP-ER or EGFP-Glc-ER (green) and DsRed2 (red)

pIRES2-DsRed2 vector is a bicistronic expression vector, which due to the presence of an internal ribosomal entry site (IRES) allows a simultaneous expression of two different mRNA from the same plasmid. This facilitates a specific selection of transfected cells. Both *EGFP-Glc-ER* and *EGFP-ER* cDNA were amplified from the pcDNA-*EGFP-Glc-ER* and pcDNA-*EGFP-ER* plasmids, respectively, using primers introducing *NheI* and *BamHI* restriction sites at 5' and 3' ends, respectively. The enzyme used in the procedure was a *PfuUltra* II Fussion HS DNA polymerase (Agilent

Technologies, 600670). Its proof-reading activity reduces the risk of PCR-induced mutations. The PCR products and pIRES2-DsRed2 vector were digested with *NheI* and *BamHI* restriction enzymes, and the appropriate DNA fragments were ligated. The success of the ligation was verified by digestion with *NdeI* and *NotI* endonucleases.

IV.Outline of cloning of *COLQ* cDNA

All constructs described in this section were sequenced to ensure the lack of any nucleotide changes. The primer sequences used in the sequencing reactions, site-directed mutagenesis and for cloning of specific inserts are specified in Chapter 2 and Appendix I.

IV.1. Cloning of *COLQ-CASPR2TM*

Collagen Q (COLQ) is an anchoring protein, essential for the concentration of acetylcholinesterase (AChE) at the neuromuscular junction (NMJ). It is expressed at the cell surface, but does not possess a transmembrane domain (TM). Attachment to the cell surface is mediated by interactions of the COLQ heparan sulphate binding domains (HSBD) and its C-terminal peptide with perlecan (Kimbell et al., 2004, Rotundo et al., 2005), which itself associates with dystroglycan (Peng et al., 1999, Peng et al., 1998), and by potential interactions with muscle-specific tyrosine kinase (MuSK) (Cartaud et al., 2004). For expression at the cell surface, COLQ was fused with a transmembrane domain (TM) originating from a different protein. A TM from contactin-associated protein-like 2 (CASPR2) (CASPR2TM) was chosen since it has been reported to be used successfully in similar experiments, which required an over-expression of TM-lacking proteins at the cell surface (Irani et al., 2010) (Figures IV.1. and IV.2.).

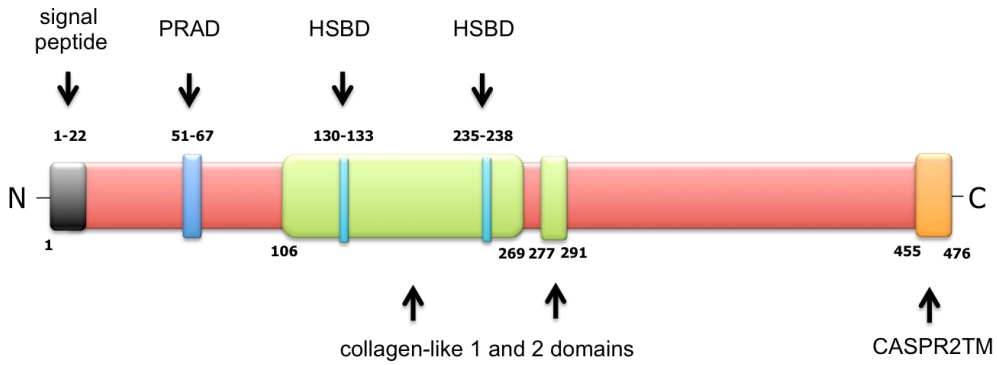

Fig.IV.1. Schematic representation of COLQ-CASPR2TM
The COLQ structure was based on the data stored in the UniProt database [Q9Y215].
PRAD – proline-rich attachment domain; HSBD – heparan sulphate binding domain
CASPR2TM – transmembrane domain of contactin-associated protein-like 2

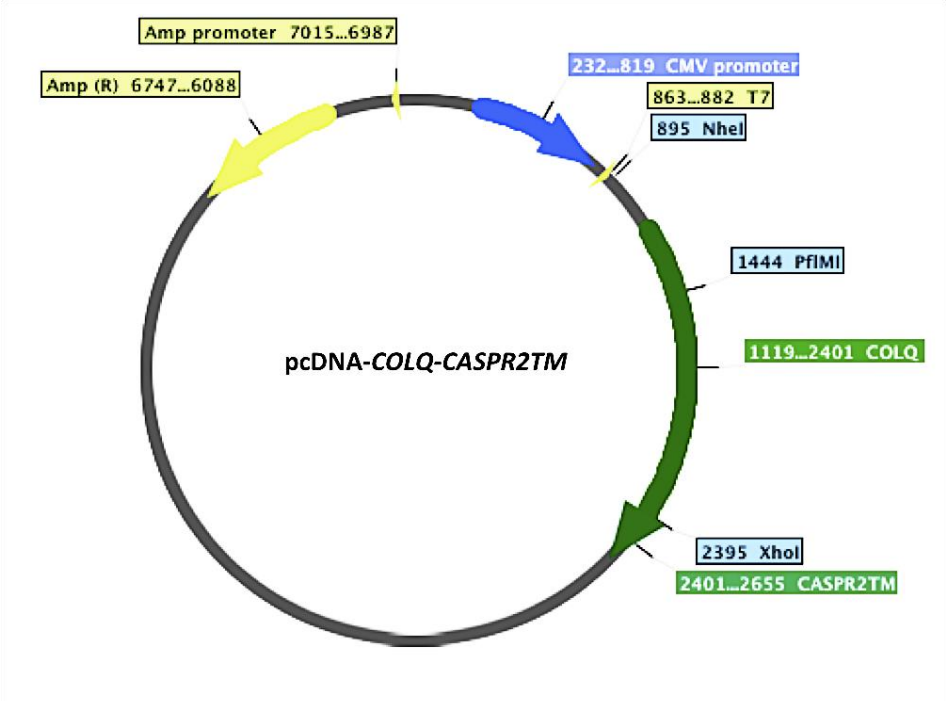

Fig.IV.2. Schematic representation of pcDNA™3.1(+) plasmid encoding human COLQ with CASPR2TM (dark green)

Constructs encoding *COLQ* in pcDNA™3.1/Hygro(+) (Invitrogen, V87020) and *Lgi1-CASPR2TM* in pcDNA™3.1(+) (Invitrogen, V79020) were kindly provided by Dr Janet Kenyon and Dr Patrick Waters, respectively. The experiment was designed such as to exchange the *Lgi1* cDNA for *COLQ* cDNA. The C-terminus of COLQ was chosen for the fusion with CASPR2TM, and thus the STOP codon needed to be removed from the *COLQ* cDNA. This was done by site-directed mutagenesis using

GeneArt® Site-Directed Mutagenesis System (Invitrogen, A13282) and mutagenesis primers. Both plasmids were then digested with *NheI* and *XhoI* endonucleases and the appropriate DNA fragments (*CASPR2TM* in pcDNA™3.1(+) as a backbone and *COLQ* cDNA as an insert) were ligated. The success of the ligation was verified by digestion of the constructs with a *PflMI* endonuclease.

IV.2. Construction of an N-terminal Myc-tagged *COLQ-CASPR2TM* expression vector

Lack of commercially available anti-COLQ antibodies required us to attach a Myc tag to the N-terminus of COLQ (Figures IV.3. and IV.4.).

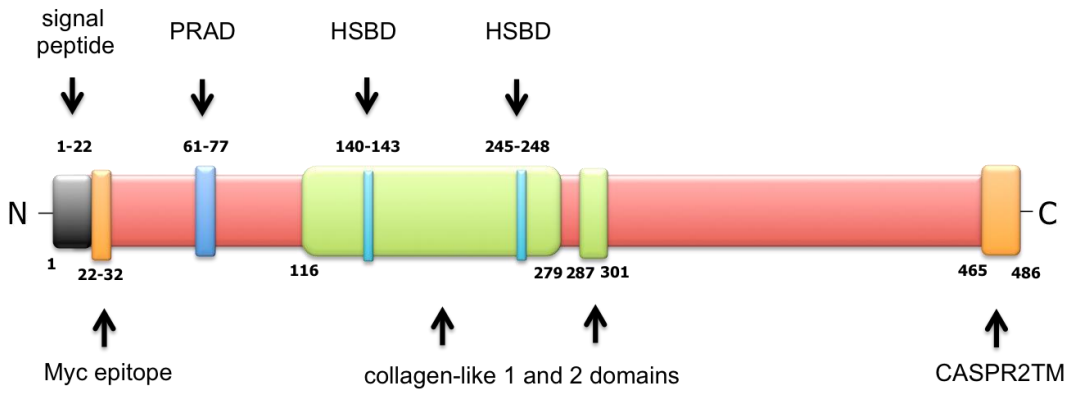

Fig.IV.3. Schematic representation of Myc-COLQ-CASPR2TM
The COLQ structure was based on the data stored in the UniProt database [Q9Y215].
PRAD – proline-rich attachment domain; HSBD – heparan sulphate binding domain
CASPR2TM – transmembrane domain of contactin-associated protein-like 2

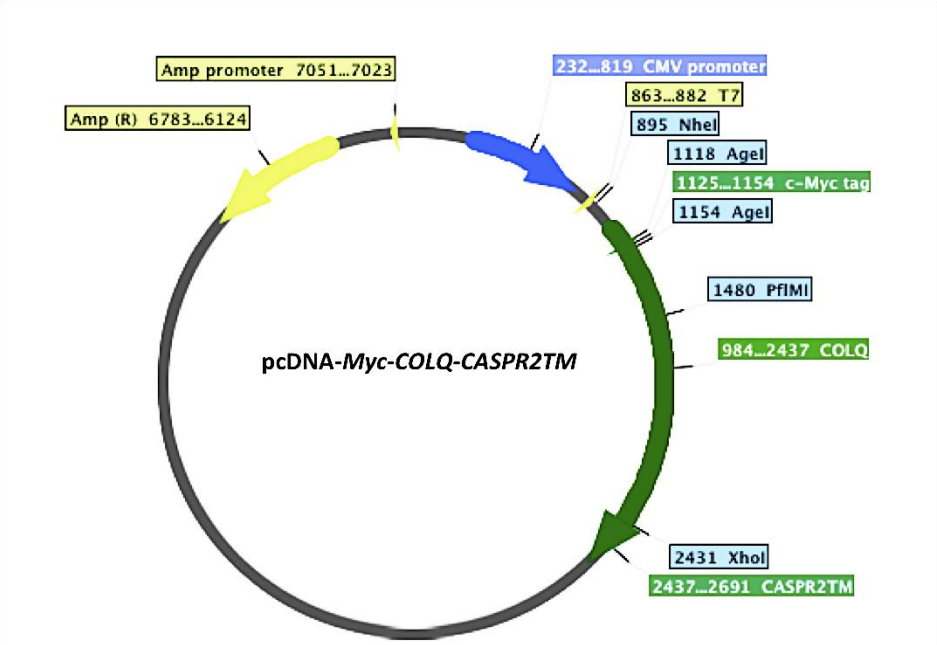

Fig.IV.4. Schematic representation of pcDNA™3.1(+) plasmid encoding human COLQ with CASPR2TM and with an N-terminal Myc tag (dark green)

The Myc tag was introduced immediately downstream of the N-terminal signal peptide, which is required for extracellular expression of COLQ and cleaved after secretion of the protein. The tag was cloned at the desired position using an *AgeI* restriction site introduced by site-directed mutagenesis performed with GeneArt® Site-Directed Mutagenesis System (Invitrogen, A13282) and mutagenesis primers. Correct *AgeI*-mutated plasmid was identified by sequencing, linearised by digestion with an *AgeI* restriction enzyme and dephosphorylated to prevent its self-ligation during subsequent cloning steps. The fragment encoding the Myc tag was obtained by annealing Myc-encoding oligonucleotides possessing overhangs with *AgeI* restriction sites and modified with phosphate groups at their 5' ends. The annealed oligonucleotides and the digested backbone were ligated.

IV.3. Cloning of a Myc-tag to the N-terminus of *COLQ*

To investigate potential interactions of COLQ with MuSK a construct encoding Myc-tagged COLQ without CASPR2TM was needed (Figures IV.5. and IV.6.).

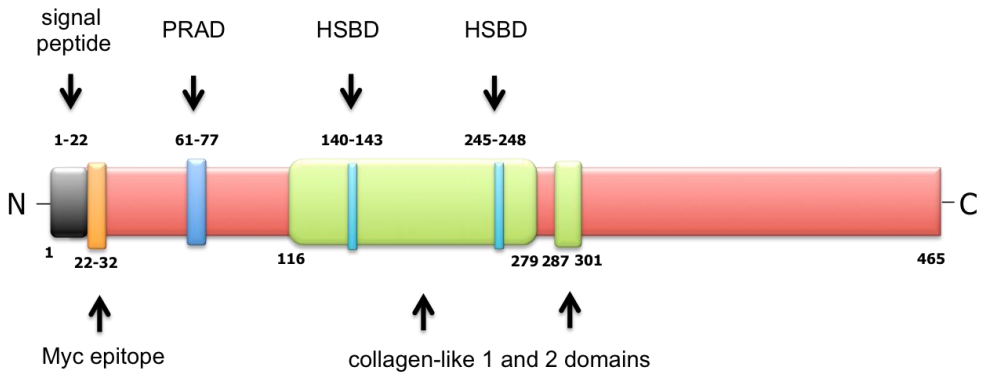

Fig.IV.5. Schematic representation of Myc-COLQ
The COLQ structure was based on the data stored in the UniProt database [Q9Y215].
PRAD – proline-rich attachment domain; HSBD – heparan sulphate binding domain
CASPR2TM – transmembrane domain of contactin-associated protein-like 2

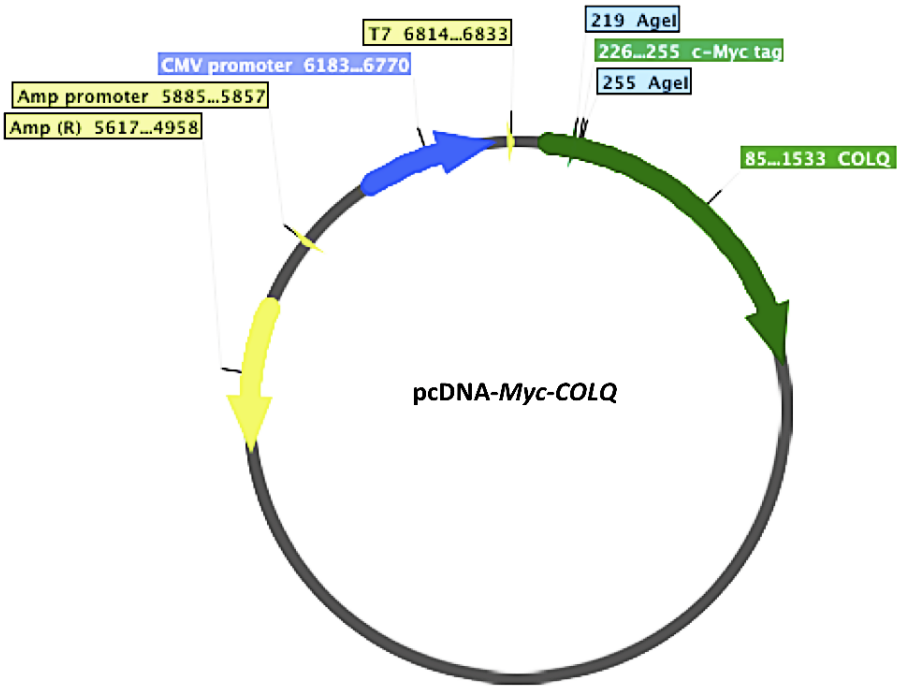

Fig.IV.6. Schematic representation of pcDNA™3.1/Hygro(+) plasmid encoding human COLQ with N-terminal Myc tag (dark green)

The pcDNA-*Myc-COLQ* plasmid was obtained by introducing an N-terminal Myc tag into pcDNA-*COLQ.* The choice of the N-terminus was determined by the fact that the C-terminal end of COLQ could be important for potential associations of the protein with MuSK (Cartaud et al., 2004). Similarly, as before, the Myc tag was inserted into a pcDNA™3.1/Hygro(+) vector encoding COLQ using an *AgeI* restriction site introduced in the desired position by site-directed mutagenesis performed with GeneArt® Site-Directed Mutagenesis System (Invitrogen, A13282) and a pair of mutagenesis primers. The *AgeI*-mutated vector was digested with an *AgeI* endonuclease, dephosphorylated and ligated with annealed Myc-encoding oligonucleotides possessing *AgeI* complementary overhangs and phosphate groups at their 5' ends.

V. Vectors available in the laboratory

V.1. pcDNA-*AGRN*

A pcDNA™3.1/Hygro(+) (Invitrogen, V87020) plasmid encoding full-length human agrin (AGRN) was kindly provided by Dr Katsiaryna Belaya (Figure V.1.).

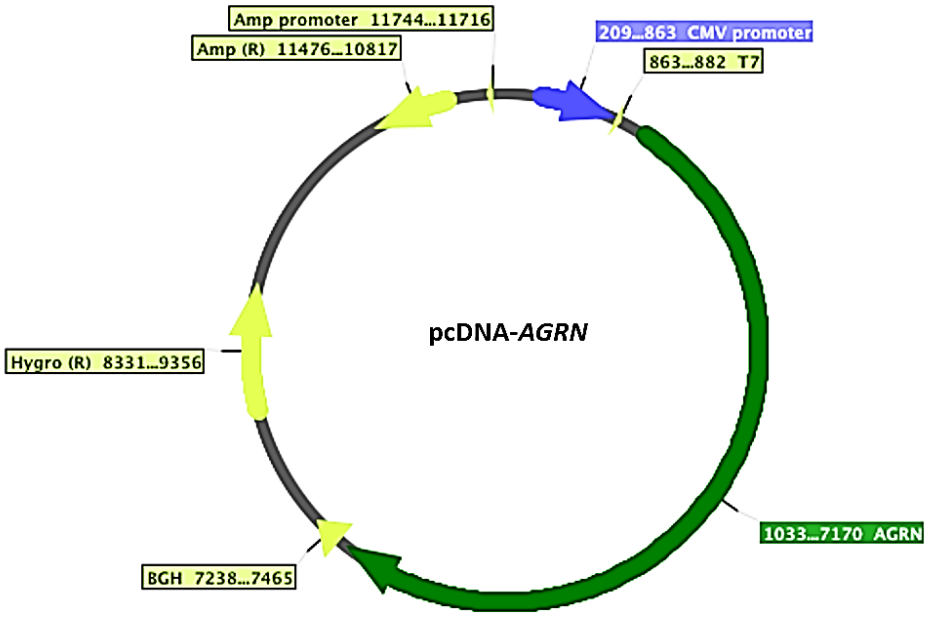

Fig.V.1. Schematic representation of pcDNA™3.1/Hygro(+) plasmid encoding full-length AGRN (dark green)

V.2. pcDNA-*CHRNA1/CHRNB1/CHRND/CHRNE*

A pcDNA™3.1/Hygro(-) (Invitrogen, V87520) plasmid encoding respective acetylcholine receptor (AChR) subunits (α, β, δ or ε) was used in the studies into AChR expression in *GFPT1*-silenced cells (Figure V.2.).

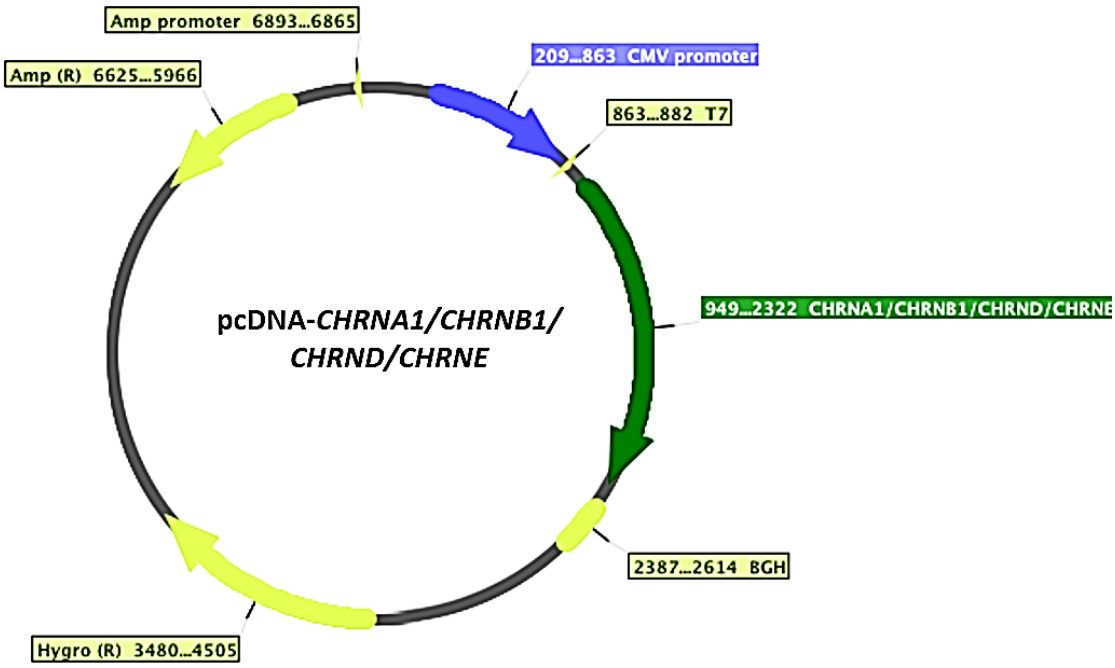

Fig.V.2. Schematic representation of pcDNA™3.1/Hygro(-) plasmid encoding AChR α, β, δ and ε subunits (dark green), respectively

V.3. pcDNA-*LRP4*

A pcDNA™3.1/Hygro(-) vector (Invitrogen, V87020) encoding human low-density lipoprotein receptor-related protein 4 (LRP4) was used as a control in the investigations into molecular interactions between muscle-specific tyrosine kinase (MuSK) and collagen Q (COLQ) (Figure V.3.).

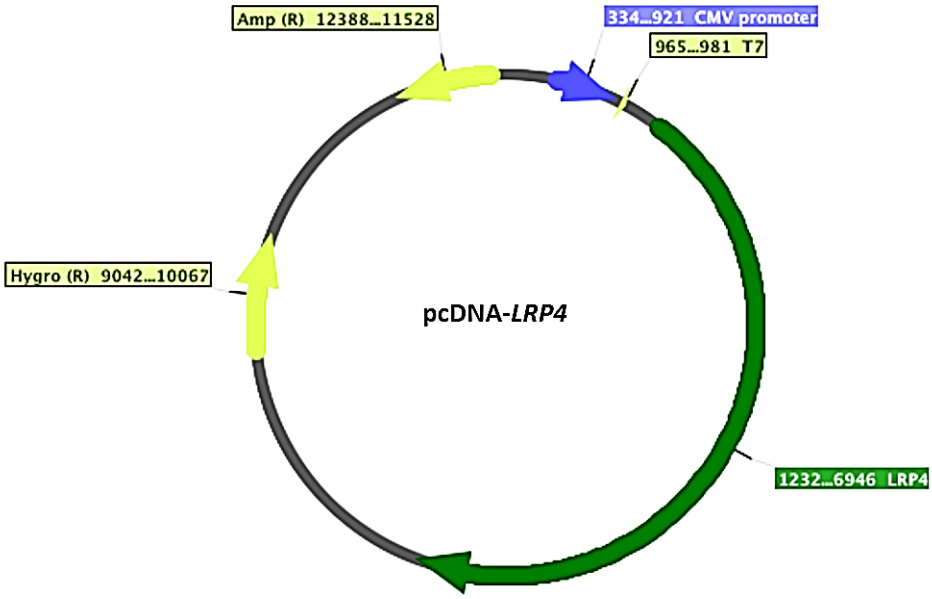

Fig.V.3. Schematic representation of pcDNA™3.1/Hygro(+) plasmid encoding LRP4 (dark green)

V.4. pcDNA-*MUSK*

A pcDNA™3.1/Hygro(+) (Invitrogen, V87020) plasmid encoding MuSK was used in the research, the main objective of which was to analyse potential interactions between MuSK and COLQ (Figure V.4.).

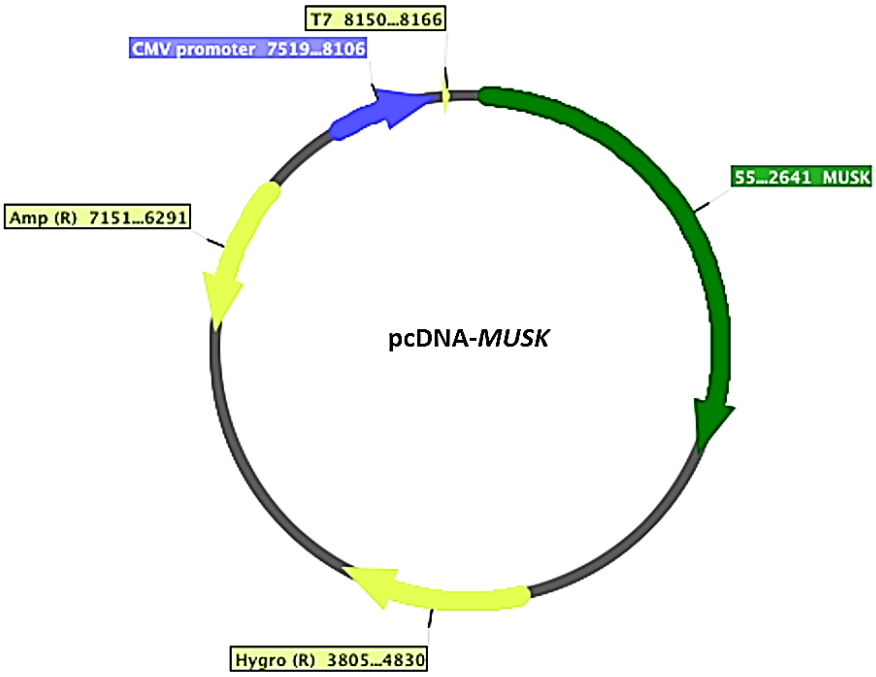

Fig.V.4. Schematic representation of pcDNA™3.1/Hygro(+) plasmid encoding MuSK (dark green)

V.5. pcDNA-*MUSK-mCherry*

A pcDNA™3.1(+) (Invitrogen, V79020) plasmid encoding MuSK with a C-terminal mCherry tag was used in the experiments, which aimed at investigating the cell surface expression of MuSK in *GFPT1*-silenced cells (Figure V.5.).

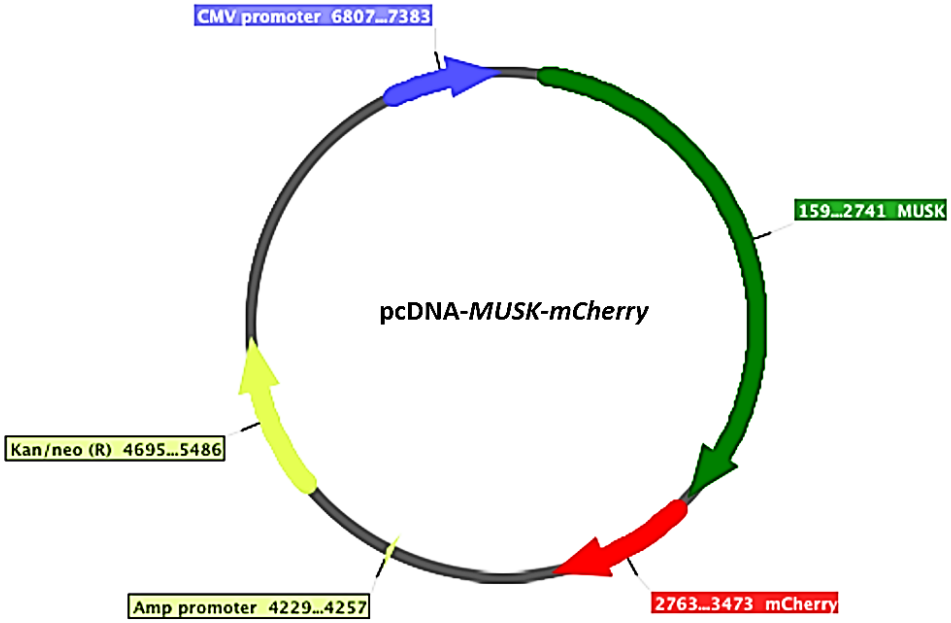

Fig.V.5. Schematic representation of pcDNA™3.1 plasmid encoding MuSK (dark green) tagged with mCherry (red) at its C-terminus

VI. Reporter plasmids and markers of transfection efficiency

VI.1. pDsRed-Monomer-N1

A pDsRed-Monomer-N1 vector encoding a red fluorescent protein (DsRed) was obtained from a commercial source (Clontech, 632465).

VI.2. pEGFP-N1

A pEGFP-N1 vector encoding an enhanced green fluorescent protein (EGFP) was obtained from a commercial source (Clontech, 6085-1).

VI.3. pGL4.29[*luc2P*/CRE/Hygro]

The pGL4.29[*luc2P*/CRE/Hygro] vector containing a cAMP response element (CRE) that drives the transcription of the luciferase reporter gene *luc2P* (*Photinus pyralis*) was obtained from a commercial source (Promega, E847A).

VI.4. pcDNA-*mCherry*

A pcDNA™3.1/Hygro(-) (Invitrogen, V87520) plasmid encoding mCherry – a red fluorescent protein – was a generous gift from Dr Patrick Waters.

VII. Publications

The chapter originally presented here cannot currently be made freely available via ORA. The content has been published as:

VII.1. Zoltowska, K., Webster, R., Finlayson, S., Maxwell, S., Cossins, J., Beeson, D. (2013) Mutations in *GFPT1* that underlie limb-girdle congenital myasthenic syndrome result in reduced cell-surface expression of muscle AChR. *Hum. Mol. Genet*. [Epub ahead of print]; doi: 10.1093/hmg/ddt145

VII.2. Cossins, J., Belaya, K., **Zoltowska, K.**, Koneczny, I., Maxwell, S., Jacobson, L., Leite, M.I., Waters, P., Vincent, A. Beeson, D. (2012) The search for new antigenic targets in myasthenia gravis. *Ann N Y Acad Sci*. *1275(1):123-8*.; doi: 10.1111/j.1749-6632.2012.06833.x

VII.3. Cossins, J., Belaya, K., Hicks, D., Salih, M.A., Finlayson, S., Carboni, N., Liu, W.W., Maxwell, S., **Zoltowska, K.**, Farsani, G.T. *et al.* (2013) Congenital myasthenic syndromes due to mutations in ALG2 and ALG14. *Brain*. *136(Pt 3):944-56.*; doi: 10.1093/brain/awt01